Prediction of Macrodispersivity in Heterogeneous Aquifers

by

Kenneth Robert Rehfeldt

B.A., Geological Sciences, University of Wisconsin-Milwaukee - 1978
M.S., Hydrology, New Mexico Institute of Mining and Technology - 1980

Submitted in Partial Fulfillment of the
Requirements for the Degree of
Doctor of Philosophy

at the

Massachusetts Institute of Technology

March 1988

Signature of Author.....
Department of Civil Engineering
March, 1988

Certified by.....
Lynn W. Gelhar
Professor , Civil Engineering
Thesis Supervisor

Accepted by.....
Ole S. Madsen, Chairman
Departmental Graduate Committee
Department of Civil Engineering

PREDICTION OF MACRODISPERSIVITIES IN HETEROGENEOUS AQUIFERS

by

KENNETH ROBERT REHFELDT

Submitted to the Department of Civil Engineering
on March 8, 1988,
in partial fulfillment of the requirements
for the Degree of Doctor of Philosophy
in Civil Engineering

ABSTRACT

At the site of an ongoing large-scale tracer experiment on the Columbus Air Force Base, Mississippi, the feasibility of estimating the autocovariance parameters of log conductivity from variability measurements and of predicting the asymptotic macrodispersivities using recent stochastic theories is demonstrated. Extensive measurements of the hydraulic conductivity (K) in three dimensions, obtained using a borehole flowmeter method, were analyzed in detail to estimate the parameters of the lnK covariance. Special emphasis was placed on estimating the uncertainty in the parameter values due to finite data sets, measurement errors, and nonstationarity. A pragmatic methodology was developed based on the uncertainty in covariance parameter estimates and observed site characteristics to assess whether the random field contains a trend and how to decide on the appropriate level of detrending. The uncertainty in the parameter estimates yields a range of parameter values that encompassed the case of a second order trend removed by ordinary least squares methods, which was analyzed for the effects of correlated residuals and variogram bias. Covariance parameter estimates from preliminary analyses of secondary measurements such as surface geophysical surveys, grain size data, and large-scale aquifer tests were generally within the uncertainty from the extensive

measurements suggesting the possibility that the covariance parameters can be estimated without exhaustive sampling. Most likely and bounding values of the covariance parameters were used to predict a range of macrodispersivities.

The possibility of an additional dispersive flux caused by an unsteady flow system was investigated using a spectral-method based perturbation analysis. The analysis treats the temporal variability of the hydraulic gradient as the primary manifestation of unsteady boundary influences. The results suggest that temporal variation in the direction of the hydraulic gradient enhances transverse dispersive mixing, but has little influence on the longitudinal dispersive flux. Temporal variation in the magnitude of the hydraulic gradient produces little enhancement of the dispersive flux in any direction. Based on the observed temporal variability in the direction of the hydraulic gradient at the CAFB site, predicted transverse macrodispersivities may be up to two orders of magnitude larger than when the effect of temporal variability is not included. At two other less heterogeneous sites, the lateral dispersivities calculated with the unsteady flow theory in this work are the first calculated values to be in agreement with measured values.

Thesis Supervisor: Dr. Lynn W. Gelhar
Title: Professor of Civil Engineering

ACKNOWLEDGMENTS

The dissertation has but one author, yet many have contributed to this work in one way or another.

This research was supported at MIT in part by the Electric Power Research Institute through research project 2485-5 under subcontract with the Tennessee Valley Authority (TVA contract No. TV-61664A) and by the National Science Foundation (Grant No. ECE-8311786).

J. Mark Boggs, Steve Young, and Sam Long of TVA graciously provided logistical support during the flowmeter measurements and supplied all of the secondary data for analysis. Mark Schaefer, former MIT colleague, helped trouble-shoot the equipment when it failed, performed some flowmeter measurements, and provided a helpful critique of the work. My brother, Bob shared part of one summer with me making flowmeter measurements, thanks for the help and the company.

The proposal for this research was developed during a six month visit to the Centre d'Information Geologique of the Ecole des Mines de Paris in Fontainebleau, France, which was supported the National Science Foundation (Grant No. 8212574-INT). I am grateful for the guidance of Dr. Ghislain deMarsily, Director of the Centre d'Information Geologique and the lively discussions and friendship of Dr. Alain Dieulin during my stay.

I am grateful to my Thesis Committee and others for their help and support. My advisor, Professor Lynn W. Gelhar gave me the opportunity to come to MIT and to work on a problem of special interest to me. I appreciated the freedom to explore on my own knowing that if I got lost I always had someone to turn to for directions. My thanks to Professor Michael Celia for his insightful analysis of the flow physics and to Professor Dennis McLaughlin for helpful discussions on the fine points of statistics. Professor Harry Hemond shared his wealth of field experience and Professor John Southard's geologic insights help relate the measured variability to geologic depositional processes. Dr. Allan Gutjahr, of New Mexico Institute of Mining and Technology, provided the key to the unsteady flow analyses by confirming that I could use the delta function spectra in the analyses. Dr. Peter Hufschmied, former Parson's Lab Post Doctoral Fellow and now of NAGRA, Switzerland, was an enthusiastic supporter of the borehole flowmeter method and was instrumental in obtaining our equipment.

Many folks from the Parson's Lab made the past four plus years enjoyable. Patricia Dixon was a constant source of information, strength, and support. The comradery and goodwill within the lab are due in large part to her efforts. Elaine Healy was an understanding recipient of my many kid stories and always a source of encouragement and humor.

To the students in the lab, Thank You. The atmosphere you provide is much like that of a family where the members can share their triumphs and defeats. Particular thanks to Neil Fennessey for becoming a valued friend and for reminding me that there is more to life than work. To Claire Welty, a friend whose enthusiasm and unwavering integrity are an inspiration to us all. To Don Polmann, Mike Jasinski, and Jim Bowen, my office support group who have struggled through the final months with me and remained cheerful. I want to thank Ronni Schwartz for typing the draft of the thesis and for her sense of humor. Thanks also to Harihar Rajaram for help with some of the figures and to Andy Dasinger for proofreading, figure preparation and the analyses of the gravel pit facies map.

My parents have contributed to my success more than simply through genetics. Early in life they instilled in me a desire to do my best. Their constant support and love were often called upon to carry us over some rough roads along the way. Thank you! Last, but never least, my family. My wife, Dawn, has been a beacon of strength. You were always there when I needed you and patiently tolerated the cramped and simple quarters in which graduate students are forced to live. Thank you, Dawn! My sons; Brian, Thomas, Jason, and Matthew are a constant joy. Their total disconcern for my work forced me to put it behind me for at least a few hours each day. Thanks guys for letting me clear my head and for always having a big hug for me at night.

TABLE OF CONTENTS

LIST OF FIGURES

LIST OF TABLES

Section 1

INTRODUCTION

RELEVANCE AND PROBLEM

Anyone who has walked along a road cut or examined cuttings or cores from a borehole will recognize that even within sedimentologically similar units there is considerable variability of grain size, texture, and sorting. The variability is not completely random, but rather is structured, often occurring in lense-like forms of varying size and geometry that are not easily characterized deterministically. These physical characteristics of the aquifer influence the hydraulic conductivity and consequently the conductivity is spatially variable also.

The movement and spreading of solutes in groundwater is an issue of much concern. Through the work of many investigators (e.g., Skibitzke and Robertson, 1963; Warren and Skiba, 1964; and Gelhar and Axness, 1983), we now appreciate the strong influence of hydraulic conductivity (K) heterogeneity on the movement, spreading, and dilution of solutes in groundwater.

Near the source of contamination, local heterogeneities strongly influence the solute plume. Solute shoots out along pathways of large hydraulic conductivity, but tends to lag behind in regions of small K. To accurately model the near-source behavior, one would need a detailed understanding of the local heterogeneity.

Much farther from the source, the spreading of the solute is larger than one would expect based on laboratory measurements of dispersion (Gelhar et al., 1985). This enhanced field-scale mixing is caused, in large part, by the variability of K. Attempts to measure the heterogeneous K field in detail over large regions would be futile. Additionally, tracer experiments to measure dispersion over large distances (on the order of kilometers) are not practical.

A number of researchers (Dagan, 1982, 1984; Gelhar and Axness, 1983) have described the variability of K as a random field and have used stochastic methods to better understand the role of heterogeneity in

field-scale dispersion. Dagan (1982, 1984) and Gelhar and Axness (1983) derived expressions for the asymptotic field-scale macrodispersivities that are functions of the autocovariance function of the natural logarithm of K (lnK). However, detailed quantification of the autocovariance of lnK in three dimensions is difficult because a large number of K values are needed.

Although these predictive expressions have the potential to be a powerful tool in the analysis of solute transport problems, the predictions must be verified by comparison with measured macrodispersivities and practical methodologies developed to obtain the autocovariance function before it becomes possible to predict macrodispersivities for real problems.

PREVIOUS CALCULATIONS OF MACRODISPERSIVITY

Macrodispersivities have been calculated using the theories of Gelhar and Axness (1983) and Dagan (1982, 1984) and compared to the macrodispersivities from tracer tests by Sudicky (1986) and Hufschmied (1986). At the Borden site, Sudicky (1986) used the hydraulic conductivity data from laboratory permeameter measurements of repacked cores collected along two perpendicular transects in a subregion of the tracer test site to estimate the variance (σ_f^2), horizontal correlation scales (λ_1 or λ_2), and vertical correlation scale (λ_3) of the log hydraulic conductivity field. Assuming a horizontally isotropic random field (characterized by $\sigma_f^2 = 0.29$, $\lambda_1 = \lambda_2 = 2.8$ m, $\lambda_3 = 0.12$ m) with mean flow parallel to the bedding, Sudicky calculated the components of the macrodispersivity tensor using the expressions in Gelhar and Axness (1983)

$$\begin{bmatrix} A_{11} & & A_{13} \\ & A_{22} & \\ A_{31} & & A_{33} \end{bmatrix} = \begin{bmatrix} 0.61\text{m} & & \approx 0 \\ & \approx 0 & \\ \approx 0 & & \approx 0 \end{bmatrix} \qquad (1\text{-}1)$$

which are compared to the measured macrodispersivities obtained by analyzing the spatial moments of depth-averaged concentration with the x_1 direction oriented in the direction of mean flow (Freyberg, 1986)

$$\begin{bmatrix} A_{11} & A_{12} \\ A_{21} & A_{22} \end{bmatrix} = \begin{bmatrix} 0.36m & 0.023m \\ 0.023m & 0.039m \end{bmatrix} \quad (1-2)$$

The predicted longitudinal macrodispersivity was overestimated and the A_{12}, A_{22} terms were underestimated, in part because of the somewhat restrictive assumptions of horizontal isotropy and mean flow parallel to bedding used by Sudicky (1986). Vomvoris (1986) also calculated macrodispersivities of the Borden site for a range of covariance parameters and various orientations of the mean flow with respect to the major principal direction of the autocovariance in an attempt to match the measured plume results. The parameters most similar to the measured values

$$\begin{bmatrix} A_{11} & A_{12} & A_{13} \\ A_{21} & A_{22} & A_{23} \\ A_{31} & A_{32} & A_{33} \end{bmatrix} = \begin{bmatrix} 0.31m & -0.0024m & 0 \\ -0.0024m & 0.0019m & 0 \\ 0 & 0 & 0.00033m \end{bmatrix} \quad (1-3)$$

were obtained with a horizontally anisotropic covariance ($\sigma_f^2 = 1.5$, $\lambda_1 = 5$ m, $\lambda_2 = 0.5$ m, $\lambda_3 = 0.01$ m) and mean flow oriented parallel to bedding, but at an angle of 20 degrees to the λ_1 direction. Yet the A_{12} and A_{22} terms were still one order of magnitude smaller than the measured values of Freyberg (1986).

The theory of Gelhar and Axness (1983) is able to predict the longitudinal macrodispersivity, A_{11}, quite well, but underpredicts the other components of A_{ij}. The underprediction of the transverse terms of A_{ij} may be due to incorrect measured A_{ij} from the tracer test, incorrect covariance parameters, or to a dispersive mechanism not included in the analyses of Gelhar and Axness (1983). Perhaps the tracer data should be reanalyzed to include the vertical component of A_{ij} or perhaps the autocovariance of lnK obtained by Sudicky (1986) from a subsection of the tracer test site may not be representative of the spatial variabilty of the entire path of the plume. There may be other factors also. As Sudicky (1986) notes, the theory of Gelhar and Axness (1983) was derived for steady flow and neutrally buoyant tracer solutions, yet, at the Borden site, the hydraulic gradient was observed to fluctuate in time, and it appears that some density-induced sinking of the plume occurred

following injection. There is clearly a need to extend the theoretical results of Gelhar and Axness (1983) to cases of unsteady flow and nonuniform density.

At the site of a cold water and salinity tracer experiment, Hufschmied (1986) estimated the autocovariance function of lnK using hydraulic conductivity values obtained using a borehole flowmeter technique(Hufschmied, 1983) and predicted a range of A_{ij} values for a range of spatial orientations of the autocovariance function using the theory of Gelhar and Axness (1983). The ranges of calculated macrodispersivities

A_{11} : 1.3 - 3.8 m
A_{22}/A_{11} : 0 - 2×10^{-2}
A_{33}/A_{11} : 0 - 6×10^{-2}

are in reasonable agreement with the measured A_{ij} obtained by analyzing breakthrough curves for temperature and electrical conductivity with one-dimensional models and by numerical simulations (Hufschmied, 1986):

A_{11} : 2.2 - 22.1 m
A_{33} : 0.07 m

Unlike the results from the Borden site, the calculated longitudinal macrodispersivity appears to be less than the observed value. It is difficult to compare the transverse or off-diagonal terms of A_{ij} because the measured value of A_{33} was obtained from a simple one-dimensional analysis and may be in error. If the measured value of A_{33} is correct, then it would appear that that component can be predicted for some orientations of the stratification with respect to the mean flow. Hufschmied (1986) recognized the importance of the orientation of the mean flow with respect to the principal components of the autocovariance function and presented a range of A_{ij} values corresponding to a range of angles. However, neither Hufschmied nor Sudicky examined the effect that uncertainty in the sample autocovariance has on the calculated macrodispersivities.

OBJECTIVES AND SCOPE

The goal of the thesis is to demonstrate the feasibility of predicting macrodispersivities at the site of a Macrodispersion Experiment (MADE) conducted by the Tennessee Valley Authority and the Massachusetts Institute of Technology located on the Columbus Air Force Base (CAFB), Mississippi. One step toward that goal is the development and evaluation of methods for characterizing the spatial variability of hydraulic conductivity at the CAFB site. A second step toward the goal is the evaluation of the variability data to determine the variance and correlation scales of the three-dimensional autocovariance function of the natural logarithm of hydraulic conductivity, which are required to predict macrodispersivities. Early in the MADE project, large fluctuations in the hydraulic head field were observed and questions were raised about the influence of unsteady flow on dispersivity. As unsteady flow is a ubiquitous aspect of most groundwater flow systems, and hence an inportant factor at sites in addition to CAFB, a third goal became the investigation of the contribution of unsteady flow to dispersion. This preliminary investigation concentrated on defining the order of magnitude of the effect and will serve as a starting point for future investigations. The thesis has been divided into separate sections each dealing with a different aspect of the prediction of macrodispersivities.

In Section 2, the unsteady flow contribution to dispersion is developed based on the premise that the major influence of unsteady flow is embodied in the temporal variability of the hydraulic gradient. The theory is developed using a stochastic analysis method that includes the influences of both the spatial variability of hydraulic conductivity and the temporal variability of the hydraulic gradient. The unsteady analysis produces the steady-flow results of Gelhar and Axness (1983) as special cases, which serve as bench marks to evaluate the additional dispersion due to unsteady flow.

In Sections 3 and 4 both the spatial and temporal variability data are analyzed for the variance and correlation scales. In Section 3, eight possible methods of characterizing spatial variability were identified: slug tests in piezometers, grain-size distributions, surface geophysics, borehole geophysics, conventional large-scale aquifer tests, mapping of sedimentological facies, laboratory permeameter, and borehole flowmeter.

The goal was to find a method that not only characterized the variability accurately, but also could be applied routinely at other sites. The measurements of spatial variability are discussed in terms of which physical parameter is actually measured, the advantages and disadvantages of each method, and the prospect of using each method for routine analysis. The data from each method are presented, or an appropriate reference cited. Of the possible methods, the borehole flowmeter method appeared to be the most promising and was extensively tested at the CAFB site (Rehfeldt et al., 1988). Less extensive data were collected using methods other than the borehole flowmeter. These secondary data, collected prior to the flowmeter measurements, provided preliminary estimates of the variance and correlation scales that were useful in designing the flowmeter experiments. The methods for collecting the secondary data were applied in much the same way one might use them in a routine site evaluation. Much of the data collected during a routine site evaluation is for reconnaissance purposes to familiarize the investigator with the range of conditions at the site. These measurements are not designed to provide geostatistical information, yet in many cases preliminary geostatistical information can be obtained. The preliminary autocovariance parameters from the analyses of the secondary data will be compared with the values from the analyses of the flowmeter data(Section 4). From that comparison, the adequacy of the secondary data to provide estimates of the autocovariance parameters will be evaluated and improvements to those methods will be suggested.

In Section 4, the spatial autocovariance of lnK is estimated in detail using the primary data from the borehole flowmeter method. The uncertainty in the autocovariance parameters is quantified and the scope of additional work needed to improve those parameter estimates is indicated. The question of trend removal is addressed with regard to the overall accuracy of the covariance parameters and whether trend removal provides significantly improved estimates of the covariance parameter. At the end of the section, preliminary temporal covariance parameters are obtained.

In Section 5, predictions of a range of macrodispersivity values are given using the uncertain autocovariance parameters of Section 4. These predictions are preliminary and may be subject to change as additional

data, particularly from work suggested in this report, become available. The implications of these results are discussed in terms of the potential for application of the stochastic theories to the analysis of groundwater transport problems. However, no comparisons of the predicted macrodispersivities with the measured values from an ongoing tracer experiment at the CAFB site are possible at this time because the experiment is still at an early stage of dispersion development and many experimental issues remain to be resolved before meaningful analyses can be completed.

Section 2

STOCHASTIC ANALYSES OF THE UNSTEADY-FLOW CONTRIBUTION TO THE DISPERSION OF SOLUTES IN GROUNDWATER

The investigation of the effect of unsteady flow on the dispersion process was motivated by two observations: (1) predicted transverse macrodispersivities based on steady-flow stochastic theory tend to be an order of magnitude or more smaller than measured values from controlled experiments and (2) natural groundwater flow systems are rarely in steady state.

PREVIOUS STUDIES

During two natural gradient tracer experiments, researchers at the University of Waterloo (Sudicky, 1986; Sykes et al., 1982) have noted that the magnitude and direction of the mean hydraulic gradient fluctuates in time. Both Sudicky (1986) and Sykes et al. (1982) suggest that the unsteadiness of the flow system might enhance the lateral spreading but don't attempt to quantify their supposition.

Sudicky (1986) suggests that the effect of unsteady flow might be analyzed by incorporating the flow transients into a transport model where macrodispersivities are used to account for spatial variability. There are a number of problems with that approach.

1) The transients are a stochastic process in time and composed of components of various amplitudes and frequencies. To model the high-frequency component one would have to use a small time step. Additionally, the random nature of the transients would seem to dictate a Monte Carlo approach or a long total simulation time. The short time step and long simulation time would yield a computationally intensive exercise.

2) Clearly some low-frequency components of the transients can be treated as deterministic while high-frequency components are treated as random. How does one differentiate the deterministic from the random components in the model?

3) Whether unsteadiness causes dispersion at all is a question that must be addressed. Dispersion causes a dilution of the plume and a reduction in the concentration. Does a temporally variable hydraulic gradient produce dispersion (dilution), or does it simply cause the plume to be shifted laterally or vertically?

Ackerer and Kinzelbach (1985), using a two-dimensional random walk transport model, simulated a contaminant plume using both a steady and time-varying velocity field. For the steady simulation, they calibrated the model and obtained apparent (including the effect of temporal variability) longitudinal and transverse dispersivities of 80 m and 2 m, respectively. They related the apparent dispersivities to the variations in the velocity field using:

$$\alpha_{La} = \alpha_L \overline{\left(\frac{u_x^2}{u}\right)} / \bar{u} + \alpha_T \overline{\left(\frac{u_y^2}{u}\right)} / \bar{u} = 80\text{m}$$

$$\alpha_{Ta} = \alpha_T \overline{\left(\frac{u_x^2}{u}\right)} / \bar{u} + \alpha_L \overline{\left(\frac{u_y^2}{u}\right)} / \bar{u} = 2\text{m}$$

where
- $\bar{u}$ = mean velocity
- u_x = x velocity component, direction of mean flow
- u_y = transverse velocity component
- α_{La} = apparent longitudinal dispersivity
- α_{Ta} = apparent transverse dispersivity
- α_L = longitudinal dispersivity
- α_T = transverse dispersivity

The temporal velocity variations, calculated from head observations in triangular arrays of wells, were found to be small:

$$\overline{\frac{u_x^2}{u}} / \bar{u} = 0.984 \qquad \overline{\frac{u_y^2}{u}} / \bar{u} = 0.016$$

The longitudinal and transverse dispersivities after removing the influence of unsteadiness with the Schiedegger formulas above were:

$$\alpha_L = 81.3 \text{ m}; \qquad \alpha_T = 0.7 \text{ m}.$$

The apparent longitudinal component was slightly smaller than α_L, but the apparent transverse dispersivity was about a factor of 3 larger. Even for the case of relatively minor temporal perturbations in the velocity field there appears to be a significant effect on the transverse dispersivity.

From the scant available literature, there is some indication that temporal variability produces an additional transverse dispersive flux, but a number of questions need to be addressed:

1) Does temporal variability produce dispersion? Dispersion causes dilution and a decrease in the maximum concentration.

2) Can one separate deterministic components of velocity variation that would produce only a lateral shifting of the plume from stochastic components which can be viewed as producing an additional dispersive flux?

3) Can predictive expressions for the macrodispersivity values be developed as in the case of steady flow?

CONCEPTUAL FRAMEWORK AND APPROACH

For flow in a heterogeneous aquifer where the hydraulic gradient varies in space, unsteadiness will produce hydraulic gradient variation in time also. Gelhar and Axness (1983) have shown that it is the variation in the specific discharge vector that leads to the field-scale dispersive flux that is characterized by the macrodispersivity. Through Darcy's Law $\mathbf{q} = -K\mathbf{J}$ one can see that spatial variation of the hydraulic conductivity K will produce spatial variation in $\mathbf{q}$. To produce the additional temporal variation in $\mathbf{q}$, the hydraulic gradient is taken to be time-variable. To explore the effects of the gradient variation, the spectral approach of Lumley and Panofsky (1964) will be used. The spectral approach will build upon and provide a direct comparison to the previous steady-state results of Gelhar and Axness (1983). Although this work is considered a first cut at incorporating the effects of both spatial and temporal variability together, it does capture the main influences of unsteadiness and will show whether the additional dispersive flux due to unsteadiness warrants additional investigation.

GOVERNING EQUATIONS

Transport Equation

The equation describing the transport of an ideal conservative solute in saturated porous media is given by

$$n\frac{\partial c}{\partial t} = \frac{\partial}{\partial x_i}\left[E_{ij}\frac{\partial c}{\partial x_j} - cq_i \right] \tag{2-1}$$

where n = effective porosity
c = dimensionless solute concentration
E_{ij} = local bulk dispersion coefficient tensor
q_i = component of the specific discharge vector

and conservation of total mass requires

$$\frac{\partial q_i}{\partial x_i} = 0 \tag{2-2}$$

The local bulk dispersion coefficient tensor is assumed to be constant. The concentration and specific discharge are assumed random variables composed of the sum of a mean and a small perturbation.

$$\begin{aligned} c &= \bar{c}(x_i,t) + c'(x_i,t) \\ q_i &= \bar{q}_i(x_i,t) + q_i'(x_i,t) \end{aligned} \tag{2-3}$$

where the mean quantities are indicated with an overbar and the primed quantities are zero mean perturbations. Substituting Eq. 2-3 into 2-1 and rearranging produces

$$n\frac{\partial \bar{c}}{\partial t} + n\frac{\partial c'}{\partial t} + \frac{\partial}{\partial x_i}(\bar{q}_i\bar{c} + \bar{q}_ic' + q_i'\bar{c} + q_i'c') = \frac{\partial}{\partial x_i}\left[E_{ij}\frac{\partial}{\partial x_j}(\bar{c} + c') \right] \tag{2-4}$$

The expected value of Eq. 2-4 is the mean equation

$$n\frac{\partial \bar{c}}{\partial t} + \frac{\partial}{\partial x_i}(\bar{q}_i\bar{c} + \overline{q_i'c'}) = \frac{\partial}{\partial x_i}\left[E_{ij}\frac{\partial \bar{c}}{\partial x_j}\right] \tag{2-5}$$

The term $\overline{q_i'c'}$ is the macroscopic dispersive flux which, if it is Fickian in nature, can be represented by

$$\overline{q_i'c'} = -q A_{ij}\frac{\partial \bar{c}}{\partial x_j} \qquad i=1,2,3 \tag{2-6}$$

Subtracting Eq. 2-5 from 2-4 yields an equation describing the perturbations

$$n\frac{\partial c'}{\partial t} + \frac{\partial}{\partial x_i}(\bar{q}_i c' + q_i'\bar{c} + q_i'c' - \overline{q_i'c'}) = \frac{\partial}{\partial x_i}\left[E_{ij}\frac{\partial c'}{\partial x_j}\right] \tag{2-7}$$

The second order term $q_i'c' - \overline{q_i'c'}$ will be small where the individual perturbations are small and hence Eq. 2-7 can be reduced to

$$n\frac{\partial c'}{\partial t} + \frac{\partial}{\partial x_i}(\bar{q}_i c') + \frac{\partial}{\partial x_i}(q_i'\bar{c}) = \frac{\partial}{\partial x_i}\left[E_{ij}\frac{\partial c'}{\partial x_j}\right] \tag{2-8}$$

Aligning the coordinate axes along the direction of mean flow so that $\bar{q}_1 = q$ and $\bar{q}_2 = \bar{q}_3 = 0$, the local bulk dispersion tensor can be written in the form (Naff, 1978; Gelhar and Axness, 1983):

$$E_{ij} = \begin{bmatrix} \alpha_L q & 0 & 0 \\ 0 & \alpha_T q & 0 \\ 0 & 0 & \alpha_T q \end{bmatrix} \tag{2-9}$$

By invoking conservation of mass

$$\frac{\partial q_i}{\partial x_i} = 0 = \frac{\partial \bar{q}_i}{\partial x_i} + \frac{\partial q_i'}{\partial x_i} \tag{2-10}$$

and substituting Eq. 2-9 into 2-8, the equation governing the perturbations becomes

$$n\frac{\partial c'}{\partial t} + q_i'\frac{\partial \bar{c}}{\partial x_i} + q\frac{\partial c'}{\partial x_1} = q\left[\alpha_L\frac{\partial^2 c'}{\partial x_1^2} + \alpha_T\left(\frac{\partial^2 c'}{\partial x_2^2} + \frac{\partial^2 c'}{\partial x_3^2}\right)\right] \tag{2-11}$$

Spectral Solution

By assuming statistical homogeneity in space and time, the solution of Eq. 2-11 can be developed using Fourier-Stieltjes representations for the perturbed quantities (Lumley and Panofsky, 1964)

$$c' = \int_{-\infty}^{\infty} e^{ikx + i\omega t}\, dZ_c(\mathbf{k}, \omega)$$

$$q_i' = \int_{-\infty}^{\infty} e^{ikx + i\omega t}\, dZ_{q_i}(\mathbf{k}, \omega) \tag{2-12}$$

Substituting Eq. 2-12 into 2-11 and recalling the uniqueness of the spectral representation

$$\{ni\omega + [ik_1 + \alpha_L k_1^2 + \alpha_T(k_2^2 + k_3^2)]\, q\}\, dZ_c = G_i\, dZ_{q_i} \tag{2-13}$$

where $G_i = -\partial\bar{c}/\partial x_i$ is assumed to be constant at the local scale over which Eq. 2-13 applies. Multiplying Eq. 2-13 by the complex conjugate $dZ_{q_j}^*$ and taking the expected value

$$\{ni\omega + [ik_1 + \alpha_L k_1^2 + \alpha_T(k_2^2 + k_3^2)]\, q\}\, S_{cq_i}(\mathbf{k}, \omega) = G_j\, S_{q_i q_j}(\mathbf{k}, \omega) \tag{2-14}$$

Using Eqs. 2-6 and 2-14, the mean macrodispersive flux can be evaluated; specifically the macrodispersivity is given by

$$A_{ij} = \int_{-\infty}^{\infty} \frac{S_{q_i q_j}(\mathbf{k}, \omega)\quad d\mathbf{k}\, d\omega}{ni\omega\, q + [ik_1 + \alpha_L k_1^2 + \alpha_T(k_2^2 + k_3^2)]\, q^2} \tag{2-15}$$

This result is similar to that derived by Gelhar and Axness (1983) for the steady-flow case but with additional terms for frequency dependence.

To evaluate Eq. 2-15, the spectrum of specific discharge must be determined. Following the work of Gelhar and Axness (1983), $S_{q_iq_j}$ is developed in terms of more fundamental quantities.

Development of the Specific Discharge Spectrum

The unsteady groundwater flow equation in three dimensions, written in terms of the natural logarithm of K, is

$$\frac{\partial^2\phi}{\partial x_i \partial x_j} + \frac{\partial \ln K}{\partial x_i}\frac{\partial \phi}{\partial x_i} = \frac{S_s}{K}\frac{\partial \phi}{\partial t} \qquad (2\text{-}16)$$

where ϕ = hydraulic head
S_s = specific storage coefficient.

Equation 2-16, which includes a change-in-storage term on the right-hand side, is inconsistent with Eq. 2-2, which implies no change in storage. The nonzero right-hand side is retained because it is a more complete treatment of the problem and because it will be shown later that the change-in-storage term does not contribute to the additional dispersive flux. The right-hand side can be expanded as follows. If we write

$$\ln K = F + f\,, \qquad E[f] = 0 \qquad (2\text{-}17)$$

then it follows that

$$K = e^F e^f = K_g e^f\,, \qquad \ln K_g = F = E[\ln K] \qquad (2\text{-}18)$$

Substituting K into Eq. 2-16 and approximating e^{-f} by a Taylor series expansion, Eq. 2-16 becomes

$$\frac{\partial^2\phi}{\partial x_i \partial x_j} + \frac{\partial \ln K}{\partial x_i}\frac{\partial \phi}{\partial x_i} = \frac{S_s}{K_g}(1-f)\frac{\partial \phi}{\partial t} \qquad (2\text{-}19)$$

where only first-order terms are retained.

Equation 2-19 applies to unsteady flow in three dimensions where the temporal forcing is supplied by the boundary conditions. The spectral method, as it will be applied here, does not allow boundary conditions to be modeled explicitly. To circumvent that limitation, the

unsteadiness will be brought into the equations through the mean hydraulic gradient, $J = -\partial H/\partial x_i$, and the mean hydraulic head. The variables in Eq. 2-19 are decomposed into the sum of a slowly varying mean in space and time and a perturbation about that mean

$$\phi(\mathbf{x},t) = \bar{H}(\mathbf{x},t) + H'(\mathbf{x},t) + h(\mathbf{x},t) \qquad (2-20)$$

The hydraulic head, ϕ, is decomposed into three terms: the slowly varying ensemble mean, $\bar{H}$; a temporally variable term, H'; and the local perturbations in space and time. The term H' serves as the temporal forcing to the flow system and is treated independently of the local perturbations, h, which one can view as the response of the flow system to the spatial variability in K and the temporal variability of the boundary conditions manifested in H'. The question one must ask is: What characteristics of the variability of H' are likely to influence dispersion?

In the most general case, the boundary-influenced term, H', will vary in time due to precipitation and in space due to nonuniform recharge caused by spatially variable soil properties. Trying to solve for the recharge through a spatially variable soil zone is beyond the scope of this work. However, some intuition can be gleaned from the work of previous investigators.

Yeh et al. (1985a,b,c) and Mantoglou and Gelhar (1987a,b,c) have shown that for vertical flow in the vadose zone, the effective hydraulic conductivity is anisotropic, with the lateral component larger than the vertical component. The anisotropy ratio is largest during the initial stages of wetting a dry soil and decreases as the moisture content increases. If we assume that a recharge event does not saturate the vadose zone, then we might expect the anisotropy of unsaturated hydraulic conductivity to yield recharge to the aquifer that is correlated over distances larger than the correlation scale of lnK. Therefore the perturbations will likely be slowly varying in space with respect to the scale of variation of lnK. One could choose to ignore the effect of the spatial variability of H' and simply assume that it applies uniformly in space. However, the simple rising and falling of the hydraulic head in time does not affect dispersion.

Recall that field-scale dispersion in the steady-flow case (Gelhar and Axness, 1983) results from the randomness in the specific discharge vector, **q**, induced by hydraulic conductivity variations. The specific discharge is defined by Darcy's Law

$$q_i = -K \frac{\partial \phi}{\partial x_i} \tag{2-21}$$

Changes in ϕ that are random in time but uniform in space do not change q_i. Therefore simple rising and falling of H' does not strongly influence dispersion at the field scale. For temporal variability of ϕ to have an influence on q_i, and hence dispersion, the spatial gradient of ϕ must be variable in time.

As a first step, assume that the hydraulic gradient can be decomposed into a slowly varying mean and a perturbation

$$-\frac{\partial \bar{H}}{\partial x_i} = \bar{J}_i \; ; \; -\frac{\partial H'}{\partial x_i} = J_i' \tag{2-22}$$

The perturbation, J'_i, is assumed to be random in time, but at the local scale, constant in space. This assumption is applicable whether one views the temporal forcing as the result of distant boundary influences (a river, for example) or as caused by recharge on site.

Changes in the stage of a river, or rivers, located some distance from the site could cause the potentiometric surface gradient to change magnitude and direction. One would expect such influences to be relatively uniform when viewed locally. The bulk anisotropy of the unsaturated zone should yield a recharge process that is correlated over distances larger than the correlation scale of lnK. The temporal variability of the hydraulic gradient is the direct result of a nonuniform recharge process. But at the local scale, the temporal variation of the hydraulic gradient will be uniform in space.

The arguments for treating temporal fluctuations as spatially uniform on the local scale are admittedly based on conjecture about the influence of the unsaturated zone. In any event, the purpose of this work is to develop a first estimate of the magnitude of the unsteady effect, and to that end it is felt that the assumption of a spatially uniform gradient will be adequate.

Substituting Eqns. 2-20 and 2-22 into 2-19 and expanding gives

$$\frac{\partial^2 \bar{H}}{\partial x_i \partial x_j} + \frac{\partial^2 H'}{\partial x_i \partial x_j} + \frac{\partial^2 h}{\partial x_i \partial x_j} + \left(\frac{\partial F}{\partial x_i} + \frac{\partial f}{\partial x_i}\right)\left(-\bar{J}_i - J_i' + \frac{\partial h}{\partial x_i}\right) =$$

$$\frac{S_s}{K_g}(1 - f)\left(\frac{\partial \bar{H}}{\partial t} + \frac{\partial H'}{\partial t} + \frac{\partial h}{\partial t}\right) \qquad (2\text{-}23)$$

The ensemble mean of Eq. 2-23 is

$$\frac{\partial^2 \bar{H}}{\partial x_i \partial x_j} - \frac{\partial F}{\partial x_i}\bar{J}_i - \overline{\frac{\partial f}{\partial x_i} J_i'} \; \overline{\frac{\partial f}{\partial x_i}\frac{\partial h}{\partial x_i}} = \frac{S_s}{K_g}\left(\frac{\partial \bar{H}}{\partial t} + \overline{f\frac{\partial H'}{\partial t}} + \overline{f'\frac{\partial h}{\partial t}}\right) \qquad (2\text{-}24)$$

Subtracting Eq. 2-24 from 2-23, and dropping terms of second order in the perturbations yields the perturbation equation

$$-\frac{\partial J_i'}{\partial x_i} + \frac{\partial^2 h}{\partial x_i \partial x_i} - \frac{\partial F}{\partial x_i} J_i' + \frac{\partial F}{\partial x_i}\frac{\partial h}{\partial x_i} - \bar{J}_i \frac{\partial f}{\partial x_i} = \frac{S_s}{K_g}\left(-f\frac{\partial \bar{H}}{\partial t} + \frac{\partial H'}{\partial t} + \frac{\partial h}{\partial t}\right) \qquad (2\text{-}25)$$

Recognizing that at the local scale F is constant, $\bar{H}$ is slowly varying, and J'_i is uniform in space, Eq. 2-25 can be simplified to

$$\frac{\partial^2 h}{\partial x_i \partial x_i} - \bar{J}_i \frac{\partial f}{\partial x_i} = \frac{S_s}{K_g}\left(\frac{\partial H'}{\partial t} + \frac{\partial h}{\partial t}\right) \qquad (2\text{-}26)$$

In a similar manner, the specific discharge perturbations are obtained from the Darcy equation with locally isotropic hydraulic conductivity (Gelhar and Axness, 1983)

$$q_i = -K_g e^f \frac{\partial \phi}{\partial x_i} \approx -K_g(1+f)\frac{\partial \phi}{\partial x_i} \qquad (2\text{-}27)$$

Substituting Eqs. 2-3, 2-20, and 2-22 into Eq. 2-27 and taking the expected value gives the equation for the ensemble mean

$$\bar{q}_i = -K_g\left[-\bar{J}_i - \overline{J_i' f} + \overline{f\frac{\partial h}{\partial x_i}}\right] \tag{2-28}$$

Subtracting Eq. 2-28 from 2-27 and dropping products of perturbed quantities, the mean-removed equation is

$$q_i' = -K_g\left[-J_i' + \frac{\partial h}{\partial x_i} - \bar{J}_i f\right] \tag{2-29}$$

The perturbed quantities in Eqs. 2-26 and 2-29 are represented by Fourier-Stieltjes integrals in wave number and frequency

$$\begin{aligned}
h &= \int_{-\infty}^{\infty} e^{i\mathbf{k}\cdot\mathbf{x}+i\omega t}\, dZ_h(\mathbf{k},\omega) \\
f &= \int_{-\infty}^{\infty} e^{i\mathbf{k}\cdot\mathbf{x}+i\omega t}\, dZ_f(\mathbf{k},\omega) \\
J_i' &= \int_{-\infty}^{\infty} e^{i\mathbf{k}\cdot\mathbf{x}+i\omega t}\, dZ_{J_i}(\mathbf{k},\omega) \\
q_i' &= \int_{-\infty}^{\infty} e^{i\mathbf{k}\cdot\mathbf{x}+i\omega t}\, dZ_{q_i}(\mathbf{k},\omega) \\
H' &= \int_{-\infty}^{\infty} e^{i\mathbf{k}\cdot\mathbf{x}+i\omega t}\, dZ_H(\mathbf{k},\omega)
\end{aligned} \tag{2-30}$$

Note that f, H', and J'_i have been represented as space-time random processes even though f is time invariant and J'_i and H' are spatially uniform. The space-time representation is necessary to produce a consistent form for the entire equation. There is no inconsistency in the above representation, because one can treat a constant as a random variable with a covariance of infinite correlation length and a spectrum with all the power concentrated at zero frequency or wave number. Substituting Eq. 2-30 into Eqs. 2-26 and 2-29 and recalling the uniqueness of the spectral representation gives

$$-k^2\, dZ_h - ik_i\bar{J}_i\, dZ_f = \frac{S_s}{K_g}(i\omega dZ_H + i\omega dZ_h) \tag{2-31}$$

for the flow equation, and

$$dZ_{q_i} = K_g[dZ_{J_i} - ik_i\, dZ_h + \bar{J}_i\, dZ_f] \tag{2-32}$$

for the Darcy equation.

Rearranging Eq. 2-31 to isolate dZ_h and substituting into Eq. 2-32 yields

$$dZ_{q_i} = K_g\left[dZ_{J_i} - \frac{\bar{J}_l k_i k_l dZ_f - \frac{S_s}{K_g} k_i \omega dZ_H}{k^2 + i\omega\frac{S_s}{K_g}} + \bar{J}_i\, dZ_f\right] \tag{2-33}$$

The specific discharge spectrum, $S_{q_iq_j}(\mathbf{k},w)$, is obtained by multiplying Eq. 2-33 by the complex conjugate $dZ_{q_j}{}^*$ and using properties of the spectral representation theorem

$$S_{q_iq_j} = K_g^2\left[S_{J_iJ_j} + \frac{\frac{S_s}{K_g}k_j\omega}{k^2 - \frac{S_s}{K_g}i\omega} S_{J_iH} + \frac{\frac{S_s}{K_g}k_i\omega}{k^2 + \frac{S_s}{K_g}i\omega} S_{J_jH} + \frac{\frac{S_s^2}{K_g^2}k_ik_j\omega^2}{k^4 + \left(\frac{S_s}{K_g}\omega\right)^2} S_{HH} + \left(\delta_{il} - \frac{k_ik_l}{k^2 + \frac{S_s}{K_g}i\omega}\right)\left(\delta_{jm} - \frac{k_jk_m}{k^2 - \frac{S_s}{K_g}i\omega}\right)\bar{J}_l\bar{J}_m\, S_{ff}\right] \tag{2-34}$$

The terms of the macrodispersivity tensor are obtained from Eq. 2-15 with the specific discharge spectrum given by Eq. 2-34. The expression for macrodispersivity can be greatly simplified by recognizing the form of the input spectra. The hydraulic conductivity is time invariant, hence, its spectrum is given by

$$S_{ff}(\mathbf{k},\omega) = S_{ff}(\mathbf{k})\,\delta(\omega) \tag{2-35}$$

where $\delta(\omega)$ is the Dirac delta function. Likewise, the variables J'_i and H' were assumed spatially uniform. Their spectra, and presumably the cross spectra, will be of a form

$$S_{J_iJ_j}(\mathbf{k},\omega) = S_{J_iJ_j}(\omega)\,\delta(\mathbf{k})$$

$$S_{HH}(\mathbf{k},\omega) = S_{HH}(\omega)\,\delta(\mathbf{k}) \qquad (2\text{-}36)$$

$$S_{J_iH}(\mathbf{k},\omega) = S_{J_iH}(\omega)\,\delta(\mathbf{k})$$

Macrodispersivity

The macrodispersivities can thus be written

$$A_{ij} = \int_{-\infty}^{\infty} \frac{K_g^2 S_{J_iJ_j}(\omega,\mathbf{k}) + K_g^2\left(\delta_{il} - \frac{k_ik_l}{k^2}\right)\left(\delta_{jm} - \frac{k_jk_m}{k^2}\right)\bar{J}_l\bar{J}_m\, S_{ff}(\omega,\mathbf{k})}{ni\omega q + [ik_1 + \alpha_L k_1^2 + \alpha_T(k_2^2+k_3^2)]q^2}\, dk d\omega \qquad (2\text{-}37)$$

Using the special forms of the spectra Eqs. 2-35 and 2-36, Eq. 2-37 decomposes into the sum of two components, one incorporating the effect of temporal variability and the other spatial variability. These components, designated by $A_{ij}^{(u)}$ and $A_{ij}^{(s)}$ for unsteady and steady, respectively, are

$$A_{ij}^{(u)} = \int_{-\infty}^{\infty} \frac{K_g^2 S_{J_iJ_j}(\omega)}{ni\omega q}\, d\omega \qquad (2\text{-}38)$$

$$A_{ij}^{(s)} = \int_{-\infty}^{\infty} \frac{K_g^2\left(\delta_{il} - \frac{k_ik_l}{k^2}\right)\left(\delta_{jm} - \frac{k_jk_m}{k^2}\right)\bar{J}_l\bar{J}_m\, S_{ff}}{[ik_1 + \alpha_L k_1^2 + \alpha_T(k_2^2+k_3^2)]q^2}\, d\mathbf{k} \qquad (2\text{-}39)$$

Equation 2-39 is the same equation derived by Gelhar and Axness (1983), hence their results can be used directly. The component from unsteady flow is evaluated as follows:

$$A_{ij}^{(u)} = \lim_{\varepsilon\to 0} K_g^2 \int_{-\infty}^{\infty} \frac{S_{J_iJ_j}(\omega)\; d\omega}{ni\omega q + \varepsilon} \qquad (2\text{-}40)$$

$$= \lim_{\varepsilon\to 0} K_g^2 \int_{-\infty}^{\infty} \frac{S_{J_iJ_j}(\omega)\; [-in\omega q + \varepsilon]\; d\omega}{n^2\omega^2 q^2 + \varepsilon^2}$$

If the spectrum, $S_{J_iJ_j}(\omega)$, is even in ω, the imaginary term in Eq. 2-40 will be zero upon integration. Upon rearrangement, Eq. 2-40 reduces to:

$$A_{ij}^{(u)} = \lim_{\varepsilon \to 0} \frac{K_g^2}{nq} \int_{-\infty}^{\infty} \frac{S_{J_iJ_j}(\omega) \frac{nq}{\varepsilon} \, d\omega}{\frac{n^2\omega^2q^2}{\varepsilon^2} + 1} \tag{2-41}$$

Making the substitution

$$v = \frac{nq}{\varepsilon} \omega$$

Equation 2-41 reduces to a simple result.

$$A_{ij}^{(u)} = \lim_{\varepsilon \to 0} \frac{K_g^2}{nq} \int_{-\infty}^{\infty} \frac{S_{J_iJ_j}\left(\frac{\varepsilon v}{nq}\right) \, dv}{v^2 + 1}$$

$$= \frac{K_g^2}{nq} S_{J_iJ_j}(0) \int_{-\infty}^{\infty} \frac{dv}{v^2 + 1}$$

$$= \frac{K_g^2 \pi}{nq} S_{J_iJ_j}(0) \tag{2-42}$$

To be consistent with the results of Gelhar and Axness (1983), Eq. 2-42 is written in the form

$$A_{ij}^{(u)} = \frac{1}{\gamma^2} \frac{q\pi}{n\bar{J}_1^2} S_{J_iJ_j}(0) \tag{2-43}$$

where γ = the flow factor defined by Gelhar and Axness as $\gamma = q/K_g\bar{J}_1$.

HYDRAULIC GRADIENT SPECTRUM

Each component of $A_{ij}^{(u)}$ requires a different gradient spectrum. The diagonal components, A_{11}, A_{22}, A_{33} require the autospectra of the three components of the gradient vector, J_1, J_2 and J_3. Cross spectra for the different components are used to calculate the off-diagonal terms of $A_{ij}^{(u)}$.

The spectra, evaluated at zero frequency, are obtained from the spectra-covariance transform (Jenkins and Watts, 1968)

$$S_{J_iJ_j}(0) = \frac{1}{2\pi}\int_{-\infty}^{\infty} R_{J_iJ_j}(\tau)\, d\tau \tag{2-44}$$

Assuming the cross- and auto-covariance functions to be exponential in form

$$R_{J_iJ_j}(\tau) = \sigma^2_{J_iJ_j} \exp\left(-\frac{\tau}{\lambda_{J_iJ_j}}\right) \tag{2-45}$$

Eq. (2-44) becomes

$$S_{J_iJ_j}(0) = \frac{1}{\pi}\,\sigma^2_{J_iJ_j}\,\lambda_{J_iJ_j} \tag{2-46}$$

where $\sigma_{J_iJ_j}{}^2$ = variance of the ith component of $\mathbf{J}$ when i=j
covariance of the i,jth components when $i \neq j$
$\lambda_{J_iJ_j}$ = correlation scale

Using the exponential spectrum for $S_{J_iJ_j}$, the components of $A_{ij}{}^{(u)}$ can be written

$$A^{(u)}_{ij} = \frac{1}{\gamma^2}\frac{q}{n}\frac{\sigma^2_{J_iJ_j}}{J_1^2}\lambda_{J_iJ_j} \tag{2-47}$$

It is instructive to examine two specific cases of hydraulic gradient variability. In the first case, only the magnitude of the gradient changes in time, and in the second case only the direction varies in time.

Hydraulic Gradient Magnitude Variation

For this special case, only the magnitude of the gradient varies in time. Assume that the hydraulic conductivity field is statistically anisotropic, then the directions of the mean hydraulic gradient, $\mathbf{J}$, and $\mathbf{q}$ may be different. Figure 2-1 illustrates the general configuration in three dimensions. For the purposes of illustration, assume that $J_2=0=J'_2$, which implies $\Gamma = 0$. This two-dimensional example is oriented

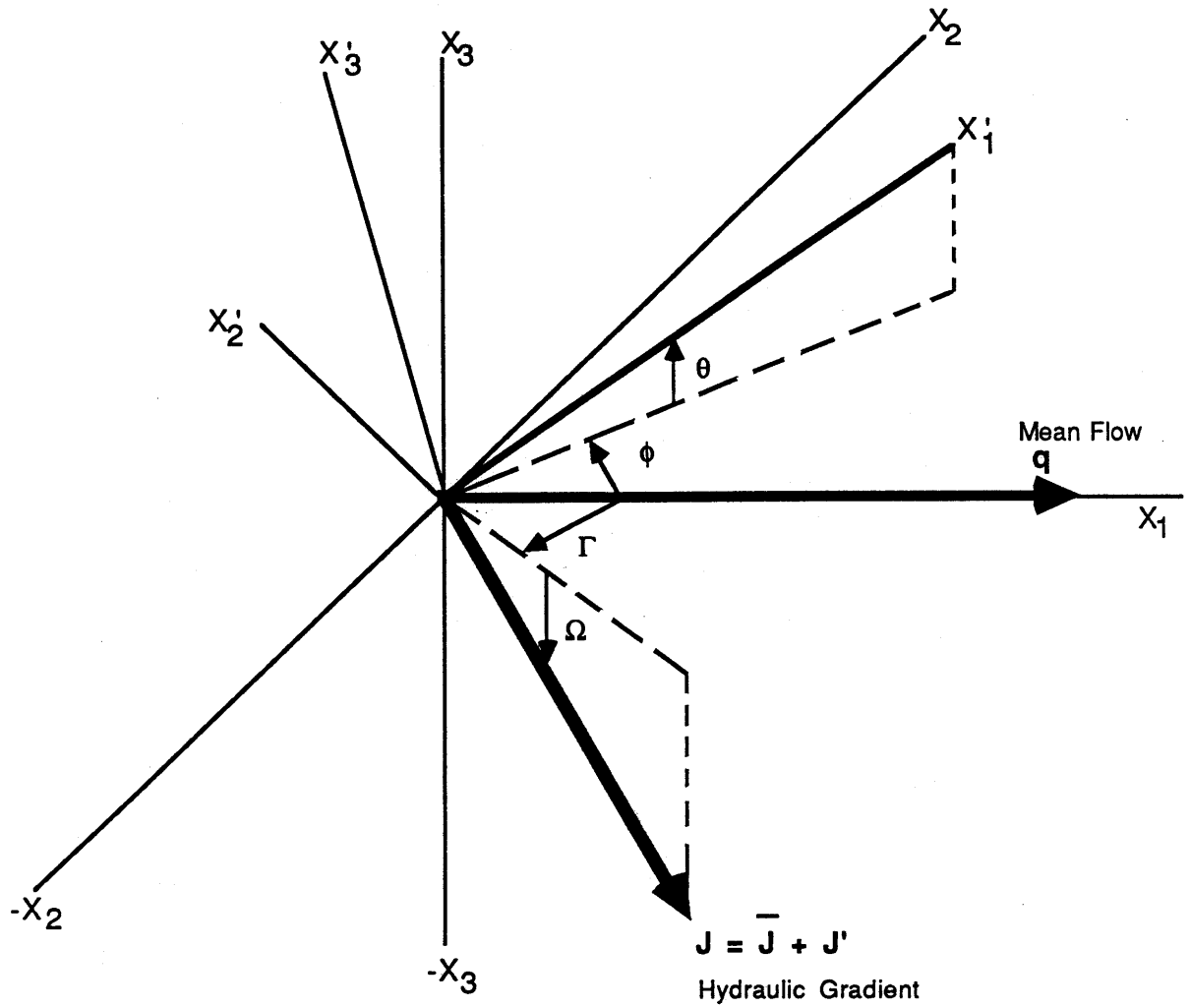

Figure 2-1. Coordinate System. The primed coordinates are the Principal Directions of the Effective Hydraulic Conductivity Tensor

in the vertical plane, and the x_1 and x_3 components of the hydraulic gradient vector are

$$J_1 = J\cos(\Omega)$$
$$J_3 = -J\sin(\Omega) \qquad (2\text{-}48)$$

where J = the magnitude of the hydraulic gradient
Ω = the angle between the mean flow direction and the hydraulic gradient.

The magnitude and the components of the gradient vector are decomposed into means and perturbations

$$\begin{aligned} J &= \bar{J} + J' \\ J_1 &= \bar{J}_1 + J_1' \\ J_3 &= \bar{J}_3 + J_3' \end{aligned} \qquad (2\text{-}49)$$

Substituting Eq. 2-49 into 2-48 and taking the expected value yields the mean and perturbation of the gradient components

$$\bar{J}_1 = \bar{J}\cos(\Omega) \qquad \bar{J}_3 = -\bar{J}\sin(\Omega)$$
$$J_1' = J'\cos(\Omega) \qquad J_3' = -J'\sin(\Omega) \qquad (2\text{-}50)$$

The perturbed quantities are described by Fourier-Stieltjes integrals

$$\begin{aligned} J_1' &= \int_{-\infty}^{\infty} e^{i\omega t}\, dZ_{J_1} \\ J_3' &= \int_{-\infty}^{\infty} e^{i\omega t}\, dZ_{J_3} \\ J' &= \int_{-\infty}^{\infty} e^{i\omega t}\, dZ_{J} \end{aligned} \qquad (2\text{-}51)$$

The auto- and cross-spectra for the components of J are obtained by substituting Eq. 2-51 into 2-50, multiplying by the complex conjugate, and taking the expected values:

$$S_{J_1J_1} = \cos^2(\Omega)\, S_{JJ}$$

$$S_{J_3J_3} = \sin^2(\Omega)\, S_{JJ} \qquad (2\text{-}52)$$

$$S_{J_1J_3} = -\sin(\Omega)\cos(\Omega)\, S_{JJ}$$

where S_{JJ} is the frequency spectrum of the gradient magnitude. For this case of temporal variation in only the magnitude of **J** the spectra ($S_{J_iJ_j}$) are functions of the angle, Ω, between the directions of **q** and **J**. Nonzero Ω is possible only in the case of bulk anisotropy of hydraulic conductivity. Gelhar and Axness (1983) have shown that statistical anisotropy of the local hydraulic conductivity field leads to anisotropy of bulk hydraulic conductivity in large scale. Therefore the spectra of the **J** components are influenced not only by the temporal characteristics of the magnitude but also by the spatial variability of hydraulic conductivity.

Taking the gradient magnitude spectrum, S_{JJ}, to be of the exponential type, the components of $A_{ij}^{(u)}$ can be found from Eqs. 2-47 and 2-52:

$$A_{11}^{(u)} = \frac{1}{\gamma^2}\frac{q}{n}\frac{\sigma_J^2}{\bar{J}^2}\lambda_J$$

$$A_{33}^{(u)} = \frac{1}{\gamma^2}\frac{q}{n}\frac{\sigma_J^2}{\bar{J}^2}\tan^2(\Omega)\,\lambda_J \qquad (2\text{-}53)$$

$$A_{13}^{(u)} = A_{31}^{(u)} = -\frac{1}{\gamma^2}\frac{q}{n}\frac{\sigma_J^2}{\bar{J}^2}\tan(\Omega)\,\lambda_J$$

Figure 2-2 presents the relationships between the components of $A_{ij}^{(u)}$ as a function of Ω. The longitudinal component, $A_{11}^{(u)}$, is larger than the other two components for Ω less than 45 degrees and smaller for Ω greater than 45 degrees. The dominant effect of the variation of the gradient magnitude is therefore in the direction of the gradient. For Ω less than 45 degrees the component of the gradient in the x_1 direction is larger than the component in the x_3 direction and it is the longitudinal component of A_{ij} that is the largest. For Ω larger than 45 degrees the component of the gradient in the x_3 direction is larger. Figure 2-2 is somewhat misleading in terms of the actual values of A_{ij} that result from Eq. 2-53 because the factor γ decreases as θ increases.

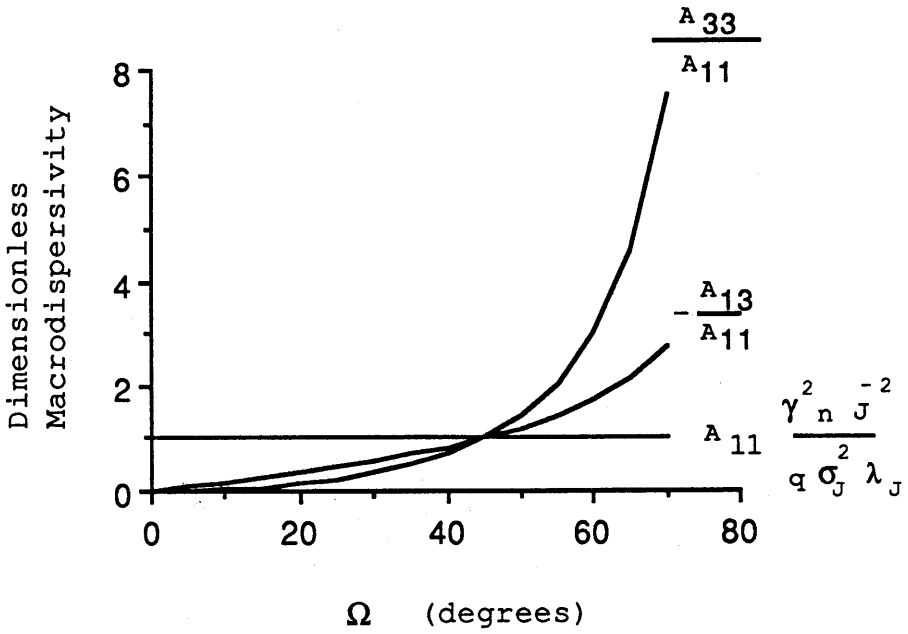

Figure 2-2. Relationship between the Macrodispersivity Tensor Components for the case of Hydraulic Gradient Magnitude Variation

The two angles θ and Ω can be related through Darcy's Law (See Eq. 2-55 below), but that relationship is nonlinear such that Ω increases with increasing θ until some critical value and then decreases for θ larger than the critical value. For θ less than the critical value, Ω increases as θ decreases, so A_{ij} increases as Ω increases. For θ larger than the critical value, it is not clear how A_{ij} changes with continued increase in θ. As Ω approaches 90 degrees the $\tan(\Omega)$ terms go to infinity, but there are physical reasons why Ω never reaches 90 degrees.

The maximum value of Ω possible in any situation is a function of the anisotropy of the bulk hydraulic conductivity and can be determined from Darcy's Law

$$\overline{q_i} = \overline{K_{ij}} J_j \tag{2-54}$$

where $\overline{K_{ij}}$ is the effective conductivity tensor. Defining the coordinate system by Figure 2-1 with $\Gamma = 0$, it is easy to derive the relation

$$\tan(\Omega + \theta) = \frac{\overline{K_{11}}}{\overline{K_{33}}} \tan(\theta) \tag{2-55}$$

Table 2-1 gives the maximum value for Ω and the critical θ values at which it occurs as a function of $\overline{K_{11}}/\overline{K_{33}}$. The maximum value for Ω is nearly 70° for $\overline{K_{11}}/\overline{K_{33}} = 30$, an anisotropy ratio that is possible in stratified aquifers. In the limit, Ω approaches 90 degrees only as $\overline{K_{11}}/\overline{K_{33}}$ approaches infinity.

Table 2-1

MAXIMUM VALUE OF Ω AS A FUNCTION OF ANISOTROPY RATIO

$\overline{K_{11}}/\overline{K_{33}}$	θ degrees	Ω_{max} to the nearest degree
1	0	0
3	30	30
10	18	55
30	10	69
100	6	78

When Ω is nonzero, the negative value for $A_{13}^{(u)}$ implies that principal axes of $A_{ij}^{(u)}$ are rotated with respect to the mean flow and away from the principal direction of the autocovariance function. For the steady-flow case, Gelhar and Axness (1983) also found that the principal axis of the macrodispersivity tensor was rotated away from the principal component direction of the autocovariance function. The rotation of the whole plume will be governed by the components of the sum of the steady and unsteady parts of the full dispersivity tensor $A_{ij} = A_{ij}^{(u)} + A_{ij}^{(s)}$. Therefore, the combined effect of gradient magnitude variation and spatial variability could produce enhanced rotation of the solute plume. Values for the specific terms in Eq. 2-53 will be presented later for the CAFB site. Recall that this special case is of variation in the vertical plane only. For magnitude variation in the horizontal plane, replace Ω by Γ, θ by ϕ and subscript 3 by 2 in the relationships above.

Hydraulic Gradient Direction Variation

For this example, the magnitude of the hydraulic gradient will remain constant, but the direction of the gradient will vary in time. The components of the hydraulic gradient are as in Eq. 2-48. Again, for illustration, only variation in the vertical plane will be examined. To investigate the temporal variation in the direction of J (Figure 2-1), characterized by fluctuations about the angle, $\overline{\Omega}$, the trigonometric terms are given by

$$
\begin{aligned}
J_1 &= J\cos(\Omega) \\
&= J\cos(\bar{\Omega}+\Omega') \\
&= J\{\cos(\bar{\Omega})\cos(\Omega') - \sin(\bar{\Omega})\sin(\Omega')\} \\
J_3 &= -J\sin(\Omega) \\
&= -J\sin(\bar{\Omega}+\Omega') \\
&= -J\{\sin(\bar{\Omega})\cos(\Omega') - \cos(\bar{\Omega})\sin(\Omega')\}
\end{aligned}
\tag{2-56}
$$

where $\bar{\Omega}$ defines the mean direction of the gradient, and Ω' is the variation about the mean. The trigonometric functions of primed quantities are approximated by the first term of a Taylor expansion such that

$$
\begin{aligned}
&\cos(\Omega') \approx 1 \\
&\sin(\Omega') \approx \Omega'
\end{aligned}
\tag{2-57}
$$

Substituting Eq. 2-57 into 2-56, evaluating the mean, and subtracting it from Eq. 2-56 produces the mean and perturbation equations

$$
\begin{aligned}
&\bar{J}_1 = J\cos(\bar{\Omega}) \\
&J_1' = J\{-\Omega'\sin(\bar{\Omega})\}
\end{aligned}
\tag{2-58}
$$

$$
\begin{aligned}
&\bar{J}_3 = -J\sin(\bar{\Omega}) \\
&J_3' = -J\{\Omega'\cos(\bar{\Omega})\}
\end{aligned}
\tag{2-59}
$$

The perturbed quantities are represented by Fourier-Stieltjes integrals

$$
\begin{aligned}
J_1' &= \int_{-\infty}^{\infty} e^{i\omega t}\, dZ_{J_1} \\
J_3' &= \int_{-\infty}^{\infty} e^{i\omega t}\, dZ_{J_3} \\
\Omega' &= \int_{-\infty}^{\infty} e^{i\omega t}\, dZ_{\Omega}
\end{aligned}
\tag{2-60}
$$

The auto- and cross-spectra are obtained by substituting Eq. 2-60 into 2-58 and 2-59 and evaluating the required expected values

$$S_{J_1J_1} = J \sin^2(\bar{\Omega})\, S_{\Omega\Omega}$$
$$S_{J_3J_3} = J \cos^2(\bar{\Omega})\, S_{\Omega\Omega} \qquad (2\text{-}61)$$
$$S_{J_1J_3} = J \sin(\bar{\Omega})\cos(\bar{\Omega})\, S_{\Omega\Omega}$$

As was observed for the case where J varied in time, the hydraulic gradient spectra are functions of the mean angle, $\overline{\Omega}$, between the mean flow and the mean hydraulic gradient. Again, properties of the spatial variability of K will influence the spectra in Eq. 2-61 through the γ term and Eq. 2-55.

Assuming that the spectrum, $S_{\Omega\Omega}$, is of exponential form, the components of $A_{ij}^{(u)}$ are given by

$$A_{11}^{(u)} = \frac{q}{n\gamma^2}\tan^2(\bar{\Omega})\, \sigma_\Omega^2 \lambda_\Omega$$
$$A_{33}^{(u)} = \frac{q}{n\gamma^2}\, \sigma_\Omega^2 \lambda_\Omega \qquad (2\text{-}62)$$
$$A_{13}^{(u)} = \frac{q}{n\gamma^2}\tan(\bar{\Omega})\, \sigma_\Omega^2 \lambda_\Omega$$

where $\overline{\Omega}$ = mean gradient direction
σ_Ω^2 = variance of the direction (radians)^2
λ_Ω = correlation scale (days)

Figure 2-3 shows the relationships between A_{11}, A_{33}, and A_{13} as a function of $\overline{\Omega}$. Much of the discussion regarding the previous case of gradient magnitude fluctuation applies to this case also. For Ω less than 45 degrees it is the A_{33} component that is largest. The temporal fluctuation of the gradient direction increases the macrodispersivity of the component perpendicular to the gradient more than the component parallel to the gradient. Another important difference between the influence of the gradient magnitude and direction on A_{ij} is that the sign of the off-diagonal term is different. For the case of Ω nonzero, gradient direction fluctuations yield a positive A_{13} term, which implies

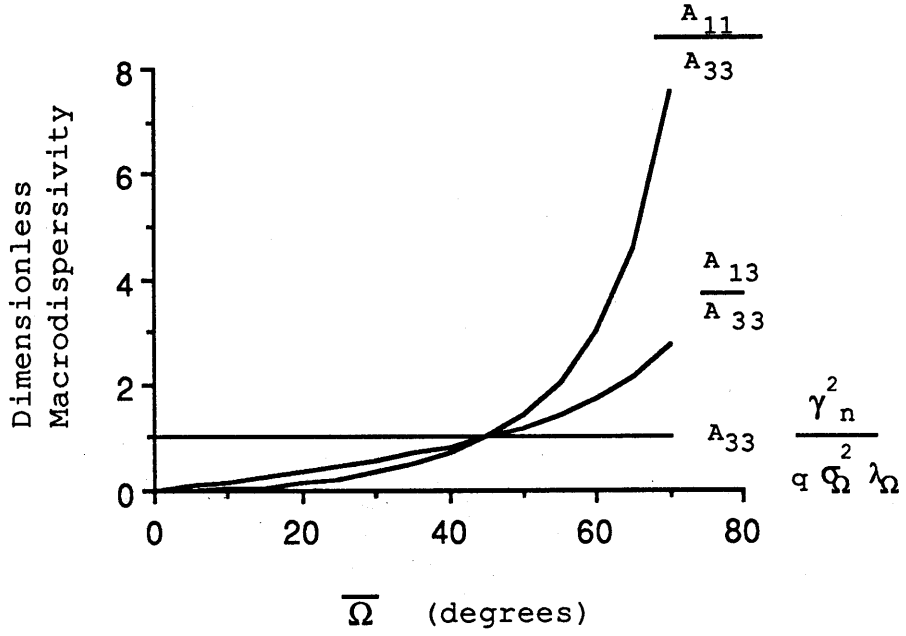

Figure 2-3. Relationship between the Macrodispersivity Tensor Components for the case of Hydraulic Gradient Direction Variation

that the plume will rotate toward the direction of the principal component of the autocovariance function. In the case of the gradient direction fluctuations, the rotation is in the direction opposite to that due to spatial variability and the combined effect of spatial and temporal variability, could produce zero rotation of the plume. Again, if variation in the horizontal plane is desired, replace Ω by Γ, θ by ϕ, 3 by 2 in the subscripts.

DISCUSSION OF THE EFFECT OF UNSTEADY FLOW ON MACRODISPERSION

The preceding analysis of the effect of unsteady flow on the predicted values of macrodispersivity resulted in a very simple relationship (see Eq. 2-47) involving the temporal variation of the hydraulic gradient. The temporal variability contribution and the spatial variability contribution to A_{ij} are additive. Therefore the dispersive flux due to unsteady flow will yield larger predicted macrodispersivities than have been obtained with the steady-state theory alone. The two special cases provide some insight into the influence of temporal variability of the hydraulic gradient on the macrodispersivities. The following points are of particular interest.

1) The relative magnitudes of the components of $A_{ij}^{(u)}$ are dependent on the angle between the mean flow and mean hydraulic gradient. That angle, Ω or Γ, can be nonzero only in the case of flow through an anisotropic aquifer. Gelhar and Axness (1983) have shown that bulk anisotropy is a consequence of aquifer heterogeneity. In addition, the macrodispersivity components are all divided by the flow factor term, γ^2. From Gelhar and Axness (1983) we know that, for any given direction of flow, γ^2 increases as the variance of lnK, σ_f^2, increases. There the effect of temporal variability of the hydraulic gradient on the macrodispersivities is a function of both the time variability and the spatial variability.

2) Variability in the magnitude of the hydraulic gradient increases the dispersive flux in the direction of the hydraulic gradient vector. Variability in the direction of the hydraulic gradient vector produces an increased dispersive flux in the direction perpendicular to the gradient vector. If the porous medium is anisotropic and the directions of **q** and **J** differ by more than 45 degrees, then variation in the magnitude of the gradient will enhance the transverse macrodispersivities. If the flow is in the direction of the mean gradient, or the medium is isotropic, the variation in the direction of the gradient will produce enhanced transverse dispersion.

3) The sign of the off-diagonal component, $A_{31}^{(u)}=A_{13}^{(u)}$ is opposite for the two cases. The direction of the principal components of the macrodispersivity will be rotated away from the direction of the principal axes of the effective hydraulic conductivity tensor when only the magnitude of the gradient fluctuates. When the direction of **J** fluctuates, the directions of the principal components are rotated toward the principal axes of the effective hydraulic conductivity tensor.

At the beginning of this section, three questions were posed regarding unsteady flow and dispersion. Two of those questions have been answered. Random unsteady fluctuations do lead to an enhanced dispersive flux, and therefore temporal variability does lead to an increase in dispersion. Secondly, simple predictive expressions for the macrodispersivities were developed based on the variance and correlation scales of the covariance and cross-covariance of the cartesian components of the hydraulic gradient. One question that was not answered is: How can one separate the deterministic components from the stochastic or random components? That question will be addressed in Section 4, where the covariance parameters of the time series are estimated.

Recall that the unsteady analysis produced a predictive expression for A_{ij} (Eq. 2-37) that was the sum of the spatial and temporal contributions. To make predictions of the macrodispersivities for a solute in a hetergeneous aquifer under unsteady flow conditions, both the spatial autocovariance function of log conductivity and the temporal covariance function of the hydraulic gradient are needed. The next section describes the measurements and analyses of the spatial variability at the CAFB site.

Section 3

MEASURES OF SPATIAL VARIABILITY AND PRELIMINARY COVARIANCE PARAMETER ESTIMATES

In this section various methods of measuring spatial variability are explored. Some of the methods measure hydraulic conductivity, others measure some other aquifer property such as electrical resistivity or the grain-size distribution of the material. Detailed measurements of the three-dimensional hydraulic conductivity are expensive and time-consuming. The goal of this phase of the research was to identify methods that could be used to characterize the aquifer heterogeneity with particular emphasis on methods that yield accurate estimates of the autocovariance parameter values and are simple enough to be used routinely. Clearly, if a method is very accurate but very tedious and expensive to use, it will not find its way into routine application. Simple, inexpensive measurements that do not produce suitably accurate estimates of the autocovariance parameters are equally unacceptable for routine application. The following eight methods were used to measure the spatial variability of hydraulic conductivity at the CAFB site:

1) Slug tests in piezometers
2) Hydraulic conductivity based on grain size
3) Surface geophysics
4) Borehole geophysics
5) Conventional large-scale aquifer test
6) Mapping of sedimentological facies
7) Laboratory permeability of minimally disturbed cores
8) Borehole flowmeter

Each method will be discussed in turn with respect to: (1) the physical parameter that is actually measured, (2) the advantages and disadvantages of each method, and (3) the prospect of using the method to characterize variability on a routine basis. The data and resulting variance and correlation scale estimates will then be presented and discussed.

DESCRIPTION OF METHODS TO MEASURE VARIABILITY

Piezometer Slug Tests

A slug of water is instantaneously added to or removed from a piezometer. The subsequent water-level response is governed by the shape of the screened section of the piezometer and by the hydraulic conductivity of the aquifer immediately outside the well screen. Hvorslev (1951) outlines measurement procedures and presents formulas for calculating the hydraulic conductivity for various well screen configurations.

In a short-screened piezometer, the slug-test method can be applied easily by raising or lowering a cylinder of known volume and measuring the water-table response with a recording transducer. The method can also be applied to sections of a long-screened well isolated by inflatable packers. In this case the method is more complicated because of the additional plumbing required. The time needed to complete a measurement is governed by the hydraulic conductivity and can range from a few seconds to a few hours or more. To be useful on a routine basis, the method is restricted to regions of moderate or large hydraulic conductivity.

The advantages of the slug-test method are that it is relatively simple, it is a direct measure of hydraulic conductivity, and measurements can be made in existing piezometers.

A disadvantage of the method is that it provides a very localized measurement, and hence is strongly influenced by the disturbed zone around the well. At the CAFB site, the piezometers were installed with augers and developed by air for about 2 hours. It is difficult to know if the material immediately surrounding the piezometer is representative of the undisturbed aquifer. A second disadvantage is that a single hydraulic conductivity value representing only a short vertical section of the aquifer is obtained from each piezometer. Measurements in intervals set off by packers along the length of a fully screened piezometer could take a prohibitively long time to complete if several layers of small hydraulic conductivity were present. The slug-test method appears to be useful for obtaining a few estimates of hydraulic conductivity but may not be practical for making many measurements on a routine basis.

Hydraulic Conductivity From Grain Size

Since Hazen (1892) a number of formulas have been proposed that relate some measure of grain size to hydraulic conductivity (for example, Krumbein and Monk, 1942; Masch and Denny, 1966; and Seiler, 1973). These formulas are empirical, with hydraulic conductivity being proportional to some function of representative grain diameters. The formulas are all of the form

$$K = \chi d^2 \tag{3-1}$$

where K = hydraulic conductivity (cm/sec)
d = representative grain diameter (cm or mm)
χ = proportionality factor

The factor χ is a function of not only the units but also of the degree of sorting. The uniformity coefficient is one measure of the sorting and is given by

$$U = d_{60}/d_{10} \tag{3-2}$$

where d_{60} = diameter such that 60% of the sample (by weight) is of diameter less than d_{60}.
d_{10} = diameter such that 10% of the sample (by weight) is of diameter less than d_{10}.

We will use the formulas presented by Seiler (1973) to convert the grain-size distributions into hydraulic conductivity. Seiler (1973) presents the relations

$$K = \chi(U)\, d_{10}^2 \qquad 5 \leq U \leq 17$$

$$K = \chi(U)\, d_{25}^2 \qquad U \geq 17 \tag{3-3}$$

where K(cm/sec), d_{10}(cm), and d_{25}(cm). Values of $\chi(U)$ for both d_{10} and d_{25} are given in Table 3-1. Seiler (1973) does not present values of $\chi(U)$ for $U < 5$, so in those cases we will use the Hazen (1892) formula

$$K = d_{10}^2 \tag{3-4}$$

where K(cm/sec) and d_{10}(mm).

Table 3-1

PROPORTIONALITY FACTOR $\chi(U)$

d_{25}

U tens \ ones	0	1	2	3	4	5	6	7	8	9
0						50.0	32.0	23.5	17.5	15.0
1	13.0	12.0	11.0	10.0	9.5	9.0	8.9	8.8	8.8	8.9
2	9.0	9.2	9.4	9.6	9.8	10.0	10.2	10.4	10.6	10.8
3	11.0	11.3	11.6	11.9	12.2	12.5	12.8	13.1	13.4	13.7
4	14.0	14.4	14.8	15.2	15.6	16.0	16.5	17.0	17.5	18.0
5	18.5	19.0	19.5	20.0	20.5	21.0	21.8	22.6	23.4	24.2
6	25.0	25.8	26.6	27.4	28.2	29.0	29.8	30.6	31.4	32.2
7	33.0	34.0	35.0	36.0	37.0	38.0	39.2	40.4	41.6	42.8
8	44.0	45.4	46.8	48.2	49.6	51.0	52.6	54.2	55.8	57.4
9	59.0	60.8	62.6	64.4	66.2	68.0	70.2	72.4	74.6	76.8
10	79.0									

d_{10}

U tens \ ones	0	1	2	3	4	5	6	7	8	9
0						215	190	170	150	135
1	120	105	94	84	75	67	61	57	57	58
2	62	66	70	74	78	82	86	90	94	98
3	102	110	118	126	134	142	150	158	166	174
4	182	192	202	212	222	232	246	260	274	288
5	302	318	334	350	366	382	402	422	442	462
6	482	502	522	542	562	582	612	642	672	702
7	732	772	812	852	892	932	986	1040	1094	1148
8	1202	1268	1334	1400	1466	1532	1606	1680	1754	1828
9	1902	1994	2086	2178	2270	2362	2402	2542	2682	2822
10	2962	3130	3298	3466	3634	3802	4002	4202	4402	4602
11	4802									

Source: Seiler, 1973, p. 356

The grain-size method has the advantage that samples of aquifer material for grain-size analyses can be taken continuously, or at specified depth intervals in almost any location. The sampling process increases the time necessary to auger into the aquifer, but the additional time is governed more by the number of samples taken rather than by the hydraulic conductivity, as is the case with slug tests.

There are several disadvantages of using grain size to measure K. First, the formulas are empirical and the accuracy of the resulting K value is uncertain. Second, the formulas are not appropriate for samples that are predominantly silt and clay. Hence no hydraulic conductivity values are estimated for the least conductive portions of the aquifer, and the resulting data set is biased toward the higher conductivity values. The biased sampling is expected to produce an overestimate of the mean and an underestimate of the variance of lnK. A third disadvantage is that samples must be taken to the laboratory for grain-size analyses and the results are not available until some time later.

Surface Geophysics

Surface geophysical methods remotely sense some property of the subsurface. Descriptions of surface geophysical techniques as applied to groundwater investigations can be found in Zohdy et al. (1974), Sendlein and Yazicigal (1981), and Yazicigal and Sendlein (1982).

Three electrical methods were utilized at the CAFB site: (1) direct current resistivity, (2) electromagnetic induction, and (3) streaming potential. The measurements were performed by the Tennessee Valley Authority's Geology and Geotechnical Engineering Group and are described in a forthcoming report (Boggs et al., 1988).

Direct-current resistivity, in a horizontal profile mode, gives the variation of the apparent resistivity of the subsurface material along a transect or a series of transects. The depth of investigation increases as the spacing between electrodes increases; an often-applied rule of thumb is that the depth of investigation is about equal to the distance between electrodes, or the "a-spacing", of the Wenner array. The depth of investigation is actually a complex function of the aquifer material

electrical properties, and Zohdy et al. (1974) state that "This rule of thumb is wrong and leads to erroneous interpretations."

The apparent resistivity is a function of the resistivity of the aquifer material and the pore fluid. If there is fresh water in the pores, the apparent resistivity decreases as the clay content increases. Thus, under ideal conditions, variations in apparent resistivity may be indicative of changes in hydraulic conductivity, because as the clay content increases the hydraulic conductivity decreases. For clay-free fluvial sands, Huntley and Mishler (1984) indicated that the matrix resistivity also increased with increasing hydraulic conductivity. They caution, however, that other researchers have found an inverse relationship for clay-free sediments and suggest that any relationship be used with caution.

Electromagnetic (EM) induction methods measure the electrical conductivity of the subsurface. A magnetic field produced at the surface induces an electric field below the surface (Zohdy et al., 1974). The current flow in the ground produces a second magnetic field which produces a current, out of phase with the induced current, that is measured in a receiver coil at the surface. Electrical conductivity is the inverse of resistivity, hence variations in resistivity are also reflected in conductivity.

Electrical currents occur naturally within the earth. Local variations in the electric potential or streaming potential (SP) develop due to electrochemical activity, electrofiltration activity, and man-made influences. In an aquifer, SP responds to the motion of fluids, and in laboratory sand columns it has been shown to be proportional to the pressure head driving the fluid (Ogilvy et al., 1969; Albireo, 1983). Anomalies in SP surveys have been useful for detecting leakage from dams and reservoirs (Bogoslovsky and Ogilvy, 1970; Ogilvy et al., 1969). Regions of increased leakage are often more permeable than the surrounding material, hence there is some hope that variations in a map of SP could be indicative of variations in hydraulic conductivity.

The three surface geophysical methods yield a remotely sensed description of the subsurface conditions and can yield a large amount of data in the horizontal plane in a relatively short time. A disadvantage of these methods is that the hydraulic conductivity is not measured

directly and the measurements can be influenced by factors other than the hydraulic conductivity such as the concentration of solutes in the groundwater and human influences such as buried pipes and cables. Hence one cannot be sure that variability in the geophysical measurement represents the variability of K. A second disadvantage is that the measurements generally do not yield much information on the variation in the vertical direction. This may not be a serious drawback, because detailed information about vertical variation can be obtained from borehole measurements.

Borehole Geophysics

As with surface geophysics, borehole geophysical instruments measure some physical property of the aquifer matrix-fluid system. The borehole measurements are not remotely sensed, rather they give a physical parameter at a specific depth.

The borehole geophysical logs of most interest are: (1) the natural gamma, (2) the gamma-gamma density, (3) single-point resistance and (4) neutron. The physics of each log is presented in a clear and concise manner in Serra (1984). Wheatcraft et al. (1986) discuss the application of borehole sensing methods for groundwater applications.

The natural gamma log measures the ambient flux of gamma particles produced by the decay of radioactive elements, particularly potassium 40, in the aquifer. Generally, the radioactive elements are concentrated in the clay fraction, hence the natural gamma log can differentiate between clean sands, clayey sands, and clay. The higher the clay content, the less permeable an interval will be. The production of gamma particles is a random process in time and Wyllie (1963) and Patten and Bennett (1963) state that it is difficult to interpret natural gamma logs quantitatively and that they are generally used for correlation between boreholes. Nonetheless, it is worthwhile to obtain some logs of natural gamma radiation for examination.

The gamma-gamma density log is a measure of the bulk density. Clays are less dense than sands or sands and gravels. Within sandier layers, the bulk density decreases as the porosity increases. If a uniform grain density is assumed, then variation in the gamma-gamma log response can be viewed as variation in porosity. Within a sandy unit, the hydraulic conductivity is expected to increase as the porosity increases, but if a

clay unit is encountered the hydraulic conductivity will decrease with increasing porosity. To use the gamma-gamma log as an indicator of hydraulic conductivity one would need another log such as the electrical resistance log or the natural gamma log to first distinguish between clay and sand and then try to define hydraulic conductivity variation within the sandier units.

The single point resistance measurements are sensitive to lithologic variations. As with the other logs, the change in log response can be used as an indicator of clay content. The neutron log measures the amount of hydrogen present. In saturated groundwater systems it is also an indicator of porosity.

An advantage of borehole geophysical logs is the speed with which the measurements can be made. The nuclear logs can be obtained in all the cased holes whether they are screened or not.

There are two disadvantages to using borehole geophysics. First, hydraulic conductivity is not measured directly. Often hydraulic conductivity must be inferred from porosity, which in turn has been inferred from the log measurements. The second disadvantage is that the tool response is often strongly influenced by the disturbed zone around the well. The gamma-gamma and neutron logs are especially sensitive to borehole influences. In sections of wells that are screened, well development will help repair the damage caused by drilling, or augering. In blank sections, no such repair can be made.

Large-Scale Aquifer Test

A conventional aquifer test, with a large capacity pumping well and numerous observation wells, influences an area of the aquifer much larger than the local scale of hydraulic conductivity variability. The hydraulic conductivity values obtained from a large-scale aquifer test are bulk values (or mean values) that apply over an area larger than the local scale of variability. Gelhar and Axness (1983) derive expressions that relate the anisotropy ratios from the aquifer test (K_{11}/K_{22}, K_{11}/K_{33}) to the lnK variance and to the ratios of the autocovariance correlation scales (λ_1/λ_2, λ_1/λ_3). In principle, then, anisotropy in bulk hydraulic conductivity can be used to obtain the relationships between the parameters of the autocovariance of the log hydraulic conductivity field.

The attractiveness of the large-scale aquifer test is the bulk parameters it can provide. If the variance and the vertical correlation scale λ_3 can be estimated by other means (for example, some borehole measurements in a few wells) then an exhaustive sampling program would not be necessary. The major disadvantage at this time is that the expressions in Gelhar and Axness (1983) have yet to be verified.

Geologic Mapping of Sedimentological Facies

When an aquifer exposure is viewed, for example along a gravel pit wall, a number of identifiable features such as gravel stringers and clay lenses stand out. Texturally distinct facies such as sand, sand and gravel, and clay can be identified and mapped along the exposed face. If the textural differences of each facies are distinct and the bulk hydraulic conductivity is relatively uniform within a single facies, but differs between facies, then the facies map becomes a surrogate map of hydraulic conductivity.

An advantage of mapping is that a continuous description of the heterogeneity can be obtained in both the horizontal and vertical direction. In addition, one can examine the fine-scale structure of the aquifer material in an undisturbed state.

One disadvantage is that one must work above the water table and extrapolate the results to deeper portions of the aquifer. Secondly, the map is only a two-dimensional view of the aquifer. If the moving face of an active gravel pit could be mapped successively, then information in the third dimension could be pieced together. To use the map to quantify the variability of hydraulic conductivity, a value of K for each facies must be assigned or measured in some way.

Continuous Core

A nearly continuous sample of the aquifer can be obtained by driving a lined split-spoon sampler into the aquifer ahead of a hollow-stem auger bit. Such cores that have been collected by TVA are 0.76 m long, 8.9 cm in diameter, and are considered slightly disturbed. In the laboratory the hydraulic conductivity is measured for each 0.076 m section along the length of the core with a permeameter.

The method yields a true physical sample to examine. In addition to hydraulic testing, the sample can be analyzed for grain size or chemical and mineralogical content.

Obtaining the cores from a single borehole can take a long time, several days in some cases. Although the samples are not undisturbed, they are not homogenized either, because layering is visible when the cores are split open. Nonetheless, one must establish precise procedures in order to obtain reproducible results (Wolf, 1988).

Borehole Flowmeter

The borehole flowmeter measures the amount of water entering a well from different levels in the aquifer. The analyses of the flowmeter logs collected during the pumping of a fully screened well (Hufschmied, 1983; Rehfeldt et al., 1988) yields the variation of hydraulic conductivity over the depth of the aquifer.

The flowmeter logs are as close to a direct measurement of hydraulic conductivity in the field as is possible at the present time. In the simplest terms, the borehole flowmeter method is analogous to a conventional aquifer test except that the discharge from each layer is measured directly with the flowmeter. The hydraulic conductivity of each layer is proportional to the measured layer discharge. The flowmeter measurements are easily performed on a routine basis and the analyses are based on the established principles of flow to a pumped well.

Of the eight methods, the borehole flowmeter was found to be the most promising for accurately measuring hydraulic conductivity variations on a routine basis. The flowmeter method is based on well established principles of well hydraulics and does not require dubious assumptions about the relationship between hydraulic conductivity and grain size, or geophysical properties. The method has been used successfully in Switzerland (Hufschmied, 1983) to measure the variability of hydraulic conductivity. The only other method of comparable accuracy and spatial resolution was the laboratory analyses of cores. Procuring and analyzing the cores is much more labor intensive, and hence more expensive, than the borehole flowmeter method. The borehole flowmeter method is a promising technique, but because it is a new method, it will take some time before the method finds its way into routine application.

As a consequence, the other measurements of variability are also important.

Extensive testing and experimentation with the borehole flowmeter method was performed at the CAFB site, and the hydraulic conductivity values are reported in Rehfeldt et al. (1988). The hydraulic conductivity data are the primary data which are analyzed in detail in Section 4 for the parameters of the autocovariance function. Preliminary spatial variability analyses of the data collected by the other seven methods, herein named secondary data, are described next.

PRELIMINARY SPATIAL COVARIANCE ANALYSES OF SECONDARY DATA

The locations of the various wells, piezometers, and sample holes that will be referred to in the following material are shown in Figure 3-1 and in Boggs et al. (1988). Only preliminary spatial analyses of secondary data were performed. I was interested in seeing if simple analyses could yield useful information on the parameters of the autocovariance, and I am fully aware that my often naive use of the geophysical measurements is far from a complete analysis of the data. Nonetheless, the preliminary analysis of the secondary measurements is a useful way to approach the question of spatial variability measurement because more detailed analyses can be performed at a later time if deemed appropriate. The preliminary analyses were used to guide the initial design of the flowmeter well network. The preliminary covariance parameter estimates are compared to the final covariance parameters from the flowmeter conductivities to test how useful the secondary data may be for estimating the parameters of the autocovariance. Based on the comparison, further analyses of some of the secondary data are suggested.

Definition of Preliminary Parameters

Three parameters describing the autocovariance, the variance, σ_f^2, the horizontal isotropic correlation scale, λ_h, and the vertical correlation scale, λ_v, will be determined from the preliminary analyses of the secondary data. In the case of the large-scale aquifer test horizontally anisotropic correlation scales also are considered.

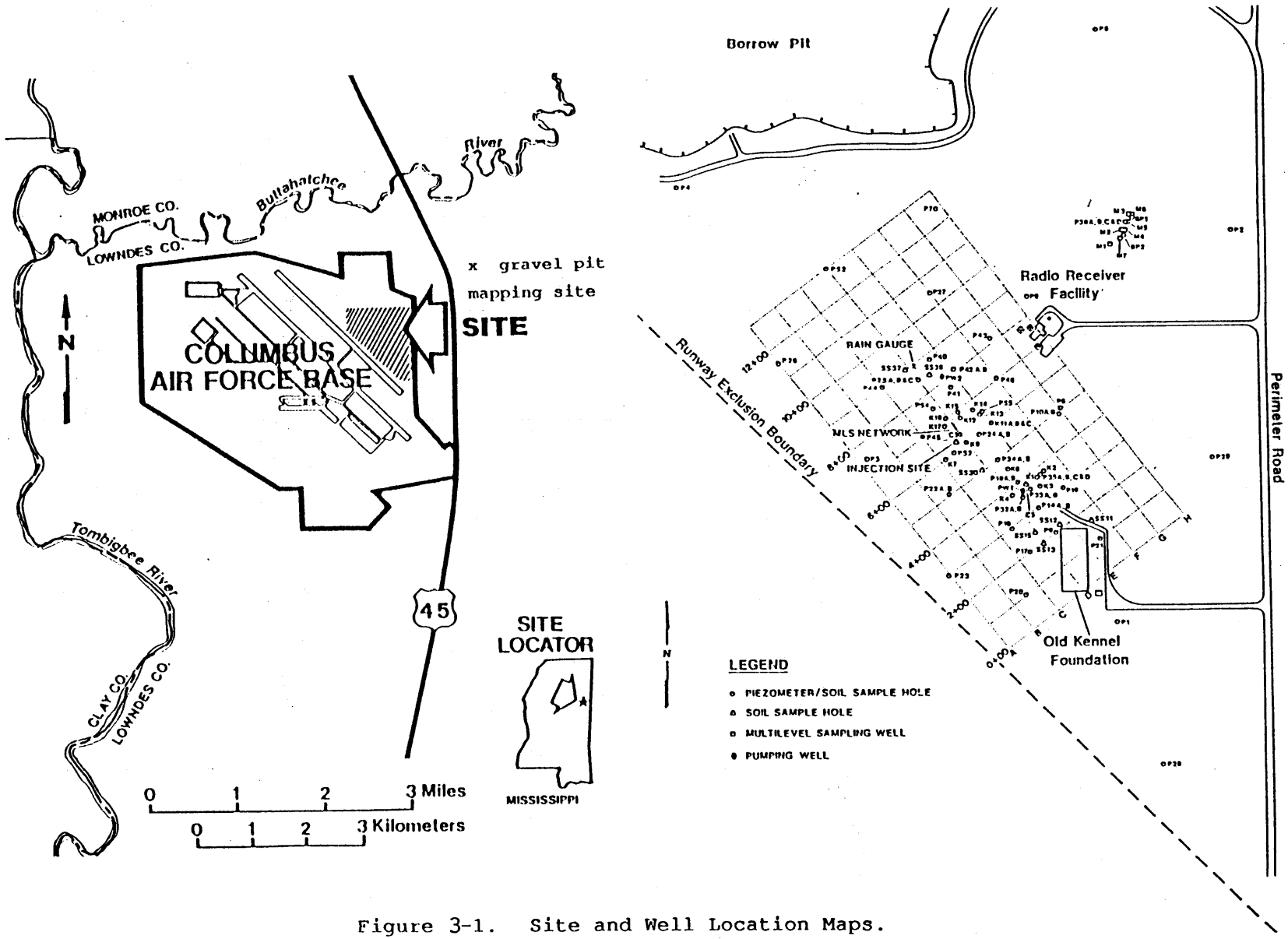

Figure 3-1. Site and Well Location Maps.

The sample variance of N data points T_i, i = 1 to N, is defined by

$$S^2 = \frac{1}{N-1}\sum_{i=1}^{N}(T_i - \bar{T}) \tag{3-5}$$

where the mean T is:

$$\bar{T} = \frac{1}{N}\sum_{i=1}^{N} T_i \tag{3-6}$$

The sample variogram (de Marsily, 1986) is defined as

$$G(r) = \frac{1}{2N_1}\sum_{i=1}^{N_1}[T_i - T_j]^2 \tag{3-7}$$

where r = average lag distance between pairs of measurements in an interval $r \pm \Delta r/2$

Δr = step size

G = average sample variogram value in the interval $r \pm \Delta r/2$

N_1 = number of pairs $(T_i - T_j)$ in the interval $r \pm \Delta r/2$

To calculate the variogram, the distribution of distances between measurements is divided into a finite number of equal length segments. The length of the segment is called the step size in this report. For a step size of Δr, the first segment is $0 < r \leq \Delta r$, the second $\Delta r < r \leq 2\Delta r$, and so on. The arthmetic average of the lag distance and the arithmetic average of the squared difference for pairs of points falling within a specific interval, or segment, yield a sample variogram value for that lag interval. Where data permitted, different sample variograms were calculated for data pairs oriented horizontally and vertically. The correlation scales in the vertical and horizontal were obtained from fitting a stationary exponential variogram of the form

$$\gamma(r) = \sigma_z^2(1 - e^{-r/\lambda}) \tag{3-8}$$

where σ_z^2 = sill value

λ = correlation scale

to the sample variogram. The sill value was assumed to be equal to the sample variance ($\sigma_z^2 = S^2$) and Eq. 3-8 was fitted by eye to the short-lag portion of the sample variogram to find λ. To use the spatial variability of the secondary measurements to infer properties of the variability of hydraulic conductivity it is assumed that K is proportional to the secondary measurement

$$K = AX^a \tag{3-9}$$

where K = hydraulic conductivity
A = proportionality constant that incorporates unit conversion
a = constant to account for higher order dependence
X = secondary measurement. This could be K from grain size or a geophysical measurement such as streaming potential.

The natural logarithm of Eq. 3-9 yields the data for spatial analysis:

$$\ln K = \ln A + a \ln X \tag{3-10}$$

Assume that A and a are constants and that lnK and lnX can be written in terms of a mean and a perturbation

$$\ln K = F + f \tag{3-11}$$

$$\ln X = W + w$$

Then the mean of Eq. 3-10 becomes

$$F = \ln A + aW \tag{3-12}$$

and the variance is

$$\sigma_f^2 = a^2 \sigma_w^2 \tag{3-13}$$

If a is known, then the secondary data will yield an estimate of σ_f^2 directly. Similarly, one can show that if Eq. 3-9 is valid then the variogram of lnK is related to the variogram of the secondary measurement by

$$\gamma_f = a^2 \gamma_w \qquad (3\text{-}14)$$

where γ_f = the variogram of the mean removed lnK process

γ_w = the variogram of the mean removed secondary measurement

If the spatial structure of the w process is assumed to be the same as the f process, then the correlation scale of f can be estimated from the variogram of w.

Piezometer Slug Tests

Betson et al. (1985) report hydraulic conductivity values from four short-screened piezometers. These were the first four piezometers installed at the site; the slug tests gave preliminary hydraulic conductivity values as part of an initial site evaluation. The slug tests were analyzed in two ways: (1) assuming local isotropy and (2) assuming a local 10:1 horizontal-to-vertical anisotropy. The measured K (cm/sec) and the mean and variance of lnK are given in Table 3-2. Because there are only four data points, the variance estimate is very uncertain and the correlation scales can not be estimated.

Table 3-2
SPATIAL ANALYSIS OF PIEZOMETER SLUG TEST

		K (cm/sec)	
Piezometer		Isotropic	Anisotropic
P1		3.6×10^{-3}	4.6×10^{-3}
P2		2.8×10^{-3}	3.6×10^{-3}
P3		4.6×10^{-3}	5.8×10^{-3}
P4		7.0×10^{-5}	1.0×10^{-4}
lnK mean	$E[\ln K] = \ln K_g$	-6.6	-6.3
Geometric mean	K_g (cm/sec)	1.4×10^{-3}	1.8×10^{-3}
lnK variance	σ_f^2	3.9	3.7

Hydraulic Conductivity from Grain Size

During the installation of the many piezometers at the CAFB site, the Tennessee Valley Authority obtained disturbed samples of the aquifer material at different depths with a split-spoon sampler. Mechanical sieve analyses of the samples are reported in Boggs et al. (1988). Table 3-3 summarizes the hydraulic conductivity values calculated from the grain-size distributions using Eqs. 3-3 and 3-4 for most of the wells installed through December 1984. Only the hydraulic conductivities from samples for which the d_{10} grain size was larger than about 0.07 mm are reported, because the smallest sieve size was 0.075 mm and no reliable estimates of d_{10} could be made if d_{10} was much smaller that 0.075 mm.

Variograms of lnK (Figure 3-2) were calculated in the horizontal and vertical directions. The resulting parameter estimates are given in Table 3-4.

Table 3-4

PRELIMINARY COVARIANCE PARAMETERS OF THE GRAIN SIZE lnK

Mean	Variance	Correlation Scales	
		λ_h (m)	λ_v (m)
-3.0	3.9	<24	1.1

The correlation scale estimates must be interpreted cautiously. The variogram was assumed to be exponential in form, yet one could easily interpret the horizontal variogram as indicating a nearly uncorrelated random set of data or as indicating a strong nugget effect implying large measurement errors (Journel and Huijbregts, 1978). A large nugget value (say 2.5) is probably not reasonable because the rising portion of the vertical variogram is defined by the value of 1.7 at a lag distance of 0.6 m. More likely, the distance between the wells is larger than the correlation scale. Hence, λ_h is interpreted to be an upper bound on the horizontal correlation scale. The vertical correlation scale appears to be more precisely defined; however, the number of couples for each lag distance is small (20 to 30) and the sample variogram values are widely scattered around the fitted exponential variogram.

Table 3-3

HYDRAULIC CONDUCTIVITY FROM GRAIN SIZE

Location	Depth Below Grade (m)	d_{10} (mm)	d_{25} (mm)	U	χ	K (cm/sec)
P-3	4.9	0.35	3.5	40	14.0	1.7
	6.4	0.32	1.4	20	9.0	1.8×10^{-1}
	7.9	0.23	0.7	43	15.2	7.4×10^{-2}
P-6	6.4	0.36	2.2	40	14.0	6.5×10^{-1}
	8.1	0.23	1.8	44	15.6	5.1×10^{-1}
	8.7	0.25	2.1	42	14.8	6.8×10^{-1}
SS-13	7.9	0.24	1.6	40	14.0	3.6×10^{-1}
	9.4	0.21	0.33	5	215.0	9.5×10^{-2}
	10.1	0.28	0.63	24	9.8	3.9×10^{-2}
	10.7	0.17	0.73	44	15.6	8.3×10^{-2}
P-14	6.4	0.34	1.3	30	11.0	1.9×10^{-1}
	7.9	0.085	0.17	14	75.0	5.4×10^{-3}
	8.5	0.08	0.15	3		6.4×10^{-3}
	9.1	0.07	0.18	3		4.9×10^{-3}
	9.8	1.3	6.8	12	94.0	1.6
P-15	6.4	2.04	4.6	6	190.0	7.9
	7.9	0.08	0.15	4		6.4×10^{-3}
	8.5	0.095	0.30	66	29.8	2.7×10^{-2}
	9.8	0.07	0.20	34	12.2	4.9×10^{-3}
P-17	6.4	0.10	0.22	50	18.5	8.6×10^{-3}
	7.9	0.12	0.16	2		1.4×10^{-2}
	9.4	0.27	1.6	27	10.4	2.7×10^{-1}
	10.1	0.17	0.31	3		2.9×10^{-2}
	10.7	0.18	0.56	39	13.7	4.3×10^{-2}
P-18	6.4	0.19	0.34	52	19.5	2.2×10^{-2}
	7.9	0.18	0.30	3		3.2×10^{-2}
	8.5	0.20	0.50	30	11.0	2.8×10^{-2}
	9.1	0.13	0.77	30	11.0	6.5×10^{-2}
	10.4	0.06	0.32	32	11.6	1.2×10^{-2}
	11.0	0.13	0.35	31	11.3	1.4×10^{-2}

Table 3-3 (con't)

Location	Depth Below Grade (m)	d_{10} (mm)	d_{25} (mm)	U	χ	K (cm/sec)
P-19	6.4	0.38	1.8	24	9.8	3.2×10^{-1}
	7.9	0.20	0.42	33	11.9	2.1×10^{-2}
	9.4	0.18	0.54	50	18.5	5.4×10^{-2}
	10.0	0.21	1.3	41	14.4	2.4×10^{-1}
	10.7	0.16	0.36	68	31.4	4.1×10^{-2}
P-20	6.4	0.25	2.9	61	25.8	2.2
	7.9	0.17	0.30	21	9.2	8.3×10^{-3}
	9.4	0.18	0.40	45	16.0	2.6×10^{-2}
	10.1	0.36	0.72	28	10.6	5.5×10^{-2}
P-22	6.4	0.18	0.33	57	22.6	2.5×10^{-2}
	7.9	0.32	2.0	35	12.5	5.0×10^{-1}
	9.4	0.21	0.90	39	13.7	1.1×10^{-1}
	10.1	0.26	3.8	74	37.0	5.3
	11.3	0.078	0.12	3		6.1×10^{-3}
P-23	6.4	1.86	4.6	7	170.0	5.9
	7.9	0.53	3.5	18	8.8	1.1
	8.5	0.073	0.11	3		5.3×10^{-3}
	9.1	0.070	0.12	3		4.9×10^{-3}
	10.2	0.086	0.13	2		7.4×10^{-3}
	11.0	0.13	0.25	75	38.0	2.4×10^{-2}
	12.8	0.077	0.11	2		5.9×10^{-3}
P-24	6.4	0.62	2.2	12	94.0	3.6×10^{-1}
	7.9	0.19	0.68	41	14.4	6.7×10^{-2}
	9.1	0.13	0.47	55	21.0	4.6×10^{-2}
	9.8	0.07	0.30	60	25.0	2.3×10^{-2}
	10.4	0.14	0.30	55	21.0	1.9×10^{-2}
	11.0	0.07	0.09	2		4.9×10^{-3}
P-25	6.4	0.085	0.15	4		7.2×10^{-3}
	7.9	0.16	0.33	33	11.9	1.3×10^{-2}
	8.5	0.16	0.23	13	84.0	2.2×10^{-2}
	9.1	0.21	0.53	56	21.8	1.2×10^{-2}
	9.8	0.15	0.18	2		2.3×10^{-2}
	10.4	0.073	0.085	2		5.3×10^{-3}
	11.6	0.077	0.12	3		5.9×10^{-3}
	12.8	0.075	0.10	2		5.6×10^{-3}
	13.4	0.09	0.14	2		8.1×10^{-3}

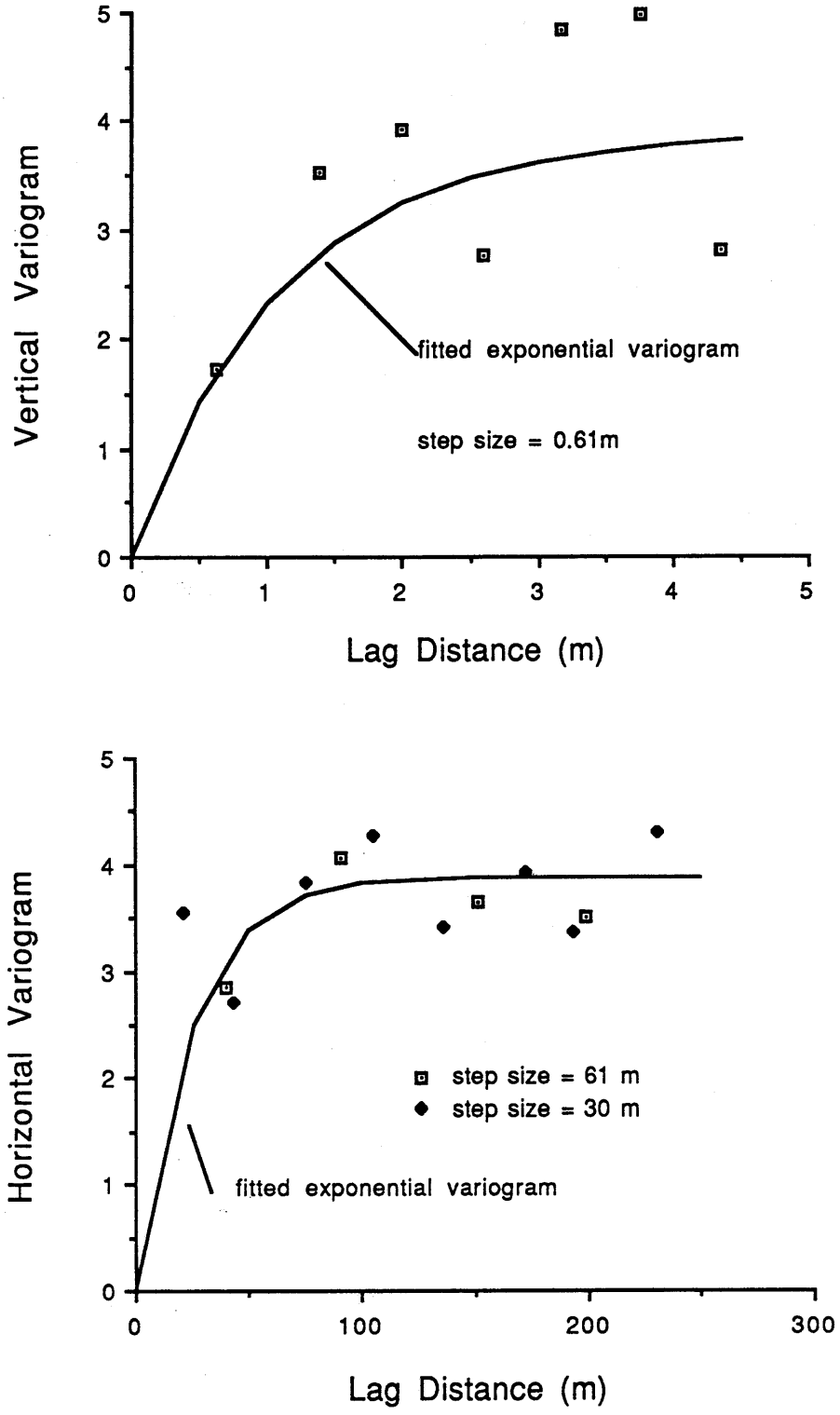

Figure 3-2. Variograms of Hydraulic Conductivity From Grain Size

The variance estimate may be quite good, assuming of course that the conductivity values in Table 3-3 are accurate. From the variograms it appears that the spacing between most of the samples is larger than the correlation scale. Therefore, the samples can be interpreted as independent observations of the random field, and by the central limit theorem we would expect the variance estimate to be a good approximation to the true value.

Surface Geophysics

Three of the surface geophysical techniques that were used at the CAFB site, direct current resistivity, electromagnetic induction, and streaming potential (SP), were examined in terms of spatial variability. Boggs et al. (1988) present the geophysical measurements made by the Tennessee Valley Authority's Geology and Geotechnical Engineering Group. Contour plots of some of the surface geophysical data that will be used for spatial analyses are given in Appendix A. Except for human influences like buried cables, the electromagnetic measurements showed very little variability over the site and were not considered for spatial analyses. The direct-current resistivity and the SP showed significant variability independent of human influences.

To use the surface geophysical data, assume that a relation between the geophysical measurement and the hydraulic conductivity can be described by Eq. 3-9. For direct resistivity, Heigold et al. (1979) and Kelly (1977) found relationships between hydraulic conductivity and the apparent formation factor of the form

$$K = A F_a^{\alpha} \tag{3-15}$$

where: A , α = constants
F_a = ρ_T/ρ_w = apparent formation factor
ρ_T = measured resistivity
ρ_w = resistivity of the pore water

If the resistivity of the water is assumed to be constant over the site, then the measured resistivity can be substituted for the apparent formation factor in Eq. 3-15. Huntley and Mishler (1984) warn that the parameters A and α in Eq. 3-15 are highly uncertain. In fact, α was found to be negative by Heigold et al. (1979), but positive by Kelly

(1977). Nonetheless, Eq. 3-15 is of the same form as 3-9, and for this preliminary analysis resistivity variability will be used as a surrogate for hydraulic conductivity variability. The variance, σ_f^2, cannot be estimated using Eq. 3-13 because of the large uncertainty in the parameter "a", but the correlation scale will be estimated from the resistivity variograms. Direct-current resistivity measurements were performed with three different electrode spacings: 1.52 m, 3.05 m, and 6.10 m. Qualitatively, the larger the electrode spacing, the greater the depth of investigation, but there is no simple way to determine the true depth of measurement (Zohdy et al., 1974).

It is also possible to hypothesize a relationship of the form in Eq. 3-9 for the SP data. Recall that SP anomalies are, in part, due to flowing groundwater and are proportional to the change in head. Although SP anomalies have been useful in detecting the movement of water and have been used to delineate zones of leakage from dams and reservoirs, it is not clear that a relationship between heterogeneity and SP exists. As a first approximation, the streaming potential will be assumed to be related to K through Eq. 3-9. As was the case with direct resistivity, the parameter "a" in Eq. 3-13 is unknown so the variance, σ_f^2, cannot be estimated. The correlation scale will be estimated from the lnSP variogram.

The variograms of ln(resistivity) and ln(SP) are given in Figure 3-3 and the correlation scale estimates are provided in Table 3-5. Note that the correlation scales are approximately equal to the sample spacing. As was true for the grain size data, the sample spacing was apparently too large to capture the rising portion of the variograms. If the correlation scales in Table 3-5 are indicative of the lnK correlation scales, then we must conclude that 16 to 30 m is an upper bound for λ_h.

Table 3-5

PRELIMINARY COVARIANCE PARAMETERS - SURFACE GEOPHYSICS

Method	a-spacing(m)	Sample Spacing (m)	λ_h-estimate (m)
Resistivity	(1.52)	30.48	< 31
Resistivity	(3.05)	30.48	< 24
Resistivity	(6.10)	30.48	< 27
Streaming Potential		15.24	< 16

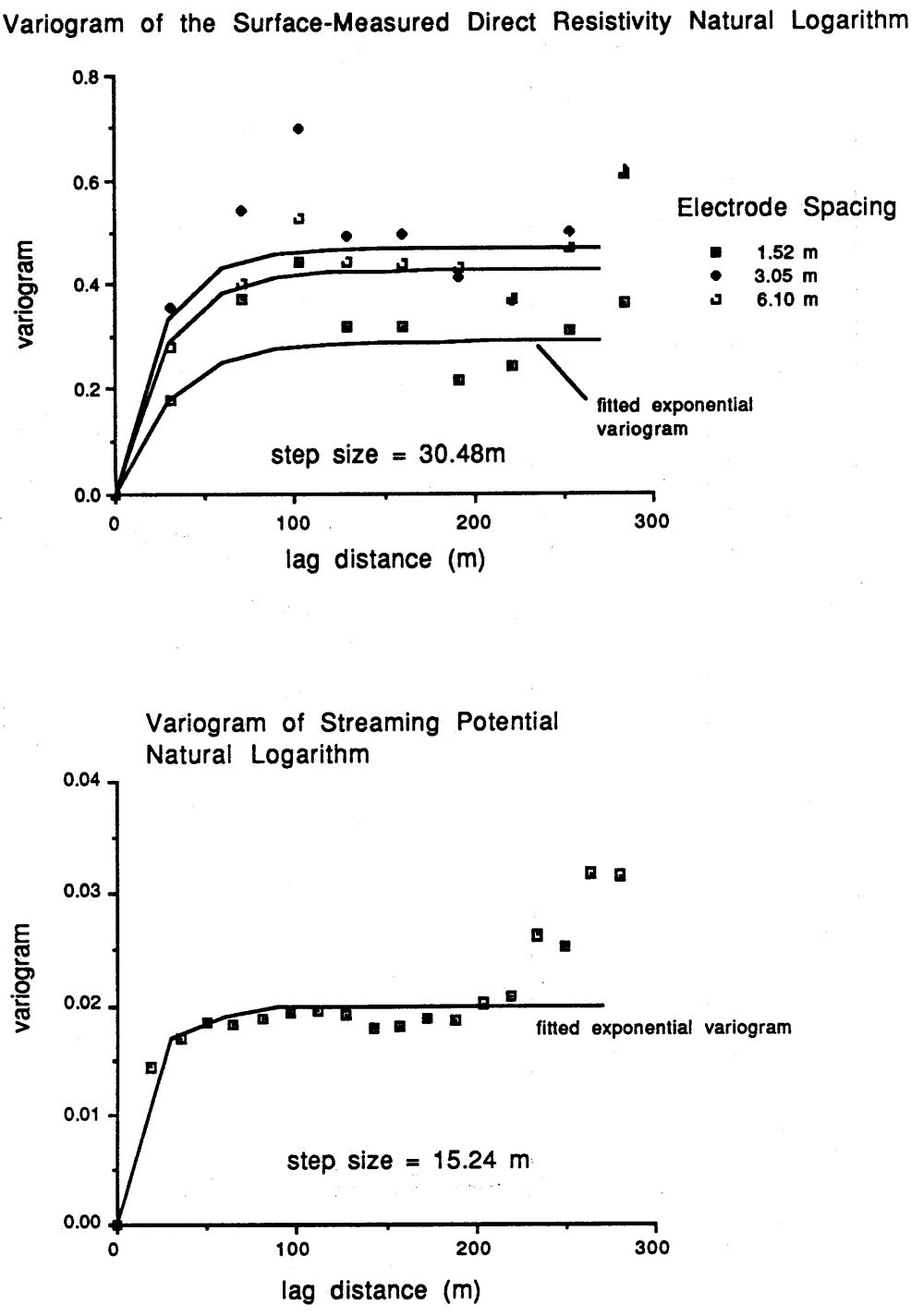

Figure 3-3. Variograms of the Direct Current Resistivity and Streaming Potential

Borehole Geophysics

Some selected borehole geophysics logs are presented and discussed in Appendix B. From a visual inspection of the logs it was concluded that the logs would not be adequate as an indicator of lnK variability and therefore no preliminary spatial analyses were performed.

Large-Scale Aquifer Test

The spatial analysis of the aquifer test data is approached from a conceptually different perspective than the other measurements. Variogram analyses of the other data are performed in order to infer some average properties of the variability from many small-scale measurements. The hydraulic conductivity obtained from the large-scale aquifer test is an average over a large volume of the aquifer. As such, it reflects the bulk character of the heterogeneity.

Gelhar and Axness (1983) derived expressions that relate the lnK variance and the statistical anisotropy (i.e., $\lambda_1 \neq \lambda_2 \neq \lambda_3$) to the anisotropy of hydraulic conductivity from large-scale aquifer tests ($K_{11} \neq K_{22} \neq K_{33}$). To estimate the correlation scale ratios (λ_1/λ_3) and (λ_1/λ_2) using Gelhar and Axness (1983), independent estimates of the variance, σ_f^2, and the hydraulic anisotropy ratios (K_{11}/K_{33}) and (K_{11}/K_{33}) are needed.

From the piezometer slug tests and the grain-size data an estimate of the variance is $\sigma_f^2=3.8$. Preliminary analyses of the aquifer test (Boggs et al., 1988) using the method of Neuman (1975), which assumes horizontal isotropy, gives a range for $\sqrt{(K_{11}K_{22})}/K_{33}$ of 3.5 to 33. The aquifer test results are preliminary because both specific yield and $\sqrt{(K_{11}K_{22})}/K_{33}$ were found to vary with radial distance from the well (Boggs et al., 1988) in contrast to the theory (Neuman, 1975), where S_y and $\sqrt{(K_{11}K_{22})}/K_{33}$ are assumed constant. For the purpose of the preliminary spatial analyses here, the preliminary aquifer test results are adequate. However, we recommend a more careful analysis of the aquifer test to obtain more accurate parameter estimates. The horizontal anisotropy ratio K_{11}/K_{22} was obtained from a map of drawdown (Figure 3-4) in deep piezometers (all at about the same elevation) near the end of pumping using the analysis in Hantush and Thomas (1966). We emphasize that this analysis is preliminary and that improved parameter estimates will be obtained after a careful reanalysis of the aquifer test data.

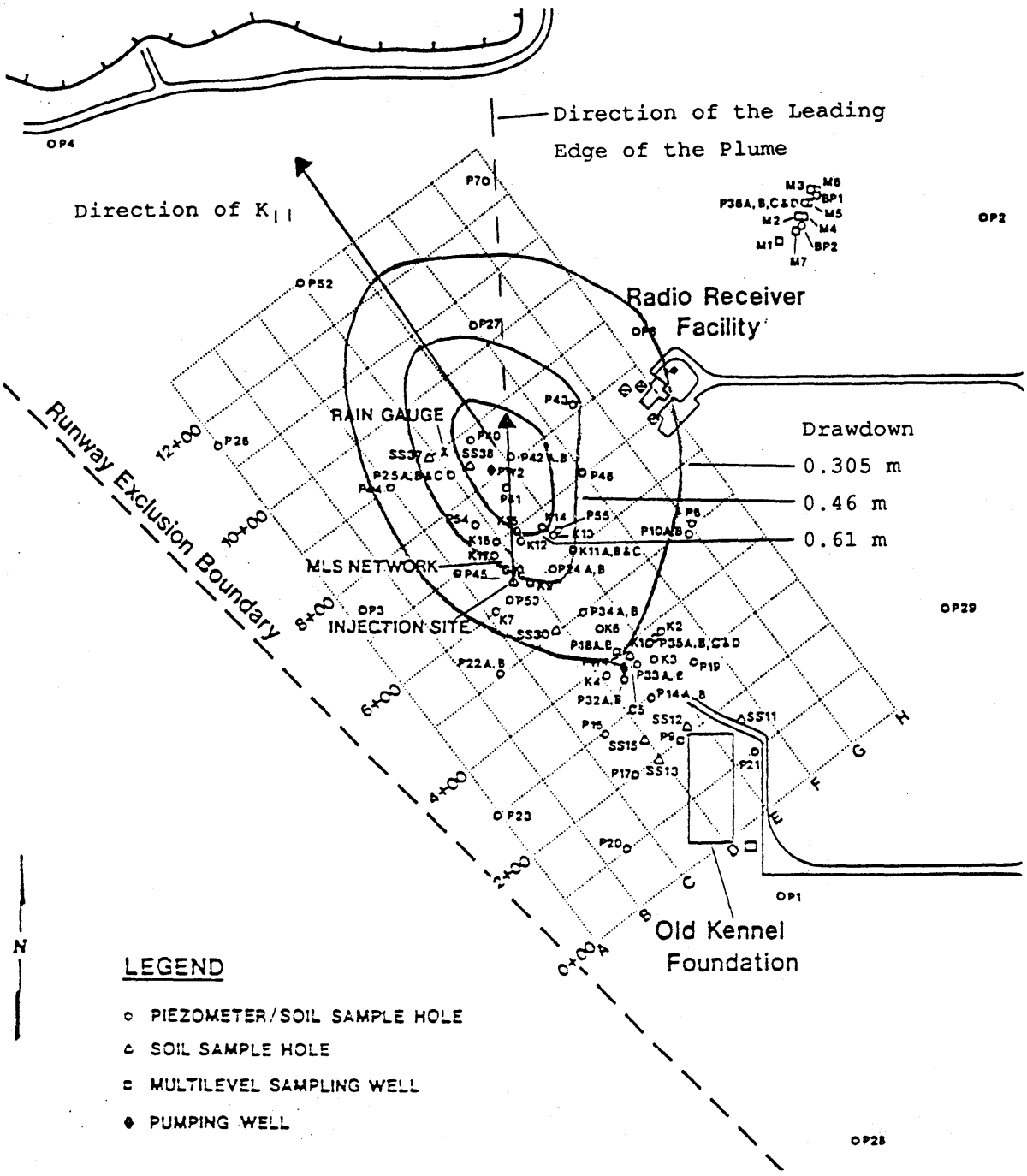

Figure 3 -4. Approximate Drawdown Contours at the Completion of the Pumping Phase of Aquifer Test Three. Direction of the Major Principal Component of the Hydraulic Conductivity Tensor and the Direction of Movement of the Leading Edge of the Tracer Plume are Indicated.

From σ_f^2 and $\sqrt{(K_{11}K_{22})}/K_{33}$ the ratio $\sqrt{(\lambda_1\lambda_2)}/\lambda_3$ can be obtained from Gelhar and Axness (1983, Figure 6, p. 168) after approximating λ_1/λ_3 by $\sqrt{(\lambda_1\lambda_2)}/\lambda_3$; an estimate of λ_1/λ_2 is obtained from Gelhar and Axness (1983, Figure 4a, p. 167 and Eq. 69, p. 170) where the difference $g_{11}-g_{22}$ comes from K_{11}/K_{22}. Then multiply $\sqrt{(\lambda_1\lambda_2)}/\lambda_3$ by $\sqrt{(\lambda_1/\lambda_2)}$ to update the λ_1/λ_3 value and obtain a new estimate of λ_1/λ_2. This process is repeated until stable parameters are obtained. Table 3-6 summarizes the results.

Table 3-6

PRELIMINARY COVARIANCE PARAMETERS - LARGE SCALE AQUIFER TEST

Input:

$\sigma_f^2 = 3.8$

$\sqrt{K_{11}K_{22}}/K_{33} = 3.5$ to 33.0

$K_{11}/K_{22} = 2.6$

λ_1/λ_3	λ_1/λ_2	$\sqrt{\lambda_1\lambda_2}/\lambda_3$
3	2	2
9	4	4.5
20	7	7.5

Geologic Mapping of Sedimentological Facies

I want to note at this point that the portions of the dissertation not concerned with unsteady flow were submitted as a technical report to the project sponsor, The Electric Power Research Institute. Professor John B. Southard of the Department of Earth, Atmospheric, and Planetary Sciences at MIT wrote the following sections on the description of the gravel deposits and the mapping technique for the technical report.

Most thick gravels of interest as aquifers are braided-stream deposits, either fluvial or glaciofluvial. The complex and poorly understood depositional setting of braided streams is characterized by a network of short-lived branching and rejoining shallow channels. Local aggradation

and degradation in these laterally shifting channels, together with variable grain size of the load from channel to channel, leads to complexly interfingering depositional bodies with irregular shapes.

The local depositional bodies in a braided-stream system usually have at least one lateral dimension greater than their thickness, although smaller bodies are often not much more extensive laterally than vertically. The scale of the depositional bodies depends upon the overall scale of the river: horizontal scales are meters to tens or even hundreds of meters, and vertical scales are centimeters to a few meters. The shapes of the depositional bodies might best be described as irregular tongues, shoestrings, wedges, and pods.

Owing to partial truncation by subsequent channels, the deposits produced in the various local depositional environments tend to show a much wider range of shapes and sizes in their final state of preservation than when they are first deposited. For this reason, and also because conditions commonly change gradually with time within a local depositional setting, the correlation between the size and shape of a depositional body, on the one hand, and its grain-size characteristics, on the other hand, tends to be low. It is usually possible, however, to recognize certain distinctive kinds of deposits in terms of mean size and sorting, whether or not such sediment types also show any clear tendency to be in a certain range of deposit size and deposit shape. Such sediment types can be termed *facies*.

The Gravel Deposit at the CAFB Site. The aquifer at the CAFB site, lying within the old floodplain of the Buttahatchee River near its confluence with the Tombigbee River, is clearly a braided-stream deposit, although the details of its interpretation are unclear. That there is substantial vertical and lateral variability in the aquifer is therefore not surprising. Full three-dimensional mapping of facies within the gravel would be of great value because it would provide a complete description of both the vertical and lateral spatial scales of variability of the deposit.

There are several gravel quarries within about one kilometer of the field site. These quarries have been worked from the surface down to the prevailing water table with drag lines, giving largely planar vertical faces showing a thickness of about three meters for inspection

and study. A major question, which cannot be fully resolved, is the extent to which these uppermost three meters of the deposit are representative of the bulk of the deposit below the water table. The close similarity in grain-size characteristics and bed thickness between the quarry faces and the cores at the field site lead us to believe that the deposit is largely similar in texture and structure in the upper and lower parts. An important qualification is that cementation is much more prominent above the water table than below, and this could have an important effect on hydraulic conductivity.

In practice three-dimensional mapping could be achieved only by examining a series of parallel vertical planar cuts in the deposit, each taken after a thin tabular volume of the deposit had been removed. This was not possible near the field site because none of the gravel quarries within the area has been worked regularly during the study. The next-best approach was to map a single quarry face to obtain a continuous two-dimensional picture of the deposit, in the hope that the mapping could be repeated at some later time, after the face had been worked again.

In addition to providing continuous information on both vertical and horizontal variability, mapping of quarry faces also allows close inspection of the deposit undisturbed by coring. In the mapping we obtained large and completely undisturbed cubic samples of each of the three dominant facies in the deposit for later laboratory measurement of hydraulic conductivity. These measurements have not yet been completed.

Techniques of Study. All of the quarries within a few kilometers of the field site were examined to find the one most suitable for mapping. Fortunately, one quarry just east of US Route 45 and along the low bluff bordering the present floodplain of the Buttahatchee River on the south, 1.5 km east-northeast of the field site (See Figure 3-1), had been worked not long before our mapping, and provided a very favorably exposed vertical planar face oriented almost east-west and extending for almost 100 meters. This face showed about three meters of section suitable for mapping below the surficial soil layer.

We first examined a 20-meter segment of the face in detail in order to distinguish the characteristic facies, or grain-size types. Boundaries between depositional bodies characterized by the various facies were identified on the face and spray-painted for added photographic

visibility. In large part the boundaries were well defined and readily distinguishable, although in many cases gradation between adjacent facies made placement of boundaries somewhat arbitrary.

A series of overlapping color photographs, each perpendicular to the face and at the same distance from it, was taken along the length of the study segment. Along the base of the face was a horizontal line marked in meters. A facies map of the face was compiled by combining the photographs into a long composite and tracing the facies boundaries onto an acetate overlay (Figure 3-5). Interpretation of the geometry of the depositional bodies and tracing of the boundaries onto the overlay was done independently by two investigators; comparison of the results showed only a few minor discrepancies.

Description of Facies. The deposit consists of sediment ranging from fairly coarse gravel (up to a few centimeters in diameter) at the coarse end, through fine gravel and sand, to clay-size sediment at the fine end. Sediment in the size range from silt to fine sand is mostly lacking, and clay is prominent only locally; most of the sediment is gravel and medium to coarse sand. The size distribution of this coarser fraction is prominently bimodal, with very coarse sand and finest gravel strongly deficient. Four facies based on grain-size characteristics were recognized and mapped:

Sandy Gravel: This facies, the most abundant, consists of bimodal mixtures of gravel and sand in varying proportions. Finer sediment is mostly absent. Variations in grain size within this facies are substantial but largely gradational.

Sand: This facies consists of fairly well sorted sand without pebbles or with only small percentages of scattered pebbles. There are gradations to sandy gravel, but for the most part contacts with other facies are well defined.

Sandy Clayey Gravel: This facies, the most variable of the four, consists of sand-gravel mixtures with appreciable clay in the pore spaces. This facies grades into sandy gravel on the one hand and to a much lesser extent into openwork gravel, by loss of sand and clay, on the other hand. Contacts with other facies are in part well defined and in part gradational.

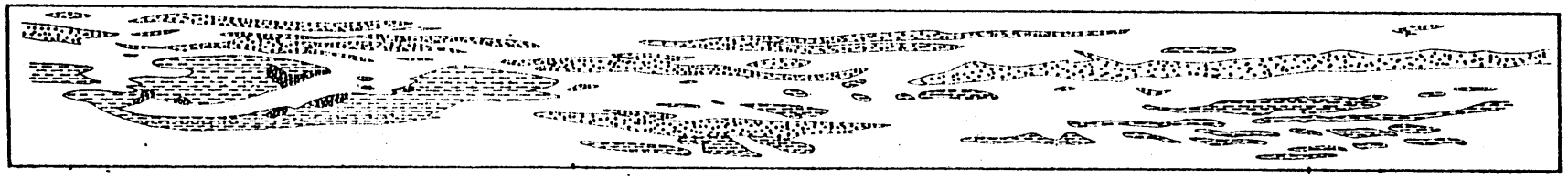

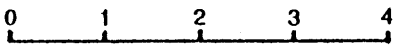

Legend

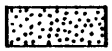
Sand


Sandy clayey gravel


Openwork gravel


Undifferentiated sandy gravel

Figure 3-5. Geologic Section Facies Map.

Openwork Gravel: This facies, the least abundant, ranges from well sorted openwork gravel to gravel with small percentages of clay in the interstices. Sand is wholly absent. The interstitial clay is not abundant enough to restrict passageways among gravel clasts. Boundaries of this facies are for the most part well defined, although there is some gradation into sandy clayey gravel.

Arrangement of Facies. The sandy gravel facies is the most abundant and appears as a matrix into which the other facies are embedded. The other facies are scattered throughout the section, although there is a paucity of clean sand in the lower half. The facies are lenticular with the ratio of length to thickness ranging from nearly one for small lenses to more than 20.

The longest dimension of the lenses is horizontal, although some variation is evident and there appears to be a channel-fill deposit near the left edge of the section. The section is rather small (2 x 20 m) compared to the area investigated by some of the other methods. Yet within this smaller area the information is continuous in both the horizontal and vertical directions.

The wide variety in the shape and size of the lenses precludes an estimate of the correlation scale by visual inspection alone. To quantify the correlation scales, hydraulic conductivity values were assigned to the different facies. The map was then "sampled" by reading the hydraulic conductivity at the vertices of a fine grid superimposed on the map and those values were used to calculate a variogram.

Assigning hydraulic conductivity values to the different facies is done in a series of stages, with each successive stage utilizing more precise values of K. Initially, hydraulic conductivity is assigned based on the description of the facies and some generic range of values (Driscoll, 1986, p. 75). These estimates are improved by incorporating knowledge about the range of hydraulic conductivity as measured by other means on the tracer test site itself. Based on the range of hydraulic conductivity values measured by the borehole flowmeter technique (Rehfeldt et al., 1988) an initial set of hydraulic conductivity values was assigned to the different facies and are designated by set 1 in Table 3-7. In the second set, the range of hydraulic conductivities was increased to reflect possible greater heterogeneity on a scale smaller than the flowmeter measurements.

Table 3-7

HYDRAULIC CONDUCTIVITY ASSIGNED TO FACIES

Facies	Hydraulic Conductivity (cm/sec)	
	Set 1	Set 2
Open Work Gravel	10^{0}	10^{2}
Sand	10^{-2}	10^{-1}
Sandy Gravel	10^{-3}	10^{-3}
Sandy Clayey Gravel	10^{-5}	10^{-7}

The next level of refinement would involve collecting numerous samples of each of the facies and measuring the hydraulic conductivity in a laboratory permeameter or based on grain size analyses. To refine the assigned hydraulic conductivity even further, undisturbed cores, or blocks, of each facies would be removed and tested in the laboratory. Work is planned to collect samples and refine the values in Table 3-7.

To discretize Figure 3-5, an 80 by 320 grid was overlain and the value of K at each vertex recorded. The spatial discretization was very fine, about 2.8 cm in the vertical and 6.9 cm in the horizontal. The fine discretization was chosen to insure that even the smallest heterogeneity in Figure 3-5 was represented by at least two points in each direction.

The full data set (25,600 points) was too large to use directly for repeated variogram calculation. To reduce the data set, coarser grids were superimposed on the finer one with the geometric mean hydraulic conductivity value of surrounding finer grid points assigned to the coarser grid. Figure 3-6 shows the averaging procedure used to reduce the size of the data set for the case of averaging over 9 points. Figure 3-7 shows the horizontal istropic variograms for data set 2 for different size coarse grids. As the data are averaged, the variance is reduced from 2.65 with no averaging to 1.54 with averages over 49 points. The correlation scale, about 1.2 m in each case, was obtained from fitting an exponential variogram to the sample variograms (with the sill value equal to the sample variance). Vanmarcke (1983) showed that theoretically, as the averaging area increases, the sample variance

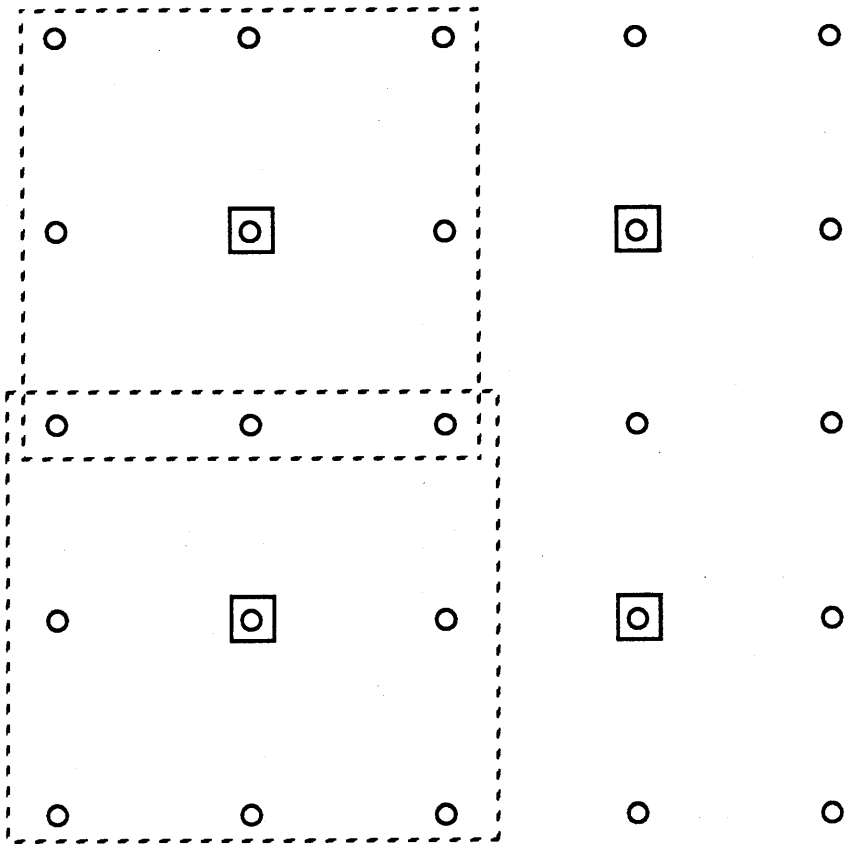

vertices of fine grid

vertices of coarse grid
The value of K assigned to each coarse grid vertex is the geometric mean of the K values at the 9 points within the box denoted by the dashed line.

Figure 3-6. Schematic Representation of the Averaging of the Fine Grid Data to a Coarse Grid.

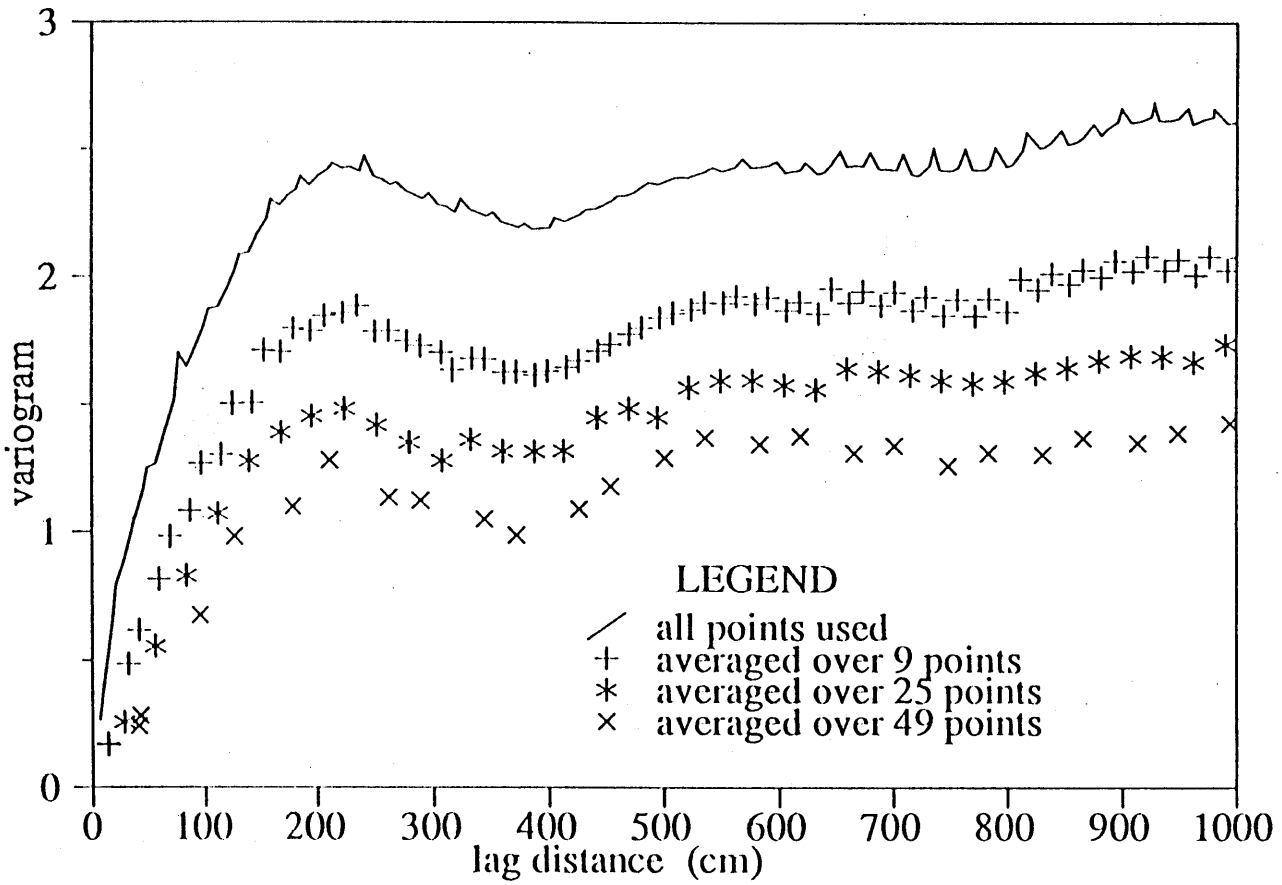

Figure 3-7. Variograms of the Gravel-Pit Map Data Before and After Averaging.

decreases and the correlation scale increases such that the product $\sigma_f^2\lambda$ remains constant. It is somewhat surprising that the correlation scale did not increase as averaging area increased.

For the remaining analyses of the the gravel-pit data, an average over nine points was used to reduce the data set to a more manageable 6,200 points. The variograms in the vertical and horizontal directions are presented in Figure 3-8 for set 1 and Figure 3-9 for set 2 and the covariance parameter values are summarized in Table 3-8 for both sets.

Not surprisingly, the variance for hydraulic conductivity set 2, which had a wider range of K values, is larger than for set 1. The variance of the assigned values should not be used as an indicator of σ_f^2 for two reasons: (1) the values of K in Table 3-7 assigned to the facies have not yet been confirmed by independent measurements and (2) the length and

Table 3-8

PRELIMINARY COVARIANCE PARAMETERS - FACIES MAP

	Set 1	Set 2
Variance	0.54	2.11
Horizontal Correlation Scale	1.15 m	1.15 m
Vertical Correlation Scale	0.15 m	0.15 m

depth of the mapped section is on the order of the correlation scales obtained from measurements on the CAFB site and therefore the mapped gravel pit face may not exhibit the full range of variability present on a larger scale such as the tracer test site.

Both sets of K values yield the same estimates for the correlation scales which are about a factor of 10 smaller than the correlation scales obtained from the other measurements at the CAFB site. The ratio of horizontal to vertical correlation scales of 7.7, however, is in general agreement. The smaller correlation scales may be due to the overall small size of the gravel pit face, which is slightly less than

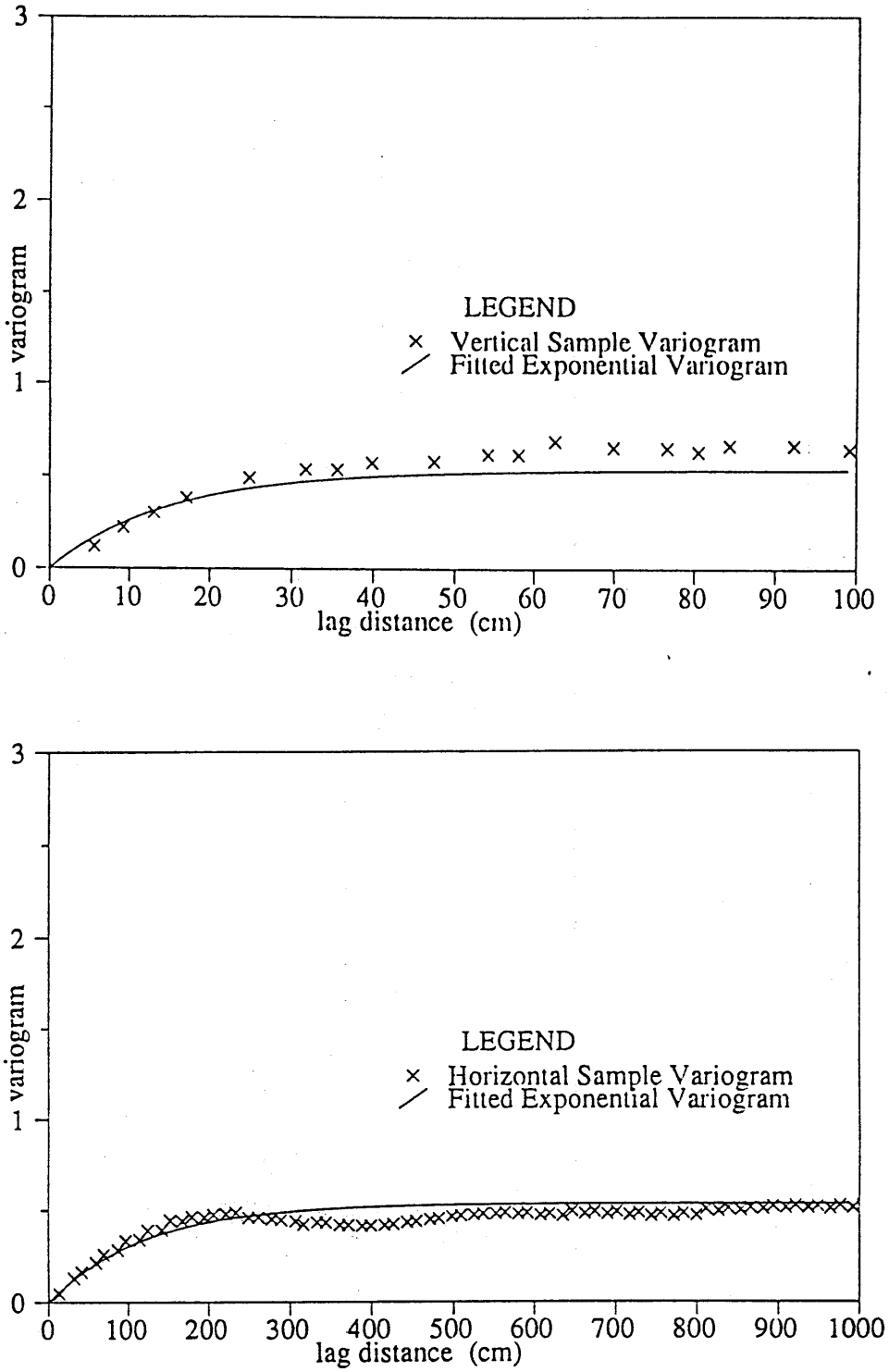

Figure 3-8. Vertical and Horizontal Variograms of Gravel Pit Data Set 1.

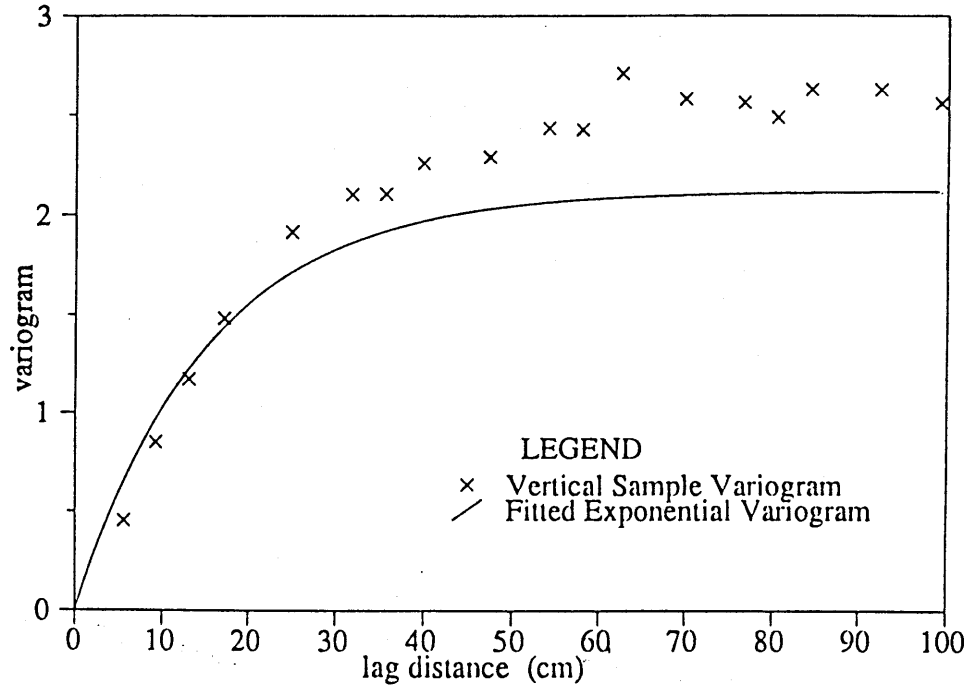

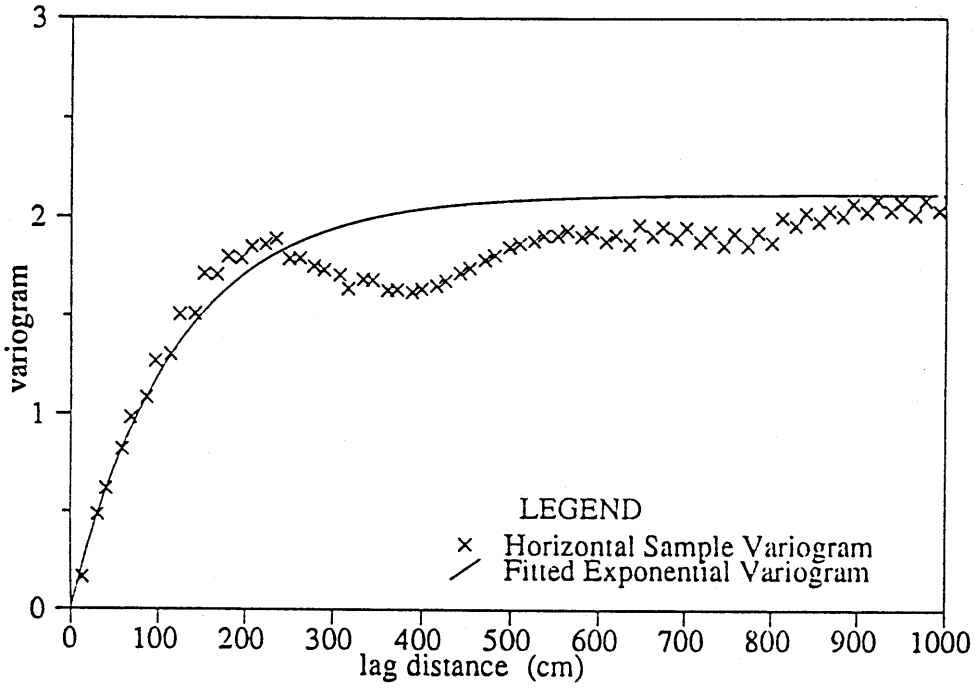

Figure 3-9. Vertical and Horizontal Variograms of Gravel Pit Data Set 2.

twice the correlation scale estimate from the other secondary measurements at CAFB. A longer face should be mapped to see if the scale of investigation affects the measurements.

Continuous Core

Each 0.76 m core of material collected by TVA was taken to their Singleton Materials Engineering Laboratory for testing. A schematic diagram of the permeameter system, designed jointly by MIT and TVA, is given in Figure 3-10. The concept of the core permeameter is quite simple. A constant head difference is maintained across the full length of the core and a steady flow is established. The drop in hydraulic head is measured across each 7.6 cm (3 inch) interval along the entire length of the core. The hydraulic conductivity of each interval is calculated from Darcy's Law

$$K = \frac{Q}{A}\frac{\Delta h}{\Delta L} \qquad (3\text{-}16)$$

where Q = discharge through the core

A = cross-sectional area of the core

$\Delta h/\Delta L$ = the hydraulic gradient over each 7.6 cm interval.

The hydraulic conductivity profile from Core C-11 is presented in Figure 3-11 along with the profile obtained using the borehole flowmeter in a fully screened well located about 1.5 m away. Near the top and bottom of the aquifer the methods correlate quite well, but in the middle the two methods differ by up to three orders of magnitude. We believe the permeameter method to be reliable. Other work at MIT using a similar laboratory permeameter, but smaller-diameter cores (Wolf, 1988), has shown that reproducible results can be obtained if careful measurements are made. In Rehfeldt et al. (1988) the borehole flowmeter method was also shown to yield reliable results. It is puzzling, then, that some of the measurements correlate well and others do not.

Part of the difference may be due to horizontal variations in hydraulic conductivity between the two boreholes. From the facies section in Figure 3-5 it is evident that major changes in conductivity could occur over a horizontal distance of one meter. The difference may also lie in the fact that the cores were stored in the laboratory for one year before they were tested. During that time the cores may have partially desaturated resulting in entrapped air within the core, or bacterial or

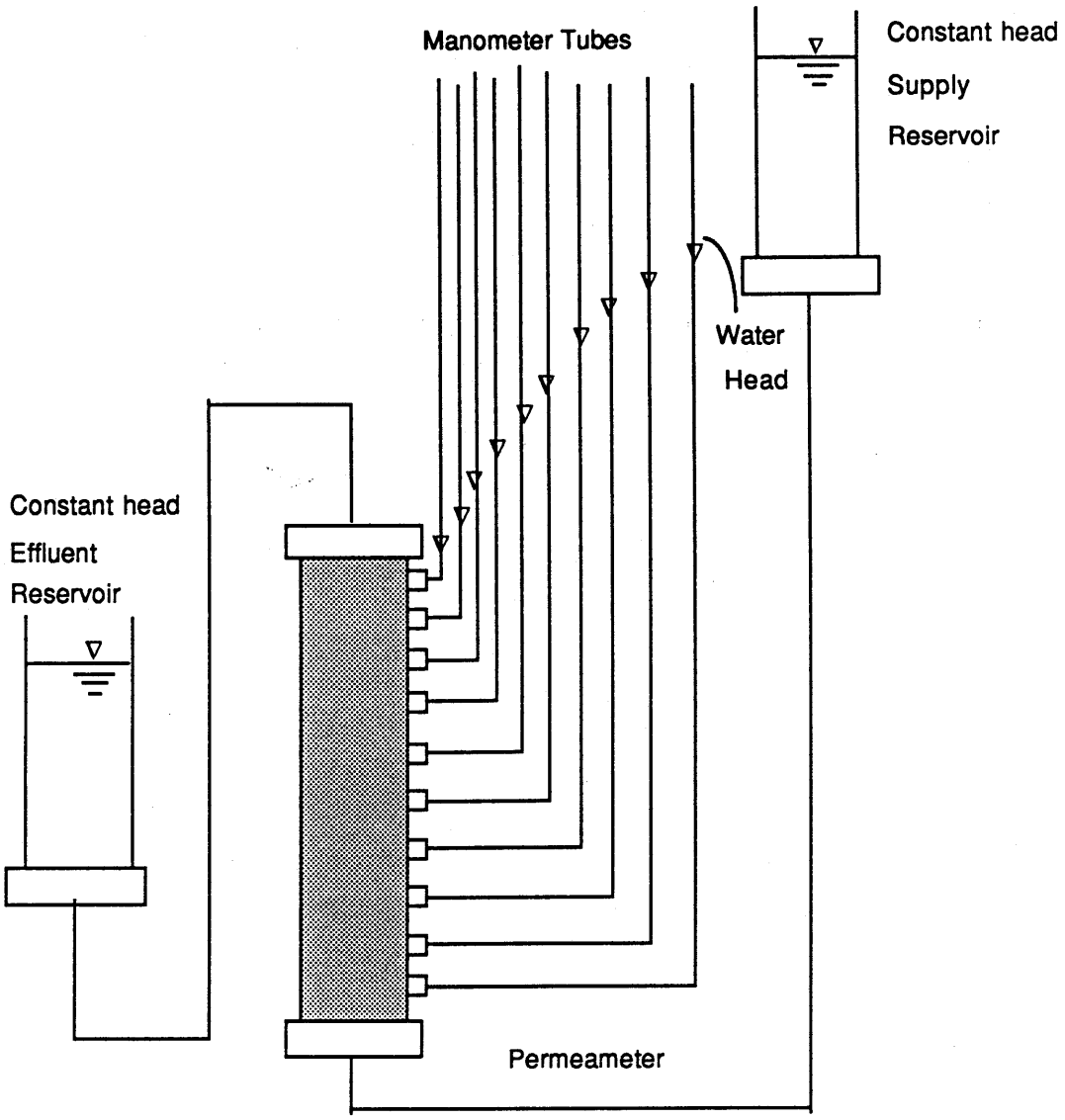

Figure 3-10. Schematic Diagram of Core Sampler Permeameter System

Source: Boggs et al., 1988

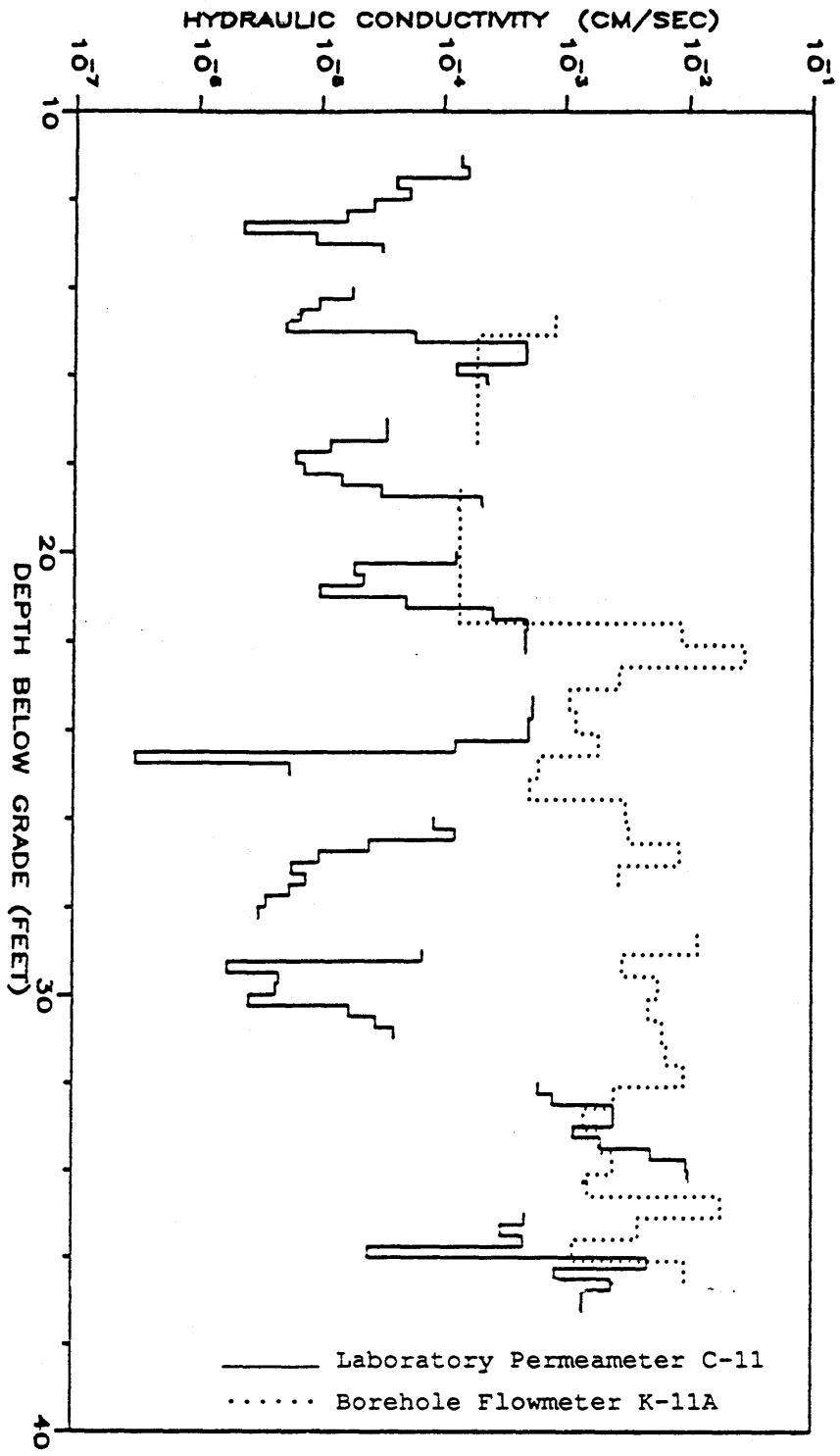

Figure 3-11. Comparison of the Hydraulic Conductivity Profiles from Laboratory Measurements in Core Hole C-11 and Borehole Flowmeter Measurements in Well K-11A.

algal growth within some of the cores easily could have partially plugged some of the pores. The one-year delay was not due to oversight on the part of MIT or TVA, but rather was caused by budget cuts handed down in mid year by EPRI.

Based on Wolf (1988) we feel the lab permeameter technique holds promise and should be pursued. However, the present core data from CAFB are unreliable and any core presently in storage should be opened and analyzed descriptively and for grain size. Additional permeameter testing should be done on fresh cores.

Borehole Flowmeter

The borehole flowmeter is considered the most reliable of the above methods for measuring the spatial variability of K on a routine basis. Detailed description of the method and experiments at CAFB can be found in Rehfeldt et al. (1988). The detailed spatial covariance analyses of the flowmeter hydraulic conductivity data are presented in Section 4 of this report.

SUMMARY OF SPATIAL COVARIANCE PARAMETERS FROM SECONDARY MEASUREMENTS

Table 3-9 is a summary of the preliminary spatial covariance parameters obtained from the secondary measurements. Except for the facies map, the data used to calculate the parameters in Table 3-9 are those typically collected during a routine site investigation. We will compare these preliminary parameters to the results of detailed spatial covariance analyses of the more comprehensive flowmeter data at the end of the next section and discuss the implications.

Table 3-9

PRELIMINARY SPATIAL COVARIANCE PARAMETERS

Method	σ_f^2	λ_h (m)	λ_3 (m)	λ_1/λ_2	λ_h/λ_3
Piezometer	3.7				
Slug Tests	3.9				
Grain Size	3.9	< 24	1.1		< 22
Resistivity (1.52)		< 31			
Resistivity (3.05)		< 24			
Resistivity (6.10)		< 27			
Streaming Potential		< 16			
Large-Scale Aquifer Test				2 to 7	2 to 7.5
Gravel Pit Facies Map		1.2	0.15		7.6

Section 4

STATISTICAL PROPERTIES OF THE NATURAL LOG HYDRAULIC CONDUCTIVITY FIELD AND THE HYDRAULIC GRADIENT

DEFINITION OF THE AUTOCOVARIANCE FUNCTION

The hydraulic conductivity values from the borehole flowmeter method are the most extensive set of variability data at CAFB. These data will be examined carefully to yield the best possible estimate of the autocovariance function.

The autocovariance function is assumed to be that of a second-order stationary stochastic process. This implies that the covariance of two points depends only on the distance between them and not on their spatial location. The covariance function is defined by

$$R_{ff}(\xi) = E[f(\mathbf{x}+\xi)\, f(\mathbf{x})] \tag{4-1}$$

where f is a zero-mean, correlated random process, ξ is the separation vector, $\mathbf{x}$ is the position vector, and E[ ] is the expectation operator.

An alternative description of the structure of the random field is given by the variogram

$$\gamma_{ff}(\xi) = \frac{1}{2} E[\{f(\mathbf{x}+\xi) - f(\mathbf{x})\}^2] \tag{4-2}$$

When the process, f, is second-order stationary, the covariance and variogram are linearly related (Matheron, 1971; deMarsily, 1986) by

$$\gamma_{ff}(\xi) = \sigma_f^2 - R_{ff}(\xi) \tag{4-3}$$

where σ_f^2 is the variance of the f process.

The expressions for predicted macrodispersivities (Gelhar and Axness, 1983) were derived using a negative exponential autocovariance:

$$R_{ff}(\xi_1,\xi_2,\xi_3) = \sigma_f^2 \exp[-(\xi_1^2/\lambda_1^2 + \xi_2^2/\lambda_2^2 + \xi_3^2/\lambda_3^2)^{1/2}] \tag{4-4}$$

where: σ_f^2 = the variance
λ_i = the correlation scale in the x_i direction; i=1,2,3
ξ_i = component of the separation vector; i=1,2,3

For the analyses that follow, the exponential covariance will be assumed. Other covariances could also be used, particularly those of the hole-function type. Vomvoris (1986) has shown that the longitudinal macrodispersivity, A_{11}, predicted by the stochastic theory was smaller by a factor of 0.58 to 0.92 when various hole covariances were used in place of the negative exponential. In general, one cannot determine the functional form from the sample variogram, or covariance, because the amount of data necessary to define the functional form of the covariance is beyond the scope of any practical investigation. Therefore the choice of the negative-exponential covariance is a pragmatic one. The parameters, σ_f^2, λ_i, and the orientation of the covariance with respect to the mean flow will have a greater impact on the predicted values of the macrodispersivity tensor A_{ij} than the functional form of the autocovariance.

VARIANCE AND CORRELATION SCALE ESTIMATES FROM SAMPLE DATA

Discussion of the Literature

In the fully three-dimensional case the exponential covariance is defined by four parameters, σ_f^2, λ_1, λ_2, and λ_3. To estimate these parameters, the exponential covariance, or variogram, is fitted to the sample variogram obtained from Eq. 3-7. How the sample variogram is calculated, potential biases in the variogram calculation, and how the exponential variogram is actually fitted to the sample variogram all influence the parameters that result.

The sample variogram may be biased due to a number of causes (Armstrong, 1984):

(1) artifacts in the data (typographical errors)
(2) poor choice of step size
(3) geographically distinct populations (nonstationarity)
(4) outliers, skewed distributions, and mixed populations.

In addition, Omre (1984) identified the non-randomized grid as a potential source of bias. A number of studies in addition to these have

tried to address the problem of obtaining the sample variogram: Cressie and Hawkins, 1980; Warrick and Myers, 1987; Sharp, 1982; Dowd, 1984; Chung, 1984; and Cressie, 1985. Many of these studies have dealt with the problem of anomalous or outlier data points common in data from the mining industry. For two of the problems most likely to occur at the MADE site, skewed distributions and non-randomized sampling, Omre (1984) found that the nonparametric estimator, Eq. 3-7, yielded unbiased estimates of the variogram except in the one hypothetical case where about 40% of the sample locations were intentionally placed to obtain values from the tail of a highly skewed distribution.

Given the sample variogram, one can either fit the functional form by eye or fit a form using a weighted or unweighted regression technique. This process of calculating the sample variogram and fitting a functional form will be referred to as conventional variogram analysis (CVA) in later discussions. If one is interested in using the fitted variogram for kriging, Journel and Huijbregts (1978) suggest a validation procedure where one data point is removed and its value predicted using kriging and the fitted variogram. This procedure is performed for each data point and the statistics of the residuals are examined to see if they are uncorrelated, of zero mean, and variance one. If not, a different variogram is fit and the procedure repeated. Davis (1987) points out that in principle this "leave-one-out" procedure can be used to determine if one variogram is more appropriate than another, but in no way determines if any particular variogram is the optimum. In addition, Davis (1987) notes that the variogram chosen to be most appropriate may depend on how one measures discrepancy between measured and predicted values, the partition set size, predictive function, and the models chosen for comparison.

This problem of validating the variogram and the potential for biased estimates of the sample variogram led to the development of other variogram estimators. Kitanidis and Lane (1985), Kitanidis (1983), Hoeksema and Kitanidis (1985) and Kitanidis (1985), among others, developed parametric procedures to estimate parameters of the covariance function from measurements. In the case of the maximum likelihood estimation procedure (Kitanidis and Lane, 1985), the parameter estimates are asymptotically unbiased (for large samples) and of minimum variance. The maximum likelihood procedure was applied to regional aquifer

hydraulic properties from Iowa by Hoeksema and Kitanidis (1985). In nearly 75% of the examples they presented, the estimated correlation scale was one of the constraint values imposed by the authors. Although the inability of the method to determine a correlation scale may have been caused by inadequate data, the method was not demonstrated to be reliable.

In a recent study, Russo and Jury (1987a) used conventional variogram analyses (CVA), maximum likelihood (ML) and restricted maximum likelihood (RML) methods to determine the variance and correlation scale of synthetic, two-dimensional, stationary random fields generated by the turning-bands method (Mantoglou and Wilson, 1982). Among the many interesting results of Russo and Jury's paper, one can interpret from the single realizations they present that the maximum-likelihood procedure produced estimates of the correlation scale and variance of accuracy comparable with the estimates from the conventional variogram-analysis method. However, the ML method is computationally burdensome, and can be applied only to relatively small data sets (for example Russo and Jury, 1987a, use 72 points).

From the same single realizations in Russo and Jury (1987a) one can observe that the restricted maximum-likelihood method (Kitanidis and Lane, 1985) produced estimates of the variance and correlation scales that were in error by a factor of 4 in some cases. Interestingly, the verification techniques based on the "leave-one-out" method failed to distinguish between CVA, ML and RML. Although Russo and Jury note that examining only a few realizations is not a conclusive test, it would appear that CVA and ML can be used to obtain estimates of σ_f^2 and λ for a stationary random field.

Nonstationary Random Fields. If the mean of the random field varies over the region of interest, the field is considered nonstationary. To estimate the covariance of the stationary portion of the random field, one must first remove the mean, or detrend the data. As was the case for stationary random fields, a number of methods have been proposed:

1) Ordinary least squares (OLS) to remove the trend and calculate the covariance of the residuals.
2) Iterative generalized least squares (IGLS) to remove the trend and calculate the covariance of the residuals.
3) ML to simultaneously estimate the trend and the covariance.

4) RML to estimate the covariance without having to estimate the trend first.
5) Minimum-Variance Unbiased Quadratic Estimation
6) Generalized Covariances.

The OLS procedure is by far the simplest to implement. The primary criticism of OLS is that the residuals are assumed to be independent and uncorrelated when, in fact, it is the correlated nature of those residuals one hopes to define by the covariance. The IGLS accounts for the correlated structure of the residuals when estimating the trend parameters. Neuman and Jacobson (1984) provide the general formulation and an example of the IGLS method. They and Cressie (1987) note that the residuals from the IGLS estimator are biased and will yield a biased estimate of the sample variogram. However, one can estimate the bias in the residual variogram from expressions in Neuman and Jacobson (1984) or Cressie (1987).

The ML method also produces biased estimates of the covariance (Kitanidis, 1985). Both RML and GC are designed to remove the influence of the drift without having to explicitly estimate it, and will, in theory, yield asymptotically unbiased estimates of the covariance parameters. For real problems, it is difficult to know which of the different methods is best.

Russo and Jury (1987b) have attempted to address the question of the best way to obtain the stationary covariance of a field with a trend. The authors generated synthetic two-dimensional stationary random fields using the turning-bands method and then corrupted those random fields by adding a deterministic trend. They then attempted to obtain the covariance of the underlying, stationary random field by applying the OLS, IGLS, ML and RML methods mentioned above. Table 4-1 summarizes the covariance parameters, σ_f^2 and λ, obtained from the different methods for various added trends. Although these are the results of only a few realizations, it appears that the OLS and IGLS methods yield covariance parameters that are usually close to the true values (within 30% or so). In general, both OLS and IGLS tended to underestimate the correlation scale and overestimate the variance, and only in one case (nonlinear trend, example 2) did the IGLS method improve the parameter estimates over the OLS method. Validation tests failed to discriminate between

Table 4-1

SUMMARY OF COVARIANCE PARAMETER ESTIMATES
FOR SYNTHETIC NONSTATIONARY RANDOM FIELDS
FROM RUSSO AND JURY (1987b)

Linear trend #1 n = 72 points

Method	σ_f^2	λ
Input	1.0	0.07
OLS	1.267	0.062
IGLS	1.273	0.062
ML	1.375	0.174
RML	1.615	0.223

Linear trend #2 n = 72 points

	random field 1		random field 2	
Method	σ_f^2	λ	σ_f^2	λ
Input	1.0	0.07	1.0	0.28
OLS	1.267	0.062	0.703	0.17
IGLS	1.272	0.062	0.728	0.17
ML	1.375	0.174	1.154	0.443
RML	1.614	0.223	2.916	1.414

Non linear n = 288 points

	random field 1		random field 2	
Method	σ_f^2	λ	σ_f^2	λ
Input	1.0	0.07	1.0	0.28
OLS	1.097	0.170	1.006	0.187
IGLS	1.170	0.170	1.209	0.259
RML	5.845	0.989	5.265	1.386

the parameter estimates from the various methods even though the RML method produced estimates that were clearly in error.

As a final comment, Russo and Jury (1987b) offered a pessimistic view of the prospects of estimating independently the parameters σ_f^2 and λ when a trend is present. Using the OLS or IGLS methods, the product $\sigma_f^2 \lambda$ for all the examples in Russo and Jury (1987a, 1987b) ranged from 40% of the true value to 280% of the true value. This would indicate that we may be able to estimate the product $\sigma_f^2 \lambda$ to within a factor of 3 or so in real situations.

Variogram Estimation - Pragmatic View

From the work of Russo and Jury (1987a, 1987b), it appears that the removal of a trend using the OLS or IGLS method is possible, and that the resulting product, $\sigma_f^2 \lambda$, is likely within a factor of 3 or so of the true value. Of practical concern in the application of the techniques is that we do not know the form of the trend to be removed. If the trend is linear and significant, then we can easily diagnose the presence of the trend from the variogram. When the trend is not strong, or if it is nonlinear, then identifying the presence of a trend from the sample variogram is, for all practical purposes, impossible. As one fits higher-order trends to the random field, the variogram of the residuals should show smaller variance and correlation scales than the undetrended field. There is no simple criterion one can use to indicate if, say, the first-order or third-order polynomial yields a more stationary random field, particularly when the variograms of the residuals from both appear nearly stationary. In fact, if the trend is actually first-order, then the third-order trend will filter out some of the true variability. This will lead to an underestimation of the variance and correlation scales. On the other hand, if the trend is actually third-order, then removing a first-order trend will yield a variogram of residuals with an overestimate of σ_f^2 and λ. In addition, it would appear that the usual verification techniques will not be useful in distinguishing two different trend functions unless the difference is quite strong. In such cases a visual inspection will lead to a similar conclusion.

To effectively remove a trend, we must rely on judgment. If one can utilize additional information about the random field, then one can strengthen the argument for choosing one trend surface over the other.

For example, one can augment the information on the trend of the hydraulic conductivity field by using knowledge of the local flow system and local geology. This is precisely the approach taken in this work.

A more fundamental question is: What do we call a trend and what is random? For the problem of estimating σ_f^2 and λ to use in stochastic flow and transport models (for example, Gelhar and Axness, 1983) we have an approximate criterion to distinguish the trend from the random component. In the stochastic solute transport theory, variation in K with scales on the order of the size of the plume are regarded as a trend and variations in K with scales on the order of 10% of the plume are treated as random. Clearly this interpretation leaves some room for judgment. Even within the same aquifer, the definition of what is trend and what is random will change depending on the time and space scales of the problem at hand.

The decision whether to detrend a set of data must, by necessity, be based on some judgment of the given problem. The scale of the problem must be known a priori because the scale dictates the size of the investigation and the scale of fluctuation that one can legitimately call a trend. If removal of a trend is clearly indicted, then the trend must be physically realistic and consistent with all known information about the site. Detrending with some automated procedure based on purely statistical arguments is questionable.

VARIOGRAM ESTIMATES AT CAFB

Rehfeldt et al. (1988) present the hydraulic conductivity values obtained using the borehole flowmeter in wells K-7 through K-36 that will be used in the estimation of the variogram. Before discussing the estimation itself, it is useful to look at the hydraulic conductivity data in order to gain a better understanding of the nature of the hydraulic conductivity field.

Sampling Scheme

The locations of the fully screened wells K-1 through K-37 on the CAFB site are shown in Figure 4-1. As discussed in Rehfeldt et al. (1988), the K-wells were installed in groups, with the locations of later wells based on preliminary calculations using the wells already in place. The data from the K-wells were obtained for two reasons: (1) as reconnaissance information on the hydraulic conductivity for use in

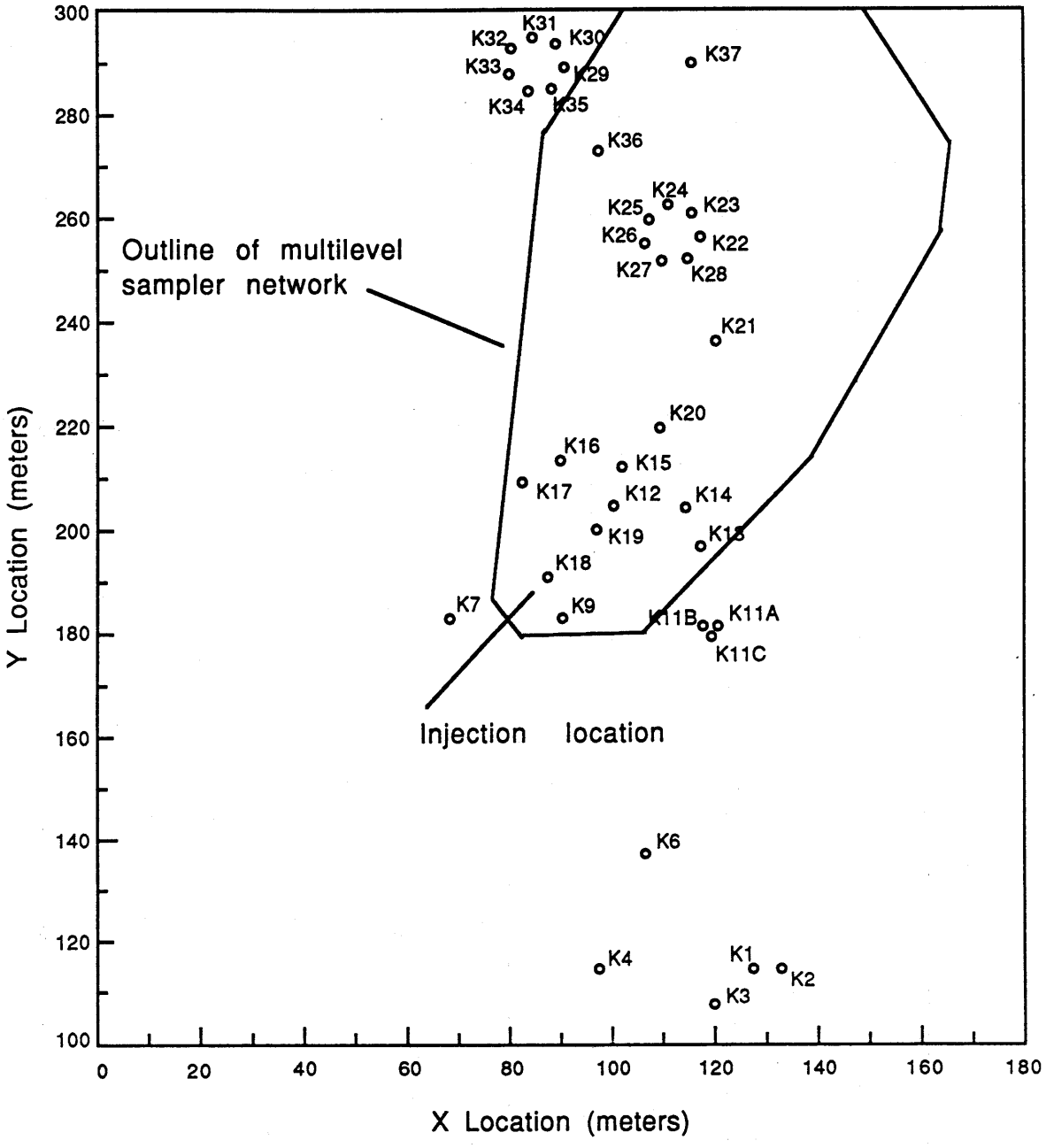

Figure 4-1. Location Map of the Flowmeter Wells

estimating the velocity of the tracer plume, and (2) as the primary data set for the covariance estimation.

The placement of wells for reconnaissance is governed by the need for information in one location or another. One tends to spread the wells out uniformly, because that maximizes the amount of information about the whole area of interest. Basically, one tries to fill holes in the existing grid.

The placement of wells for the variogram estimate is often quite different. In the simplest terms, the variogram estimation reduces to finding the variance and the correlation scales. One may also wish to determine the form of the covariance (exponential or hole function, for example) but spatial data are limited in number, and the form is usually not distinguished with confidence.

The most precise estimate of the variance will be obtained if all the hydraulic conductivity measurements are uncorrelated and independent. The maximum amount of independent information is obtained if the distance between any two measurements is greater than the correlation scale. However, to estimate the correlation scale from the sample variogram, the rising portion of the variogram must be discernible, and to do that, samples must be separated by distances less than the correlation scale. The sampling requirements for the variance and the correlation scale therefore are not compatible, and to design a sample grid one must reach a compromise. To further complicate the design of the well network, the correlation scale must be known in order to properly design the network, but one almost never knows the correlation scale a priori. The best approach is to make an educated guess of the correlation scale, then design a portion of the sample locations, collect the data, and estimate the correlation scale from the partial data set. The design can then be modified before the remainder of the wells are installed.

Network Design at CAFB

Figure 4-2 shows the initial design of the K-well network. The design network was chosen based on the following considerations:

1) The horizontal anisotropy of the lnK field, if other than one, is unknown. Two transects of wells (as used by Sudicky, 1986) do not provide enough information to determine the principal coordinates

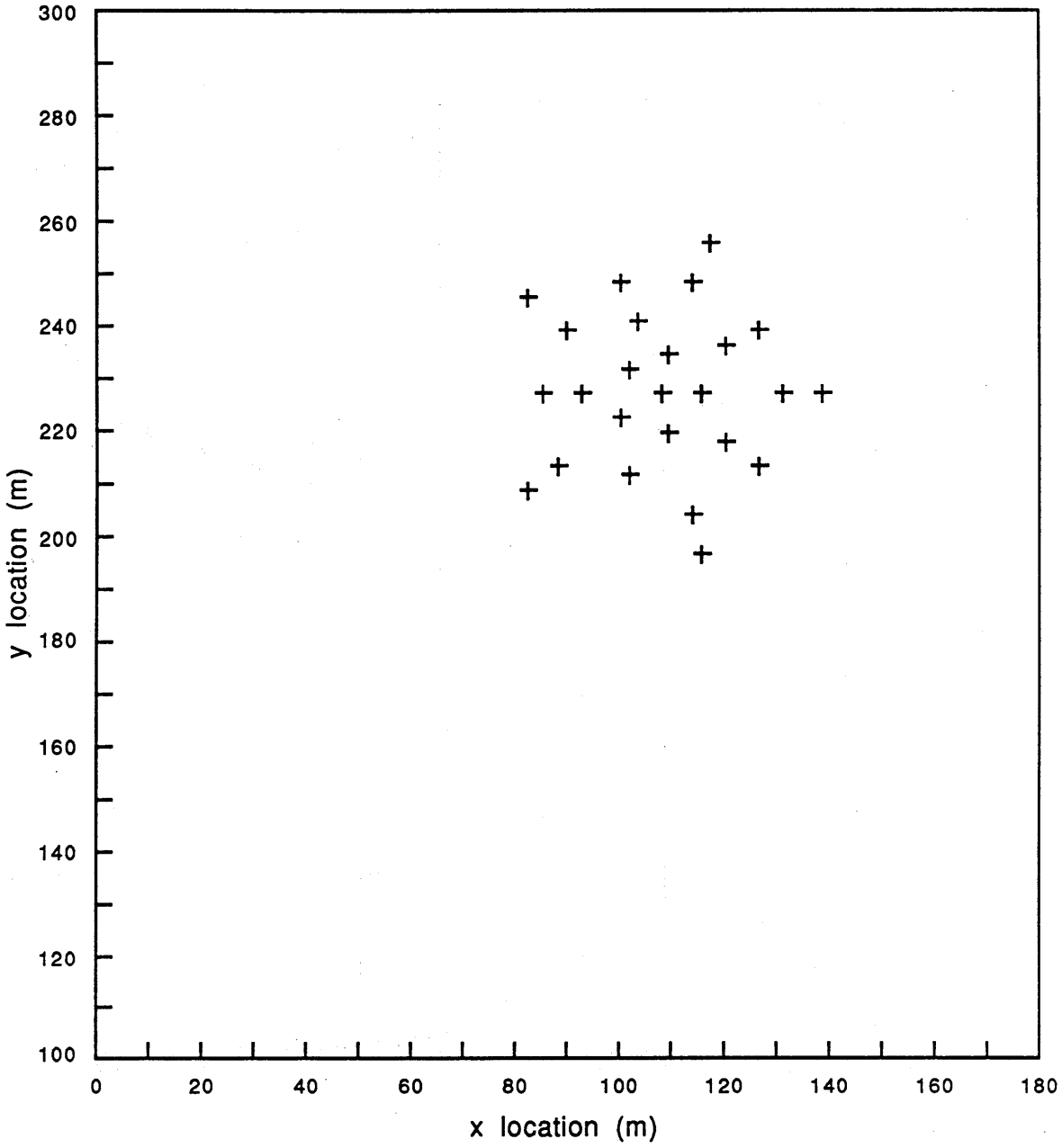

Figure 4-2. Preliminary Design Locations of 25 K-Wells

of the lnK covariance. This is analogous to the problem of estimating the large-scale anisotropy of hydraulic conductivity from an aquifer pumping test. If the principal directions are unknown, at least three rays of wells are needed (Hantush, 1966). Therefore, the star pattern was used because the variogram could be estimated in many directions.

2) When the lnK field has a trend, that trend must be identified and removed. Data from one or two transects may be adequate to remove a linear trend. However, if higher-order trends are present, two lines of information may not be adequate to identify the trend surface.

3) To adequately estimate the variance, wells must be far enough apart to be uncorrelated. The star provides for data at a spacing large enough to estimate the variance. From one side to the other side is about 4λ, where λ is obtained from the estimates in Section 2. In retrospect, it appears that 4λ may be too small and that a larger value, closer to 10λ, would be more appropriate.

4) To obtain the correlation scale, wells should be closely spaced. By pairing wells at various locations, short lag information is obtained. Intermediate lag distance data come from the remaining combinations of wells.

The design was never optimized in the sense of Warrick and Myers (1987), nor were the wells sited randomly (Russo and Jury, 1987a,b; Omre, 1984). The design is the result of weighing the various competing requirements of the sampling network and choosing a reasonable compromise.

The design is based on an estimate of λ of 15 m, which was obtained from variograms of the secondary data (see Section 2). The estimated value was expected to be an upper bound, but was used to lay out the first eight wells of the network, indicated by the circled locations in Figure 4-2.

A horizontal isotropic variogram (Figure 4-3), using flowmeter measurements from the first eight wells of the star pattern and seven wells installed for reconnaissance, indicated a horizontal correlation scale of 12 m. These first 15 wells are indicated on Figure 4-1 with numerical designations less than 23. From Figure 4-3 it appears that

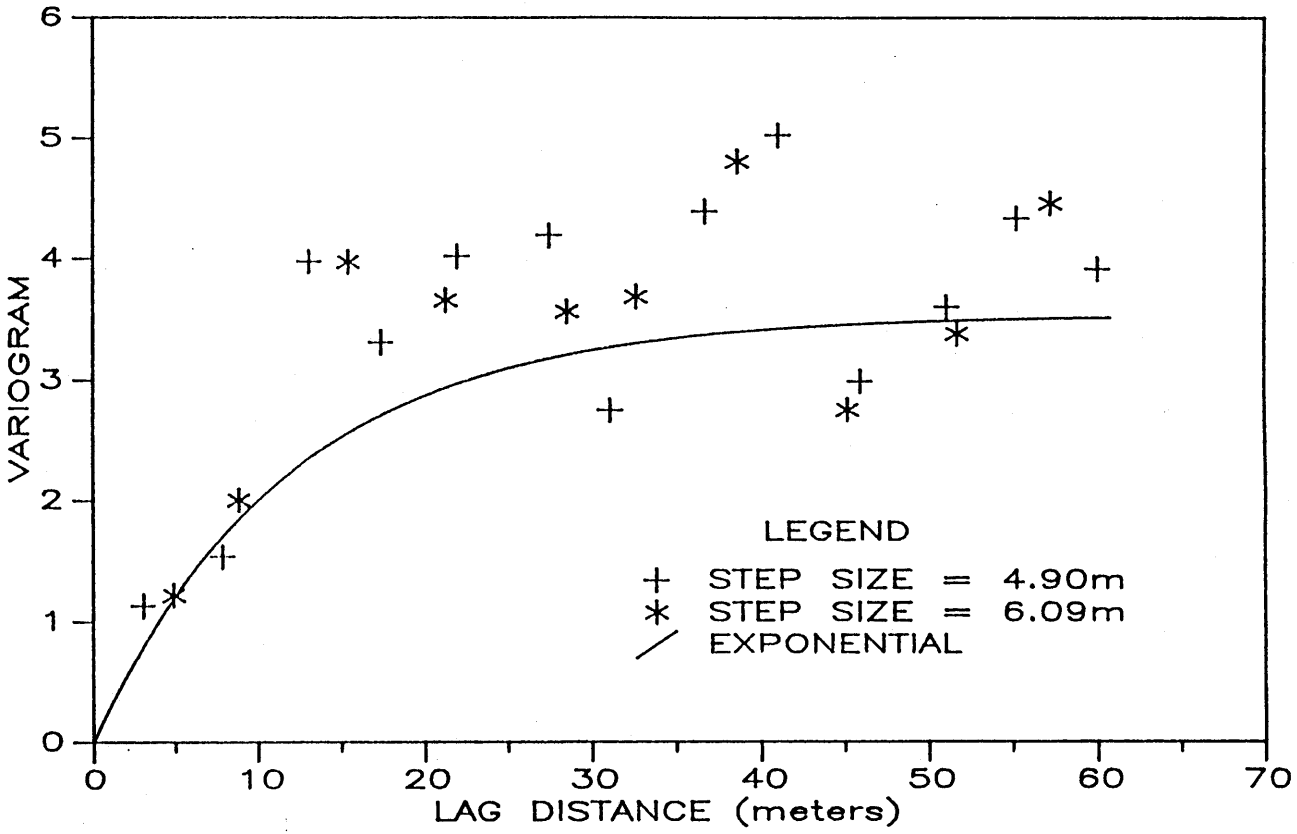

Figure -3. Horizontal Isotropic Variogram of Hydraulic Conductivity Values from the First 15 K-Wells.

the minimum well spacing was adequate to define the rising portion of the variogram. However, there were far fewer couples at the short lags (about two orders of magnitude fewer) than at larger lags, and the remaining wells were placed to improve the short lag information. To maximize information at a small scale, two circles of 7 wells were installed (See Figure 4-1). Another approach would have been to pair up some of the existing wells, but that proved impossible. Due to equipment problems, the measurements in the final wells were delayed until after the start of the large-scale tracer test. To minimize the disturbance to the tracer plume, the K wells needed to be at least 30 m away from the plume, located in the vicinity of Wells K-18 and K-19 at the time.

Presentation of the Measured Hydraulic Conductivity Data

The location of three section lines is given in Figure 4-4. Section A-A' (Figure 4-5) extends from behind the injection site, through the center of the five injection wells (Betson et al., 1985), and along nearly the center line of the tracer plume. This section represents a view of the hydraulic conductivity distribution along the longitudinal axis of the tracer plume. Along the depth of any well the hydraulic conductivity can vary by up to three orders of magnitude. There is a trend toward larger hydraulic conductivity as one moves from left to right. This region of high hydraulic conductivity could be a channel deposit and may extend to the left above the highest measured value in wells 7 and 18. The positions of high and low water table during the period Nov. 1, 1986 - Aug. 31, 1987, are marked on all the sections. During periods of high water table, the upper one-quarter of the aquifer is uncharacterized. In general, the lower part of the aquifer seems to be less conductive than the upper part.

Section D-D' (Figure 4-6) runs transverse to the plume and intersects section A-A' at Well K-15. Again, there is a channel-like deposit of higher hydraulic conductivity in the center of the section between elevations 57 and 61 m. This deposit is truncated both left and right on section D-D'. Recall that on section A-A', the deposit extends to well K-21 and probably continues for some unknown distance.

Section C-C' (Figure 4-7) runs transverse to section A-A', but near the edge of the tracer monitoring network. The hydraulic conductivity is largest near wells K-25 and K-27 and decreases sharply to the left

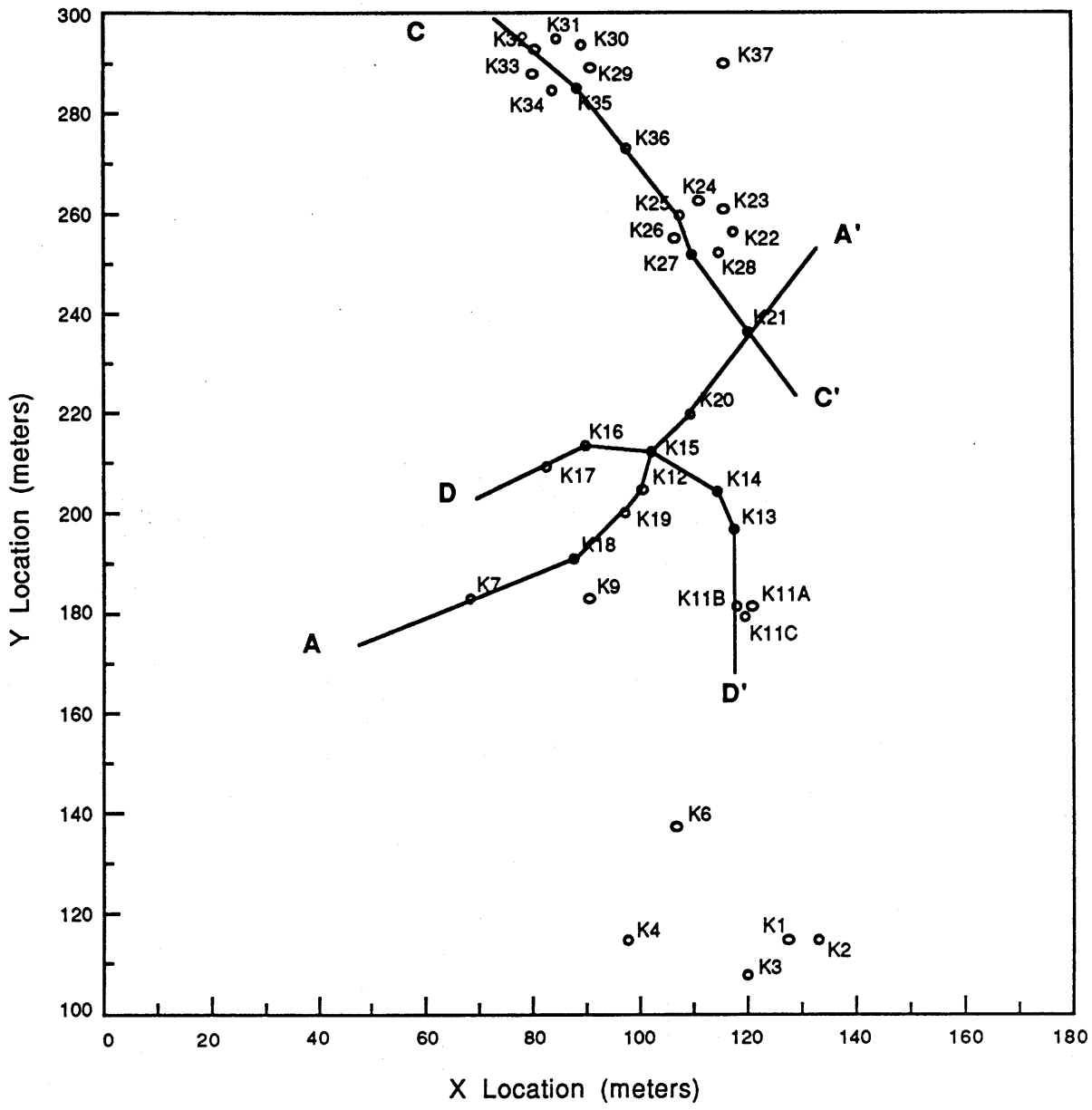

Figure 4-4. Location Map of Hydraulic Conductivity Cross Sections

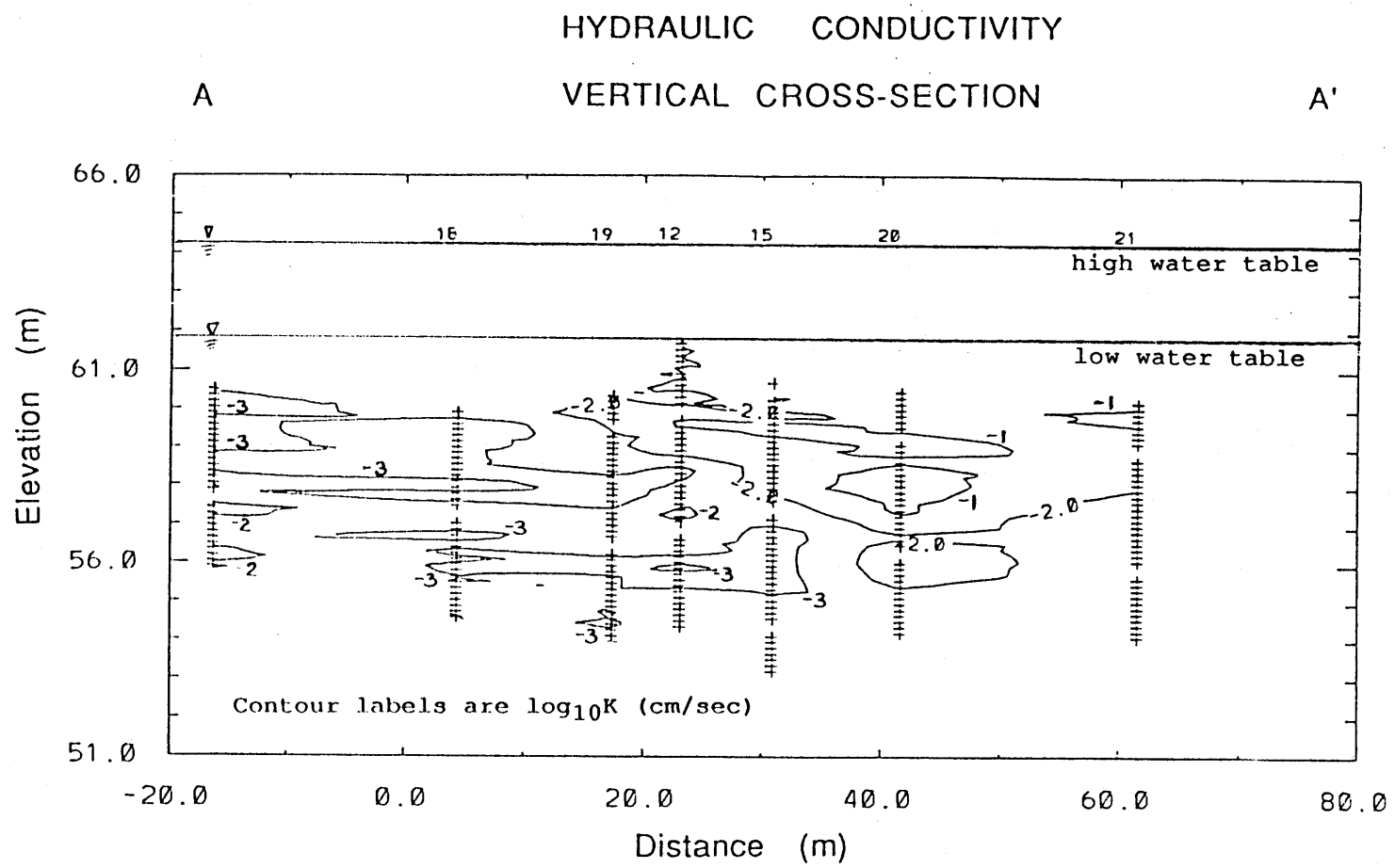

Figure 4-5. Hydraulic Conductivity Cross Section A-A'.

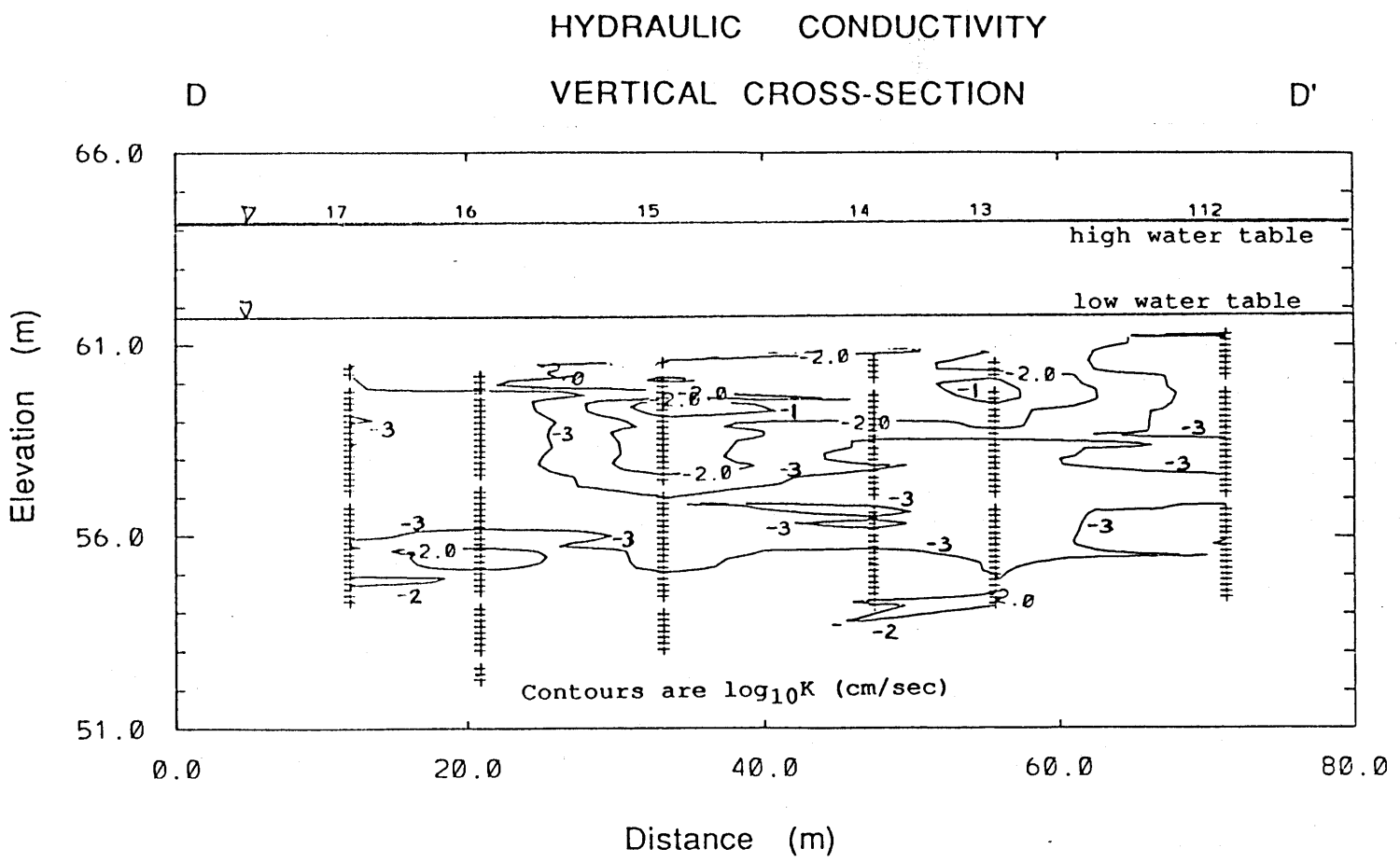

Figure 4-6. Hydraulic Conductivity Cross Section D-D'.

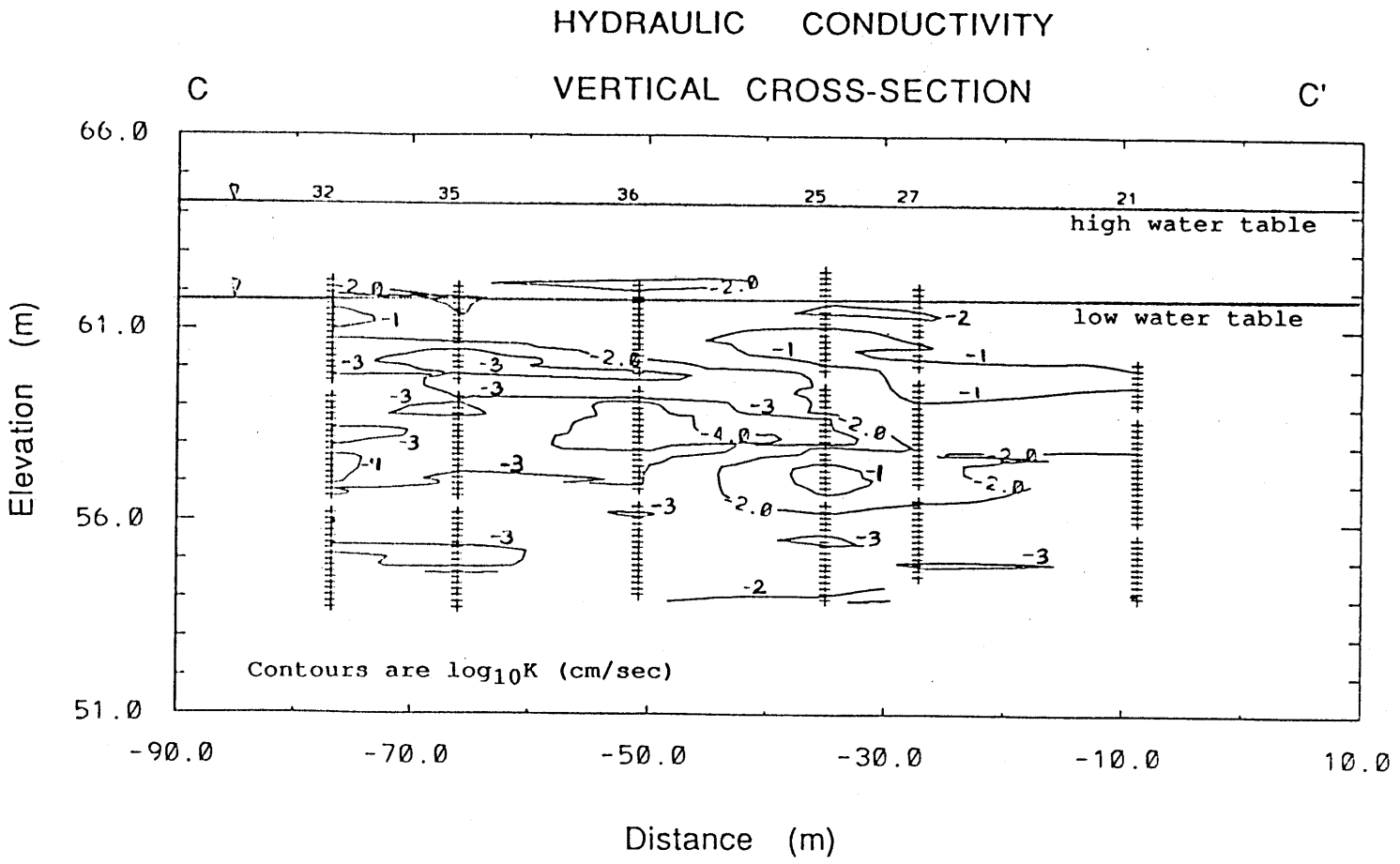

Figure 4-7. Hydraulic Conductivity Cross Section C-C'.

except above elevation 61 m, where the hydraulic conductivity in the region of wells K-32 and K-35 is also high.

From these three sections one can get a feel for the nature of the aquifer. There appears to be a channel-shaped deposit with larger hydraulic conductivity that extends from near wells K-12 out past wells K-21 and K-22. It is not clear from the data whether this channel extends beyond K-21 and K-22.

Recall that the definition of a trend depends on the scale of interest. For the tracer plume at CAFB, which as of February 1, 1988, is about 128 m long, the high-hydraulic-conductivity channel could be treated as a trend, although the dimensions of the channel are about one half the length of the plume. However, treating the channel as a trend is valid only during the early stages of plume development. During the early stages of plume development the asymptotic results of Gelhar and Axness (1983) may not apply, so it is not clear that detrending would be a useful exercise. After the plume has been in the aquifer for 3 years, it will be larger. At that time, a channel of the size observed with the K-wells will not be a trend. In fact, if one is interested in defining the asymptotic macrodispersivity of the shallow aquifer at CAFB, then one should consider the channel as a larger-scale heterogeneity. For the CAFB site, then, one can define multiple A_{ij} that would apply for problems on different scales. By treating the channel as a trend, the scale of the problem of interest is on the order of 100 m or less. If one were interested in transport over larger distances, then the channel should be treated as part of the overall aquifer heterogeneity.

Spatial Covariance Parameter Estimates of the Measured Data

In the most general case, six parameters describing the autocovariance of the random field are necessary to predict A_{ij}: the variance, σ_f^2, the correlation scales in the three principal directions $\lambda_1,\lambda_2,\lambda_3$, and two angles, θ and ϕ, (See Figure 2-1) describing the orientation of the major principal component of the autocovariance with respect to the mean flow direction. To simplify the analyses, assume the minor principal direction is vertical (θ=0) and that flow is horizontal. In horizontal layered deposits this will always be approximately correct because the lateral dimension of such deposits is much greater than the vertical dimension and flow is along the bedding plane. From a practical point

of view, even if the deposits are inclined at some small angle, say up to 5 degrees, the wells are still vertical and generally too far apart to influence the calculation. At small lags one would still be using data from the same well, and at larger lags one would be comparing the top of one well to the bottom of another; this would not be significant because the tails of the variogram are very uncertain. The inability to detect small values of θ will be shown in Section 5 to lead to large uncertainty in the prediction of A_{ij}.

In the horizontal, one can examine directional properties because the wells are distributed nonuniformly. By using data pairs oriented in preselected directions, the directional variogram is obtained (Journel and Hiujbregts, 1978).

For the measured hydraulic conductivity, the variance is 4.59, and three variograms are given in Figure 4-8. The top variogram depicts the spatial statistics in the vertical direction. In the calculation of this variogram, only couples representing data from the same well were used; no cross-well couples were allowed. The experimental variogram follows an exponential form up to a lag distance of about 2 m. Beyond 2 m, the variogram exhibits a "hole-effect" as it rises above the variance for lags up to about 5 m. The tail of the variogram falls below the variance.

The middle graph on Figure 4-8 contains the horizontal directional variograms for two directions. The two directions, 0 and 90 degrees, are defined by a counterclockwise rotation with respect to the x-axis in Figure 4-1. The lower graph on Figure 4-8 is the variogram in the horizontal direction assuming horizontal isotropy. On each variogram in Figure 4-8, a confidence interval about the variance is indicated. Before discussing the variograms, the confidence interval and its importance in the interpretation of the sample variograms will be explained.

For the fitted negative exponential variograms given in Figure 4-8, the sill value is set equal to the sample variance, which is the random variable that approximates the unknown true variance. If the lnK values are assumed to be independent samples from a population that is normally distributed, then one can define a confidence interval for the variance (Bhattacharyya and Johnson, 1977)

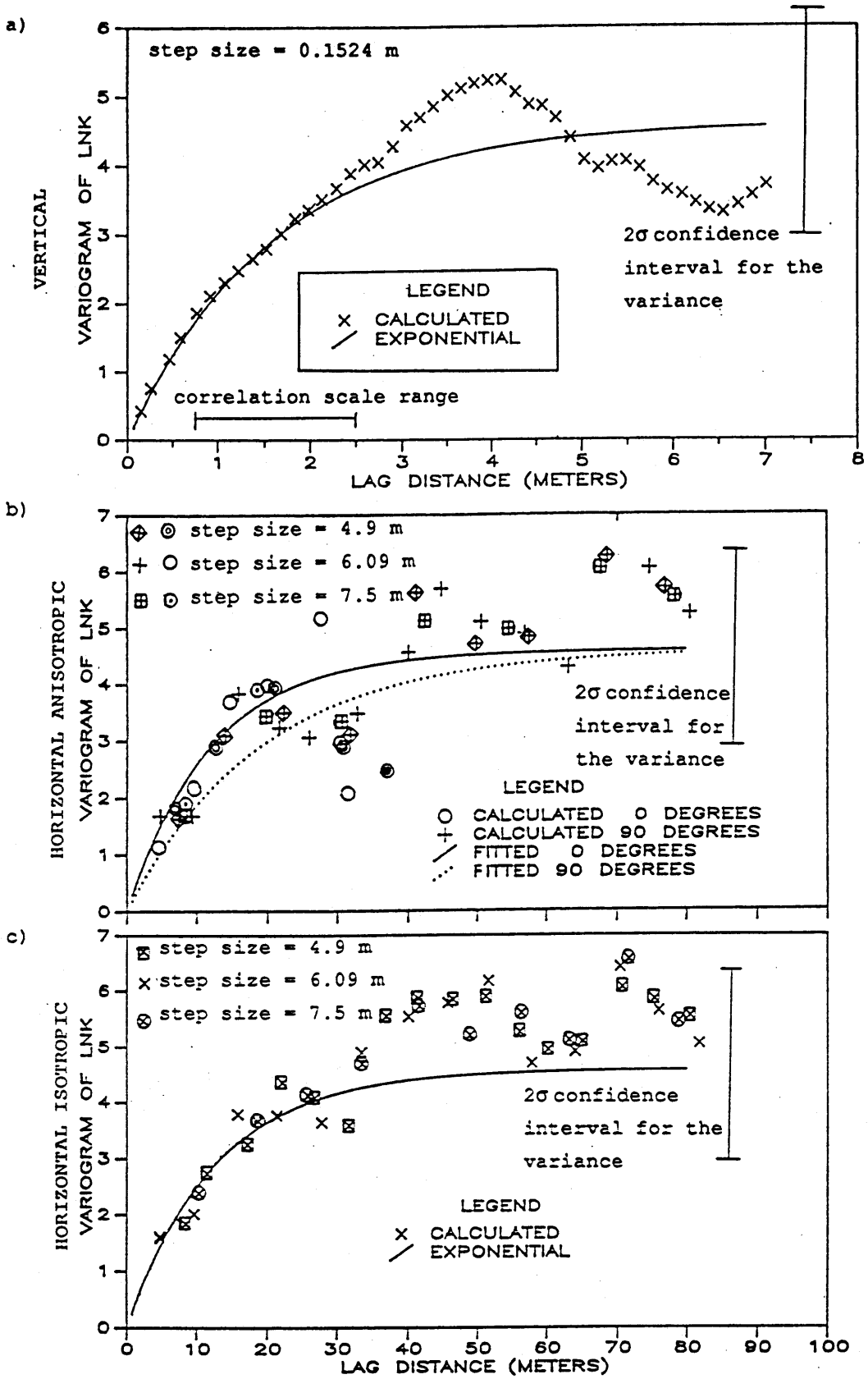

Figure 4-8. Vertical, Horizontal Anisotropic and Horizontal Isotropic Variograms of the Measured Hydraulic Conductivity.

$$P\left[\frac{(N-1)\hat{\sigma}_f^2}{\chi^2_{\alpha/2}} < \sigma_f^2 < \frac{(N-1)\hat{\sigma}_f^2}{\chi^2_{1-\alpha/2}}\right] = 1-\alpha \qquad (4-5)$$

where
- N = number of sample points
- $\hat{\sigma}_f^2$ = sample variance
- σ_f^2 = true lnK variance
- $1-\alpha$ = confidence level
- $\chi^2_{\alpha/2}$ = chi-square statistic

Equation 4-5 is a probability statement about the random interval covering σ_f^2. Although incorrect in a statistical sense, pragmatically one can say that the $(1-\alpha)$% confidence interval provides a likely range in which the true variance lies.

Another way to view the accuracy of the variance estimate, $\hat{\sigma}_f^2$, is to calculate the variance of that estimate. Benjamin and Cornell (1970), show that the variance of $\hat{\sigma}_f^2$ is given by

$$\text{VAR}[\hat{\sigma}_f^2] = \frac{2(N-1)}{N^2}\sigma_f^4 \qquad (4-6)$$

where
- N = number of samples
- σ_f^4 = squared population variance.

The data are assumed to be independent samples from a population of normally distributed random variables. For large N, and because σ_f^4 is unknown, we will approximate the variance of $\hat{\sigma}_f^2$ by

$$\text{VAR}[\hat{\sigma}_f^2] \approx \frac{2}{N}\hat{\sigma}_f^4 \qquad (4-7)$$

In this formula, as in the ones above, N is the number of independent samples. The number of independent samples at the CAFB site is unknown, although it is less than the total number of samples because correlated samples were taken intentionally to estimate the correlation structure of the lnK random field.

For the case of a time series characterized by a negative exponential autocovariance structure of known correlation scale, τ, Priestley (1981)

developed a factor M that is used to reduce the total number of samples to an equivalent number of independent samples. The number of independent samples is given by

$$N^* = \frac{N}{M_v} \tag{4-8}$$

where $M_v = (1+a^2)/(1-a^2)$
$a = \exp(-\Delta/\tau)$
Δ = sample spacing
τ = correlation scale
N = total number of samples
N* = number of independent samples

The above expression was developed for the analysis of a long time series of equally spaced data. The hydraulic conductivity profiles from each well at CAFB were constructed from equally spaced measurements along the length of the well screen. The wells, if grouped together, could be viewed as a long one-dimensional series of equally spaced data. The sample spacing is 0.15 m and, from Figure 4-8, the vertical correlation scale is 1.57 m. This yields M_v = 10.3. Therefore, the number of independent measurements is more than 10 times less than the total number of measurements due to the fine vertical spacing of samples relative to the correlation scale.

The reduction factor, M_v, can be estimated more simply by defining M as the ratio of the correlation scale to the sample spacing

$$M_v = \lambda/\Delta \tag{4-9}$$

This also yields M = 10.3. This simpler form for M is perhaps a little more intuitive than Eq. 4-8 and can be used as a model to estimate the additional reduction in the number of independent samples due to the horizontal correlation of data. In the horizontal, the reduction factor, M_h, is estimated from

$$M_h = \frac{W_t}{W_u} \tag{4-10}$$

where W_t = total number of wells
W_u = number of wells separated by a distance greater than λ_h

Wells that were separated by less than λ_h were clustered into a single well. The number of clusters, W_u, represents the number of independent horizontal sampling locations.

After correcting for the vertical and horizontal correlated structure of the data, the number of independent measurements is approximated by

$$N^* = \frac{N}{M_v M_h} \tag{4-11}$$

Using the total number of measurements, N = 1242, and the correlation scales obtained from the variograms in Figure 4-8, the vertical and horizontal correction factors are 10.3 and 2.1, respectively. Therefore, the 1242 samples yield only about 58 independent samples. The implication is that the variance of $\hat{\sigma}_f^2$ will be much larger when the correlated nature of the data set is taken into account.

If we define the variance of $\hat{\sigma}_f^2$ as

$$VAR(\hat{\sigma}_f^2) = \frac{2\hat{\sigma}_f^4}{N} M_v M_h = \frac{2\hat{\sigma}_f^4}{N^*} \tag{4-12}$$

then a two standard deviation confidence interval can be constructed about $\hat{\sigma}_f^2$ as:

$$\hat{\sigma}_f^2 - 2\sqrt{VAR(\hat{\sigma}_f^2)} < \sigma_f^2 < \hat{\sigma}_f^2 + 2\sqrt{VAR(\hat{\sigma}_f^2)} \tag{4-13}$$

The confidence interval for the variance of the measured hydraulic conductivity, with $\sigma_f^2 = 4.59$ and $N^* = 58$, is

$$2.89 < \sigma_f^2 < 6.30 \tag{4-14}$$

The width of the 95% confidence interval is quite large, but it must be remembered that the choice of the interval size is arbitrary. The 95% level implies that there is only a 5% chance that the interval does not include the true variance. The width of the one standard deviation is much narrower, 3.7 to 5.4, than the 95% interval, but one is accepting a 32% chance that the interval does not include the variance. In the remaining analyses, the 95% interval will be used, hence the bounding

values are quite unlikely. In Section 5, the influence of covariance parameter uncertainty on the predicted values of Aij is examined. The choice of the 95% level is intended to severely test the sensitivity of A_{ij} to unlikely parameter values. For comparison to the $\pm 2\sigma$ confidence interval, the 95% confidence interval about the variance calculated from the χ^2 statistic is

$$3.31 < \sigma_f^2 < 6.80 \qquad (4\text{-}15)$$

The total width of each interval estimate is about the same, 3.4 for the $\pm 2\sigma$ interval and 3.5 for the χ^2 interval. The difference between the two intervals is that the χ^2 interval is nonsymmetric, with more of the interval above the mean than below the mean. One should not view these confidence intervals as precisely defined limits because some judgment is required to determine the effective number of independent samples. However, the intervals do provide a good feel for a reasonable range for the variance that will be useful when deciding if additional refinements to the covariance parameter estimates are likely to yield statistically significant improvements in the parameter values. Clearly there is a large uncertainty in the estimate of σ_f^2 at the CAFB site.

This uncertainty has a direct impact on the theoretical variogram that is fitted to the sample variogram and hence, influences the correlation scale. In fact, by fitting the theoretical variogram to the sample variogram using the upper and lower limits of the variance, a range for the correlation scales is also determined. Figure 4-9 illustrates an objective way to put a range on the estimate of the correlation scale. If the sample variance is defined as the most likely value, then with the sill value of the negative exponential variogram set to the sample variance, the best visual fit to the rising portion of the sample variogram is used to give the most likely estimate of λ. The bounding values of λ are determined by an identical best visual fit to the rising portion of the sample variogram, where the sill value of the negative exponential covariance is set to the upper and lower confidence intervals of the variance. Although the range about λ is not a statistical confidence interval, the range does provide a useful estimate of the uncertainty in λ. The bounding values of λ also will be used to test the sensitivity of A_{ij} to parameter uncertainty. We can now return to the discussion of Figure 4-8.

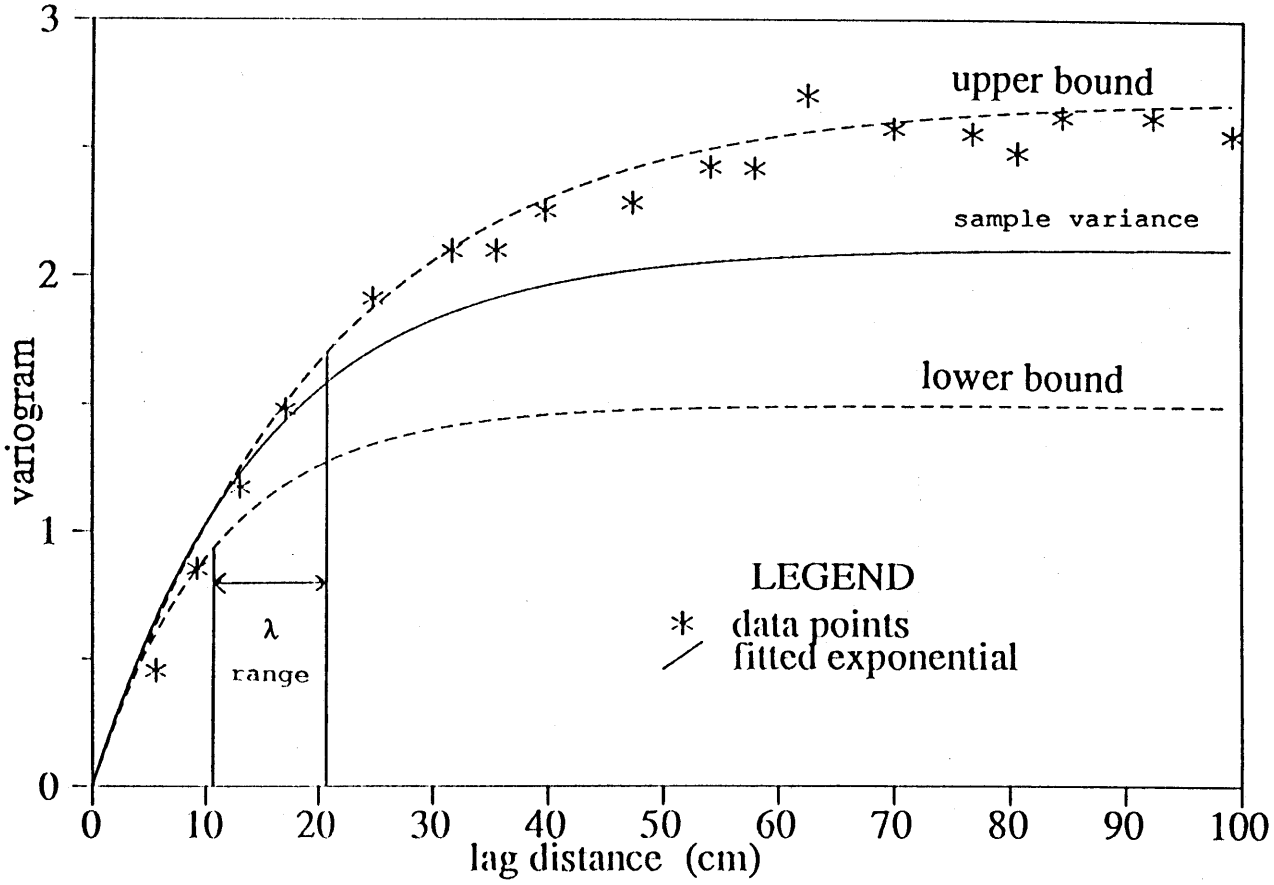

Figure 4-9. Definition of the Correlation Scale Range

The sample variogram in the vertical direction (Figure 4-8a) is closely approximated by the negative exponential covariance for lags less than 2 m. At lags greater than 2 m, the sample variogram appears to fluctuate about the variance. One might be tempted to view the larger lag fluctuations as indication of a trend. However, the question of trends in the vertical direction is a difficult one because of the problem of short data series.

Aquifers are sheet-like deposits with the lateral extent often orders of magnitude larger than the vertical dimension. At the CAFB site the K-wells were installed to the full depth of the aquifer. The shallow aquifer at CAFB is at most 8.5 m thick, and in some cases a meter or two less because of low water table. Therefore the maximum length of the data series from any well is on the order of 8 m.

When calculating the autocovariance function of a time series, Jenkins and Watts (1968) indicate that one should not consider lag distances greater than 20% of the full series length. For the wells at CAFB, the 20% criterion implies one should not consider lags greater than about 2 m. In the geostatistical literature, the conventional wisdom (Journel and Huijbregts, 1978) is to consider lags up to one-half the sample spacing (4.5 m at CAFB). Russo and Jury (1987a,b) showed some variograms from data that contained nonlinear trends that indicated that the existence of the trend could not be determined from the variogram unless lags greater than one-half the series length were considered. However, it is not the length of the data series alone that is of concern, but rather the length relative to the correlation scale. To fit an exponential covariance, one would like to have calculated the sample covariance to lags of 2 or 3 times the correlation scale. As long as 2 or 3 λ is less than 20% of the series length, or if λ is 5% to 10% of the total series length, then one can feel confident that the sample covariance is a good estimate, and if one observes significant deviation from the presumed stationary form beyond 3 or 4 λ then one should be able to determine if a data set contains a trend or not. On the other hand, when the series length is only 3 or 4 λ, then it becomes difficult to separate trend from randomness.

Identifying a trend from the variogram is particularly difficult in the vertical direction because the total length of data from each well is,

on average, 4.5 times the vertical correlation scale (λ_v); the maximum is 5.5 λ_v and the minimum is 3 λ_v.

Figures 4-10a and 4-10b show the hydraulic conductivity profiles for each of the wells after removing a constant mean value. Some wells (K-7, K-9, K-18, K-19, K-21. and K-22) appear to exhibit a linear trend. From other wells (K-14, K-15, K-20, and K-34) one might argue that a second-order trend is more appropriate. Finally, there are wells that do not exhibit any noticeable trend at all (for example, K-12, K-17, K-25, K-29, and K-35). Over the entire study region there does not appear to be a consistent vertical trend, even though what appears to be vertical trends can be observed locally. These trends may, in fact, be normal fluctuations.

In testing a maximum-entropy method for calculating the sample variogram, Sharp (1982) presented two synthetic data series generated using a first-order autoregressive process. The covariance of this process was of negative exponential form with a correlation scale of 9.5 units. The generated series and associated variograms are given in Figure 4-11.

The series are interesting because there are some subsections of length 30 to 50 units (roughly 3 to 5λ) which, if viewed alone, exhibit no trend and other subsections that exhibit marked first-order and second-order trends. If one were to construct a window of dimension 3 to 5λ, and slide it along these data series in Figure 4-11, many of the short series in the window would mimic the hydraulic conductivity profiles in Figure 4-10. It appears that although some of the hydraulic conductivity profiles show a trend, one could justifiably conclude that the hydraulic conductivity field as a whole does not contain a trend in the vertical.

Also of interest in Figure 4-11 are the variograms. The sample variograms deviate from the input exponential variogram and Sharp's maximum-entropy method. For illustration, a $\pm 2\sigma$ band has been constructed about the variance using Eqs. 4-8, 4-9, 4-12, and 4-13 with $\hat{\sigma}_f^2 = 1.0$, $\lambda = 9.5$, $\Delta = 1.0$, and $N = 250$. The deviations of the sample variogram from the exponential form fall within the $\pm 2\sigma$ band placed about the input variance of 1.0 (the sample variance was not stated in the paper). Looking at the sample variogram in Figure 4-8a, one sees

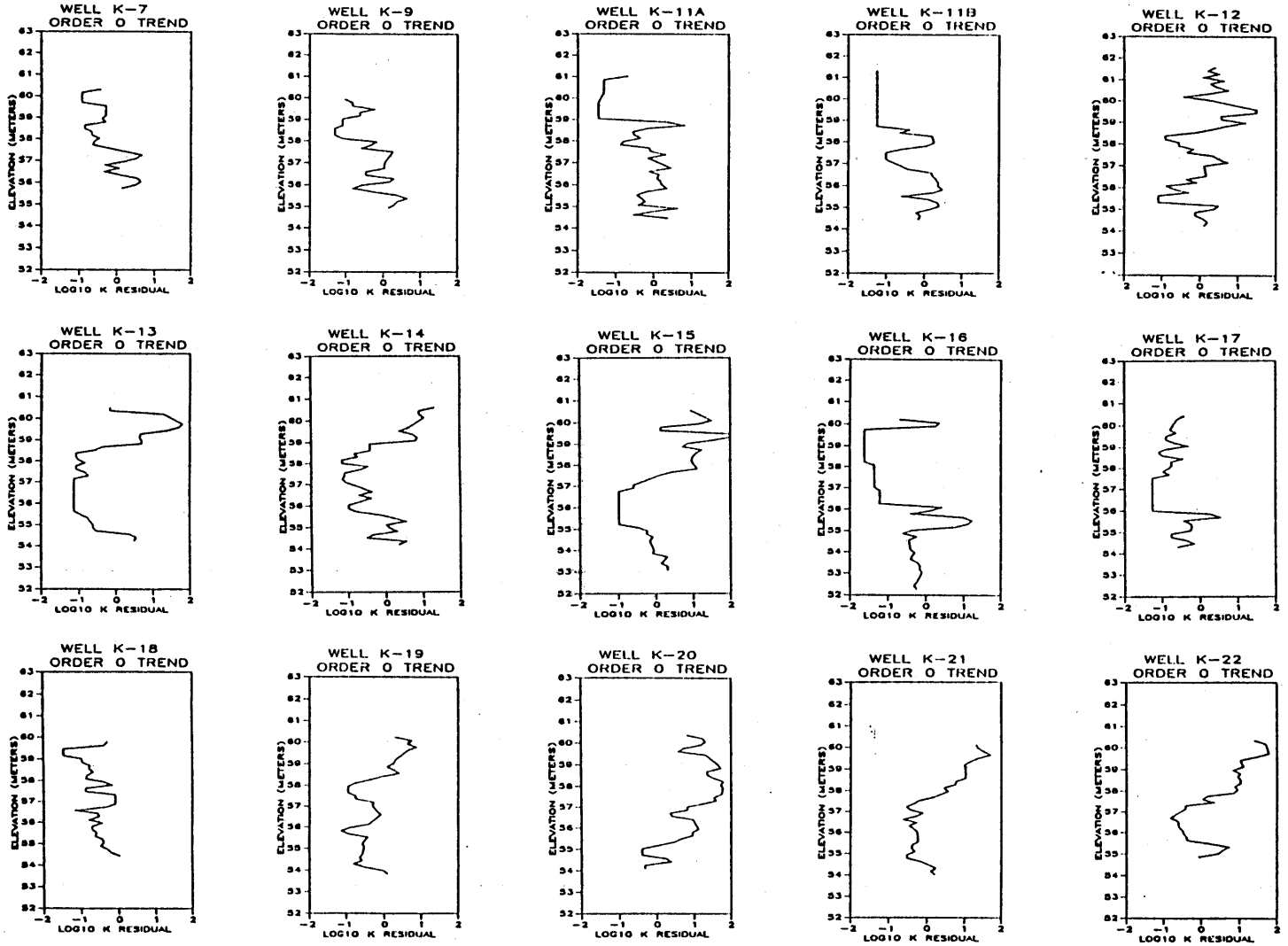

Figure 4-10a. Hydraulic Conductivity Residuals for Wells K-7 through K-22 After Removal of a Constant Mean Value.

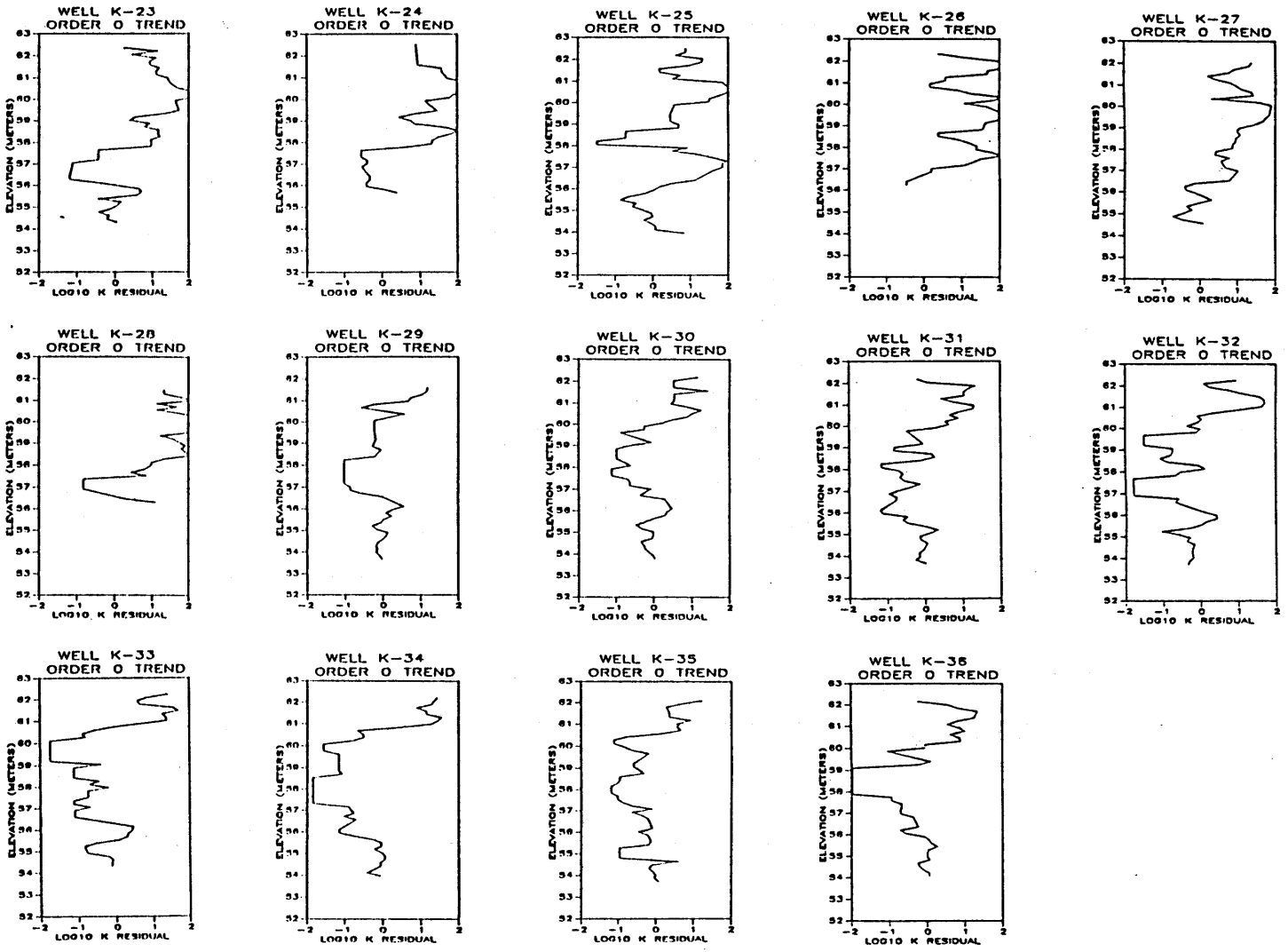

Figure 4-10b. Hydraulic Conductivity Residuals for Wells K-23 through K-36 After Removal of a Constant Mean Value.

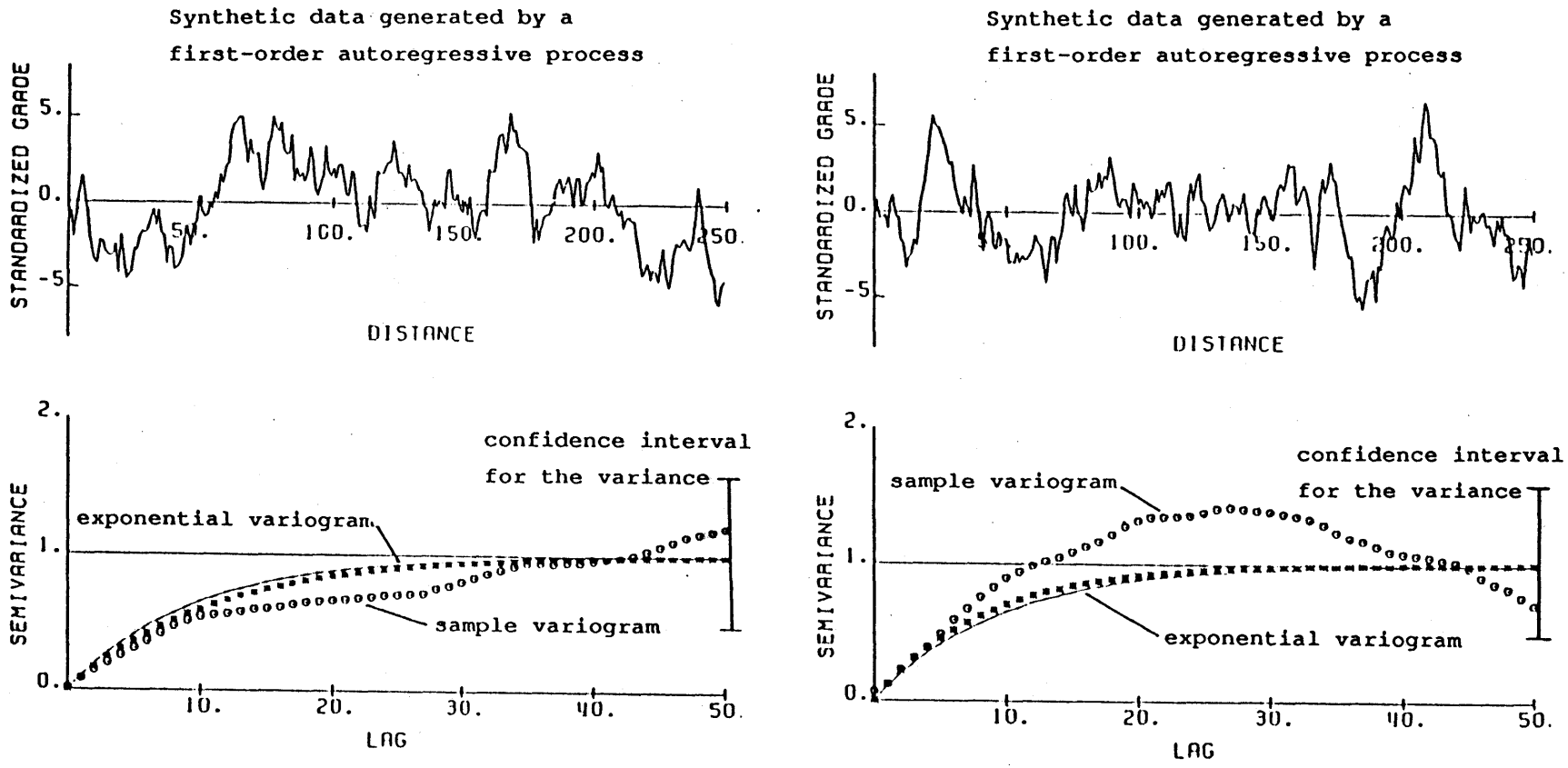

Figure 4-11. Synthetic Data Series Generated with an Exponential Variogram and the Corresponding Sample Variograms.

Source: Sharp, 1982, p. 462-463.

that the fluctuations about the exponential form also fall within the ± 2σ band and one could justifiably conclude, based on an analogy to Figure 4-11, that the hydraulic conductivity profiles observed at each well are not inconsistent with the assumption of a stationary random field.

Horizontal anisotropic variograms were calculated in two directions (Figure 4-8b). These two directions correspond to the principal components of the hydraulic conductivity tensor from Figure 3-4. For both directions, the variogram values using three different step sizes are plotted together. The wells are irregularly spaced in the horizontal, hence the choice of the step size can be important (Armstrong, 1984). By lumping the results of three step sizes together, we are less likely to be misled by a single variogram value. The two exponential variograms each rise to a sill at $\sigma_f^2 = 4.6$; the difference in the curves comes from the correlation scales, 12 m for 0 degrees and 19 m for 90 degrees. It is optimistic to think that one can confidently determine horizontal anisotropy based on the sample variogram in Figure 4-8b. Rather Figure 4-8b is presented to suggest the possible anisotropy in the variogram. However, additional study of the horizontal anisotropy of the variogram is unwarranted in light of Figure 4-8b. In the remaining analyses of the variograms, the lnK field will be assumed to be statistically isotropic in the horizontal plane.

The horizontal isotropic variogram (Figure 4-8c) is calculated by assuming no directional dependence in the horizontal plane. Again, the variogram values calculated using three step sizes (4.9, 6.1, and 7.5 m) are grouped on a single plot to give better definition to the sample variogram.

For lag distances up to 30 meters, the sample variogram follows an exponential form. At lag distances greater than 30 meters, the sample values lie above the sill of the exponential variogram, which equals the sample variance, $\sigma_f^2 = 4.6$. One might interpret the larger lag behavior as indicative of a trend; however, nearly all the sample values fall within the $\pm 2\sigma$ interval of σ_f^2.

Discussion

A number of points about the sample variograms are worth noting. In both the vertical and horizontal directions, the sample spacing of the hydraulic conductivity measurements was small enough to clearly define the rising portion of the variogram. Thus, there is a clear indication that the heterogeneity can be described as a correlated random field with a covariance structure, although the parameters of the covariance are uncertain. From the variogram in the vertical direction it would appear that the spacing of the measurements (0.1524 m) was much finer than necessary and that values as large as 0.61 m would have been adequate. Changing the vertical spacing when collecting data with the borehole flowmeter method is very simple because the operator controls the sampling interval. One does sacrifice some sensitivity by taking measurements at a larger interval because the hydraulic conductivity values are averaged over the interval. Hufschmied (1986) has shown that the integrating nature of the flowmeter measurements allows one to extract information on the variability of hydraulic conductivity on scales smaller than the measurement scale.

The horizontal spacing of measurements is controlled by the well locations. The placement of the wells is more important than the vertical sample interval because there is no way to extract information on conductivity variability in the horizontal at scales smaller than the well spacing. To obtain horizontal information at short separation distances, some of the wells must be close together. On the other hand, if too many wells are close together, then a poor estimate of the variance will result.

The sample variograms of the measured natural logarithm of K in the horizontal and vertical directions both exhibit exponential behavior up to lags that are roughly 30% of the largest sample dimension in either direction, where the maximum sample spacing in the horizontal and vertical directions is 116 and 8.5 m, respectively. Thus the sample variograms in Figure 4-8 were calculated to lags well beyond the recommended maximum value of 50% of the largest spacing (Journel and Huijbregts, 1978) or the more restrictive 20% value of Jenkins and Watts (1968). The divergence of the sample variogram from the exponential form at larger lags is therefore not unusual and is not statistically significant.

For all practical purposes, the variogram analyses are complete. The covariance is assumed exponential with a variance of 4.6 and correlation scales of 12.7 and 1.6 in the horizontal and vertical directions, respectively. From previous discussions it is clear that the variance is uncertain, hence the correlation scales are also uncertain. Using the procedure sketched out in Figure 4-9 a range for the λ's were obtained using the $\pm 2\sigma$ intervals constructed for the variance. Table 4-2 summarizes the parameters. In Section 5 these parameters will be used to estimate a range of macrodispersivities.

Table 4-2

BEST ESTIMATE AND RANGE OF VALUES OF
THE VARIANCE AND CORRELATION SCALES
OF THE MEASURED HYDRAULIC CONDUCTIVITY DATA

	Best	$\pm 2\sigma$ range	
Parameter	Estimate	Low Value	High Value
σ_f^2	4.6	2.9	6.3
λ_h	12.7	6.9	22.5
λ_v	1.6	0.75	2.5

ANALYSES OF NONSTATIONARY FIELDS

In the previous section the data on natural log hydraulic conductivity were analyzed assuming the random field was stationary. The resulting sample variograms at intermediate and large lags did not follow the exponential variogram form. On the basis of the variograms it is not possible to say if a trend is present in the data, and the parsimonious approach is to assume there is no trend. Nonetheless, until more data are collected so that a tighter band can be placed on the variance estimate one can presume a trend may be present and try to remove it to obtain the statistics of the detrended field. In this section methodologies for removing a trend and for finding the appropriate order of that trend are developed.

What is a trend?

For the purposes of this report, and for any practical application, a trend is defined as the slowly varying component of the random field. Slowly varying is a poorly defined term that implies that at a scale much smaller than the problem scale, the slowly varying term would appear nearly constant. For example, at the CAFB site, the tracer plume is about 130 meters long. At a horizontal scale of say 10 to 15 meters, a trend would appear to be nearly constant. The removal of a trend from the data will alter the variogram that is estimated form the residuals. The variance is reduced, but the trend should not influence the short lag portions of the variogram. If after removal of the trend, the short lag portion of the variogram has been affected, then the trend has removed too much of the variability.

Even with the large number of hydraulic conductivity values collected at CAFB it was not possible to prove or disprove the presence of a trend in the data. The most parsimonious solution is to assume the trend is absent because fewer parameters are required. Russo and Jury (1987b) showed that trends in the data are not often clearly discernible from the sample variogram, but that estimates of the variance and correlation scale of the underlying stationary random process may be significantly in error if the trend is not removed. The question one faces is not whether a trend is present, but rather will removing a trend change the variance and correlation scale values significantly. To address this question, the hydraulic conductivity data are detrended by fitting polynomials of order up to three and a variogram estimation is performed with the residuals. A least-squares approach will be used to detrend the lnK field and the variogram of the residuals will be calculated with the nonparametric estimator (Eq. 3-7).

Least Squares Approach

The natural log hydraulic conductivity field is decomposed into a trend vector of length m and a residual vector also of length m

$$\ln K(\mathbf{x}) = F(\mathbf{x}) + R(\mathbf{x}) \qquad (4\text{-}16)$$

where $F(\mathbf{x})$ is the trend, or drift, and $R(\mathbf{x})$ are the residuals. Following Neuman and Jacobson (1984) the residual vector is of zero mean and is characterized by the covariance matrix, $\mathbf{V}$, defined as

$$E[\mathbf{R}\mathbf{R}^T] = \mathbf{V} \tag{4-17}$$

The trend is expressed as polynomial of order N

$$F(\mathbf{x}) = \sum_{j=1}^{J_N} a_j P_j(\mathbf{x}) \tag{4-18}$$

where J_N is the number of terms in the polynomial, a_j are the coefficients to be determined and $P_j(\mathbf{x})$ are functions of the coordinate values. The trend will be assumed three-dimensional, hence there will be 4 terms for a first-order polynomial, 10 terms for second-order, and 20 terms for third-order. Eq. 4-16 is written in matrix notation

$$\ln\mathbf{K} = \mathbf{P}\mathbf{a} + \mathbf{R} \tag{4-19}$$

The generalized least-squares (GLS) problem minimizes the criterion

$$\Omega(\hat{\mathbf{a}}) = (\ln\mathbf{K} - \mathbf{P}\hat{\mathbf{a}})\,\mathbf{V}^{-1}\,(\ln\mathbf{K} - \mathbf{P}\hat{\mathbf{a}}) \tag{4-20}$$

with respect to $\hat{\mathbf{a}}$. The direct minimization (Schweppe, 1973) reduces to solving a system of linear equations of the form

$$\frac{\partial\Omega\hat{\mathbf{a}}}{\partial\hat{\mathbf{a}}} = \mathbf{P}^T\mathbf{V}^{-1}\,[\ln\mathbf{K} - \mathbf{P}\hat{\mathbf{a}}] = 0 \tag{4-21}$$

If the residuals, $R(\mathbf{x})$, are a stationary random field, we can write the i,j th term of $\mathbf{V}$ as (Neuman and Jacobson, 1984)

$$V_{ij} = \rho_R(S_{ij}) = \rho_R(0) - \gamma_R(S_{ij}) \tag{4-22}$$

where $\rho_R(S)$ = covariance function of R(x)
S_{ij} = $|x_i - x_j|$
$\rho(0)$ = variance of R(x)
$\gamma_R(S)$ = variogram of R(x)

The problem is simplified if solved as an ordinary least-squares regression because $\mathbf{V}$ is replaced by the identity matrix and Eq. 4-21 reduces to

$$\mathbf{P}^T \ln\mathbf{K} - \mathbf{P}^T\mathbf{P}\,\hat{\mathbf{a}} = 0 \qquad (4\text{-}23)$$

Neuman and Jacobson (1984) note that the OLS method is internally inconsistent because the residuals are assumed to be uncorrelated and suggest that an iterative generalized least-squares (IGLS) approach be used to properly account for correlated residuals. The IGLS method is computationally burdensome, and it is not clear that the IGLS method will yield significantly improved parameter estimates. Later it is shown that the error introduced by using the OLS method is small for the CAFB site.

Solution of the Ordinary Least Squares Equations

The solution of Eq. 4-23 proved to be more difficult than anticipated. The normal equations were solved using Gauss-Jordan elimination with full pivoting (Press et al., 1986) and QR Decomposition (Dongarra et al., 1979). The method of Singular Value Decomposition (SVD)(Press et al., 1986) was also considered. Unfortunately, SVD solves an auxiliary set of equations, and it was not clear that Eq. 4-21 could be cast in the auxiliary form. Equations 4-21 and 4-23 were to be solved with the same routine to demonstrate the improvement in the parameters estimates with the IGLS method, so the SVD routine was not considered. It was known beforehand that direct solution of the normal equations is susceptible to roundoff error (Press et al., 1986), but it was expected that double precision arithmetic on a MicroVax II (16 digits of accuracy) would be sufficient to avoid excessive roundoff error. Figure 4-12 shows the fitted trends at three wells obtained using a double precision QR routine. At all three wells the trends appear to follow the observed data, although the lack of curvature in the second order trend is suspicious. The trends do not follow each well precisely, but the regression minimizes the residuals over the entire domain, not just at three wells.

Despite the apparent reasonableness of the fitted curves in Figure 4-12, the lack of curvature in the second-order trend was suspicious. To check the QR results, a Gauss-Jordan routine using quad precision (32 digits) on a MicroVax II was implemented. The trends for the same three wells obtained using the Gauss-Jordan routine are shown in Figure 4-13. The quad-precision solution provides a better fit to the measured profiles than did the double-precision routine. All subsequent

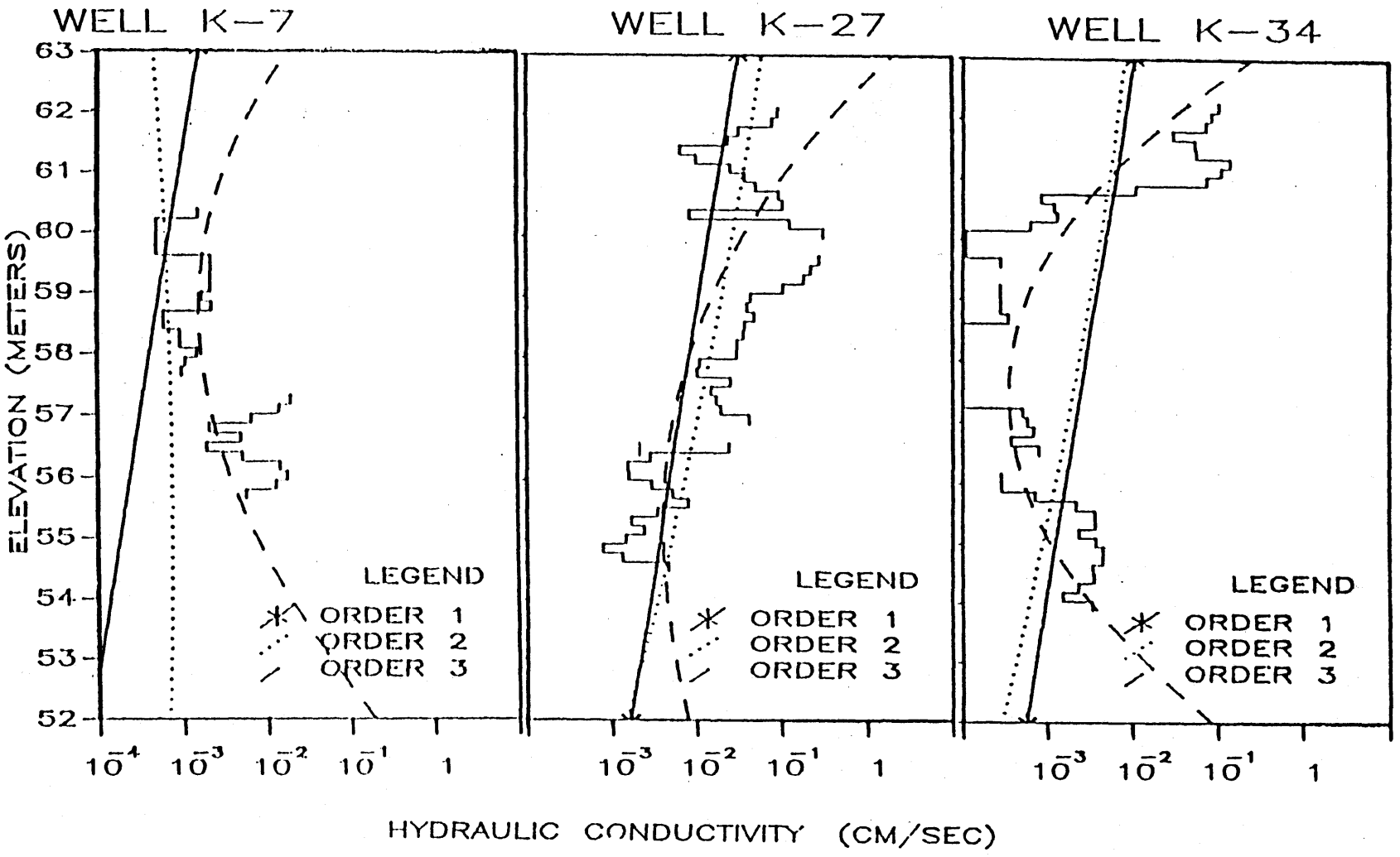

Figure 4-12. Comparison of the Fitted Trend Surfaces of Order 1, 2, and 3 from the QR Decomposition Solution and the Measured Hydraulic Conductivity Profiles of Wells K-7, K-27, and K-34.

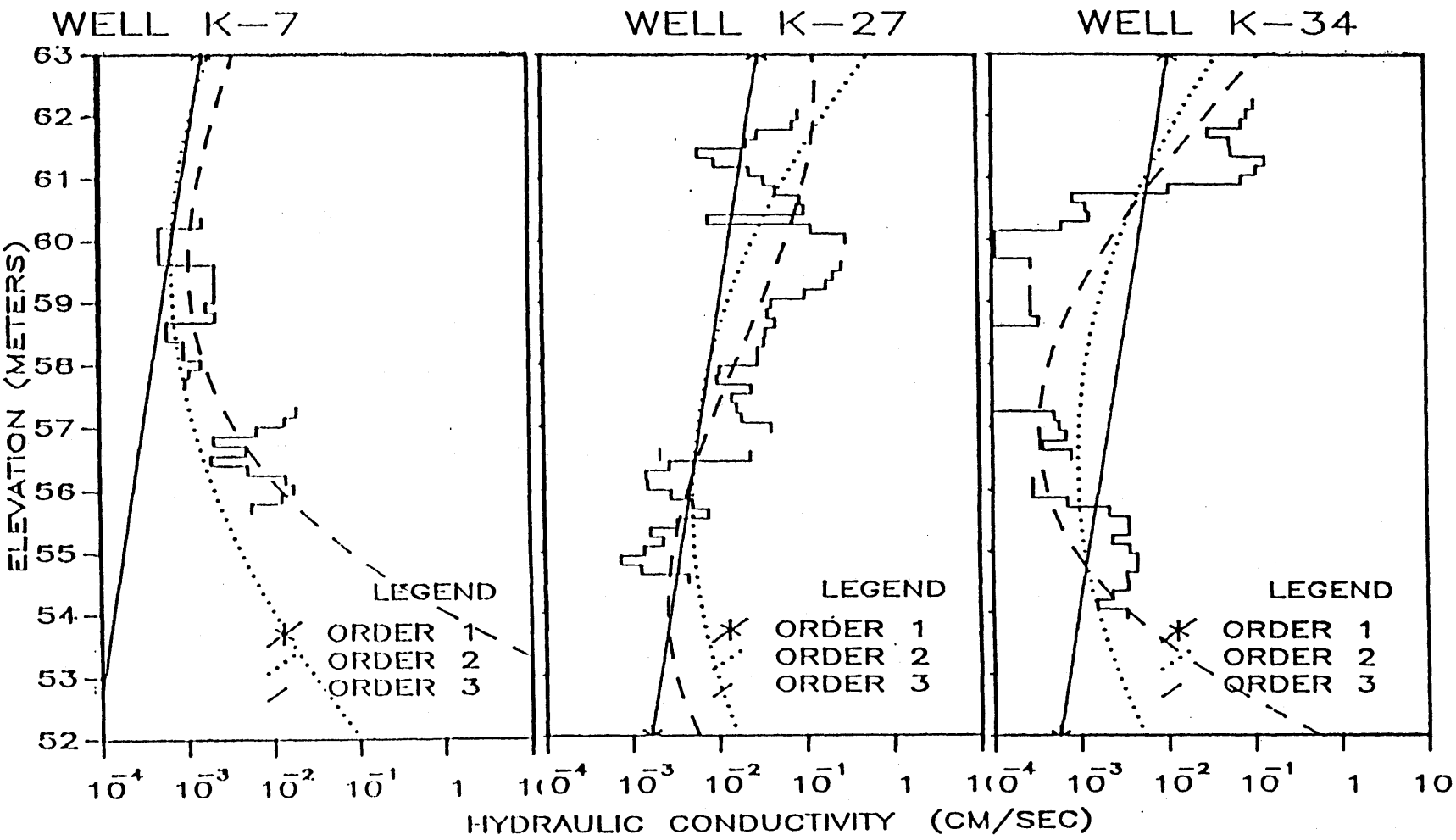

Figure 4-13. Comparison of the Fitted Trend Surfaces of Order 1, 2, and 3 from the Quad Precision Gaussian Elimination Solution and the Measured Hydraulic Conductivity Profiles of Wells K-7, K-27, and K-34.

regressions were performed using the quad-precision Gauss-Jordan Elimination routine. In retrospect, rescaling of the data would also have reduced the roundoff error.

Results of Detrending with OLS

Polynomial trends of order 1 to 3 were removed from the data using ordinary least-squares regression. The variograms of the residuals in the vertical and horizontal directions are presented in Figures 4-14 and 4-15, respectively. In the vertical, the shape of the variograms in Figure 4-14 are not changed substantially compared to Figure 4-8a until a trend of order 2 or 3 is removed. The third-order trend produces the most stationary-looking variogram; however, the curvature of the third order trend in Figure 4-13 is quite large. The question of scale becomes important in the vertical. If the tracer plume spreads over much of the vertical extent of the aquifer, then the third-order trend may be filtering out some of the true randomness.

In the horizontal, the higher the order of the polynomial, the more stationary the variogram appears. This, of course, is expected. Data at lags less than 10 m were unaffected as higher-order polynomial trends were removed, but data at lags greater than 15 m were influenced by detrending. The size of the plume is on the order of 130 m already, hence variations at lags of 15 m must be considered random. It would appear that the third-order trend is removing too much of the variability.

The log hydraulic conductivity residual profiles for all the wells are given in Figures 4-16a,b, 4-17a,b, and 4-18a,b for trends of order 1,2, and 3, respectively. These profiles are plotted as a continuous line to facilitate the visual comparison. The profiles of residuals from the first-order trend and to a large degree the second-order trend are modified only slightly compared to the original profiles. It is not until a third order trend is removed do we see substantial straightening of the profiles in some wells (for example, K-7, K-9, and K-35). Most of the other wells have profiles that still appear nonstationary. This inability to remove the trends in the vertical log profiles is another indication that in fact the variation in the profiles represents random fluctuations and not a large-large trend.

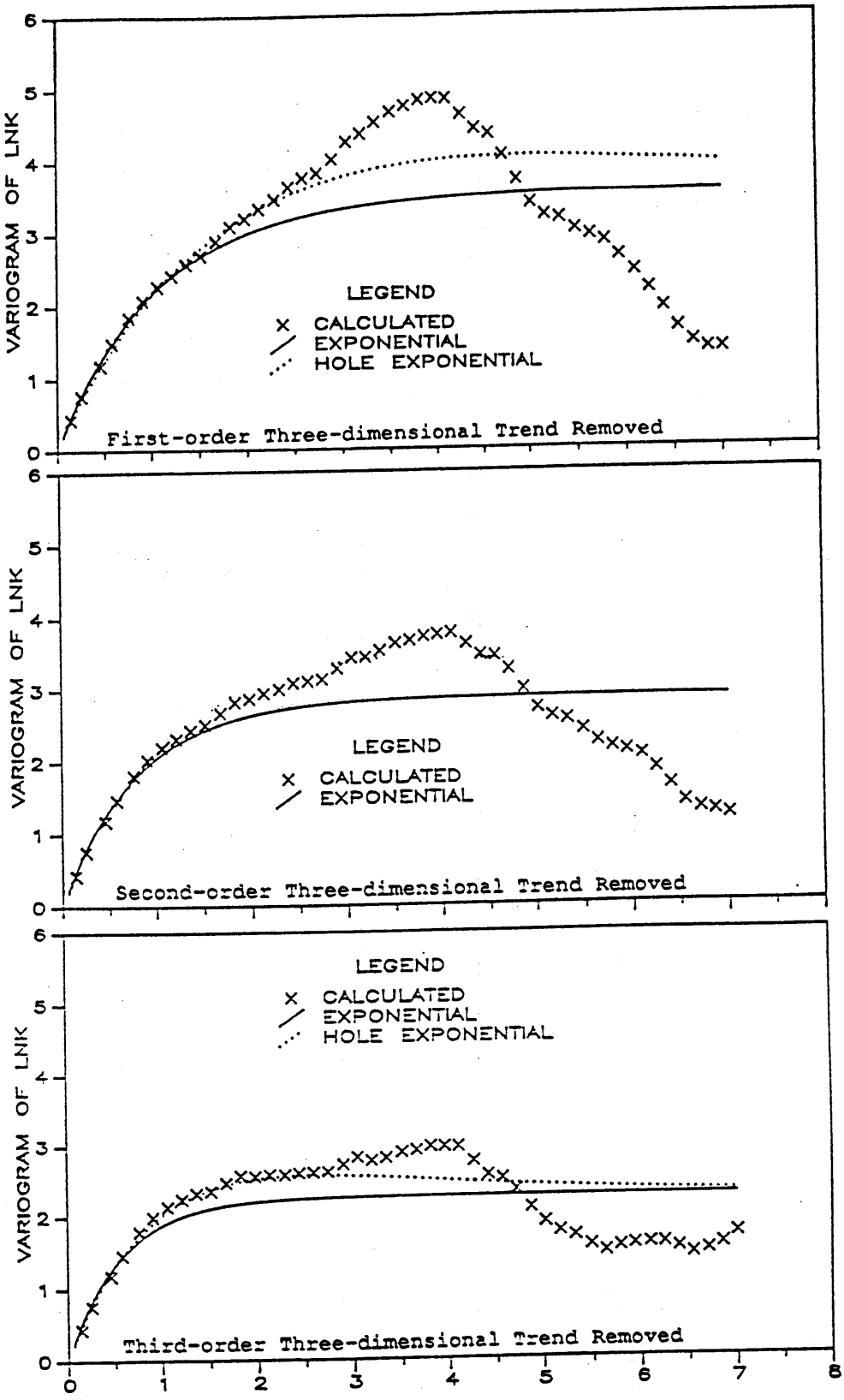

Figure 4-14. Variograms in the Vertical Direction After Removing Trends of Order 1, 2, and 3.

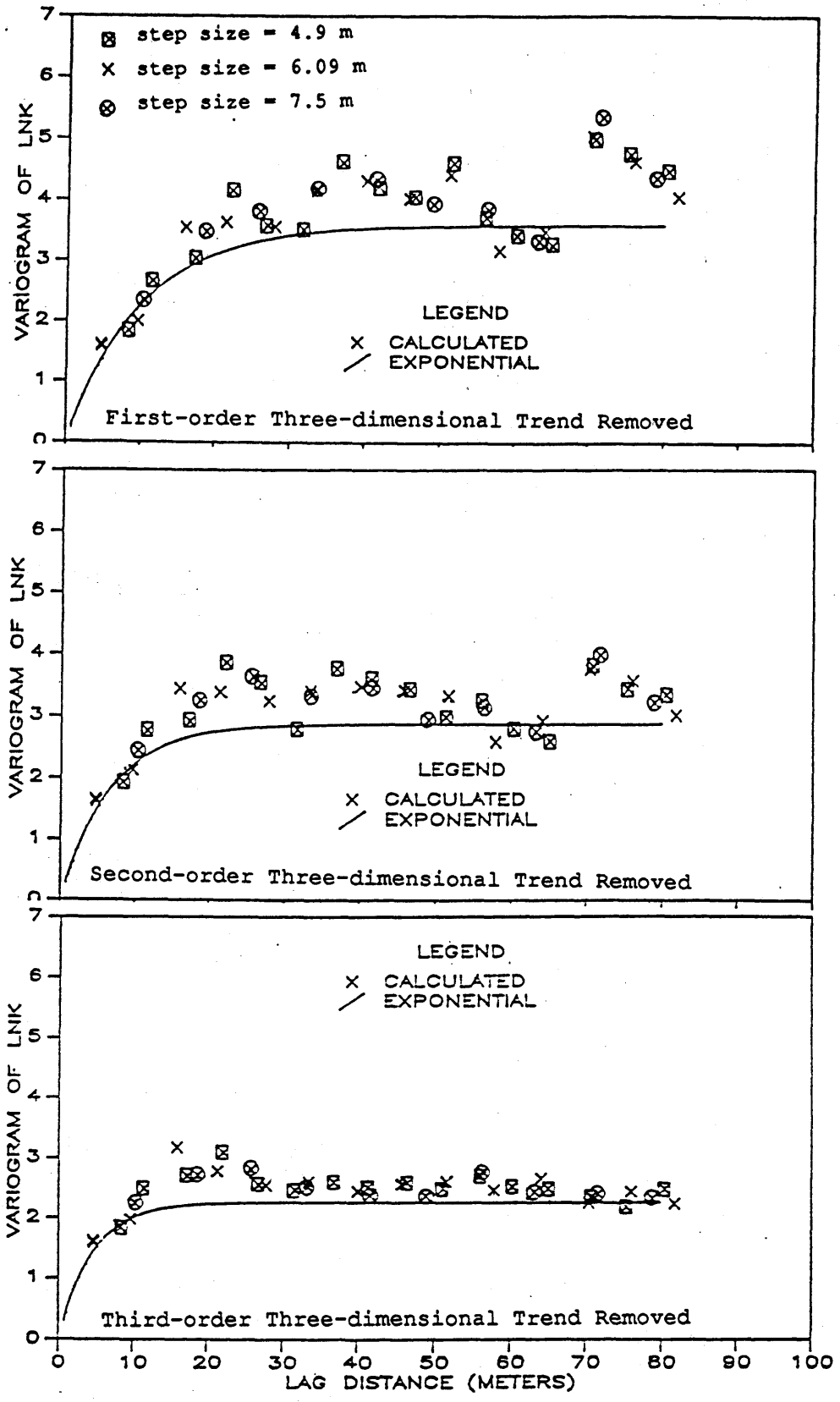

Figure 4-15. Horizontal Isotropic Variograms After Removing Trends of Order 1, 2, and 3.

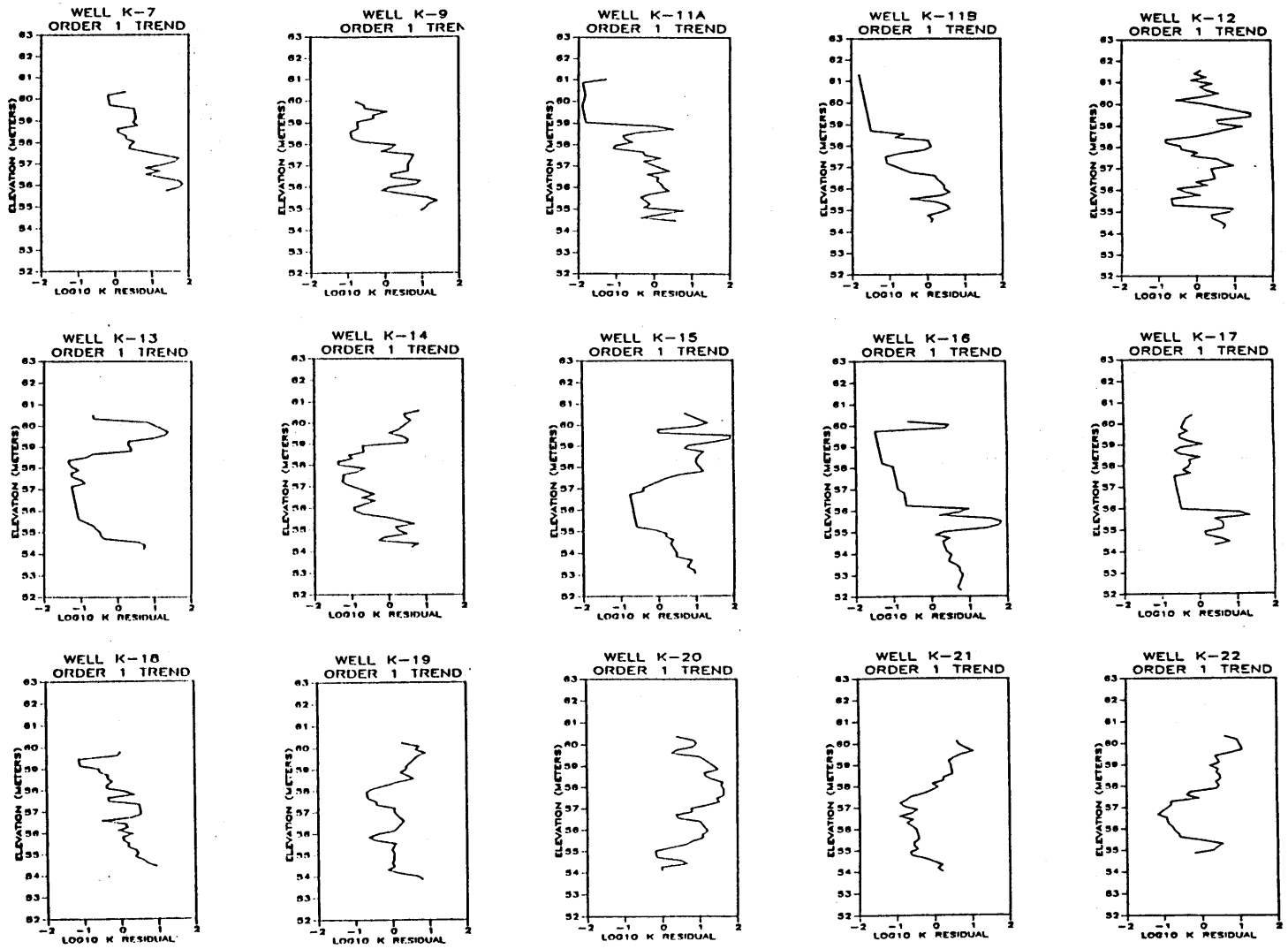

Figure 4-16a. Hydraulic Conductivity Residuals for Wells K-7 through K-22 After Removal of a First Order Trend.

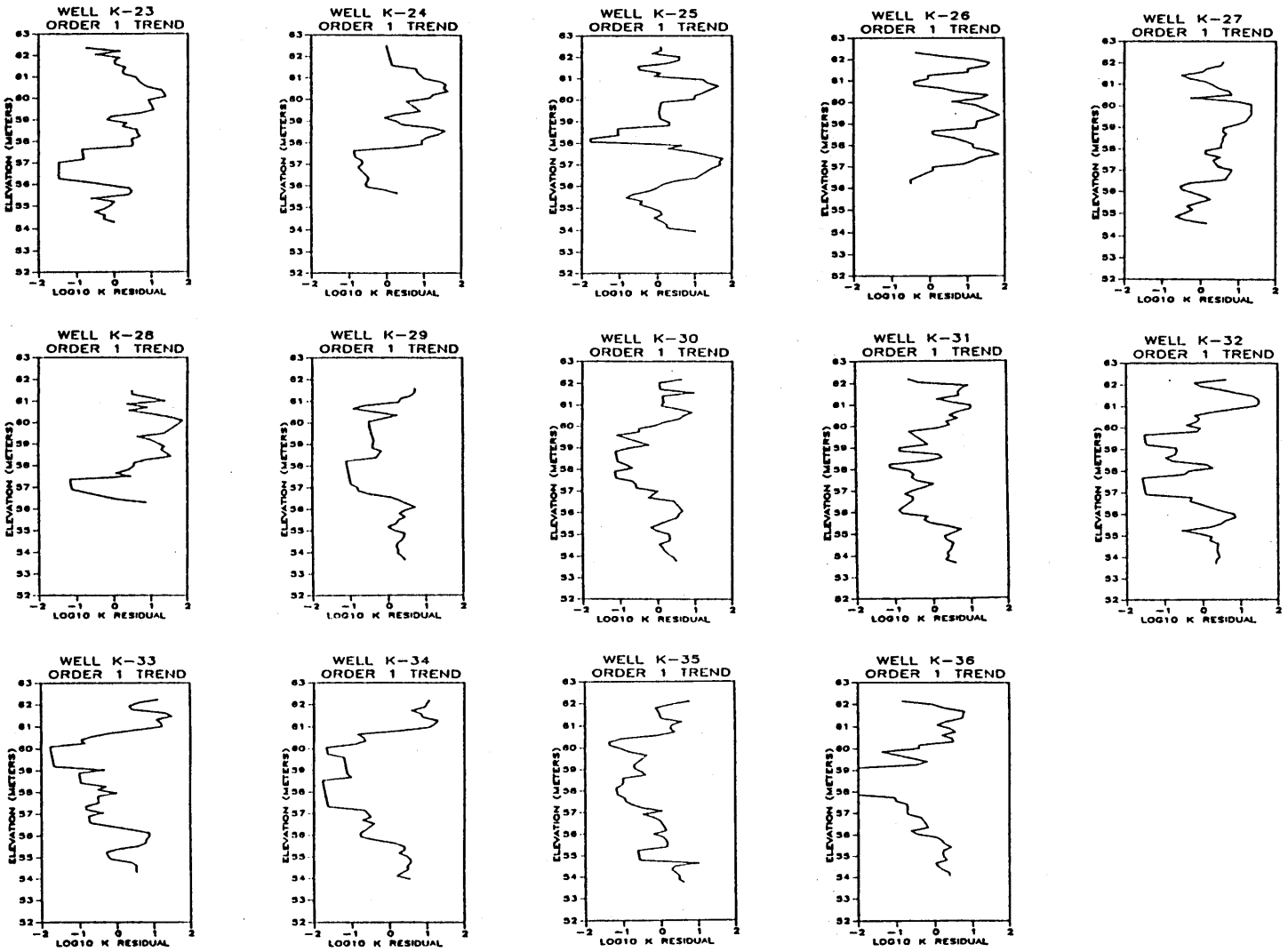

Figure 4-16b. Hydraulic Conductivity Residuals for Wells K-22 through K-36 After Removal of a First Order Trend.

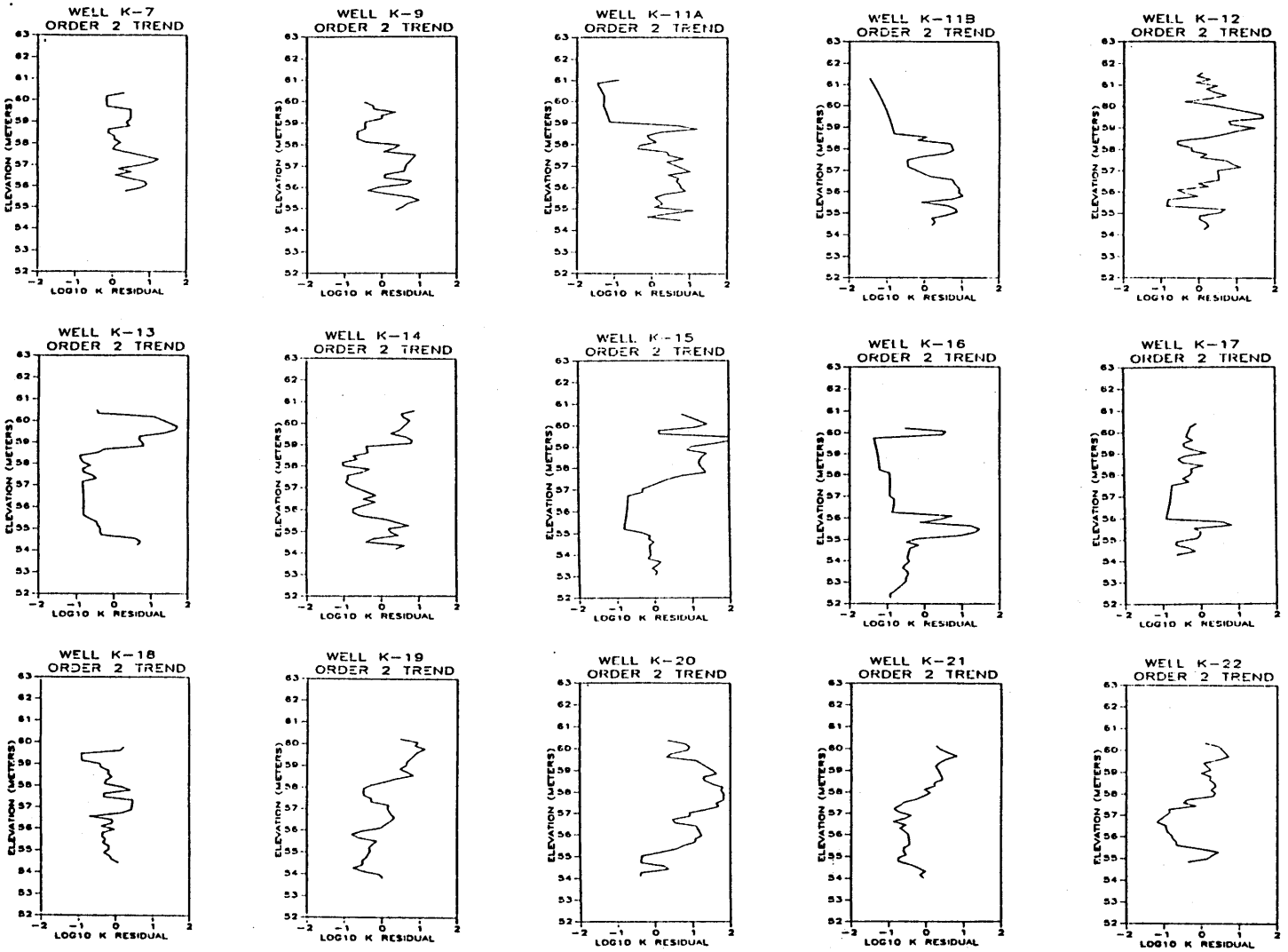

Figure 4-17a. Hydraulic Conductivity Residuals for Wells K-7 through K-22 After Removal of a Second Order Trend.

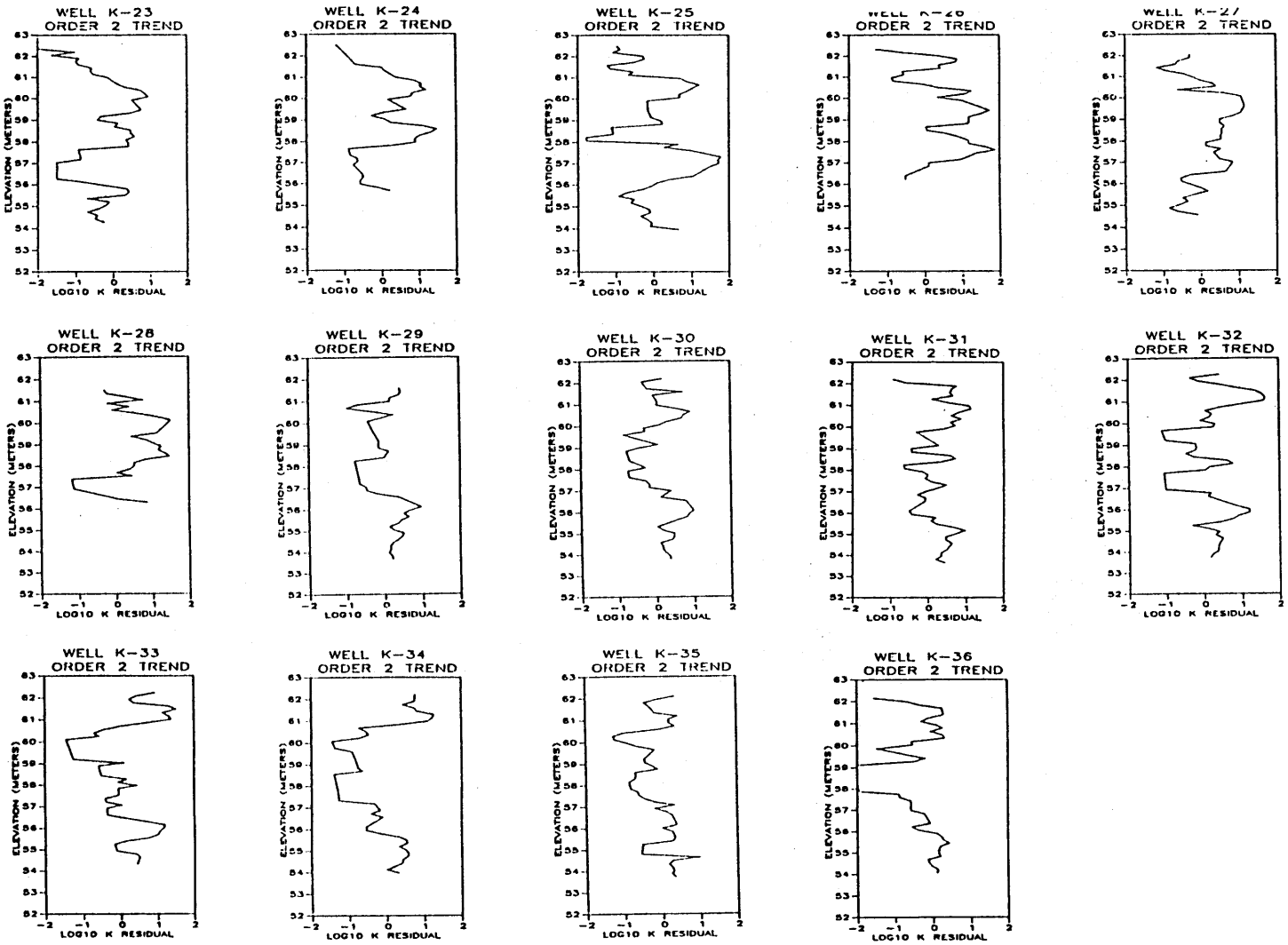

Figure 4-17b. Hydraulic Conductivity Residuals for Wells K-22 through K-36 After Removal of a Second Order Trend.

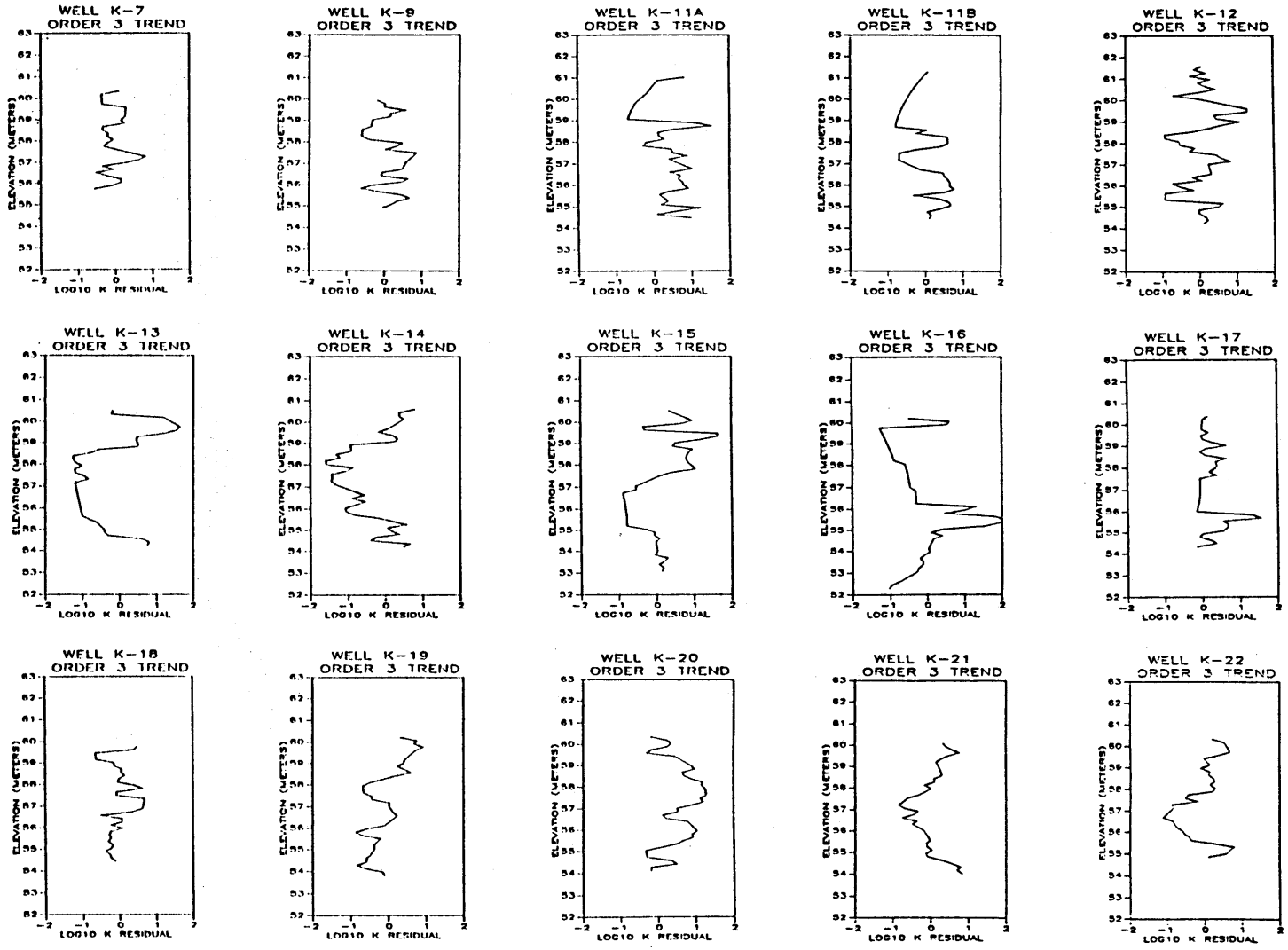

Figure 4-18a. Hydraulic Conductivity Residuals for Wells K-7 through K-22 After Removal of a Third Order Trend.

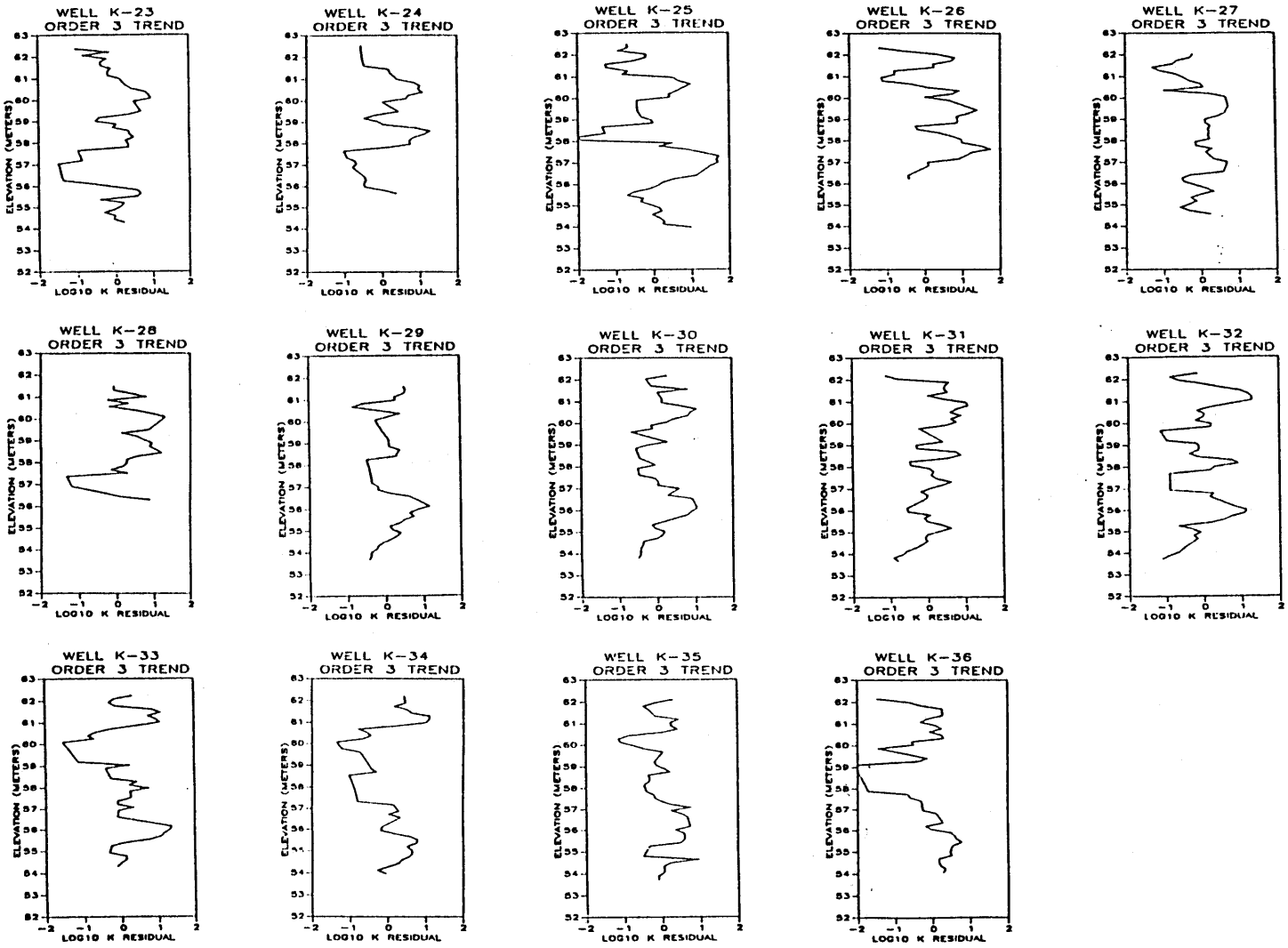

Figure 4-18b. Hydraulic Conductivity Residuals for Wells K-22 through K-36 After Removal of a Third Order Trend.

Figures 4-19 to 4-21 are the fitted trend surface as a function of depth in the aquifer. The third-order trend surface is quite contorted and takes on peculiar values immediately outside the areas of well control.

Horizontal Detrending

Additional trend surfaces were generated assuming there is no trend in the vertical direction, hence only a horizontal dependence is included in the fitted polynomial. The resulting horizontal variograms and trend surfaces are given in Figures 4-22 and 4-23. The vertical variograms are the same as in Figure 4-9a because they do not change when a two-dimensional trend is removed.

Table 4-3 summarizes all the variance and correlation scale values from the detrended data.

Table 4-3

VARIANCE AND CORRELATION SCALES
AFTER DETRENDING

HORIZONTAL AND VERTICAL TRENDS

Order	σ_f^2	λ_v (m)	λ_h (m)
1	3.6	1.08	10.0
2	2.9	0.80	6.7
3	2.3	0.57	4.7

HORIZONTAL TRENDS ONLY

Order	σ_f^2	λ_v (m)	λ_h (m)
1	4.0	1.25	11.5
2	3.6	1.10	9.5
3	3.4	0.90	9.0

Discussion

The measured hydraulic conductivity data were detrended using three-dimensional and two-dimensional polynomials of order 1, 2, and 3. As anticipated, the variograms of the residuals "look" more like the variogram of stationary random processes the larger the order of the

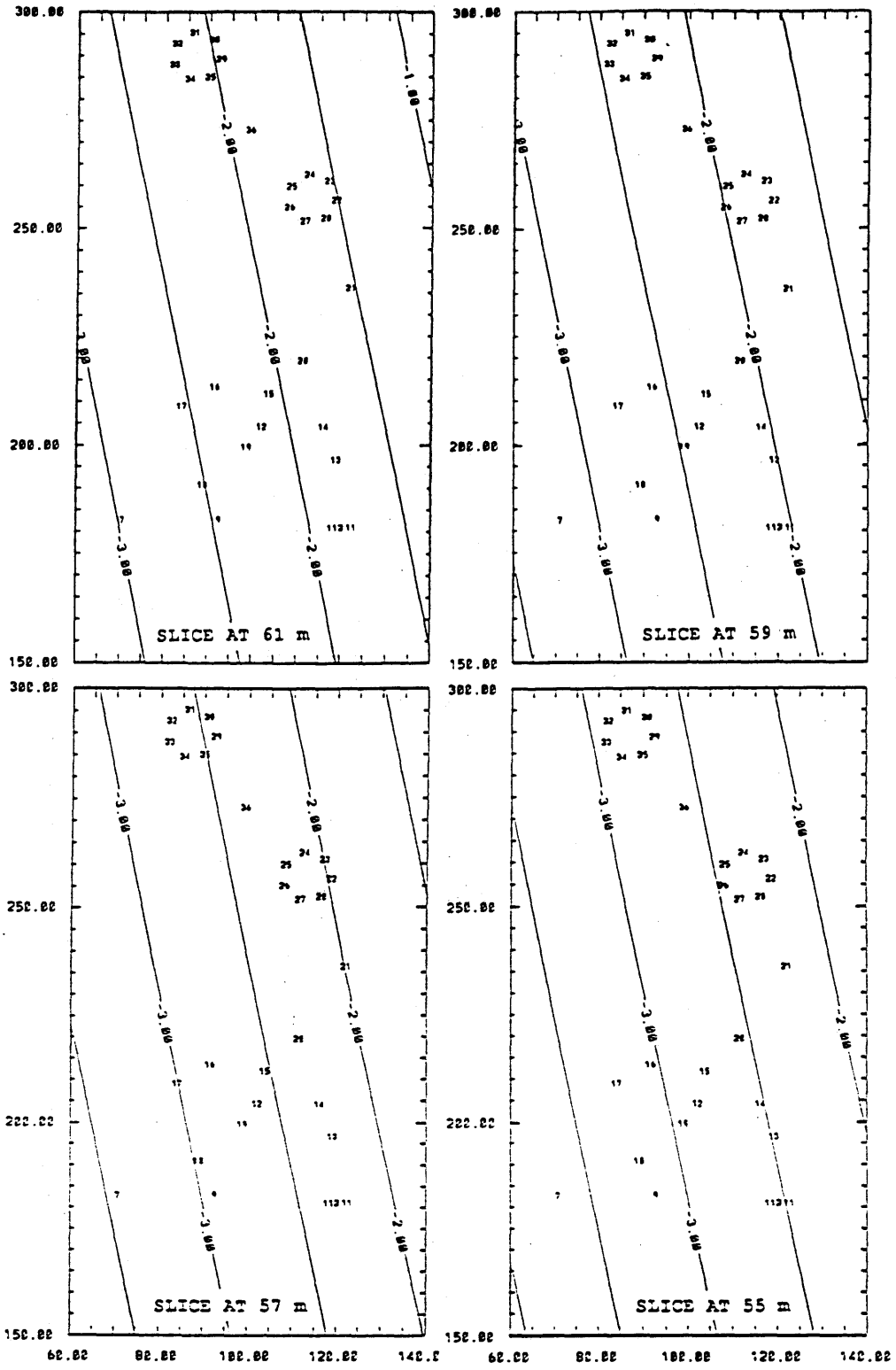

Figure 4-19. Contours of Four Horizontal Slices of the First Order Three-Dimensional Trend Surface.

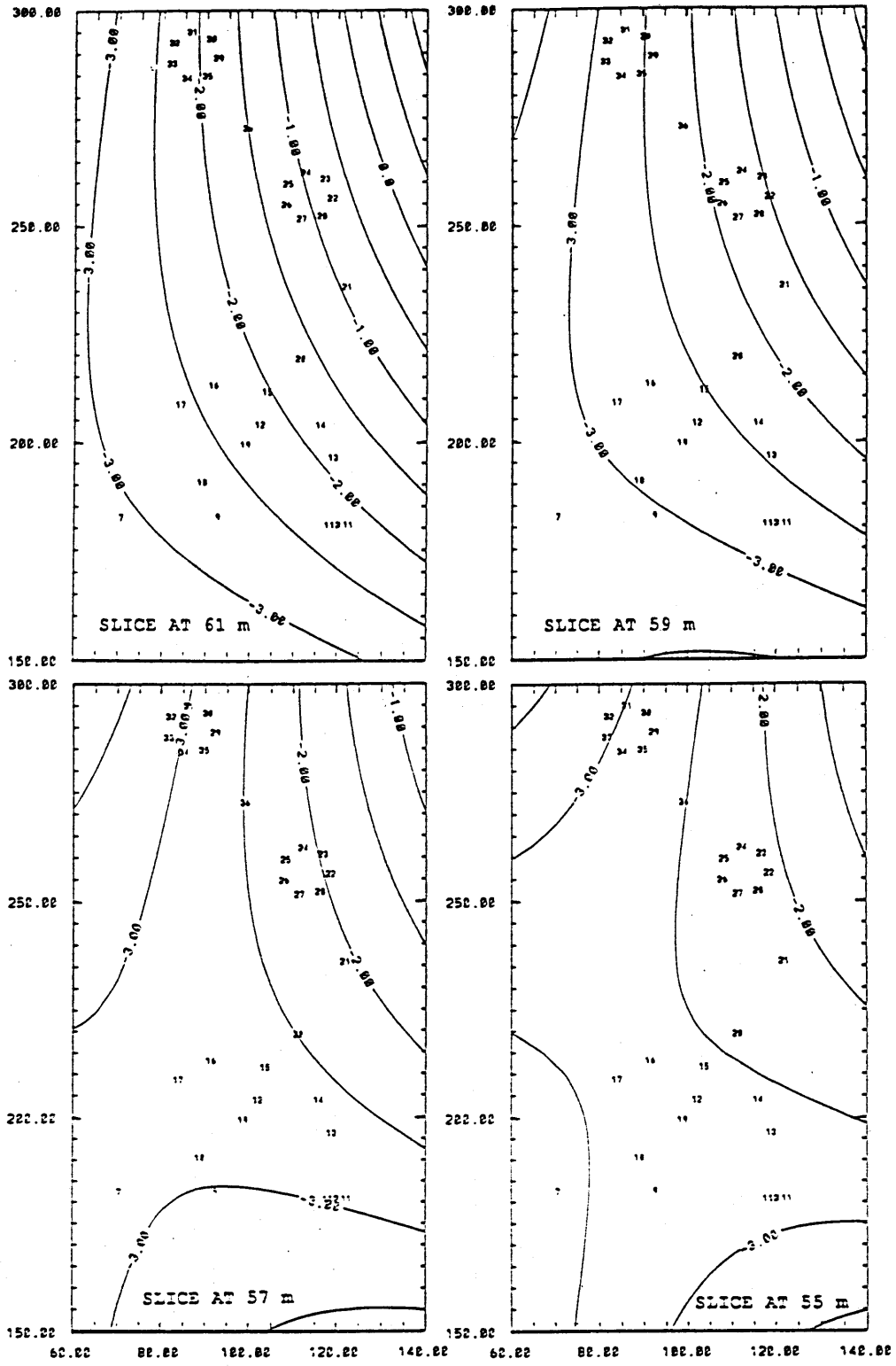

Figure 4-20. Contours of Four Horizontal Slices of the Second Order Three-Dimensional Trend Surface.

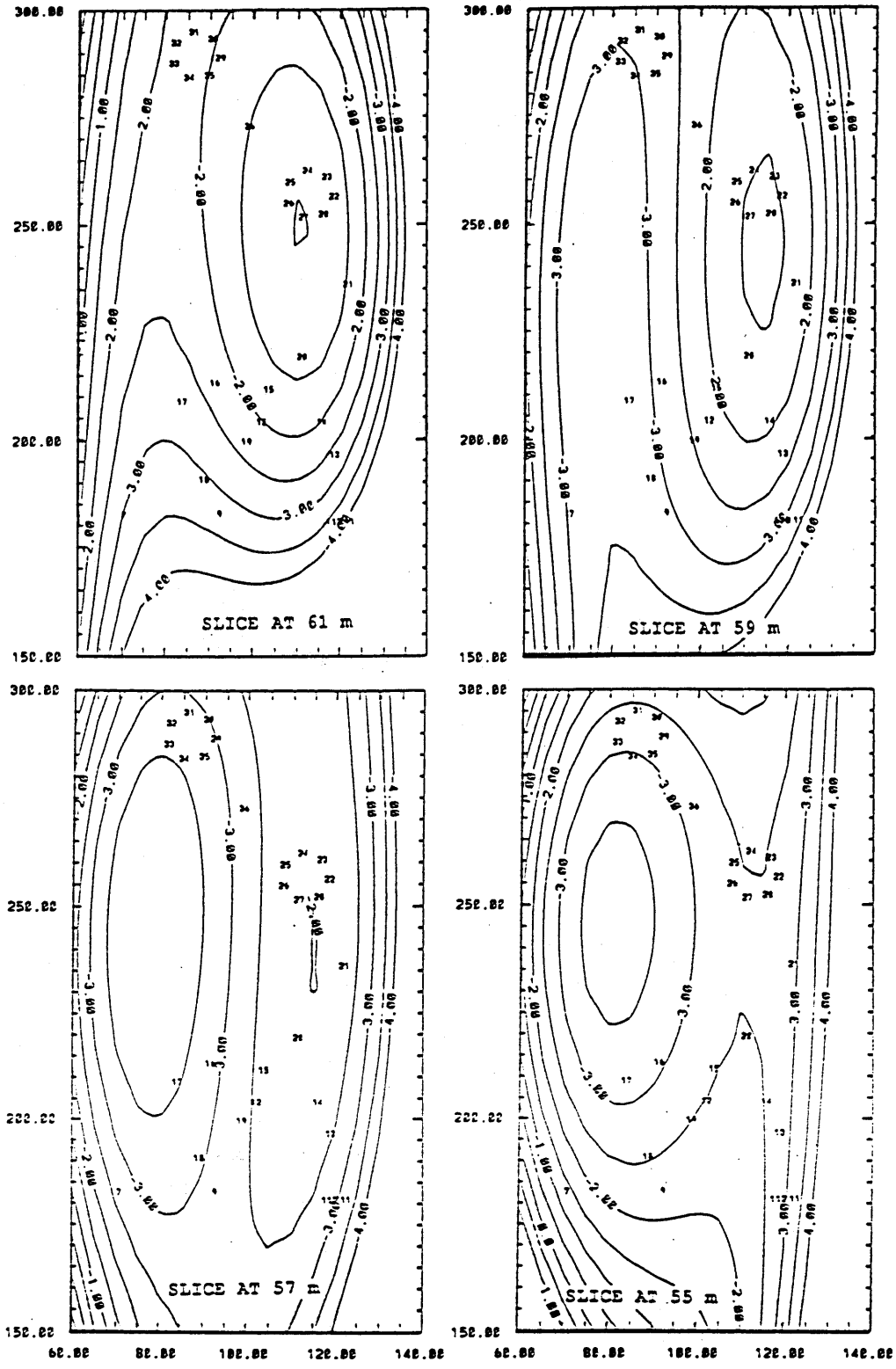

Figure 4-21. Contours of Four Horizontal Slices of the Third Order Three-Dimensional Trend Surface.

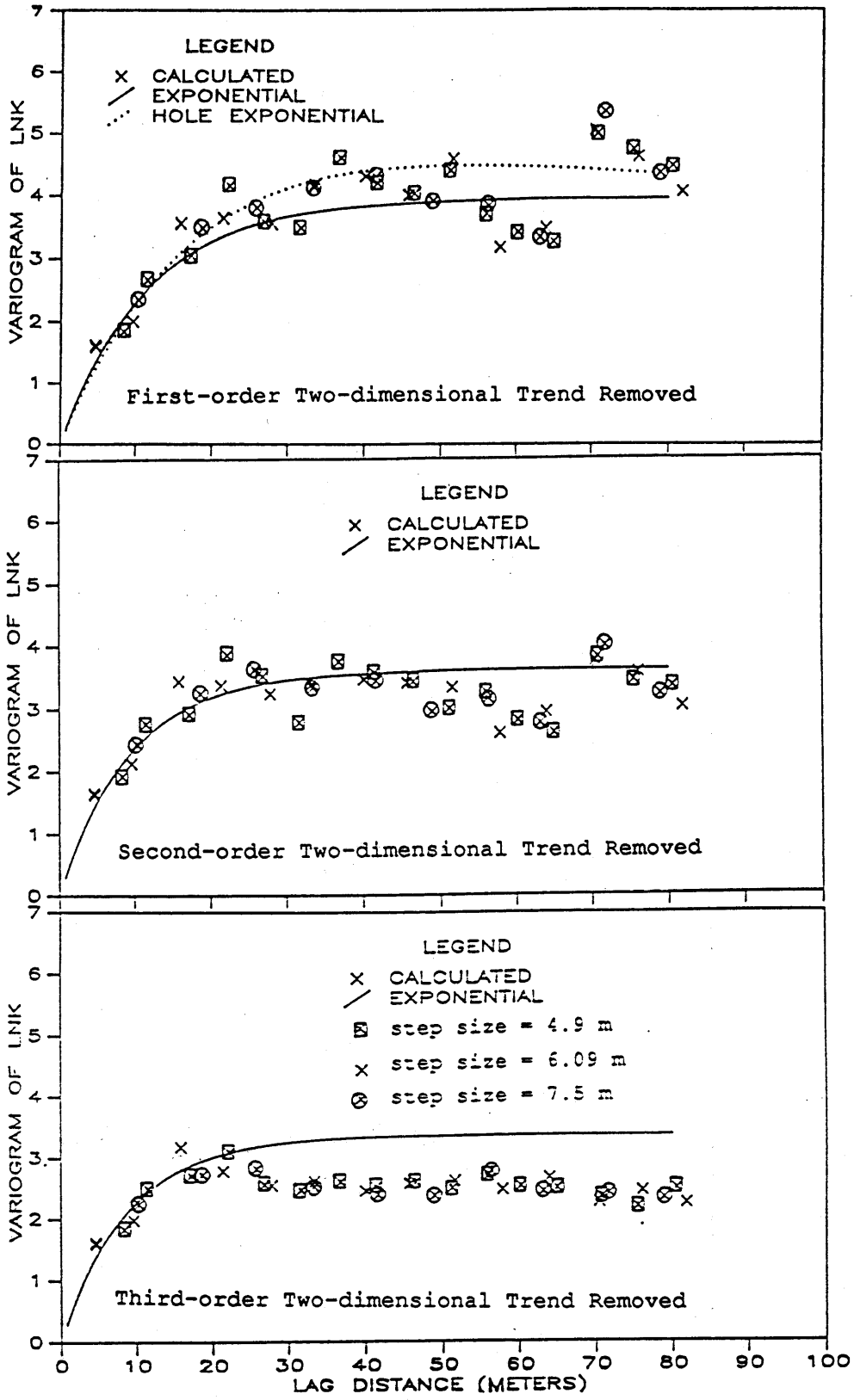

Figure 4-22. Horizontal Isotropic Variograms of the Residual Hydraulic Conductivity After Removal of Two-Dimensional Trends of Orders 1, 2,and 3.

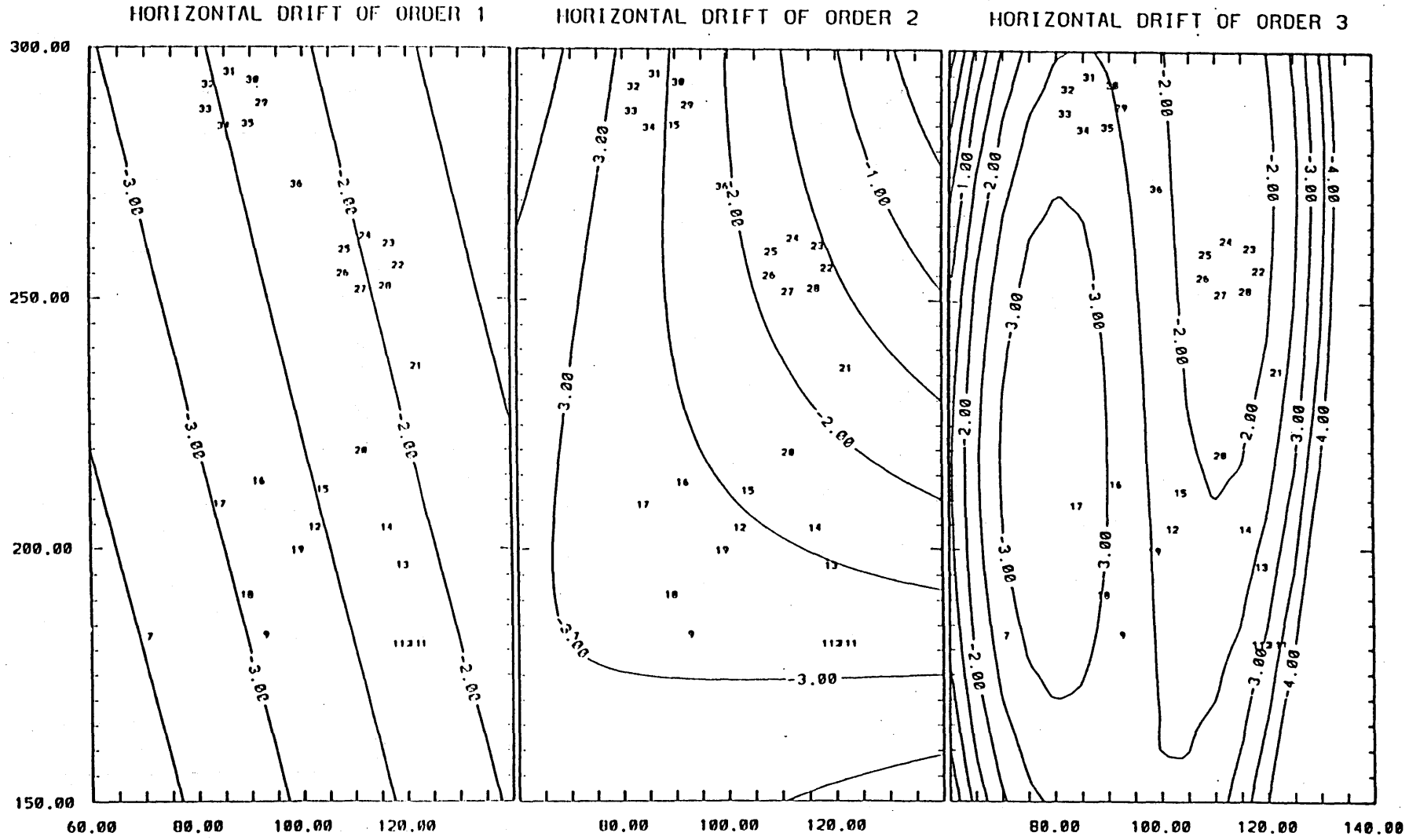

Figure 4-23. Two-Dimensional Trend Surfaces of Order 1, 2, and 3.

polynomial. Nonetheless, one would have difficulty defending a trend of order 1, 2, or 3 as being best based on the variograms in Figures 4-14, 4-15, and 4-22.

In Table 4-3 one can see that the parameters resulting from detrending with polynomials of order 1 and 2 fall within the confidence bands estimated for the covariance parameters of the measured hydraulic conductivity (Table 4-2). Only for the third-order trend do the covariance parameters fall outside the range of σ_f^2 and λ.

One way to decide on the most appropriate order trend is to examine the trend surface itself to see if it is consistent with other available information about the site. Figure 4-24 shows the contours of the two-dimensional trend surfaces and the path of the leading edge of the tracer plume as of August, 1987. The tracer is continuing in the same direction based on information as of December, 1987. The first- and second-order trends are compatible with the observed path of the tracer. Although it is unlikely that the hydraulic conductivity continues to increase in the direction of plume movement as much as the trends would indicate, the direction of tracer movement and the trend surfaces are physically compatible. The third-order surface indicates a large decrease in K just to the right of wells K-21 and K-22. That "impermeable wall" is physically inconsistent with the observed path of the tracer. Therefore the third-order trend surface should be rejected because it is physically inconsistent with the other known information at the CAFB site. Second-order is the highest-order trend that is compatible with the other data on site.

ADDITIONAL FACTORS INFLUENCING THE SAMPLE VARIOGRAMS

Three factors that could be influencing the shape and magnitude of the sample variograms are: (1) measurement error, (2) correlated residuals, (3) bias caused by detrending. Measurement error refers to the errors in hydraulic conductivity values obtained from the flowmeter method. Rehfeldt et al. (1988), showed that the hydraulic conductivity values were more reproducible for layers of larger K. In other words the measurement error is a function of the measured value. If the measurement errors were completely random, the variogram would exhibit a

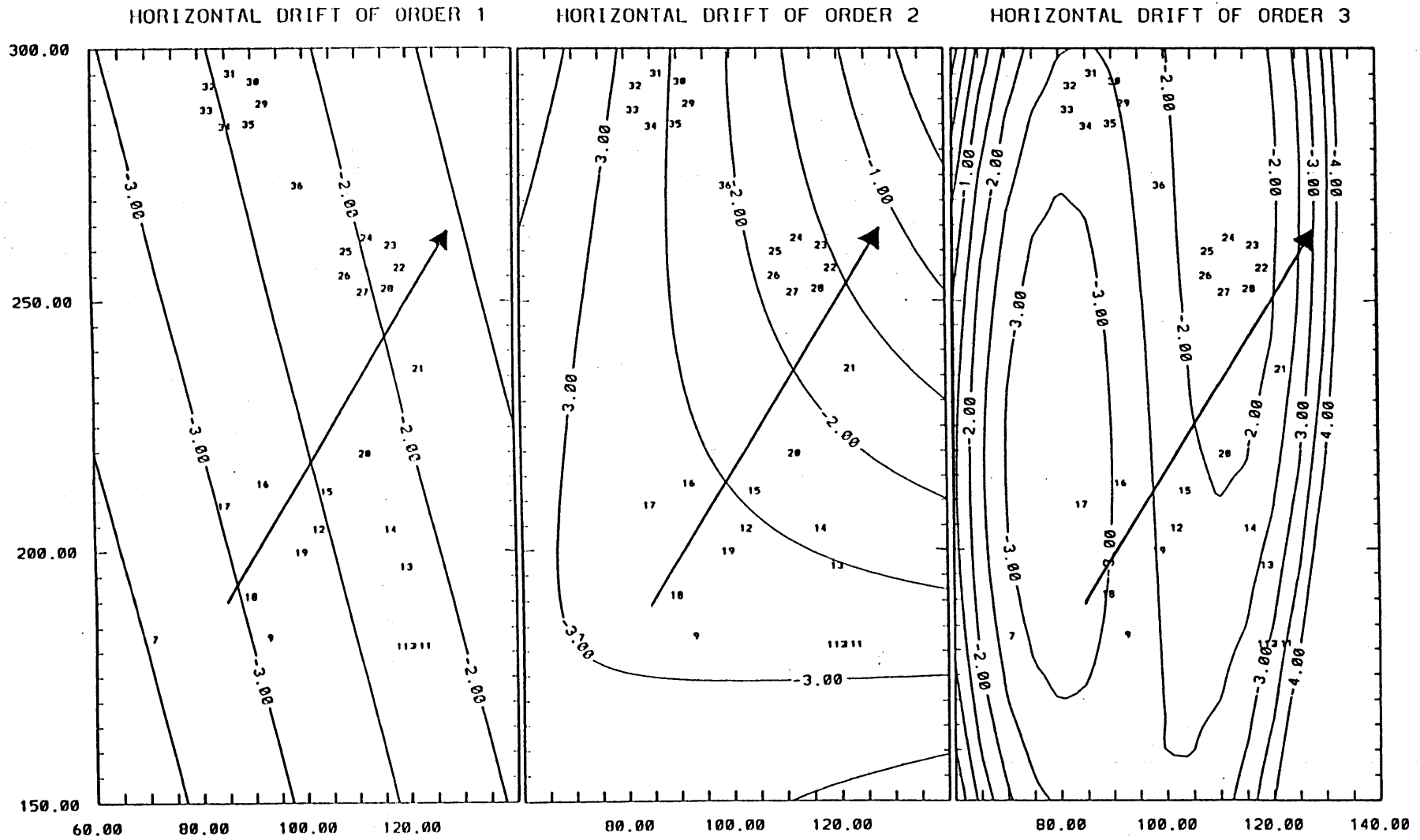

Figure 4-24. Path of the Leading Edge of the Tracer Plume as of November 2, 1987.

nugget effect (Journel and Huijbregts, 1978). The form and magnitude of the effect that the observed measurement error has on the lnK covariance will be determined.

The effect of correlated residuals and the bias caused by detrending apply only to the variograms of the residuals after removing a trend. The effect of correlated residuals was a small increase in the sill value for an example presented by Neuman and Jacobson (1984). In a letter to the editor by Gambolati and Galeati (1987) and in the response by Neuman et al. (1987) several more examples were presented where the sill value increased when the IGLS approached was used, in one case by a factor of two. Neuman and Jacobson (1984) and Cressie (1987) point out that residuals from the generalized least-squares estimator of spatial trend will yield biased estimates of the variogram.

Measurement Errors

Rehfeldt et al. (1988) presented and analyzed replicate hydraulic conductivity measurements. For layers with replicate measurements, the lnK mean and lnK deviation were defined as

$$\bar{y}_i = \frac{1}{N}\sum_{j=1}^{N} \ln K_{ij} \qquad j=1,2,\text{ or } 3 \qquad (4\text{-}24)$$

$$y'_{ij} = \ln K_{ij} - y_i \qquad (4\text{-}25)$$

where $\ln K_{ij}$ = the natural logarithm of the j^{th} replicate of layer i
N = number of replicate measurements for layer i
$\bar{y}_i$ = mean lnK value for layer i
y'_{ij} = deviation of the $\ln K_{ij}$ value from the mean $\bar{y}_i$.

When the y'_{ij} values from all the layers were pooled, they formed a continuous distribution of values from -3.0 to 3.0 that did not follow a normal distribution according to a Kolmogorov-Smirnov test. The pooled data were subdivided into three groups according to the $\bar{y}$ value. The distribution of y'_{ij} values in two of the groups, $-10<\bar{y}<-6$ and $-4<\bar{y}<0$, were found to be normally distributed at the 95% level using the Kolmogorov-Smirnov test. The variance of y'_{ij} was larger for groups containing layers of small hydraulic conductivity than for layers of large hydraulic conductivity. In Rehfeldt et al. (1988) the three groups were chosen simply to illustrate the increase in measurement

error as measured hydraulic conductivity decreased and as such were somewhat arbitrary.

To refine the analyses, the pooled y'_{ij} data were divided into eight groups according to $\bar{y}_i$. The y'_{ij} data within each group were compared to a normal distribution using the Kolmogorov-Smirnov test and the mean and variance were calculated. For each group, Table 4-4 gives the mean, the variance, the number of values, and the level at which the assumption of normality would be accepted using the Kolmogorov-Smirnov test.

Table 4-4

ANALYSIS OF REPLICATES - GROUPED BY $\bar{y}_i$

Group $\bar{y}_i$	Number of Points	Mean $\bar{y}_{ij}$	Variance $\sigma^2_{y_{ij}}$	Level at which normality accepted
-2 to -1	30	0.0	0.04	86.2%
-3 to -2	40	0.0	0.03	20.5%
-4 to -3	97	0.0	0.05	23.2%
-5 to -4	83	0.0	0.15	99.0%
-6 to -5	107	0.0	0.15	99.8%
-7 to -6	180	0.0	0.36	92.2%
-8 to -7	156	0.0	0.56	32.0%
-10 to -8	167	0.0	0.51	78.8%

The error variance of each group is plotted in Figure 4-25 along with three fitted polynomials. The polynomials will be described in a moment, but first, some discussion of the observed measurement error is in order.

The average magnitude of the measurement error, represented by the variance of y'_{ij}, increased as hydraulic conductivity decreased (indicated by more negative $\bar{y}$ values), but within each group there is a

continuous range of measurement errors. Errors in the measured discharge in the well (Rehfeldt et al., 1988) lead to precisely the observed errors in $\ln K_{ij}$. The borehole flowmeter method is more sensitive to errors in measured discharge for layers of small hydraulic conductivity than for layers of large K. If the errors in discharge are assumed to be random, then the errors in K will be random also, but the variance of the error will be the largest when K is small. Errors in the discharge caused by variation in the pumping rate and the position of the flowmeter probe in the well (Rehfeldt et al., 1988) are assumed to be independent of the measured hydraulic conductivity. The errors in measured K or lnK that were analyzed in the replicate analyses are the result of propagating the discharge errors through the borehole flowmeter equations. To determine the effect of measurement error on the calculated variogram, the details of the error propagation will be bypassed and instead the observed measurement error in $\ln K_{ij}$ will be used directly. The approach is a simple one, but it will serve to illustrate the effect of measurement error on the sample variogram.

Let the variance $\sigma_{y'}^2$, as plotted in Figure 4-25, be represented by a polynomial function of $\overline{y}$ times the variance of a random component σ_ε^2 such that

$$\sigma_{y'}^2 = (A\bar{y} + B\bar{y}^2 + C\bar{y}^3 + D)\sigma_\varepsilon^2 \qquad (4\text{-}26)$$

Assuming ε is of mean zero and variance one, the parameters for the three polynomials in Figure 4-25 were obtained by multiple regression and are given in Table 4-5

Table 4-5
MEASUREMENT ERROR - VARIANCE FUNCTION PARAMETERS

Order	A	B	C	D
1	-0.0806	0	0	-0.1762
2	0.0127	0.0092	0	0.0134
3	0.2992	0.0728	0.0041	0.3696

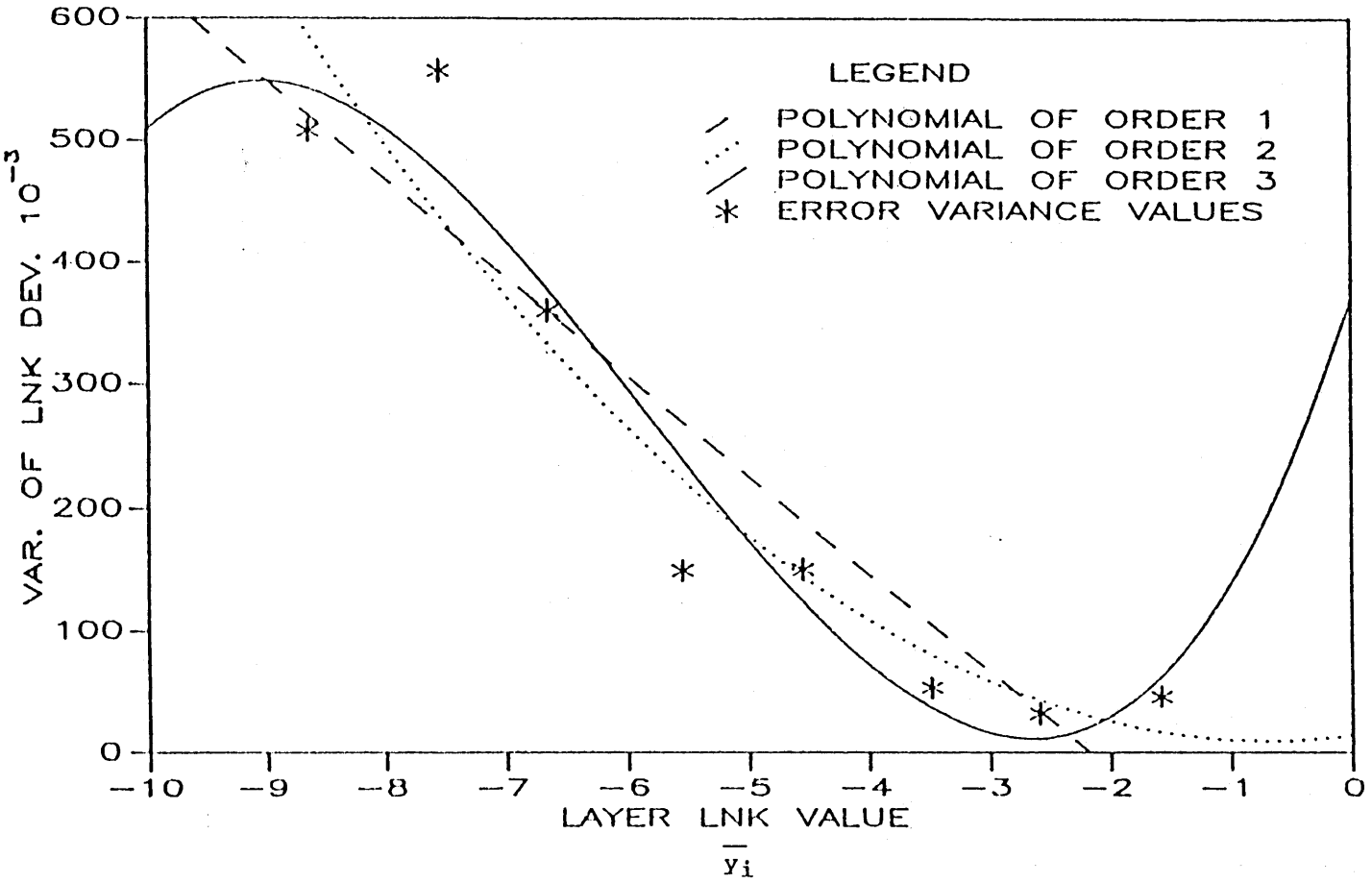

Figure 4-25. Variance of the Measurement Error.

These parameter values apply only if the units of K are cm/sec. If the units are other than cm/sec, simple expressions can be developed that will correct the parameters A, B, C, and D for K in the new units. Define the following:

$$K = \alpha K_s \tag{4-27}$$

K = hydraulic conductivity in cm/sec
K_s = hydraulic conductivity in units other than cm/sec
α = unit conversion factor

Taking the logarithm

$$\ln K = \ln\alpha + \ln K_s = S + \ln K_s \tag{4-28}$$

and after substituting for $\overline{y}$ in Eq. 4-26

$$\sigma^2_{y'} = [A(\ln K_s + S) + B(\ln K_s + S)^2 + C(\ln K_s + S)^3 + D]\sigma^2_\varepsilon \tag{4-29}$$

one gets an equation in the new units.
Expanding Eq. 4-29 and writing it in a form similar to Eq. 4-26

$$\sigma^2_{y'} = [\hat{A} \ln K_s + \hat{B} (\ln K_s)^2 + \hat{C} (\ln K_s)^3 + \hat{D}]\sigma^2_\varepsilon \tag{4-30}$$

One can solve for $\hat{A}$, $\hat{B}$, $\hat{C}$, and $\hat{D}$ in terms of the previously defined parameters A, B, C, and D. The expressions are given in Table 4-6

Table 4-6

VARIANCE PARAMETERS - UNIT CONVERSIONS

Polynomial Order	$\hat{A}$	$\hat{B}$	$\hat{C}$	$\hat{D}$
1	A	-	-	AS+D
2	A+2BS	B	-	$AS+BS^2+D$
3	$A+2BS+3CS^2$	B+3CS	C	$AS+BS^2+CS^3+D$

Only the first- or second-order polynomials given in Figure 4-25 are acceptable. The rapid increase in the third-order polynomial for $\overline{y} > -1$ is not consistent with the assumed conceptual model of the measurement error. The second-order polynomial best represents the conceptual model. For large conductivity layers ($\overline{y} > -3$) the discharge errors have only a small influence on hydraulic conductivity, but as the layer conductivity decreases (decreasing $\overline{y}$) the error will grow rapidly. The linear polynomial has similar properties, but yields a negative variance for $\overline{y} > -2$.

The coefficients of the polynomials to describe the increase in the measurement error variance with decreasing hydraulic conductivity were obtained from the sample data. To estimate the effect of measurement error on the sample variogram, the polynomial (Eq. 4-26) will be assumed to describe the errors in the whole population and not just the sample data.

Measurement model. Define the measured value of log hydraulic conductivity for layer i, y_i, as the sum of the true value plus a measurement error:

$$y_i = Y_i + V_i \tag{4-31}$$

where $Y_i = \ln K_i = F + f' =$ true value
$F =$ ensemble mean
$f =$ perturbation
$V_i =$ measurement error

The magnitude of V_i is assumed to be a function of Y_i in accordance with the observations in Table 4-4 and is given by

$$V_i = f(Y_i)\varepsilon_i \tag{4-32}$$

where ε_i = random error with zero mean and constant unit variance
$f(Y_i)$ = polynomial function of Y_i

The expected value of V_i is

$$E[V_i] = E[f(Y_i)\varepsilon_i] = E[f(Y_i)]E[\varepsilon_i] = 0 \tag{4-33}$$

and the variance is

$$E[V_i^2] = E[\{f(Y_i)\}^2 \varepsilon_i^2] = E\{f(Y_i)\}^2 \sigma_\varepsilon^2 \tag{4-34}$$

where $\{f(Y_i)\}^2$ is one of the polynomials defined by Eq. 4-26. The measurement model is now written

$$y_i = Y_i + f(Y_i)\varepsilon_i \tag{4-35}$$

The ensemble mean of the random field, assuming that the ε_i are independent of the layer hydraulic conductivity values is

$$\bar{y} = \bar{Y} = F \tag{4-36}$$

The sample variogram is defined by

$$\hat{\gamma} = \hat{\gamma}(r) = \frac{1}{2} E[(y_i - y_j)^2] = \frac{1}{2} E[\{ Y_i + f(Y_i)\,\varepsilon_i - Y_j - f(Y_j)\,\varepsilon_j \}^2] \tag{4-37}$$

where r = average lag distance between pairs of measurements in an interval Δr

$\hat{\gamma}$ = sample variogram obtained from measured values

Expanding Eq. 4-35

$$\begin{aligned} \hat{\gamma} = \; & \frac{1}{2} E\,[Y_i^2 + 2Y_i f(Y_i)\varepsilon_i - 2Y_i Y_j - 2Y_i f(Y_j)\varepsilon_j + (f(Y_i)\varepsilon_i)^2 \\ & - 2Y_j f(Y_i)\varepsilon_i - 2\, f(Y_i)\, f(Y_j)\varepsilon_i\varepsilon_j + Y_j^2 + 2Y_j f(Y_j)\varepsilon_j + (f(Y_j)\varepsilon_j)^2] \end{aligned} \tag{4-38}$$

Performing the expectation on the right-hand side under the assumption that the errors may be autocorrelated but that Y_i and ε_i are independent yields

$$\hat{\gamma} = \sigma_f^2 - R_{ff} + \frac{1}{2} E\,[\{(f(Y_i)\}^2 \varepsilon_i^2 + \{(f(Y_j)\}^2 \varepsilon_j^2 - 2\, f(Y_i)\, f(Y_j)\varepsilon_i\varepsilon_j] \tag{4-39}$$

where σ_f^2 = lnK variance

R_{ff} = lnK autocovariance

$\sigma_f^2 - R_{ff} = \gamma$ = true variogram

To complete the expectation, the functional form of $f(Y_i)$ must be known. A second-order polynomial was chosen for $[f(Y_i)]^2$ from the data analysis, therefore a linear equation will be used for $f(Y_i)$:

$$f(Y_i) = \alpha Y_i + \beta \tag{4-40}$$

Substituting Eq. 4-40 in 4-39, expanding, and completing the expectation gives

$$\hat{\gamma} = \sigma_f^2 - R_{ff} + (\alpha^2 F^2 + 2\alpha\beta F + \beta^2)(\sigma_\varepsilon^2 - R_{\varepsilon\varepsilon}) + \alpha^2(\sigma_f^2\sigma_\varepsilon^2 - R_{ff}R_{\varepsilon\varepsilon}) \tag{4-41}$$

The use of Eq. 4-40 places some restrictions on the coefficients that are used in Eq. 4-26. For the second-order polynomial form, Eq. 4-26 becomes

$$\sigma_v^2 = (AY_i + BY_i^2 + D)\,\sigma_\varepsilon^2 \tag{4-42}$$

where from Table 4-5

$$A = 0.0127$$
$$B = 0.0092$$
$$D = 0.0134$$

Squaring Eq. 4-40 and equating the coefficients in 4-42 gives

$$B = \alpha^2 \;:\; A = 2\alpha\beta \;:\; D = \beta^2 \tag{4-43}$$

which imply that $2\sqrt{(BD)} = A$. Using the coefficient values for A, B, and D above

$$2\sqrt{(BD)} = 2.22 \times 10^{-2} \neq 1.13 \times 10^{-2} = A$$

we see that the coefficients of the second-order polynomial do not satisfy the restrictions. A simple set of parameter values that satisfies the restriction and produces a reasonable fit to the data (Figure 4-26) is B = 0.01, A = 0.02, D = 0.01. Substituting the coefficients from Eq. 4-43 into 4-41 and rearranging gives the error in the sample variogram due to measurement errors

$$\hat{\gamma} - \gamma = (BF^2 + AF + D)(\alpha_\varepsilon^2 - R_{\varepsilon\varepsilon}) + B(\alpha_f^2\alpha_\varepsilon^2 - R_{ff}R_{\varepsilon\varepsilon}) \tag{4-44}$$

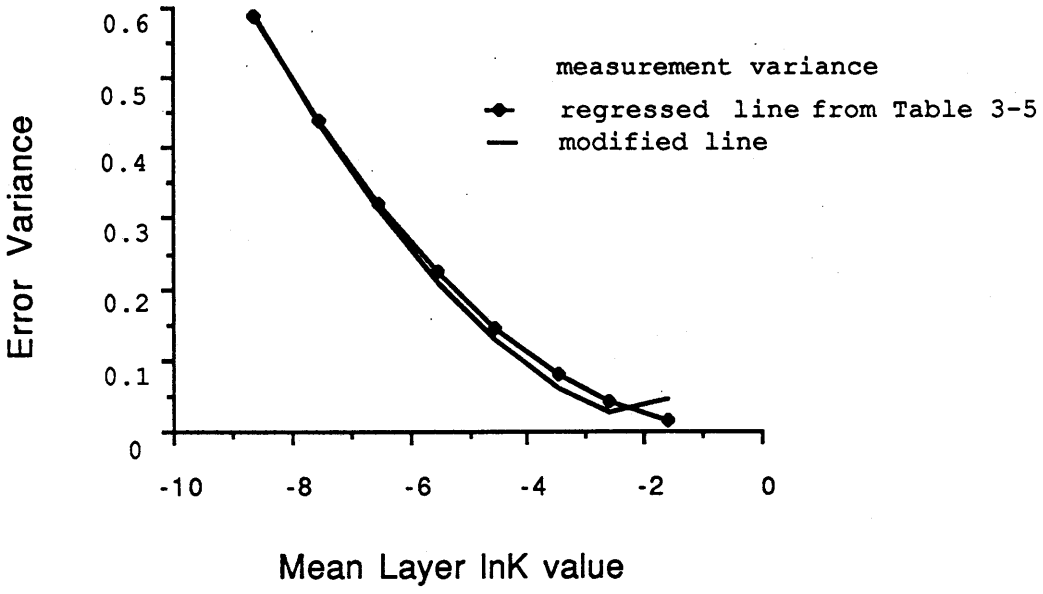

Figure 4-26. Comparison of the Regressed Curve through the Measurement Error Variance and the Curve with Coefficients that Satisfy the Parameter Restrictions.

To quantify Eq. 4-44 let the autocovariances of f and ε be of exponential form, but with different correlation scales:

$$R_{ff} = \sigma_f^2 \, e^{-x/\lambda}$$

$$R_{\varepsilon\varepsilon} = \sigma_\varepsilon^2 \, e^{-x/\lambda_\varepsilon} \qquad (4\text{-}45)$$

Two cases will be examined: (1) the measurement error is uncorrelated noise $\lambda_\varepsilon << \lambda$ and (2) the correlation scales are the same $\lambda_\varepsilon = \lambda$. The parameter values are

$$\begin{aligned} F &= -5.52 \\ \sigma_f^2 &= 4.59 \\ \sigma_\varepsilon^2 &= 1.0 \\ A &= 0.02 \\ B &= 0.01 \\ D &= 0.01 \end{aligned}$$

For Case 1:

$$\hat{\gamma} - \gamma = B(F^2 + \sigma_f^2) + AF + D = 0.25 \qquad (4\text{-}46)$$

and for Case 2:

$$\hat{\gamma} - \gamma = [BF^2 + AF + D](1 - e^{-x/\lambda}) + B\sigma_f^2(1 - e^{-2x/\lambda})$$

$$\begin{aligned} &= 0.0 && \text{for } x=0 \\ &= 0.17 && \text{for } x=\lambda \\ &= 0.25 && \text{for } x>>\lambda \end{aligned} \qquad (4\text{-}47)$$

Discussion of the Influence of Measurement Error. The error in the sample variogram caused by lnK measurement error is a function of the lnK mean (F), the lnK variance (σ_f^2), the lnK autocovariance, and the autocovariance of ε, where ε is a random noise term. If the noise is uncorrelated, the sample variogram will exhibit a small nugget effect. If the noise if autocorrelated, the sample variogram is unaffected at very small lags, but the error in the variogram grows rapidly as the lag increases.

In both cases the sample variogram values are slightly larger than the values of the true variogram. The measurement error accounts for less

than 6% of the observed variability at CAFB and for all practical purposes is insignificant. This is especially true when compared with the imprecision associated with the variance estimates.

Correlated Residuals

Neuman and Jacobson (1984) stated that the ordinary least-squares (OLS) approach for detrending a nonstationary-in-the-mean data set was inconsistent because the residuals are treated as uncorrelated when in fact it is the correlated structure of the residuals that is sought. They suggested a computationally burdensome iterative generalized least squares (IGLS) approach that treats the correlated residuals in a consistent manner. The IGLS problem reduces to solving a set of linear equations given previously by Eqs. 4-21 and 4-22. The computational burden comes from the inversion of the N X N covariance matrix (**V**), where N is the number of measured hydraulic conductivity values. The covariance matrix is initially unknown, but is estimated from the sample autocovariance of the residuals from the OLS method. With each successive solution of the IGLS equations, the covariance matrix is updated until a stable result is achieved.

Reduced Data Set. It was impossible to use the full data set (1242 values) in the IGLS approach because of the matrix inversion. The size of the data set needed to be reduced significantly without destroying the spatial structure of the random field. Fortunately, at least in this context, there is an overabundance of redundant information in the vertical because the sample spacing of 0.1524 m is more than 10 times smaller than the vertical correlation scale of 1.6 m.

An averaging length of six times the sample spacing (0.9144 m) was chosen. Beginning at the bottom of each well the hydraulic conductivity values of each 0.9144 m interval were arithmetically averaged and that value was assigned to the center of the interval. Any extra data points at the top of the well were simply truncated. The data set was reduced to 214 values and the spatial structure of the random field was preserved (Figure 4-27).

Following the procedure in Neuman and Jacobson (1984) the data were detrended using OLS for polynomials of various orders. A second-order trend was chosen based on the earlier detrending of the full data set. Three iterations of the GLS approach were performed; the horizontal and vertical variograms for each iteration are presented in Figure 4-28.

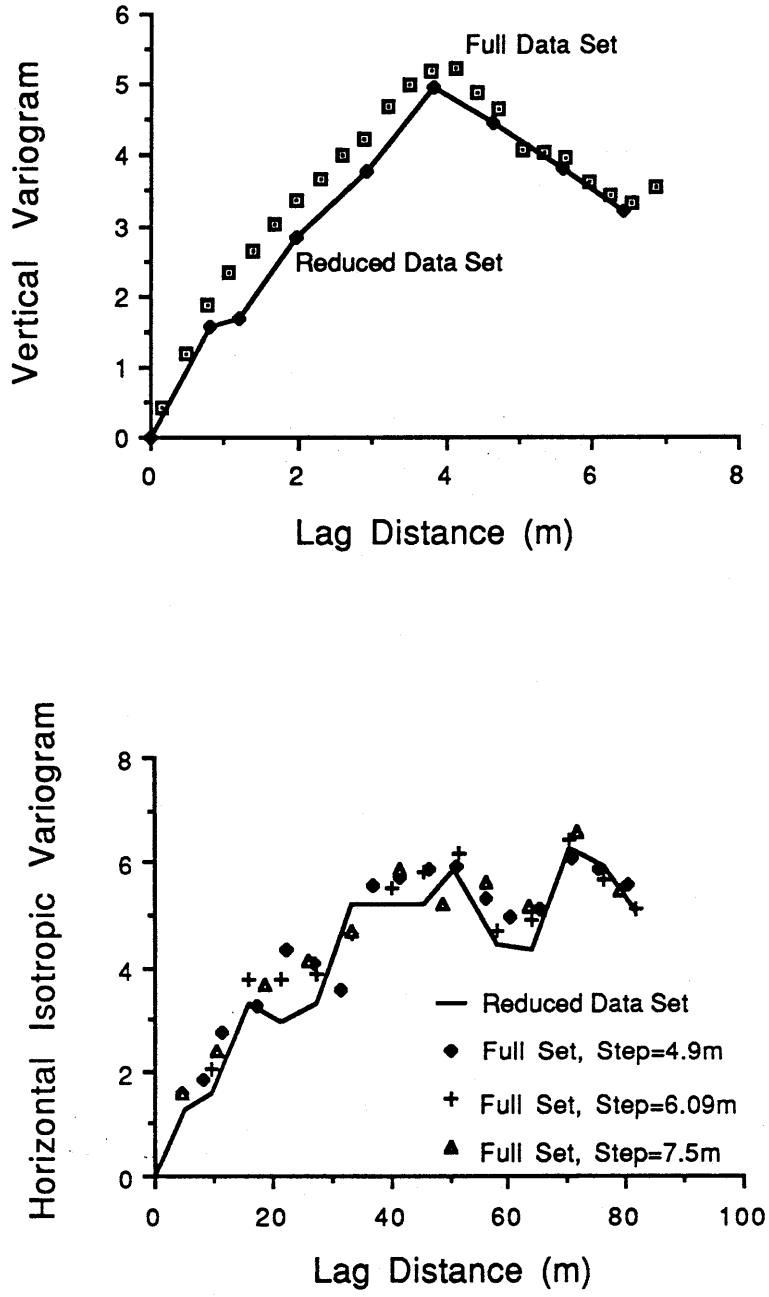

Figure 4-27. Comparison of the Variograms for the Full and and Reduced Data Sets

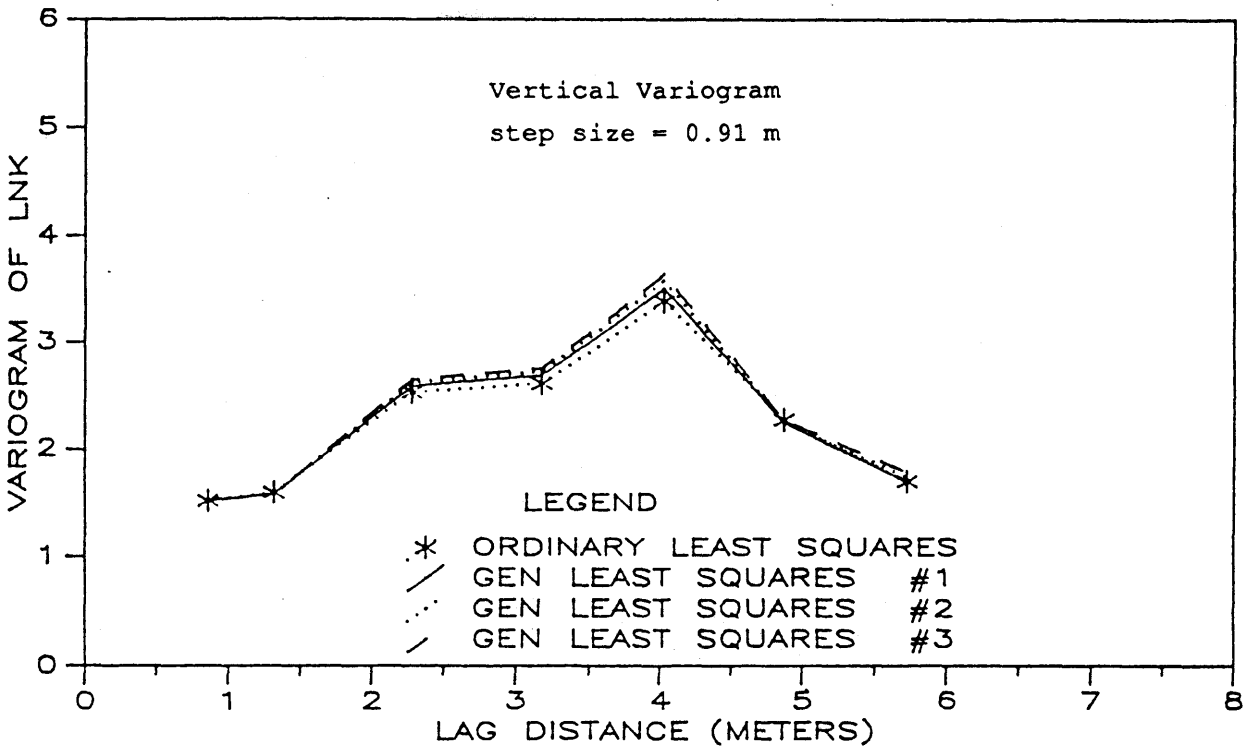

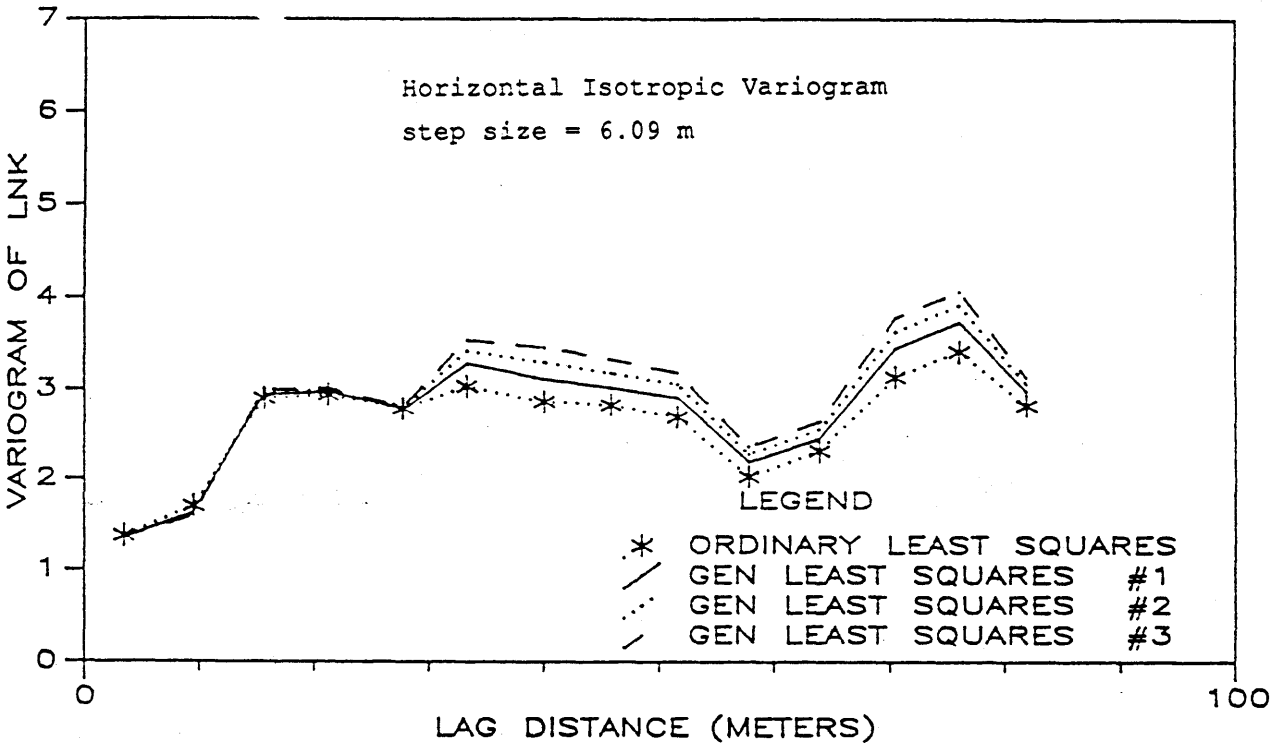

Figure 4-28. Variograms of the Residuals after Removal of a Second Order Trend for Three Iterations of the Iterative Generalized Least Squares Approach.

The changes in the variance and correlation scales from the OLS solution to the third iteration of the GLS solution are given in Table 4-7.

Table 4-7

IMPROVEMENTS IN SPATIAL COVARIANCE PARAMETERS AFTER IGLS

	σ_f^2	λ_h (m)	λ_v (m)
OLS	2.39	7.1	1.00
IGLS (third iteration)	2.61	8.8	1.25

Changes in the sample variogram occur only for lags much greater than the correlation scale. For a stationary random field, the large-lag portion of the variogram (the sill) is simply a measure of the variance, which as we have seen is not known with certainty. The change in the variance (an increase of 0.22) amounts to only a 9% correction in the variance value. It is interesting to note that one adds a correction to the variance for correlated residuals but subtracts the correction for measurement error. For the data collected at the CAFB site, the two corrections are of almost the same magnitude, and the resulting "corrected" variance is unchanged from the sample variance.

Bias Introduced by the Least-Squares Approach

The residuals that result from detrending with a least-squares approach will yield a biased estimate of the variogram (Neuman and Jacobson, 1984; Cressie, 1987). Neuman and Jacobson (1984) give the covariance estimation error as

$$\upsilon = \hat{\mathbf{R}} - \mathbf{R} \tag{4-48}$$

where $\hat{\mathbf{R}}$ is the covariance calculated from the residuals and $\mathbf{R}$ is the true covariance. They obtain the covariance of υ, $\mathbf{V}_\upsilon = E[\upsilon\upsilon^T]$, as

$$\mathbf{V}_\upsilon = \mathbf{P}\,(\mathbf{P}^T\mathbf{V}^{-1}\mathbf{P})^{-1}\,\mathbf{P}^T \tag{4-49}$$

where $\mathbf{P}$ = n x m matrix of basis functions
$\mathbf{V}$ = n x n covariance matrix
n = number of data
m = number of coefficients in the trend polynomial.

Equation 4-49 is evaluated with little additional computational burden. The covariance matrix, $\mathbf{V}$, is inverted elsewhere in the IGLS procedure, so the middle term involves two matrix multiplications and the inversion of a 10 x 10 matrix in the case of a second-order trend. The remaining terms are matrix multiplications that yield an n x n matrix of the covariance estimation error.

Each element in $\mathbf{V}_\upsilon$ is the covariance of the estimation error for a pair of data values. The covariance of the estimation error in the horizontal and vertical directions was obtained by assigning the various data pairs to predetermined lag distance and direction classes (as one does when calculating the variogram) and finding the mean of the elements of $\mathbf{V}_\upsilon$ that fell within the various classes. Figure 4-29 is a plot of the variograms of the estimation error in the horizontal and vertical direction.

The variogram of the residuals, corrected for the bias, will be the sum of the variograms from Figures 4-28 and 4-29. The bias grows as the lag distance grows, therefore the bias correction will be small for small lags. The large-lag correction can be viewed as a correction to the sill value, or the variance. For the second-order trend, the bias correction will increase the variance from 2.6 to 3.2. This variance applies only to the reduced data set. Comparing the variance of the OLS residuals using the reduced data set (σ_f^2 = 2.4, Table 4-7) to the variance of the OLS residuals using the full data set (σ_f^2 = 2.9, Table 4-3) it appears that the reduced data set yields a smaller variance upon detrending. To estimate the variance that would likely have resulted from GLS trend removal from the full data set, a factor of 0.5 is added to the reduced data set variance to yield σ_f^2 = 3.4 which is the variance of the residuals after removal of a second-order trend. With the bias corrected variance, the horizontal and vertical correlation scales increase to 10 m and 1.6 m, respectively.

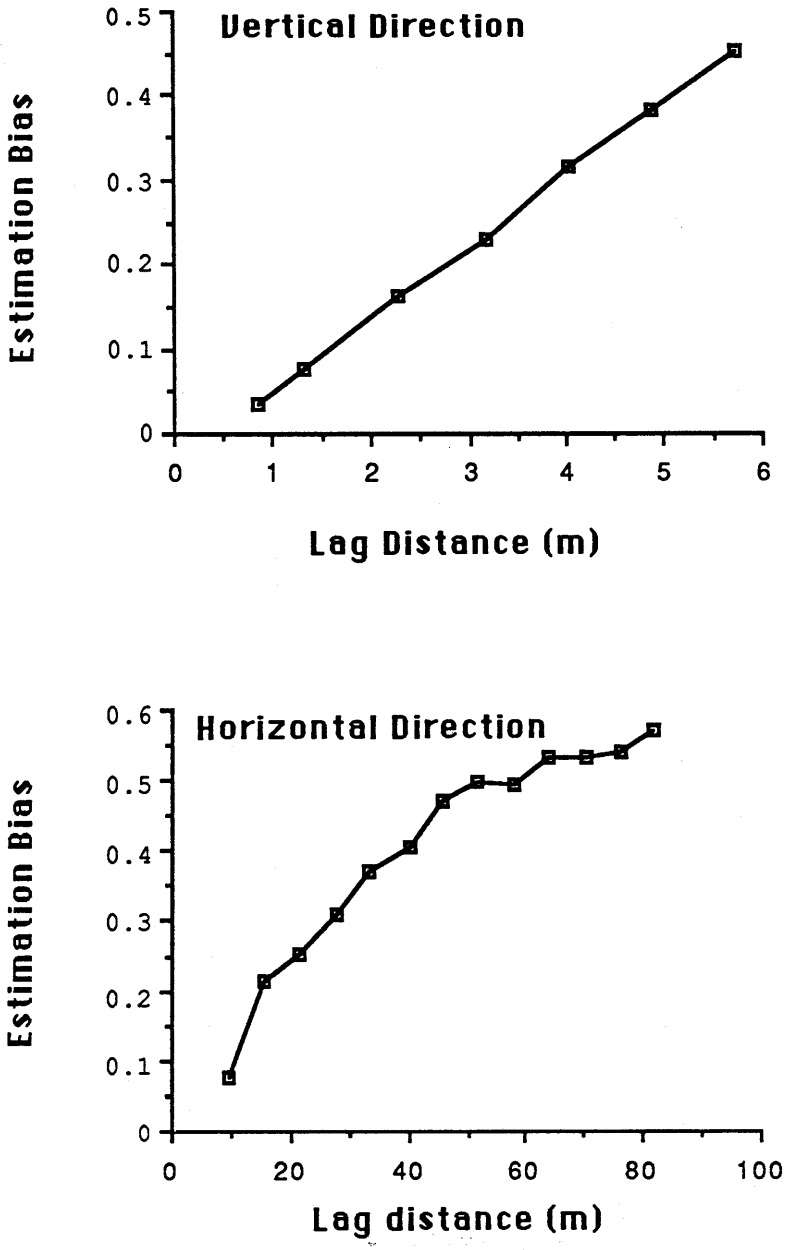

Figure 4-29. Variogram Estimation Bias Caused by Least Squares Detrending..

DISCUSSION OF THE SPATIAL COVARIANCE PARAMETERS

The measurement of the variability of hydraulic conductivity at the CAFB site was undertaken to demonstrate the feasibilty of estimating the covariance parameters necessary to predict macrodispersivities using existing stochastic theories. An extensive set of hydraulic conductivity data (1242 points), collected using a borehole flowmeter technique, were carefully analyzed to obtain the best estimate of the autocovariance parameters possible. The resulting parameters, the variance and correlation scales, were shown to be uncertain. As important as the parameter estimates themselves were the simple approaches used to quantify the uncertainty in the estimates. In a statistical sense, placing a confidence band on the autocovariance is a difficult problem and is not solved by the approach taken in this work. Rather the approach in this work is intented to be an objective way to evaluate the resulting parameters to determine whether additional, more elaborate analyses to improve the estimates are justified. The parameter estimates improve slowly with increasing data because the confidence band decreases as the inverse of the square root of the number of samples. Therefore to reduce the confidence band by a factor of two would require a four-fold increase in the number of data points. It is clear that even with an extensive data set such as the one at the CAFB site, the variance and correlation scales could not be determined with certainty and that attempts to do so would require such large amounts of data as to be impossible for practical application.

Whether the data should be detrended is a difficult problem that will never be answered with certainty in real situations. The question of detrending was approached from the pragmatist's point of view. First of all, from synthetic random fields (Ababou, 1988; Sharp, 1982) it is clear that portions of a random field of a size up to four or five times the correlation scale can be systematically above or below the ensemble mean. At the CAFB site, where the correlation scale was about 12 m in the horizontal direction, a lense or body of material 50 or 60 m long could legitimately be considered part of the expected behavior of a stationary random field. In addition, what is deemed a trend depends strongly on the scale of the problem being investigated. It is therefore very important that an investigator understand the scope of the problem before designing a sampling well network and that the design be flexible enough to allow modifications as new information is

obtained. With the data collected at the CAFB site it was not possible to show that a trend existed. In other words, the variablity that was observed could all be explained as consistent with a stationary random field. Nonetheless, the measured hydraulic conductivity data were reexamined assuming a trend might be present for two reasons: 1) to establish a methodology for removing a trend and 2) to see if removing a trend would significantly change the covariance parameter estimate from the measured data.

After examining the literature, no evidence was found to indicate that the least-squares methods of detrending would yield unsatisfactory results. In fact it was the computationally burdensome, statistically elegant and highly touted methods that often gave unreasonable results. Polynomial trends of various orders were considered. From the variograms of the residuals it was not possible to decide which order polynomial was the most appropriate. Only after including information on the path of the tracer plume did it become clear that if a trend was to be removed, it would be of second order. A second-order trend was removed using least-squares appproaches, and the variograms of the residuals were corrected for the effects of measurement error, correlated residuals, and estimation bias. The resulting spatial covariance parameters fall well within the $\pm 2\sigma$ range defined for the parameters obtained before detrending. Parameter values that fall within the $\pm 2\sigma$ range cannot be distinguished statistically. Hence, from the viewpoint of the spatial covariance parameter values, the question of whether a second-order trend is superimposed on an otherwise stationary random field is a moot point. One must not lose sight of the fact that it is the prediction of macrodispersivities that is important. The questions of whether uncertainty in the covariance parameters or the existence of a trend are important from a macrodispersivity prediction viewpoint will be explored in Section 5.

Discussion of the Preliminary Spatial Covariance Parameters

The application of the results of stochastic analyses (Gelhar and Axness, 1983, for example) to aid in the solution of routine solute transport problems has been hindered by the perception that a prohibitively large amount of data is required to estimate the model parameters. This perception is enhanced by the recent results of Russo and Jury (1987a, b) who concluded, based on the analysis of synthetic data with artificial trends, that the spatial covariance parameters

could not be determined accurately with 72 data points in two-dimensional space.

The results of the detailed spatial covariance analysis of the flowmeter data in this report could also be viewed negatively. The analysis of measurements of hydraulic conductivity in 29 wells produced upper bounds for the variance and correlation scales that were two and three times the lower bounds, respectively. To reduce the width of the 95% confidence interval for the variance so that the upper bound is 1.5 times the lower bound would require the installation of an additional 34 to 85 new wells depending on whether all the new wells were located more than one correlation apart or if on average one-half the wells were separated by distances greater than the correlation scale. As a practical matter, it is simply not possible to put tight bounds on the spatial covariance parameters.

Accepting that some uncertainty in the covariance parameters is unavoidable, the preliminary covariance parameters from the secondary measurements are of special interest. Although the borehole flowmeter method is a proven and promising technique, the method is a recent development, and it will take some time before the method finds its way into standard practice. The secondary methods: (1) split-spoon samples of the aquifer material, (2) slug tests in piezometers, (3) surface geophysics, and (4) large-scale aquifer tests are often part of a routine site investigation.

The preliminary covariance parameters (Table 3-9) are in retrospect remarkably prognostic, but with qualifications. Only the grain-size information could be used to estimate the vertical correlation scale. It was fortunate that TVA collected grain size samples in some of the boreholes at a 0.61 m (2 foot) interval. Common practice is to obtain a split-spoon sample at the end of each 1.52 m (5 foot) auger section. Based on the results of this study, it is recommended that grain-size samples be taken at least every 0.76 m (2.5 foot) during the augering of a borehole.

The preliminary horizontal correlation scale is given as an upper bound from the grain size and surface geophysical data and is equal to the smallest sample spacing. For each data set, the minimum sample spacing is larger than the horizontal correlation scale (12.7 m) from the

complete set of flowmeter data. To test if these methods will yield a reliable estimate of the horizontal correlation scale, an additional survey of the site, using either conventional resistivity with the 6.10 m "a-spacing" or the streaming potential, should be performed with a sample spacing of 6.1 m (20 feet).

The large-scale aquifer test offers the potential of extracting the ratios of correlation scales using the theory outlined in Gelhar and Axness (1983). The results the aquifer test used in this report are preliminary and the correlation scale ratios are provisional. More thorough analysis of the aquifer test data are recommended with particular attention to: (1) the assumptions in Neuman (1972, 1975) that transmissivity, specific yield, and hydraulic (horizontal-vertical) anisotropy remain constant and (2) an extension of the analysis to the horizontally anisotropic case.

In summary, some uncertainty in the spatial covariance parameters estimated from sample data is inevitable even for very large data sets. By acknowledging this uncertainty, the need for intensive sampling to define "The Autocovariance" largely disappears, and the more pragmatic (and attainable) goal becomes simply a good estimate of the autocovariance. Toward that goal we are encouraged by the results from grain size and surface geophysical data commonly gathered during routine site investigations.

ESTIMATING PARAMETERS OF THE HYDRAULIC GRADIENT VARIABILITY

The theory developed in Section 2 will be useful for estimating the magnitude of the dispersive flux due to unsteady flow if the parameters in the equations can be estimated. In the general case, six spectra, $S_{J_iJ_j}$, must be evaluated at zero frequency. However, for the purpose of obtaining the order of magnitude of the effect, it will be sufficient to use the simplified two-dimensional examples given in Chapter 2.

Hydraulic Head Data

The elevation of the water level in short-screened piezometers has been measured monthly (and sometimes more frequently) in nearly all of the piezometers at the CAFB site (Boggs et al., 1988). Figure 4-30 contains the water-level hydrographs of four of the piezometers on the site over

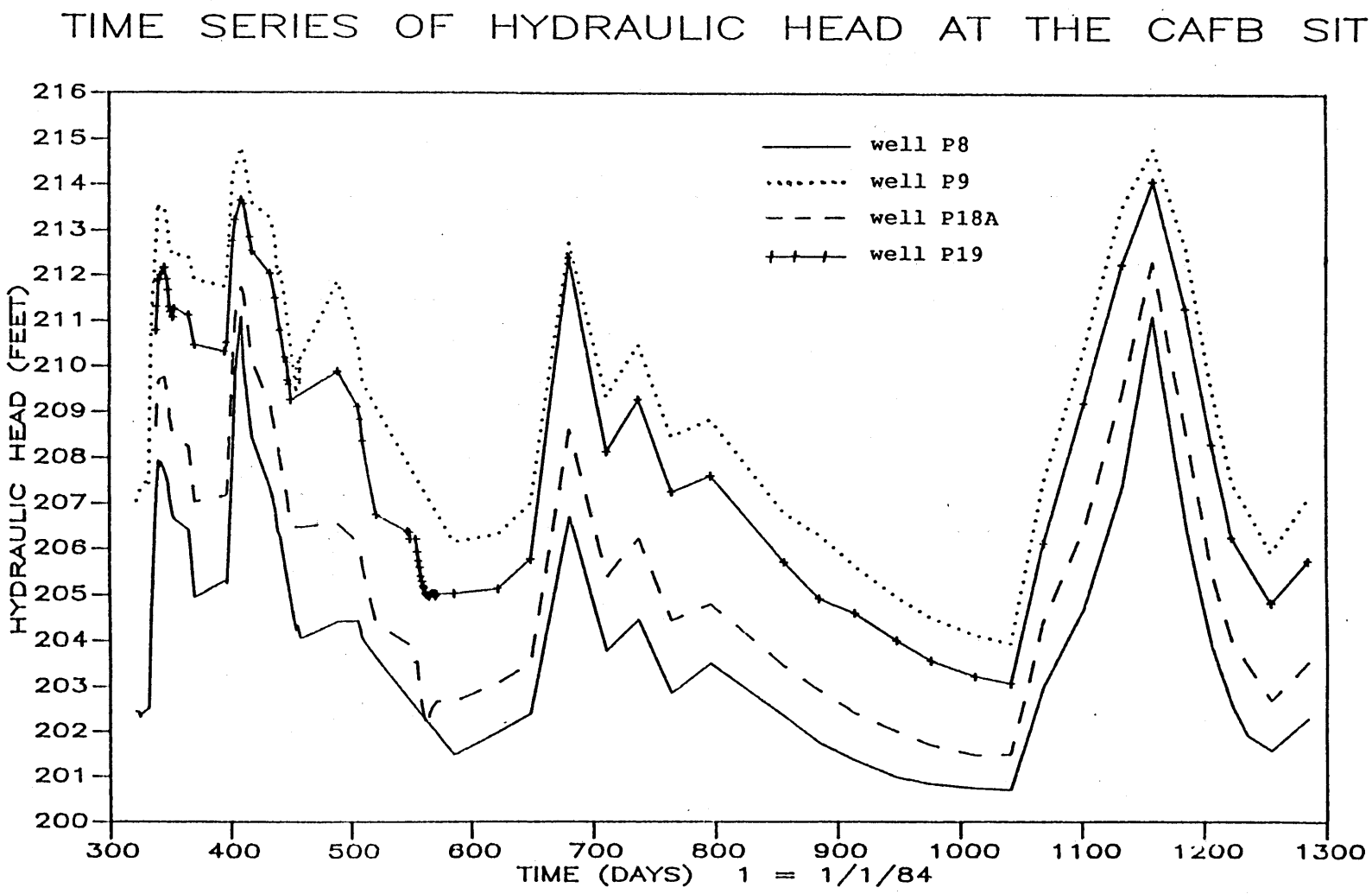

Figure 4-30. Time Series of Hydraulic Head in Four Piezometers on the CAFB Site.

almost a three-year period beginning in November, 1984. The hydrographs for these four piezometers are representative of the site as a whole and were chosen to illustrate the character of the water level fluctuations. The dates of measurement are indicated by the plus (+) signs along the curve for Well P19. For the first year (day 300 to about 600) water levels were measured much more frequently (daily during some periods) than during the last two years, when monthly sampling has been the norm.

The magnitude of the head variation observed at CAFB is quite large compared to other sites (Mackay et al., 1986; Garabedian, 1987). Over the three-year period in Figure 4-30, the water level varied by up to 3.35 m (11 feet) over a four-month interval. Although only three years of data are available, there is clearly a strong seasonal periodicity to the water levels, with maxima occurring during the winter and spring and minima generally occurring during the summer and fall. However, it is the fluctuation of the gradient, not the head elevation, that was postulated in Section 2 to be the primary temporal influence on dispersion.

Hydraulic Gradient Time Series

In the general case, the unsteady contribution to the components of the macrodispersivity tensor (Eq. 2-47) require the variance and the correlation scale of the cross-covariance function of the hydraulic gradient components. It is easier to visualize the gradient fluctuations when the gradient is described by its magnitude and direction instead of its cartesian components. Two simplified two-dimensional cases were presented in Section 2: fluctuation of the magnitude only and fluctuation of the direction only. To use those simplified cases, the time series of gradient magnitude and direction must be found and the variances and correlation scales estimated. In the development of the unsteady theory, the hydraulic gradient was assumed to be planar over the local region of interest. Fluctuations in both the magnitude and direction of the hydraulic gradient are estimated from a plane fit through the hydraulic head elevations measured at at least four piezometers. The hydraulic head is assumed to be of the form

$$H(x_1, x_2, x_3) = Ax_1 + Bx_2 + Cx_3 + D \qquad (4\text{-}50)$$

where the components of the gradient in the x_1, x_2, and x_3 directions are

$$J_1 = -\frac{\partial H}{\partial x_1} = -A \; ; \quad J_2 = -\frac{\partial H}{\partial x_2} = -B \; ; \quad J_3 = -\frac{\partial H}{\partial x_3} = -C \tag{4-51}$$

The magnitude of the hydraulic gradient is given by

$$J = \sqrt{J_1^2 + J_2^2 + J_3^2} \tag{4-52}$$

and it is convenient at this point to define a horizontal magnitude by

$$J_h = \sqrt{J_1^2 + J_2^2} \tag{4-53}$$

The direction of **J**, with respect to the direction of mean flow is described by two angles (See Figure 2-1)

$$\Gamma = \tan^{-1}(J_2/J_1) \quad \text{in the horizontal plane}$$
$$\Omega = \tan^{-1}(J_3/J_h) \quad \text{in the vertical plane} \tag{4-54}$$

The magnitude and angles describing the hydraulic gradient are decomposed into a mean and a zero mean perturbation.

$$\begin{aligned} \Omega &= \overline{\Omega} + \Omega' \\ \Gamma &= \overline{\Gamma} + \Gamma' \\ J &= \overline{J} + J' \end{aligned} \tag{4-55}$$

The variables with the overbars are mean quantities and the variances of the perturbations are given by σ_Ω^2, σ_J^2, and σ_Γ^2.

Over the entire site (Figure 3-1) many possible groups of wells could be used to calculate time series for J and Ω. Of the many possible combinations, four sets of piezometers were chosen that would exhibit a range of charateristics and were analyzed for fluctuations in the hydraulic gradient:

Set 1 : P1, P2, P3, P4

Set 2 : P8, P42B, P44, P53B, P52

Set 3 : P10A, P10B, P14A, P14B, P18A, P18B, P22A, P22B, P24A, P24B

Set 4 : 24A, 24B, 25A, 25B, 25C, 42A, 42B, 53A, 53B, 54A, 54B, 55A, 55B

The piezometers in Set 1 are widely spaced with a minimum distance between points of 300 m (1000 ft). These piezometers were chosen to examine the fluctuations on a scale that encompassed the entire site. The piezometers in Set 2 are spaced closer together (on the order of 50 m) and are located in the immediate vicinity of the tracer plume. All the piezometers in sets 1 and 2 are screened at approximately the same elevation near the base of the aquifer and will be used to estimate only the horizontal hydraulic gradient. Set 3 contains five pairs of nested piezometers located upgradient of the tracer experiment injection site. Nested piezometers are groups of two or more piezometers placed near to each other, but screened at different elevations in order to measure the vertical hydraulic gradient. The piezometers in set 3 were chosen because there is a downward vertical hydraulic gradient at each of those locations. In other regions of the site the direction of the vertical gradient is nearly zero or upward so that over the entire study area, the mean vertical gradient is likely to be small. Data set 4 contains nested piezometers located in the region of the tracer test experiment. In this region, the mean gradient is near zero or upward and the gradient direction alternates from downward to upward.

Figures 4-31, 4-32, 4-33, and 4-34 are time series of J, J_h, Γ, and Ω for data sets 1, 3, and 4. Time series of the magnitude of the gradient, J in Figures 4-32 and 4-34 and J_h in Figures 4-31 and 4-32, exhibit noticeable seasonal periodicity that mimics the hydraulic head periodicity in Figure 4-30. The time series of the direction of the hydraulic gradient show some seasonal periodicity also, although it is less pronounced in the horizontal direction (Γ in Figures 4-31 and 4-33) than in the vertical (Ω in Figures 4-32 and 4-34). Whether this seasonal periodicity constitutes a random or deterministic component will be addressed in a later section.

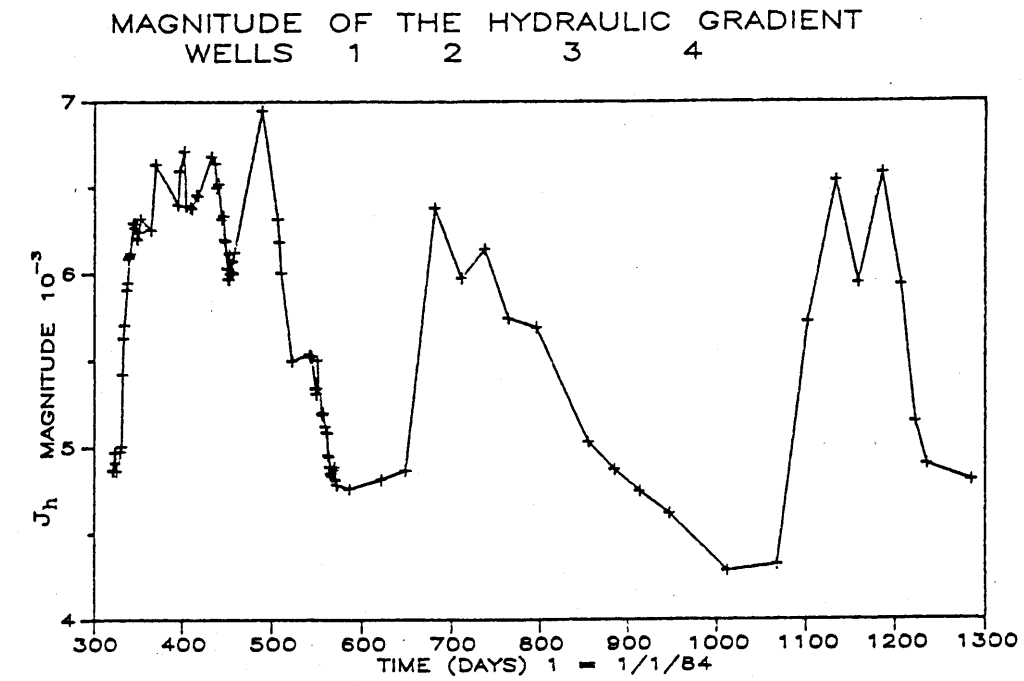

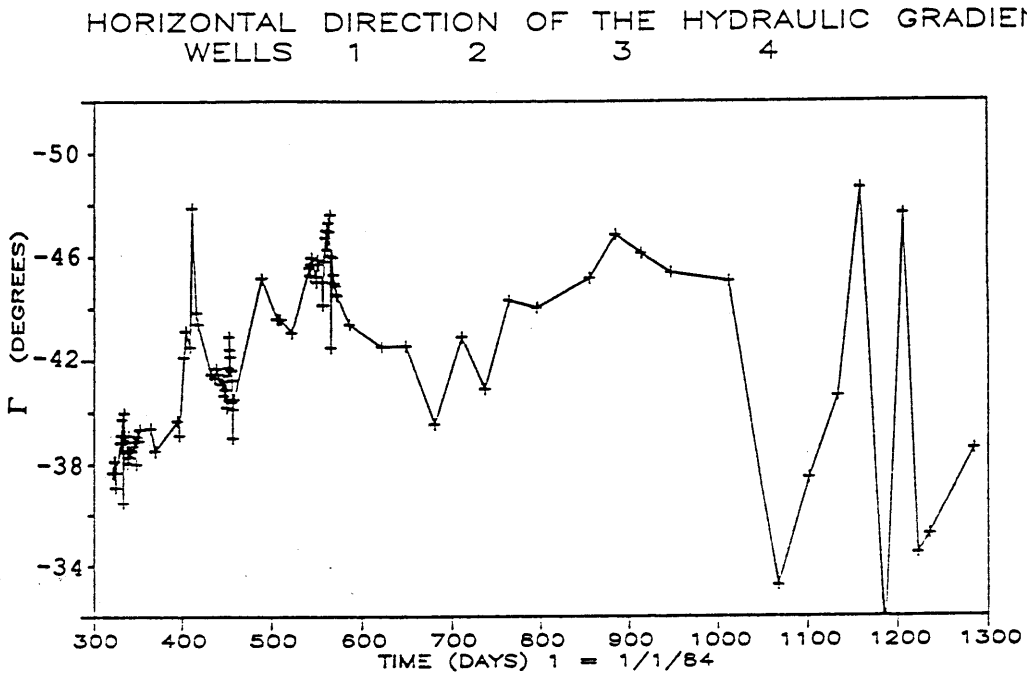

Figure 4-31. Time Series of J_h and Γ from Data Set 1.

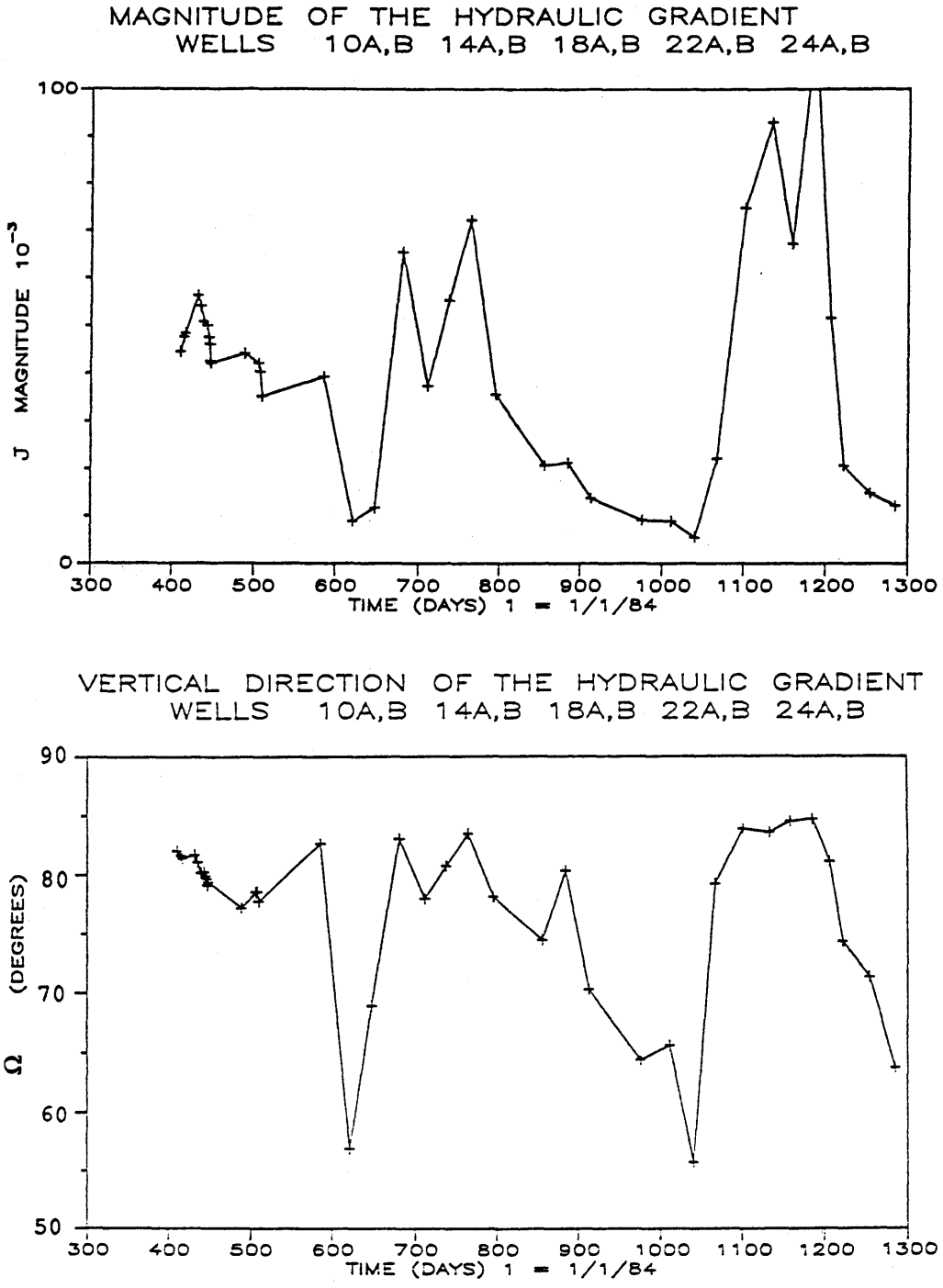

Figure 4-32. Time Series of J and Ω for Data Set 3.

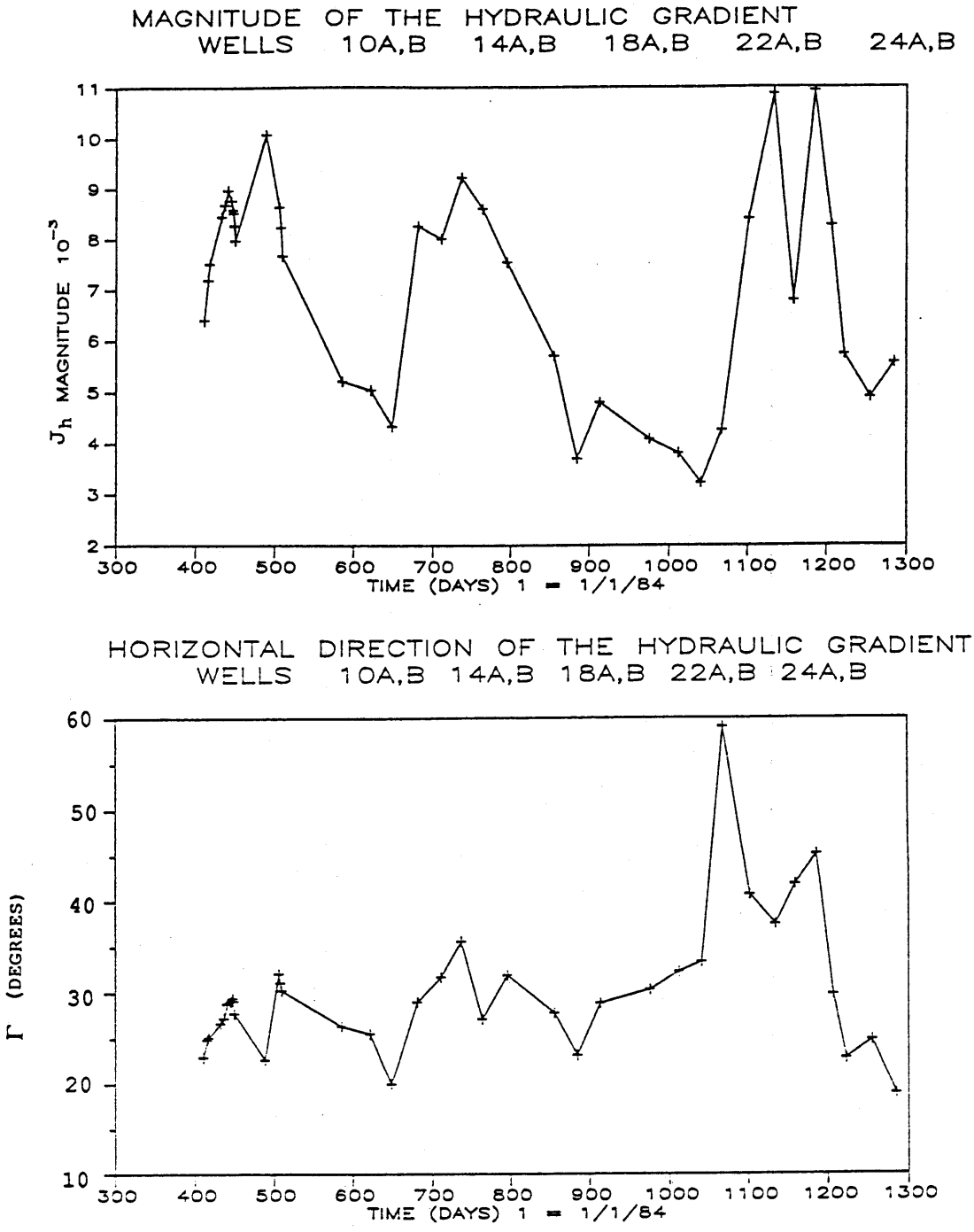

Figure 4-33. Time Series of J_h and Γ for Data Set 3.

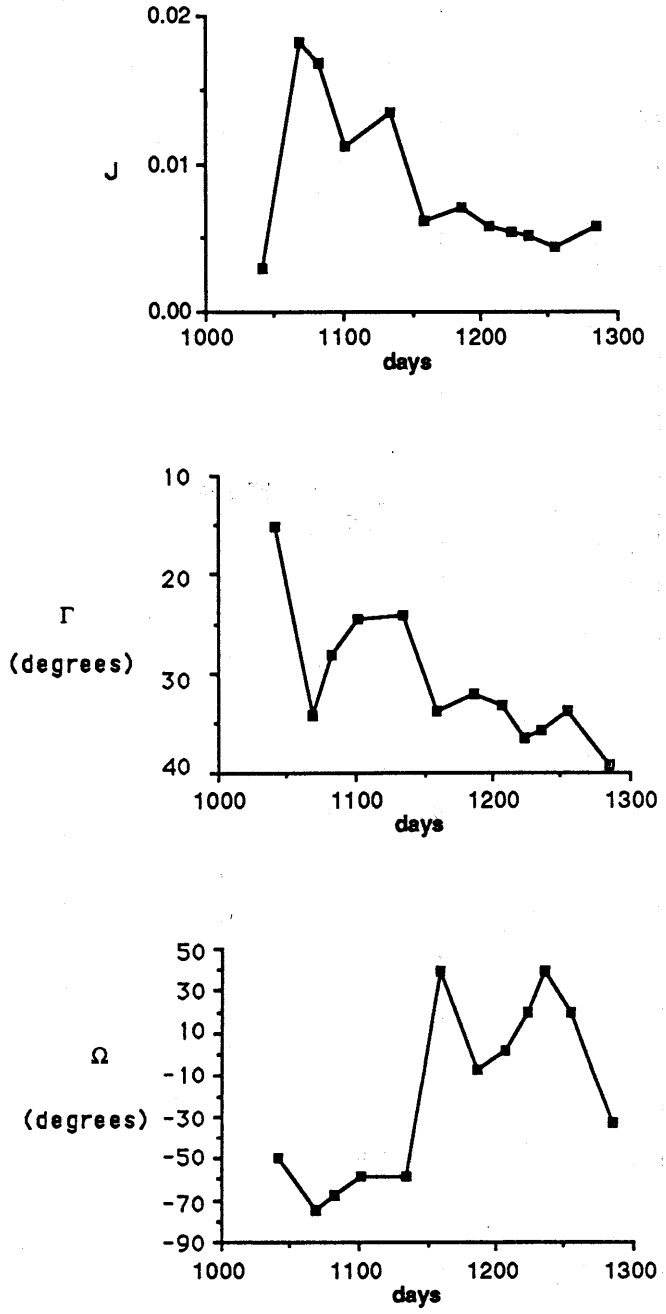

Figure 4-34. Time Series of J, Γ and Ω for data set 4

Table 4-8 summarizes the mean values of J, J_h, Ω, and Γ. The angles Γ and Ω are measured with respect to the direction of mean flow, which is assumed to be horizontal and oriented in the x_1, x_2 plane as indicated by the direction of the leading edge of the plume in Figure 3-4.

The mean value for J was an order of magnitude smaller from data set 4 than from set 3. The larger gradient magnitude and the large mean value of Ω (77 degrees) from set 3 reflect the strong downward vertical component of the hydraulic gradient in that region of the site. The piezometers of data set 4 were located in a region of where the direction of the vertical gradient changes for down to up over time. As a result the mean gradient magnitude is smaller and the mean angle Ω is -19 degrees, indicating that the mean gradient is upward in that region. Data set 4 contains more recently installed piezometers, and a longer data series is needed to provide a definitive comparison. However, from other nested piezometers on site , it is known that the vertical gradient direction changes from location to location, and presumably the mean angle Ω should be near zero when averaged over the site. The mean horizontal gradient was quite uniform, but the direction changed significantly. Negative values of Γ indicate that the gradient is rotated counterclockwise with respect to $\mathbf{q}$, and positive values of Γ indicate a clockwise rotation. Only data set 4 yields a horizontal gradient direction that is physically consistent with the observed direction of movement of the leading edge of the plume and the presumed axis of the effective hydraulic conductivity tensor in Figure 3-4.

Table 4-8

MEAN HYDRAULIC GRADIENT PARAMETERS

Data Set	J	J_h	Γ degrees	Ω degrees
1		5.6×10^{-3}	-42	
2		2.9×10^{-3}	-30	
3	4.1×10^{-2}	7.1×10^{-3}	-26	77
4	4.2×10^{-3}	5.0×10^{-3}	31	-19

Variance and Correlation Scales Estimation

There are a number of approaches to obtaining the spectra at zero frequency. Because these are one-dimensional time series, many standard spectral analysis techniques could be used. If the data were sampled at a regular interval, then the autocovariance function could be obtained directly and transformed to yield the spectrum. If the the data are unevenly spaced, as they are at CAFB, a variogram might be useful for finding the correlation scale, as was done for the spatial data. Estimating the spectrum directly is also an alternative. Marquardt and Acuff (1983) present a methodology for calculating the spectrum directly from unevenly spaced data. Calculating the spectrum, either directly or transformed from the autocovariance function, is a preferable method, because a confidence interval can be placed on the spectral estimate (Jenkins and Watts, 1968). Therefore, a confidence interval could be place upon the product $\sigma^2\lambda$.

Estimation of the spectrum is the preferable way to obtain $\sigma^2\lambda$, but the data set from CAFB simply doesn't warrant the effort at this time. Recall that there are barely three years of data, with most of the data concentrated in the first year. The number of effective independent samples could be small even if the correlation scale is on the order of 30 days or so. In addition, some of the time series are very short, particularly data set 4, so that the calculation of the variogram would be highly uncertain. Another concern is how to detrend the time series.

As in the case of spatial variability, the random component is assumed to be small relative to the scale of the experiment. The yearly cycles should not be considered as part of the random component if estimates of the unsteady effect on dispersion are desired for the tracer plume at CAFB during the first few years of the project. If one wanted to predict the longer-term dispersion, then the yearly cycle might be included. However, the spectrum of the seasonally periodic gradient fluctuations will not likely follow the exponential form. For these reasons and because this analysis is intended to provide an order-of-magnitude estimate of the parameters, a very simple alterative method is used to estimate the parameters.

As was the case with the estimates of the spatial covariance parameters, the decision to remove a trend is seldom straightforward. In the frequency domain a periodic series is more likely because of the yearly cycles of nature. If the yearly cycle is consistent, then it should be removed. However, the three years of data at CAFB are too short to estimate the cyclic mean effectively. To examine the role of the yearly periodicity, two sets of parameters will be obtained, the first without removing the seasonal periodicity and the second by making a rough calculation of the variance of the subseasonal component.

For the case without removing the seasonal component, the sample variance will be used directly and the correlation scale will be assumed to be about one year. The value of one year is chosen because it is large enough that the analysis with the seasonal trend included could be viewed as an upper bound on the unsteady contribution to A_{ij}. An approximate way to remove the seasonal periodicity is to develop a moving window of width 30 days or so that is moved along the time series. Except for a few outliers, variations within the window are considered part of the subseasonal randomness that covers a total range of 4σ, where σ is the standard deviation of the small-scale variability. Figure 4-35 is a schematic presentation of the simplified variance estimation scheme.

The correlation scale is estimated to be 30 days for J and J_h and 60 days for Ω and Γ. Table 4-9 contains the variances and correlation scales for both the seasonal and subseasonal variability. Admittedly

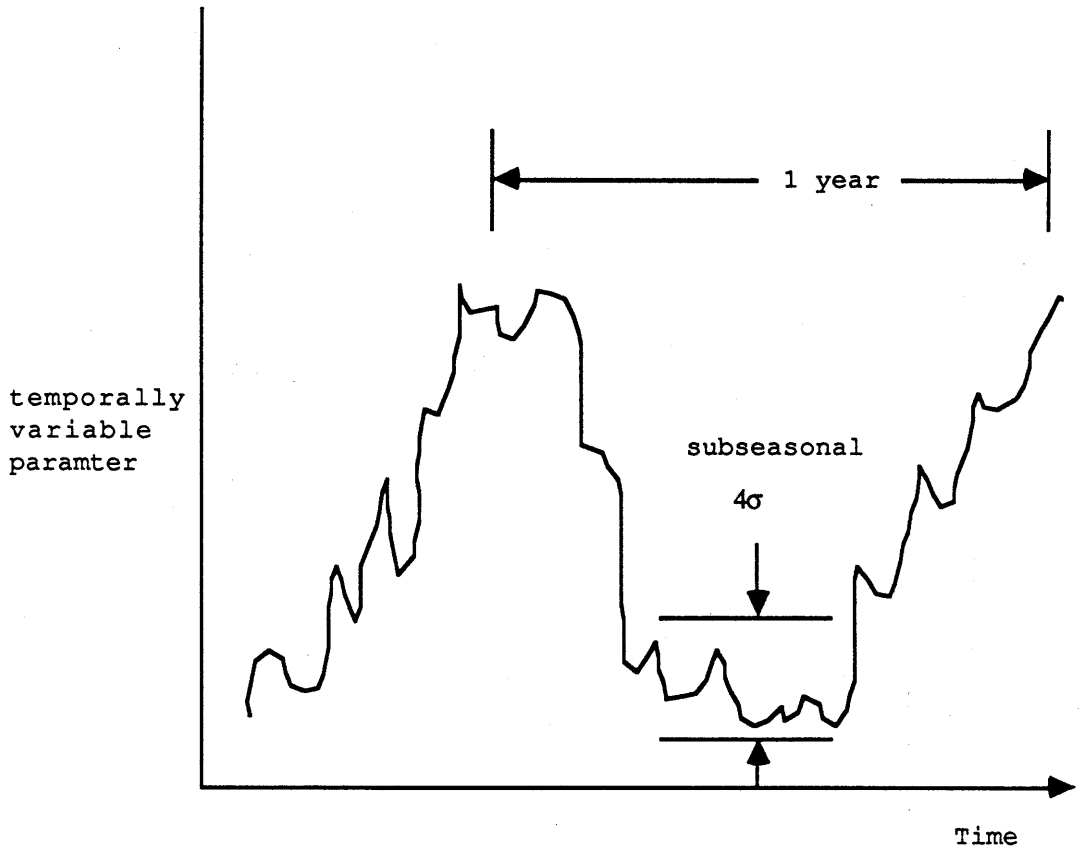

Figure 4-35. Schematic Representation of the Subseasonal Temporal Variability

Table 4-9

HYDRAULIC GRADIENT VARIABILITY PARAMETERS

Seasonal Scale

Data Set	σ_J^2	λ_J (yr)	$\sigma^2_{J_h}$	λ_{J_h} (yr)	σ^2_Ω $(deg)^2$	λ_Ω (yr)	σ^2_Γ $(deg)^2$	λ_Γ (yr)
1	-	-	$4.3x10^{-7}$	1	-	-	12	1
3	$5.6x10^{-4}$	1	$4.1x10^{-6}$	1	53	1	53	1
4	$5.2x10^{-5}$	1	$1.8x10^{-6}$	1	1684	1	40	1
mean	3.1x10-5	1	2.1x10-6	1	870	1	35	1

Subseasonal Scale

Data Set	σ_J^2	λ_J (days)	$\sigma^2_{J_h}$	λ_{J_h} (days)	σ^2_Ω $(deg)^2$	λ_Ω (days)	σ^2_Γ $(deg)^2$	λ_Γ (days)
1	-	-	$3.1x10^{-8}$	30	-	-	1.3	60
3	$5.6x10^{-5}$	30	$3.9x10^{-7}$	30	6	60	2.5	60
4	$1.6x10^{-6}$	30	-	-	160	60	2.5	60
mean	2.9x10-5	30	$2.1x10^{-7}$	30	83	60	2.1	60

these are rough estimates, but they will serve as order-of-magnitude estimates with which to evaluate the magnitude of the unsteady effect on A_{ij}.

Discussion of Parameter Estimates

Comparing the parameters from Tables 4-8, and 4-9, it is clear that the mean and variance of the gradient magnitude can be much larger in the vertical direction than in the horizontal direction. Over an area larger than data sets 3 or 4, the average vertical gradient would be expected to decrease because the regions of consistently upward or downward gradients are localized. Nonetheless, the vertical gradient, whether up or down, can be much larger than the horizontal gradient.

The seasonal variances of Ω and Γ are about the same for set 3 at a value of 53 degrees squared. The variance of Ω is much larger than the variance of Γ for set 4.

The correlation scales are really educated guesses. Clearly the correlation scale of the seasonal variability, which could be on the order of one year, is probably too large for the analyses of the plume at hand; however for prediction well into the future, it may be a reasonable choice. There is a higher-frequency variability which is on the order of a month or two, hence the estimates for λ are in the range of 30 to 60 days.

Covariances, or variograms, were not calculated because the data were insufficient to yield significantly better estimates of the parameters. The sample spacing was less than one month only during the first year of measurements. It is recommendewd that a network of piezometers be established with continuous, remote recording of water-level data for later analyses. Such a system is currently in place near the tracer plume, but data need to be collected for a number of years. In addition, nested piezometers should be included in the network to allow for the estimation of vertical gradients.

Section 5

PREDICTION OF MACRODISPERSIVITY

The predictions of macrodispersivity in this section are divided into two parts. The first part deals exclusively with the predicted macrodispersivities resulting from spatial variability alone. The spatial covariance parameters are known to be uncertain, and the effect of that uncertainty is examined by predicting A_{ij} values for the range of covariance parameters. In the second part, macrodispersivities are predicted including the effect of unsteady flow. The parameters describing the temporal variability are upper bounds, therefore the predicted A_{ij} are expected to exhibit the maximum effect that can be expected at the CAFB site. The section will close with a discussion of the results and a calculation of the influence of unsteady flow on the macrodispersivities at the Borden and Otis tracer test sites.

SPATIAL VARIABILITY

The detailed spatial covariance analyses of the borehole flowmeter data in Section 4 provided uncertain parameter values (Table 5-1). Recall that the most likely values were obtained from fitting an exponential variogram to the sample variogram of the measured hydraulic conductivity and that the ranges were based on estimates of a 95% confidence interval for the variance. Consequently the bounding values are quite unlikely. The covariance parameters for the hydraulic conductivity residuals following the removal of a second-order trend surface fell within the $\pm 2\sigma$ range, therefore the bounding covariance parameter values encompass a broad array of special cases.

Table 5-1

SPATIAL COVARIANCE PARAMETERS AND RANGES

Parameter	Most Likely Value	$\pm 2\sigma$ Range
Variance	4.6	$2.9 < \sigma_f^2 < 6.3$
Horizontal correlation scale	12.7 (m)	$6.9\ m < \lambda_h < 22.5\ m$
Vertical correlation scale	1.6 (m)	$0.75\ m < \lambda_v < 2.5\ m$

Although the uncertainty in the covariance parameters is itself a concern, this section focuses on the effect of that uncertainty on predicted macrodispersivities. The importance of uncertainty will be assessed by predicting asymptotic macrodispersivities (A_{ij}) using Gelhar and Axness (1983) for the most likely parameter values and the bounding values. In addition to the three parameters in Table 5-1, three additional parameters, which are needed to use the equations in Gelhar and Axness (1983) and were not determined from the analyses in Section 4, must also be assigned a range of values. Those additional parameters are: (1) the horizontal anisotropy ratio λ_1/λ_2 where $\lambda_h = \sqrt{(\lambda_1\lambda_2)}$, (2) the angle in the horizontal plane, ϕ, between the direction of λ_1 (if $\lambda_1 > \lambda_2$) and the direction of mean flow (Figure 5-1), and (3) the angle in the vertical plane, θ, between the direction of λ_1 and the direction of mean flow (Figure 5-2).

Marked statistical anisotropy in the horizontal plane ($\lambda_1 > \lambda_2$) was not detected in the sample variograms, although a horizontal anisotropy ratio (λ_1/λ_2) of 1.6 was shown to be possible (See Figure 4-8b). Based on the preliminary results of type curve analyses of the large-scale aquifer test and the expressions in Gelhar and Axness (1983) relating hydraulic anisotropy to statistical anisotropy, the horizontal anisotropy ratio (λ_1/λ_2) could be as large as seven (See Table 3-6). The angle ϕ could be as large as 45 degrees based on Figure 3-4.

The angle θ can be viewed as the angle between the dip of the beds and the mean flow direction. If the beds are assumed to be horizontal, then θ could be approximated by the slope of the water table, which is on the

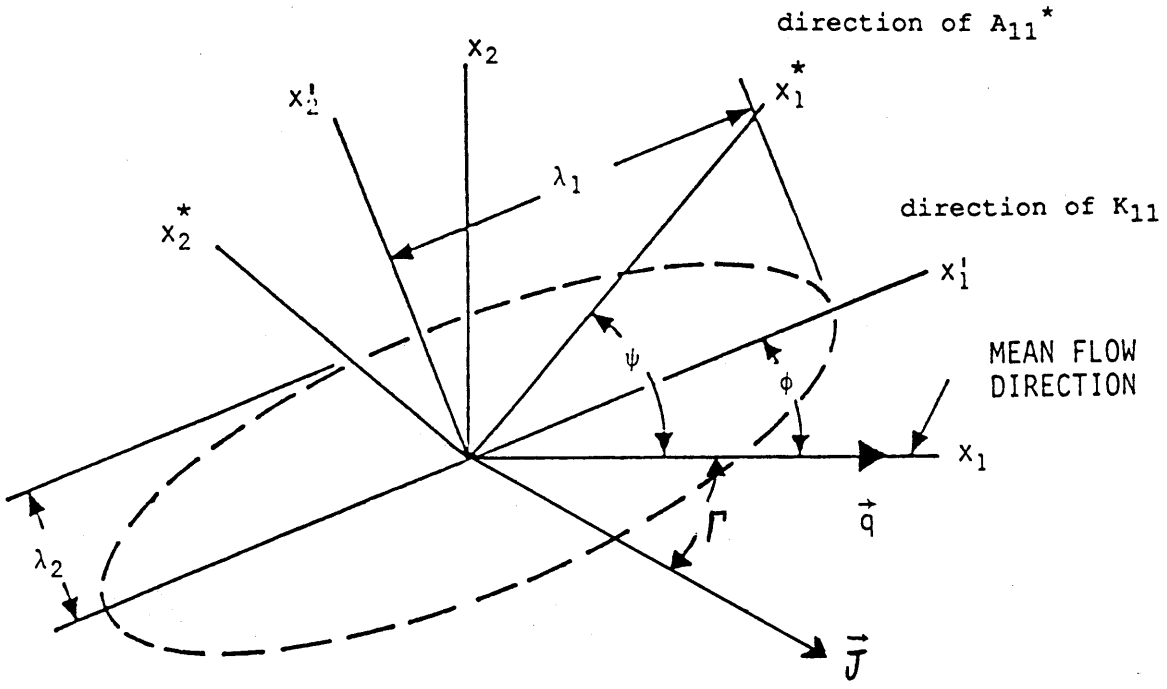

Figure 5-1. Coordinate Systems for the Case $x_3=x'_3$; the Dashed Ellipse Represents the e^{-1} Level of Correlation in the Covariance Function, the x'_1 Direction Being that of Maximum Correlation Scale in the Horizontal. The x' Coordinates are the Principal Axes of the Effective Hydraulic Conductivity Tensor and the x^* Coordinates are the Principal Axes of the Macrodispersivity Tensor.

Source: Gelhar and Axness, 1981, p. 49

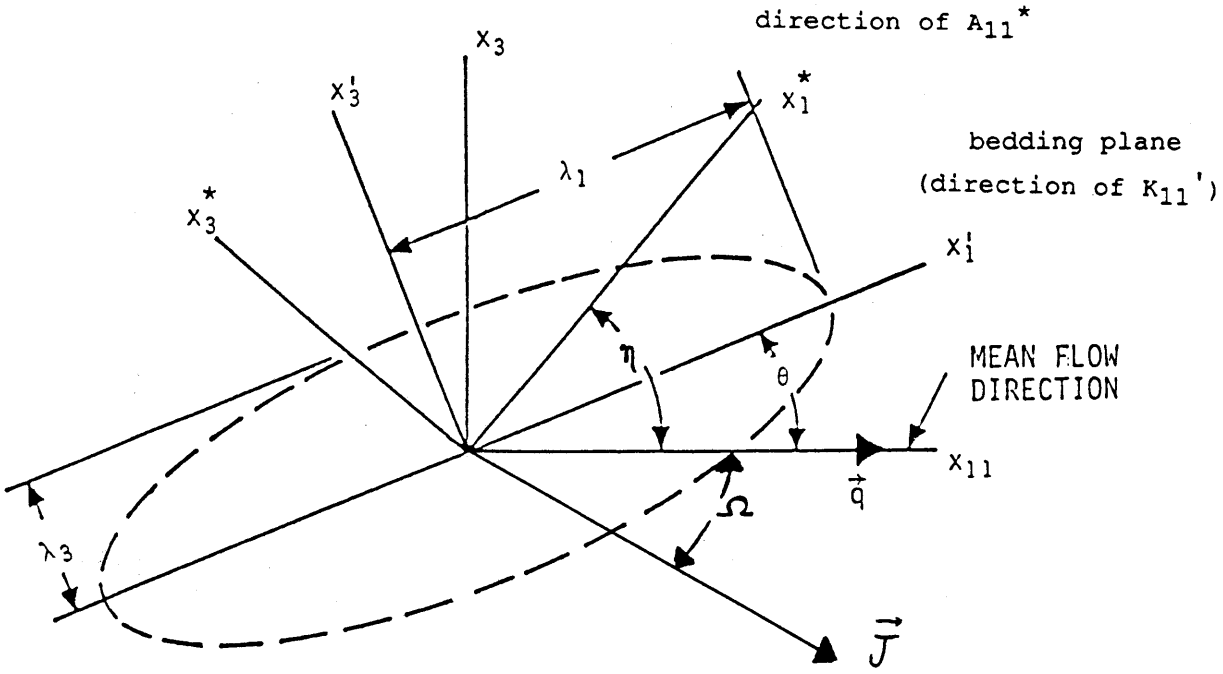

Figure 5-2. Coordinate Systems for the Case $x_2=x'_2$; the Dashed Ellipse Represents the e^{-1} Level of Correlation in the Covariance Function, the x'_1 Direction Being that of Bedding. The x' Coordinates are the Principal Axes of the Effective Hydraulic Conductivity Tensor and the x^* Coordinates are the Principal Axes of the Macrodispersivity Tensor.

Source: Gelhar and Axness, 1981, p. 34

order of 1 degree. If the beds are gently dipping at an angle of 5 degrees or so, then θ may be as large as 7 degrees.

The values of A_{ij} for various combinations of input parameters will be predicted for two somewhat idealized cases (Gelhar and Axness, 1983): (1) horizontal and vertical anisotropy with mean flow along the plane of stratification but oriented at an angle ϕ (Figure 5-1) with the direction of the major principal component of the autocovariance, and (2) horizontal isotropy ($\lambda_1=\lambda_2$) but vertical anisotropy ($\lambda_1>\lambda_3$), with mean flow oriented in the direction of the dip at an angle θ (Figure 5-2) with the bedding. Gelhar and Axness also present integral expressions for A_{ij} in the case of arbitrary orientation of the covariance and mean flow, but the computations are more cumbersome than for the idealized cases, which will be adequate to demonstrate the sensitivity of A_{ij} to the covariance parameters.

Horizontal and Vertical Anisotropy - Flow Parallel to Bedding

The equations for the components of A_{ij} for case 1 (Gelhar and Axness, 1983, Eqs. 69 and 70) are

$$\begin{aligned} A_{11} &= \sigma_f^2\lambda_1\lambda_2/(\gamma^2\lambda_3\zeta) \\ A_{22}/A_{11} &= (J_2/J_1)^2\zeta(2\zeta+1)/[2(1+\zeta)^2] \\ A_{33}/A_{11} &= (J_2/J_1)^2\zeta/[2(1+\zeta)^2] \\ A_{12}/A_{11} &= (J_2/J_1)\zeta/(1+\zeta) \\ A_{13} &= A_{23} = 0 \end{aligned} \qquad (5-1)$$

where

$$\begin{aligned} \zeta &= [(\lambda_1/\lambda_3)^2\sin^2\phi+(\lambda_2/\lambda_3)\cos^2\phi]^{1/2} \\ J_2/J_1 &= (B-1)\sin\phi\cos\phi/(\sin^2\phi+B\cos^2\phi) \\ \gamma &= \exp\left[\sigma_f^2\left(\frac{1}{2}-g_{22}\right)\right]/(\sin^2\phi+B\cos^2\phi) \\ B &= \bar{K}_{22}'/\bar{K}_{11}' = \exp[\sigma_f^2(g_{11}-g_{22})] \end{aligned}$$

The component A_{12} can be nonzero and the orientation of the principal axes of A_{ij}, x_i^*, is determined by

$$\tan 2\psi = 2A_{12}/(A_{11} - A_{22}) \qquad (5\text{-}2)$$

with ψ as shown in Figure 5-1. To use Eq. 5-1, the following parameters are needed: $\sigma_f^2, \lambda_1, \lambda_2, \lambda_3$, and ϕ. The parameters g_{11} and g_{22} in the expression for B above are estimated from Figure 5-3. Values of A_{ij} from Eq. 5-1 for various combinations of σ_f^2, λ_1, λ_2, λ_3, and ϕ are given in Table 5-2. The A_{ij}^* terms are the principal components of A_{ij}. The results in Table 5-2 are grouped according to σ_f^2 and λ. Within each group the variance and correlation scales are the same; only the angle varies. Group 1 contains the lower bound values for σ_f^2, λ_1, and λ_3; the λ_2 value was chosen so λ_1/λ_2 was equal to two. Group 2 contains the most likely parameter values and Group 3 are upper bounds. For Group 4, the values of λ_1 and λ_2 were chosen to yield a horizontal anisotropy ratio (λ_1/λ_2) of seven. Recall that only λ_h was obtained in Section 4. Except for group 1, the values of λ_1 and λ_2 were chosen such that $\sqrt{(\lambda_1\lambda_2)} = \lambda_h$, where λ_h is given in Table 5-1. Several observations from Table 5-2 to note are:

(1) When the angle ϕ is zero, only the A_{11} term is nonzero.
(2) Within each group there is very little difference in the A_{ij} components if the angle is 25 or 45 degrees.
(3) When the angle is nonzero, the off-diagonal term is always of a larger magnitude than the transverse diagonal terms. Non-zero off-diagonal terms lead to a rotation of the plume with respect to the mean flow direction.
(4) The longitudinal dispersivity, A_{11}, decreases with increasing σ_f^2 and ranged from 0.62 m to 1.94 m for all the cases considered.
(5) The transverse principal components, A_{22}^* and A_{33}^* are very small, on the order of a few millimeters, and change very little with increasing σ_f^2 or ϕ.

Figure 5-4 shows the principal components of the macrodispersivity tensor as a function of the variance and the orientation. The observations noted above are confirmed by Figure 5-4.

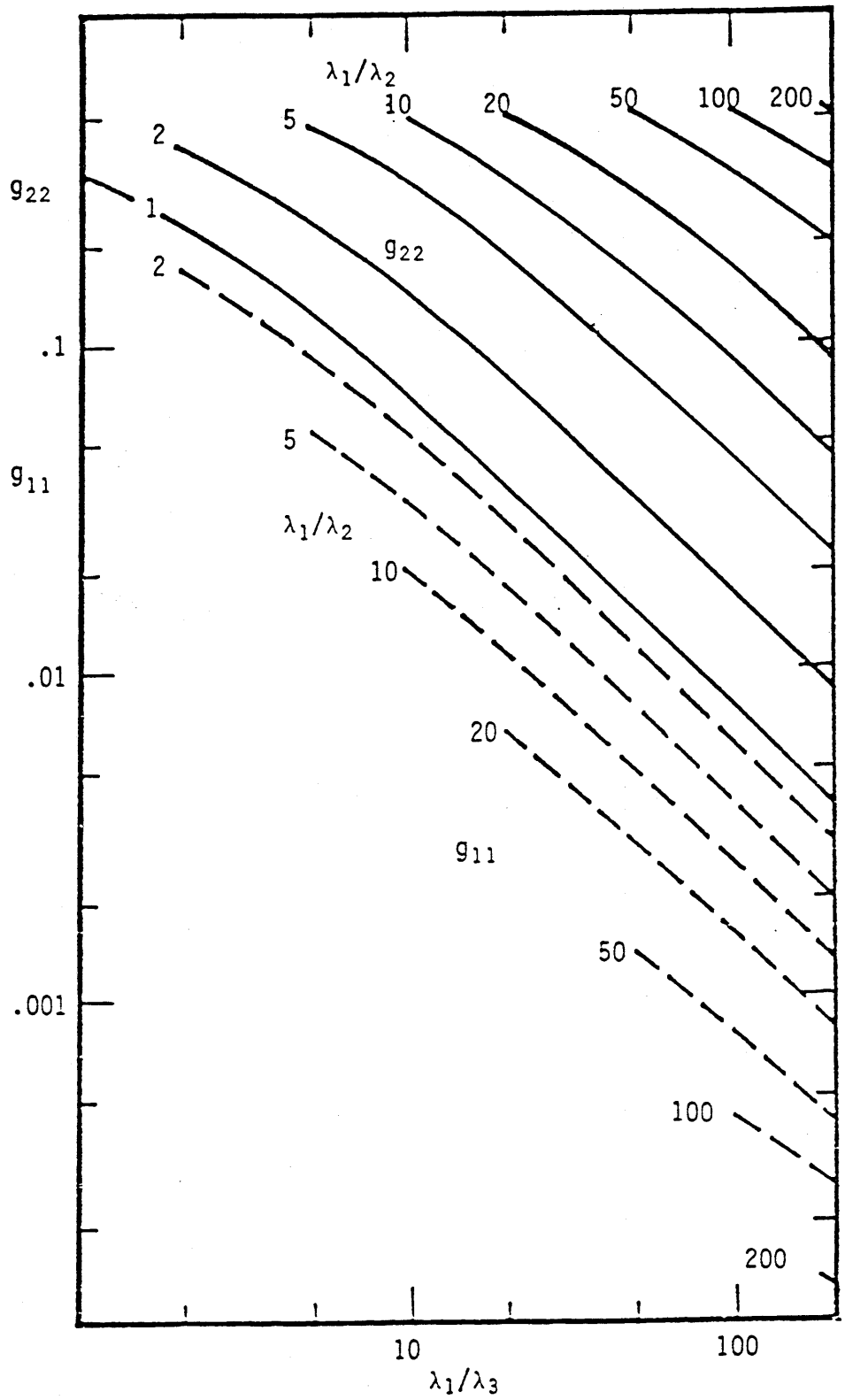

Figure 5-3. g_{11} and g_{22} as a function of λ_1/λ_3 and λ_1/λ_2.

Source: Gelhar and Axness, 1981, p. 37

Table 5-2

CALCULATED MACRODISPERSIVITIES DUE TO SPATIAL VARIABILITY

FOR THE CASE OF FLOW PARALLEL TO THE BEDDING

Horizontal and Vertical Anisotropy

Group #	σ_f^2	θ deg.	ϕ deg.	λ_1 m	λ_2 m	λ_3 m	γ	$A_{11}^{(s)}$ m	$A_{22}^{(s)}$ m	$A_{12}^{(s)}$ m	$A_{33}^{(s)}$ m	$A_{13}^{(s)}$ m	$A_{11}^{(s)*}$ m	$A_{22}^{(s)*}$ m	$A_{33}^{(s)*}$ m	ψ deg.
1	2.9	0	0	6.9	3.4	0.75	3.60	1.54	0	0	0	0	1.54	0	0	0
	2.9	0	25	6.9	3.4	0.75	3.39	1.39	0.017	-0.147	0.0014	0	1.41	0.0014	0.0014	-6.0
	2.9	0	45	6.9	3.4	0.75	3.07	1.32	0.024	-0.171	0.0015	0	1.35	0.0015	0.0015	-7.4
2	4.6	0	0	15.0	10.0	1.6	7.43	1.25	0	0	0	0	1.25	0	0	0
	4.6	0	25	15.0	10.0	1.6	7.00	1.27	0.016	-0.137	0.0011	0	1.29	0.0011	0.0011	-6.2
	4.6	0	45	15.0	10.0	1.6	6.34	1.34	0.024	-0.175	0.0014	0	1.37	0.0014	0.0014	-7.4
3	6.3	0	0	40.0	13.0	2.5	19.3	0.68	0	0	0	0	0.68	0	0	0
	6.3	0	25	40.0	13.0	2.5	16.1	0.62	0.068	-0.20	0.0039	0	0.68	0.0035	0.0039	-17.9
	6.3	0	45	40.0	13.0	2.5	12.3	0.72	0.084	-0.24	0.0034	0	0.80	0.0030	0.0034	-18.5
4	4.6	0	0	38.0	4.2	0.85	9.48	1.94	0	0	0	0	1.94	0	0	0
	4.6	0	25	38.0	4.2	0.85	8.34	0.64	0.040	-0.158	0.0010	0	0.68	0.00094	0.0010	-13.9
	4.6	0	45	38.0	4.2	0.85	6.85	0.58	0.043	-0.156	0.00066	0	0.62	0.00062	0.00066	-15.1

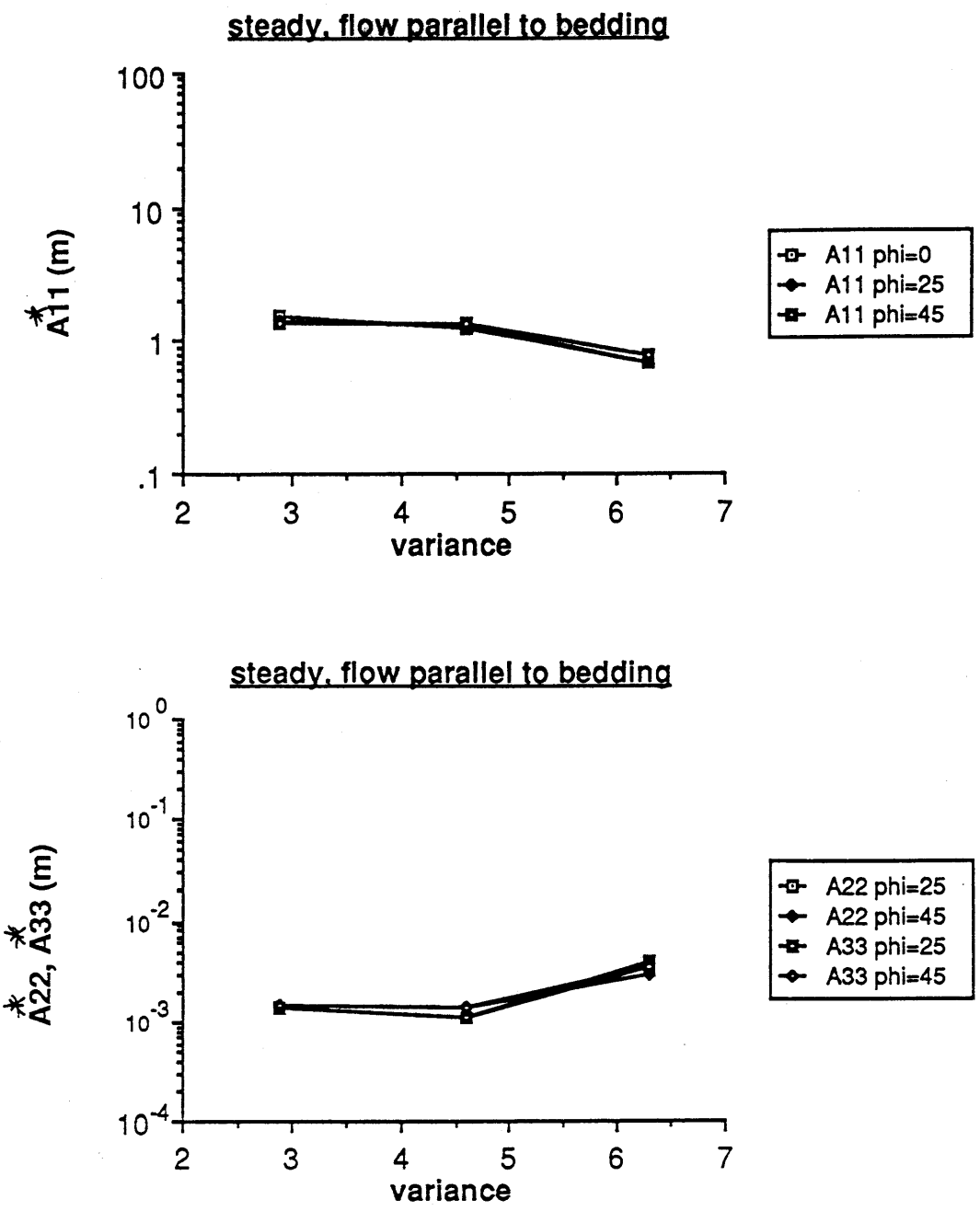

5-4. Principal Components of the Macrodispersivity Tensor for the Case of Steady Flow Parallel to Bedding.

Vertical Anisotropy - Flow Inclined to the Bedding

This case examines the effect of mean flow inclined at some angle to the bedding. To use some of the simple expressions in Gelhar and Axness (1983) we will assume the autocovariance is anisotropic only perpendicular to bedding ($\lambda_1=\lambda_2>\lambda_3$) and that either the beds are horizontal and flow is inclined, or that the flow is in the direction of maximum dip if the beds are dipping. Equation 5-3, taken from Gelhar and Axness (1983), is slightly easier to use than Eq. 5-1 because the g_{11} and g_{33} terms are defined by simple expressions and do not need to be interpolated from Figure 5-3.

$$
\begin{aligned}
A_{11} &= \sigma_f^2 \lambda_1 \mu/(\gamma^2 \xi) \\
A_{22} &= \sigma_f^2 \lambda_1 \mu J_3^2 / [2(1+\xi)^2 \gamma^2 J_1^2] \\
A_{33} &= \sigma_f^2 \lambda_1 \mu J_3^2 (1+2\xi)/ [2(1+\xi)^2 \gamma^2 J_1^2] \\
A_{13} &= A_{31} = \sigma_f^2 \lambda_1 \mu J_3 / [(1+\xi) \gamma^2 J_1]
\end{aligned}
\qquad (5\text{-}3)
$$

where

$$
\begin{aligned}
\mu &= \rho^{-1} = \lambda_3/\lambda_1 \\
\xi &= (\sin^2\theta + \mu^2 \cos^2\theta)^{1/2} \\
J_3/J_1 &= -(1-\beta)\sin\theta\cos\theta/(\sin^2\theta + \beta\cos^2\theta) \\
\beta &= \bar{K}_{33}'/\bar{K}_{11}' = \exp[\sigma_f^2 (g_{11} - g_{33})] \\
\gamma &= \exp\left[\sigma_f^2 \left(\frac{1}{2} - g_{33}\right)\right]/(\sin^2\theta + \beta\cos^2\theta) \\
g_{11} &= \frac{1}{2}\frac{1}{\rho^2-1}\left[\frac{\rho^2}{(\rho^2-1)^{1/2}}\tan^{-1}(\rho^2-1)^{1/2} - 1\right] \\
g_{33} &= \frac{\rho^2}{(\rho^2-1)}\left[1 - \frac{1}{(\rho^2-1)^{1/2}}\tan^{-1}(\rho^2-1)^{1/2}\right]
\end{aligned}
$$

The angle η (Figure 5-2) between the direction of mean flow and the principal axes of A_{ij} is given by

$$\tan 2\eta = 2 A_{13}/(A_{11} - A_{33}) \qquad (5\text{-}4)$$

Table 5-3 summarizes the calculated macrodispersivities for a range of parameters. The results are again grouped by the variance and correlation scale. Within each group, the angle between the bedding plane and the mean flow direction is varied from 0 up to 9 degrees. Although 9 degrees is rather large for essentially horizontal flow through flat-lying sediments, there are regions up to 30 m long (see Figure 4-5 between wells K-19 and K-20 for example) where a dip of 9 degrees may be appropriate. The following features are observed in Table 5-3:

(1) The transverse diagonal terms A_{22}^*, A_{33}^* are sensitive to the angle θ and increase by more than an order of magnitude in some cases as θ increases from two to nine degrees.
(2) For any fixed angle, the transverse diagonal terms increase significantly as the variance increases.
(3) The longitudinal macrodispersivity changes little with variance or angle except for σ_f^2=6.3.
(4) For large variances, the off-diagonal terms become dominant and the angle of plume rotation gets large.
(5) The transverse components attain values as large as 1 meter or more when the variance is large and θ is 5 or 9 degrees.

Figure 5-5 shows the principal components of the macrodispersivity tensor as a function of the variance and orientation. It is clear that the components are quite sensitive to θ particularly for large variance. It is not clear, however, that the stochastic theory is applicable at the large variances observed at the CAFB site.

Discussion of Predicted Macrodispersivities - Spatial Variability

In the following discussion, all values of A_{ij} will be assumed to be principal components unless stated otherwise. The wide range of predicted macrodispersivities (A_{ij}) presented in Tables 5-2 and 5-3 are summarized below:

$$0.58 \text{ m} < A_{11}^* < 17.1 \text{ m}$$
$$0.00062 \text{ m} < A_{22}^* < 10.4 \text{ m}$$
$$0.00064 \text{ m} < A_{33}^* < 4.15 \text{ m}$$

The large range of predicted A_{ij} may at first seem rather surprising. However, a very wide range of input parameters was chosen specifically to predict A_{ij} at the unlikely bounding values. Recall that the ranges

Table 5-3

CALCULATED MACRODISPERSIVITIES DUE TO SPATIAL VARIABILITY

FOR THE CASE OF FLOW INCLINED TO THE BEDDING

Vertical Anisotropy

Group #	σ_f^2	θ deg.	ϕ deg.	λ_1 m	λ_2 m	λ_3 m	γ	$A_{11}^{(s)}$ m	$A_{22}^{(s)}$ m	$A_{12}^{(s)}$ m	$A_{33}^{(s)}$ m	$A_{13}^{(s)}$ m	$A_{11}^{(s)*}$ m	$A_{22}^{(s)*}$ m	$A_{33}^{(s)*}$ m	η deg.
1	2.9	0	0	6.9	6.9	0.85	3.35	1.79	0	0	0	0	1.79	0	0	0
	2.9	2	0	6.9	6.9	0.85	3.31	1.75	0.0064	0	0.0081	-0.0537	1.75	0.0064	0.0064	-1.8
	2.9	5	0	6.9	6.9	0.85	3.16	1.64	0.038	0	0.050	-0.138	1.65	0.038	0.038	-4.9
	2.9	9	0	6.9	6.9	0.85	2.81	1.57	0.112	0	0.156	-0.264	1.62	0.112	0.108	-10.2
2	4.6	0	0	12.7	12.7	1.6	6.71	1.29	0	0	0	0	1.29	0	0	0
	4.6	2	0	12.7	12.7	1.6	6.48	1.34	0.068	0	0.086	-0.154	1.36	0.068	0.069	-6.9
	4.6	5	0	12.7	12.7	1.6	5.48	1.60	0.404	0	0.53	-0.445	1.76	0.404	0.368	-19.8
	4.6	9	0	12.7	12.7	1.6	3.89	2.42	1.18	0	1.66	-1.07	3.18	1.18	0.902	-35.0
3	6.3	0	0	22.5	22.5	2.5	14.4	0.68	0	0	0	0	0.68	0	0	0
	6.3	2	0	22.5	22.5	2.5	12.5	0.87	0.61	0	0.75	-0.35	1.16	0.61	0.45	-39.9
	6.3	5	0	22.5	22.5	2.5	7.77	2.09	3.59	0	4.60	-1.46	5.27	3.59	1.43	-65.2
	6.3	9	0	22.5	22.5	2.5	3.48	6.78	10.40	0	14.40	-5.21	17.10	10.40	4.15	-62.9

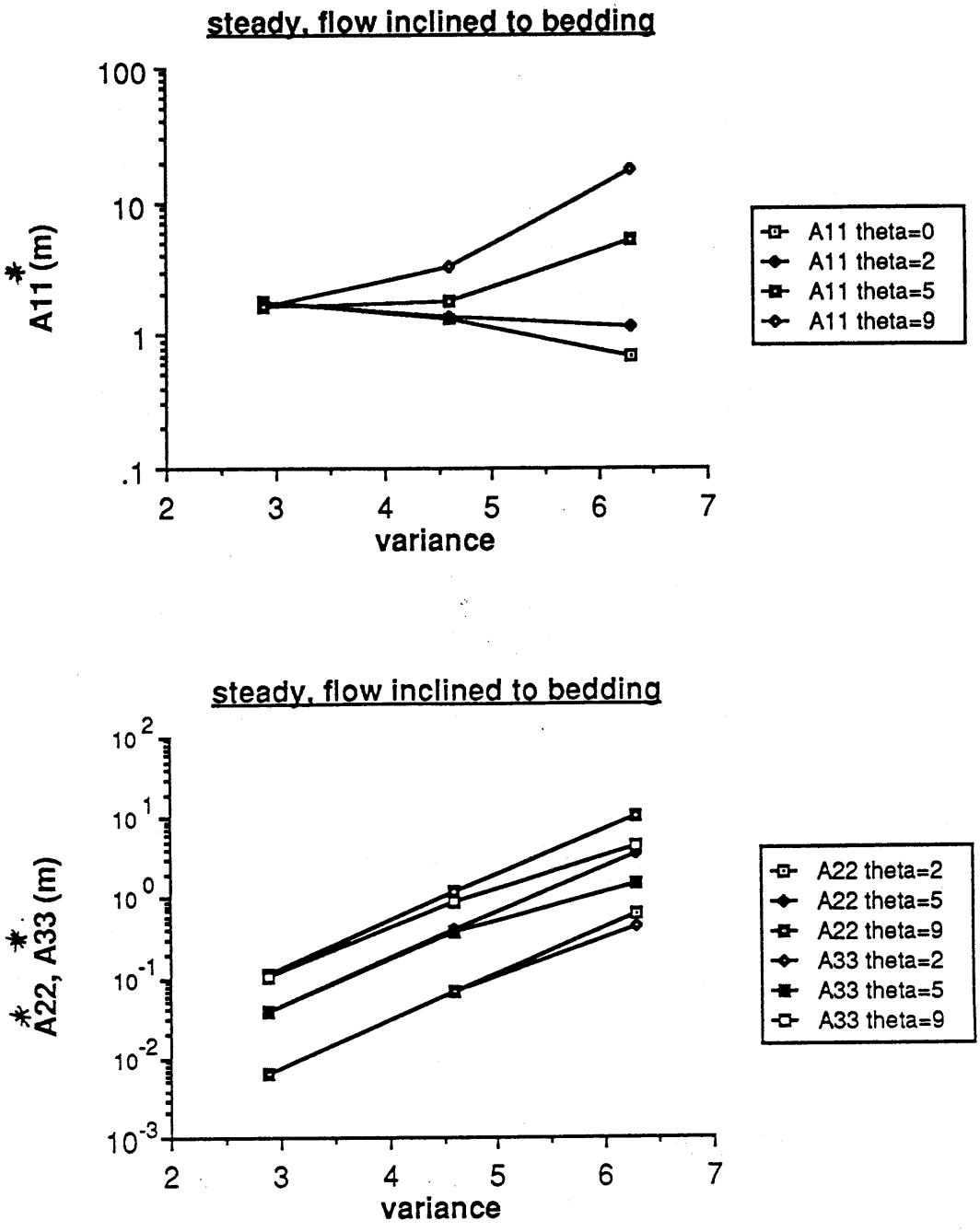

5-5. Principal Components of the Macrodispersivity Tensor for the Case of Steady Flow Inclined to Bedding.

of input variance and correlation scales were approximate 95% confidence intervals. In addition, a range of angles describing the orientation of the autocovariance function with respect to the mean flow were also considered. In the table above, the effects of parameter uncertainty and orientation uncertainty are combined. The effect of the orientation can be quite large. The following table gives the range of A_{ij} using only the most likely parameter values (σ_f^2=4.6, λ_h=12.7, λ_v=1.6), but for various orientations of the covariance with respect to the mean flow.

0.6 m	<	A_{11}^*	<	3.2 m
0.0006 m	<	A_{22}^*	<	1.2 m
0.0006 m	<	A_{33}^*	<	0.9 m

Clearly, uncertainty in the orientation of the covariance with respect to the mean flow, particularly in the vertical direction, can have almost as great an effect as parameter uncertainty. It appears that in addition to measuring the variance and the correlation scales of the lnK field, it is also important to determine the orientation of the lnK covariance, particularly if it is tilted in the vertical plane. Recall from Table 5-3 that an angle of 2 to 5 degrees has a significant influence on the predicted value of A_{ij}. From the spatial variability data available at CAFB, it is not possible to determine if the autocovariance is tilted at an angle of 2 or 5 degrees. An important area of future research should be the development of an improved spatial covariance analysis of the lnK field that would include an accurate estimate of the orientation of the autocovariance with respect to the mean flow direction, particularly in the vertical direction.

Two final points of discussion are: 1) whether the perturbation approach of Gelhar and Axness (1983) can be applied to the CAFB site, where the observed variance of lnK is large, and 2) what role do trends in the hydraulic conductivity field play in the dispersion process.

The equations in Gelhar and Axness (1983) were obtained assuming small random perturbations. In the case of an isotropic autocovariance (λ_1=λ_2=λ_3), Tompson et al. (1988) used a random-walk technique to simulate the transport of solutes through two heterogeneous random porous media using the flow field from Ababou (1988). These were carefully designed three-dimensional simulations with a total

displacement of 10 times the correlation scale of the medium. The rate of spreading of the tracer was tracked as it moved through the system, and an asymptotic macrodispersivity was obtained from the linear portion of the plot of the second moment of the plume versus displacement. The simulations are exact in the sense that the results do not depend on linearized equations or the assumption of small perturbations. To estimate the range of applicability of the theoretical results of Gelhar and Axness (1983), Tompson et al. (1988) generated two porous media using the turning-bands method (Tompson et al., 1987; Mantoglou and Wilson, 1982), one with variance 1.0 and the other with variance 5.3. Case one with σ_f^2=1.0 is a moderate test of the perturbation theory and case two with σ_f^2=5.3 is quite a severe test. In Figure 5-6 the longitudinal macrodispersivities for the two cases are compared with the theoretical results of Gelhar and Axness (1983) and Neuman (1987). It would appear that for the isotropic case, the predicted value of A_{11} using the theory of Gelhar and Axness is quite good for σ_f^2 as large as 1.0 and reasonable for σ_f^2 as large as 5.3. In contrast, the theory of Neuman (1987) yields a modest overestimate of A_{11} for σ_f^2=1.0, but is significantly in error for σ_f^2=5.3.

We emphasize that the results of Tompson et al. (1988) apply to the isotropic case only. There is a clear need to expand the simulations to cases of anisotropic porous media. Simulations in an anisotropic case would not be straightforward because of the additional questions of initial conditions, boundary conditions, and the size of the domain. Tompson et al. (1988) suggest that a model with 10^7 nodes may be necessary to simulate the problem of anisotropic flow and transport properly. Until simulations are performed for the anisotropic case it is not possible to assess the adequacy of the Gelhar and Axness (1983) theory in a manner similar to Figure 5-6 for predicting macrodispersivities in very heterogeneous, anisotropic porous media. Nonetheless, we are encouraged by the results of Tompson et al. (1988).

The results in Tables 5-2 and 5-3 were obtained under the assumption that the log hydraulic conductivity field is stationary. A tempting solution to the large-variance question is simply to reduce the variance by removing higher-order trends from data. This simple idea ignores the important point that the theoretical results of Gelhar and Axness (1983) assume the mean log conductivity is constant. The theory would need to be extended for the case of trending mean before any conclusions can be

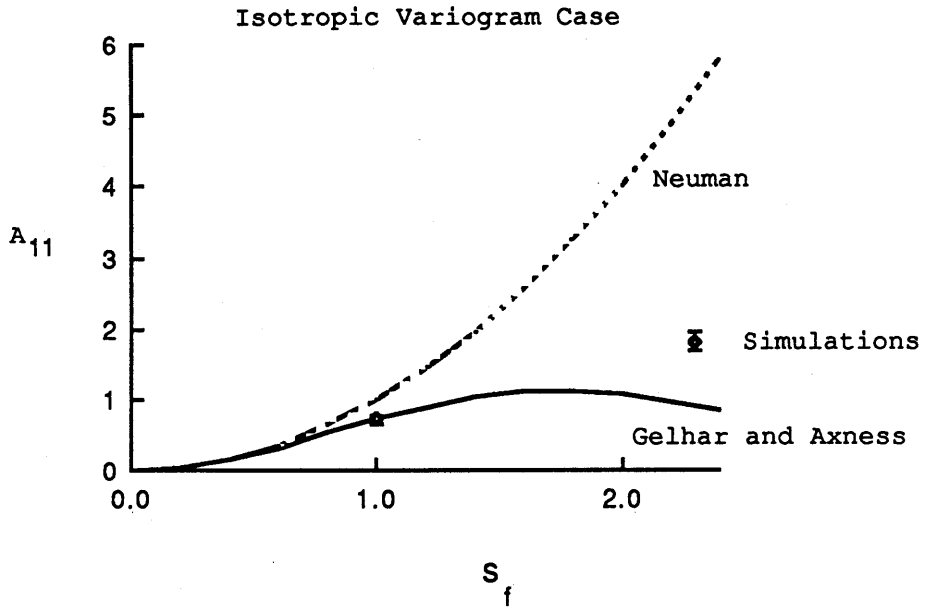

Figure 5-6. Comparison of Longitudinal Dispersivity from Three-Dimensional Simulations and Stochastic Theory

Source : Tompson et al., 1988

drawn. If for example, the hydraulic conductivity decreases monotonically with depth in the aquifer, then a tracer plume in such an aquifer would be sheared as it moves along. That shearing, however, is not dispersion. Therefore, how trends are incorporated into the prediction of macrodispersivity is an area of future research.

TEMPORAL VARIBILITY

From the theory in Section 2 and the parameters of the temporal variability in Section 4 some estimates can now be made of the effect of unsteady flow on the predicted values of macrodispersivity. As in the steady-flow case, two simplified examples, one of flow parallel to bedding and one with flow inclined to bedding, will be examined.

Equations 2-53 and 2-61 describe the unsteady contribution to A_{ij} for the two special cases of variation in gradient magnitude and gradient direction, respectively. Values of most of the parameters in those equations are given in Tables 4-8 and 4-9. Only the mean values from Table 4-9 will be used in the following calculations. The solute velocity (q/n) is assumed to be 0.055 m/day, and the flow factor γ was presented in Tables 5-2 and 5-3 for each of the special cases. The angles Γ and Ω are defined by Eq. 2-55 in terms of ϕ and θ, respectively. The observed values of Γ and Ω in Table 4-8 will serve as a check on the calculated values from Eq. 2-55.

Horizontal and Vertical Anisotropy - Flow Parallel to the Bedding

The first special case is of flow parallel to bedding in a three-dimensionally anisotropic medium. In the steady-state case (See Table 5-2) it was shown that the predicted longitudinal and transverse dispersivities remained within a narrow range of values despite a wide range of input parameters. The predicted transverse macrodispersivities were generally quite small. To determine the maximum additional transverse dispersive flux due to unsteady flow, the gradient variability parameters including seasonal periodicity from Table 4-9 will be used. It is recognized that the resulting $A_{ij}^{(u)}$ will be an upper-bound estimate of the unsteady effect. Two sets of $A_{ij}^{(u)}$ will be calculated, one examining the effect of gradient magnitude variation and the other examining the combined effects of variations in both Γ and Ω.

Table 5-4 contains the predicted $A_{ij}^{(u)}$ and the combined A_{ij} (spatial and temporal varibility) for the case of flow parallel to bedding, including the contribution from variation in hydraulic gradient magnitude. In this case, only the horizontal gradient is considered because the layers are assumed to be horizontal and the flow is horizontal also. Comparing the last four columns of Tables 5-2 and 5-4, it is evident that fluctuations in the magnitude of the horizontal hydraulic gradient produce a very small effect, particularly when one realizes that the values of σ_J^2 and λ_J may be overestimated by at least a factor of 10. The principal components of Table 5-4 are plotted in Figure 5-7. A comparison of Figure 5-4 with 5-7 demonstrates that there is little influence of temporal variability of gradient magnitude on the predicted macrodispersivity.

The direction of the hydraulic gradient fluctuates both in the horizontal plane and in the vertical plane. For the combined effects of variation in Γ and Ω, Eq. 2-62 is used twice. For flow parallel to the bedding plane, Γ can be nonzero if ϕ is nonzero. To bring in the effect of variation of the gradient in the direction perpendicular to the bedding while still maintaining the mean flow parallel to the bedding, the angle $\Omega = 0$, but σ_Ω^2 is nonzero. Recall from Table 4-9 that the variability in the vertical direction of the gradient was more than 10 times larger than in the horizontal direction. Therefore one can expect that the vertical transverse macrodispersivities will be influenced to a greater extent than the horizontal transverse value. The results are presented in Table 5-5; again the last four columns are compared to Table 5-2. The principal components are plotted in Figure 5-8. In all cases, the longitudinal component was largely unaffected by the variation in the gradient direction. For the case of small variance ($\sigma_f^2 = 2.9$) both transverse terms of A_{ij}^* increased by at least one order of magnitude due to unsteady effects. As the variance increases, the relative effect of temporal variability decreases because of the γ term in Eqs. 2-53 and 2-61 increases as the variance increases. The hydraulic gradient variability parameters were upper bounds, and therefore the increase in A_{33} due to temporal variability may not be as large as indicated in Table 5-5. Nonetheless, these results demonstrate that observed temporal variability may enhance the dispersivity. Of particular interest is the increase in the transverse terms with decreasing variance. It appears that the influence of temporal

Table 5-4

CALCULATED MACRODISPERSIVITY COMPONENTS FOR THE CASE OF FLOW PARALLEL TO BEDDING INCLUDING THE CONTRIBUTION FROM HYDAULIC GRADIENT MAGNITUDE VARIABILITY

Group #	σ_f^2	ϕ deg.	Γ deg.	λ_1 m	λ_2 m	λ_3 m	γ	K_{11}/K_{22}	$A_{11}^{(u)}$ m	$A_{22}^{(u)}$ m	$A_{12}^{(u)}$ m	$A_{33}^{(u)}$ m	A_{11}^{*} m	A_{22}^{*} m	A_{33}^{*} m	Ψ deg
1	2.9	0.0	0.0	6.9	3.4	0.75	3.60	1.34	0.1200	0.0000	0.0000	0.0	1.66	0.000	0.0000	0.0
	2.9	25.0	7.1	6.9	3.4	0.75	3.39	1.34	0.1400	0.0021	-0.0170	0.0	1.55	0.001	0.0014	-7.0
	2.9	45.0	8.4	6.9	3.4	0.75	3.07	1.34	0.1700	0.0036	-0.0240	0.0	1.52	0.002	0.0015	-8.7
2	4.6	0.0	0.0	15.0	10.0	1.60	7.43	1.34	0.0280	0.0000	0.0000	0.0	1.28	0.000	0.0000	0.0
	4.6	25.0	7.1	15.0	10.0	1.60	7.00	1.34	0.0330	0.0005	-0.0040	0.0	1.32	0.002	0.0011	-8.1
	4.6	45.0	8.4	15.0	10.0	1.60	6.34	1.34	0.0004	0.0008	-0.0056	0.0	1.36	0.001	0.0014	-6.3
3	6.3	0.0	0.0	40.0	13.0	2.50	19.30	2.13	0.0054	0.0000	0.0000	0.0	0.69	0.000	0.0000	0.0
	6.3	25.0	19.8	40.0	13.0	2.50	16.10	2.13	0.0077	0.0010	-0.0028	0.0	0.69	0.005	0.0039	-16.7
	6.3	45.0	19.9	40.0	13.0	2.50	12.30	2.13	0.0133	0.0017	-0.0048	0.0	0.81	0.006	0.0034	-18.4
4	4.6	0.0	0.0	38.0	4.2	0.85	9.48	1.77	0.0170	0.0000	0.0000	0.0	1.96	0.000	0.0000	0.0
	4.6	25.0	14.5	38.0	4.2	0.85	8.34	1.77	0.0290	0.0019	-0.0075	0.0	0.71	0.001	0.0010	-13.5
	4.6	45.0	15.5	38.0	4.2	0.85	6.85	1.77	0.0430	0.0033	-0.0119	0.0	0.67	0.000	0.0007	-16.6

Horizontal gradient variation: $J_h = 5.2 \times 10^{-3}$ $\sigma_{J_h}^2 = 2.1 \times 10^{-6}$ $\lambda_{J_h} = 365$ days

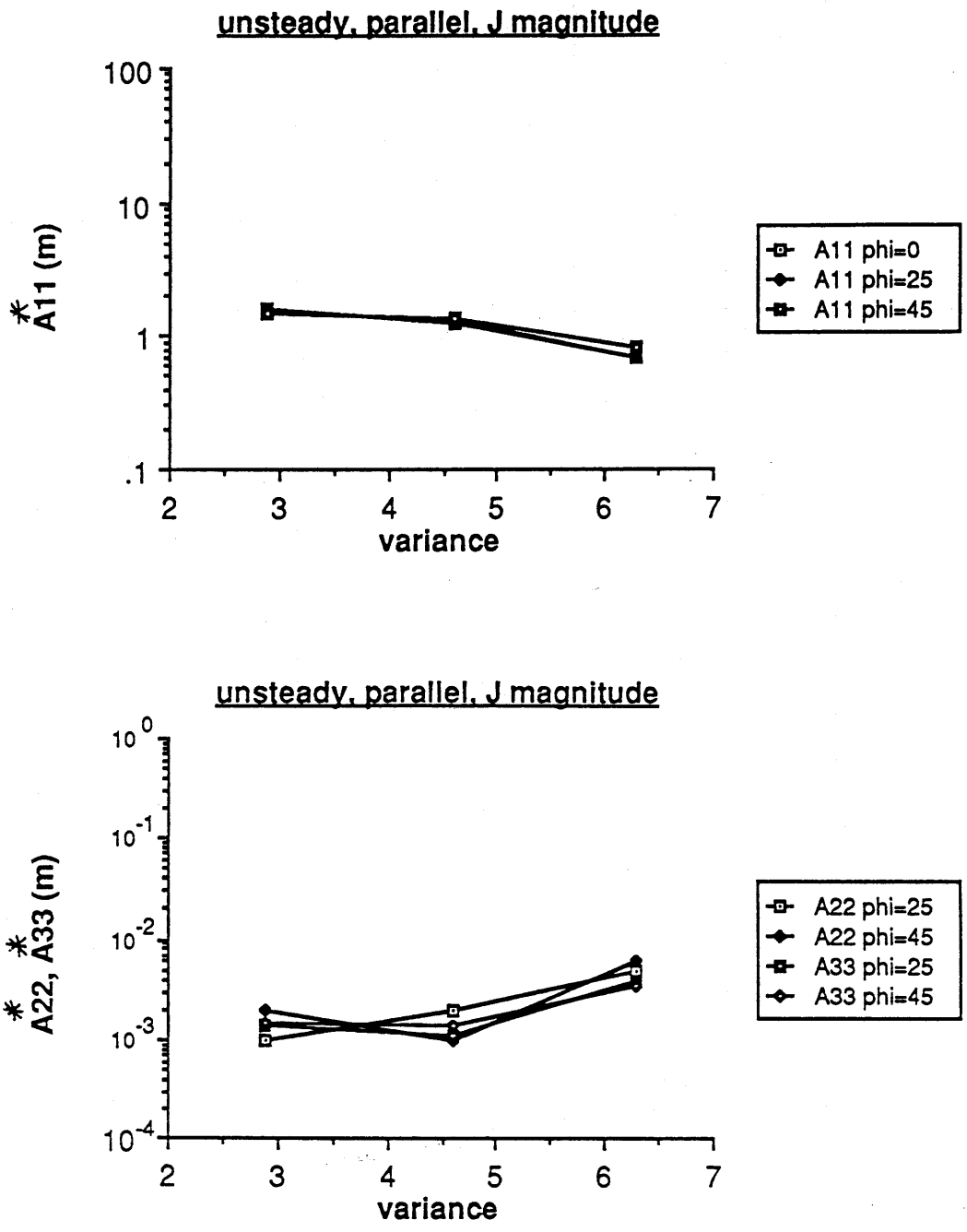

5-7. Principal Components of the Macrodispersivity Tensor for the Case of Unsteady Flow Parallel to Bedding Including Temporal Variability of the Magnitude of the Hydraulic Gradient.

Table 5-5

CALCULATED MACRODISPERSIVITY COMPONENTS FOR THE CASE OF FLOW PARALLEL TO BEDDING INCLUDING THE CONTRIBUTION FROM HYDRAULIC GRADIENT DIRECTION VARIABILITY

Group #	σ_f^2	ϕ deg.	Γ deg.	λ_1 m	λ_2 m	λ_3 m	γ	K_{11}/K_{22}	$A_{11}^{(u)}$ m	$A_{22}^{(u)}$ m	$A_{12}^{(u)}$ m	$A_{33}^{(u)}$ m	A_{11}^{*} m	A_{22}^{*} m	A_{33}^{*} m	Ψ deg
1	2.9	0.0	0.0	6.9	3.4	0.75	3.60	1.34	0.00000	0.0170	0.0000	0.390	1.54	0.0170	0.390	0.0
	2.9	25.0	7.1	6.9	3.4	0.75	3.39	1.34	0.00030	0.0190	0.0024	0.440	1.41	0.0210	0.440	-7.9
	2.9	45.0	8.4	6.9	3.4	0.75	3.07	1.34	0.00060	0.0230	0.0034	0.530	1.34	0.0250	0.530	-9.5
2	4.6	0.0	0.0	15.0	10.0	1.60	7.43	1.34	0.00000	0.0040	0.0000	0.090	1.25	0.0040	0.090	0.0
	4.6	25.0	7.1	15.0	10.0	1.60	7.00	1.34	0.00008	0.0045	0.0006	0.100	1.28	0.0060	0.100	-4.2
	4.6	45.0	8.4	15.0	10.0	1.60	6.34	1.34	0.00010	0.0055	0.0008	0.120	1.36	0.0070	0.120	-6.6
3	6.3	0.0	0.0	40.0	13.0	2.50	19.30	2.13	0.00000	0.0006	0.0000	0.014	0.68	0.0006	0.014	0.0
	6.3	25.0	19.8	40.0	13.0	2.50	16.10	2.13	0.00010	0.0008	0.0003	0.020	0.68	0.0041	0.020	-16.7
	6.3	45.0	19.9	40.0	13.0	2.50	12.30	2.13	0.00020	0.0015	0.0005	0.033	0.80	0.0036	0.033	-18.4
4	4.6	0.0	0.0	38.0	4.2	0.85	9.48	1.77	0.00000	0.0024	0.0000	0.055	1.94	0.0024	0.055	0.0
	4.6	25.0	14.5	38.0	4.2	0.85	8.34	1.77	0.00020	0.0032	0.0008	0.073	0.68	0.0042	0.073	-14.3
	4.6	45.0	15.5	38.0	4.2	0.85	6.85	1.77	0.00040	0.0047	0.0013	0.110	0.62	0.0061	0.110	-14.5

σ_Ω^2 = 870 (degrees)^2 = 0.27 (radians)^2 λ_Ω = 365 days

σ_Γ^2 = 35 (degrees)^2 = 0.011 (radians)^2 λ_Γ = 365 days

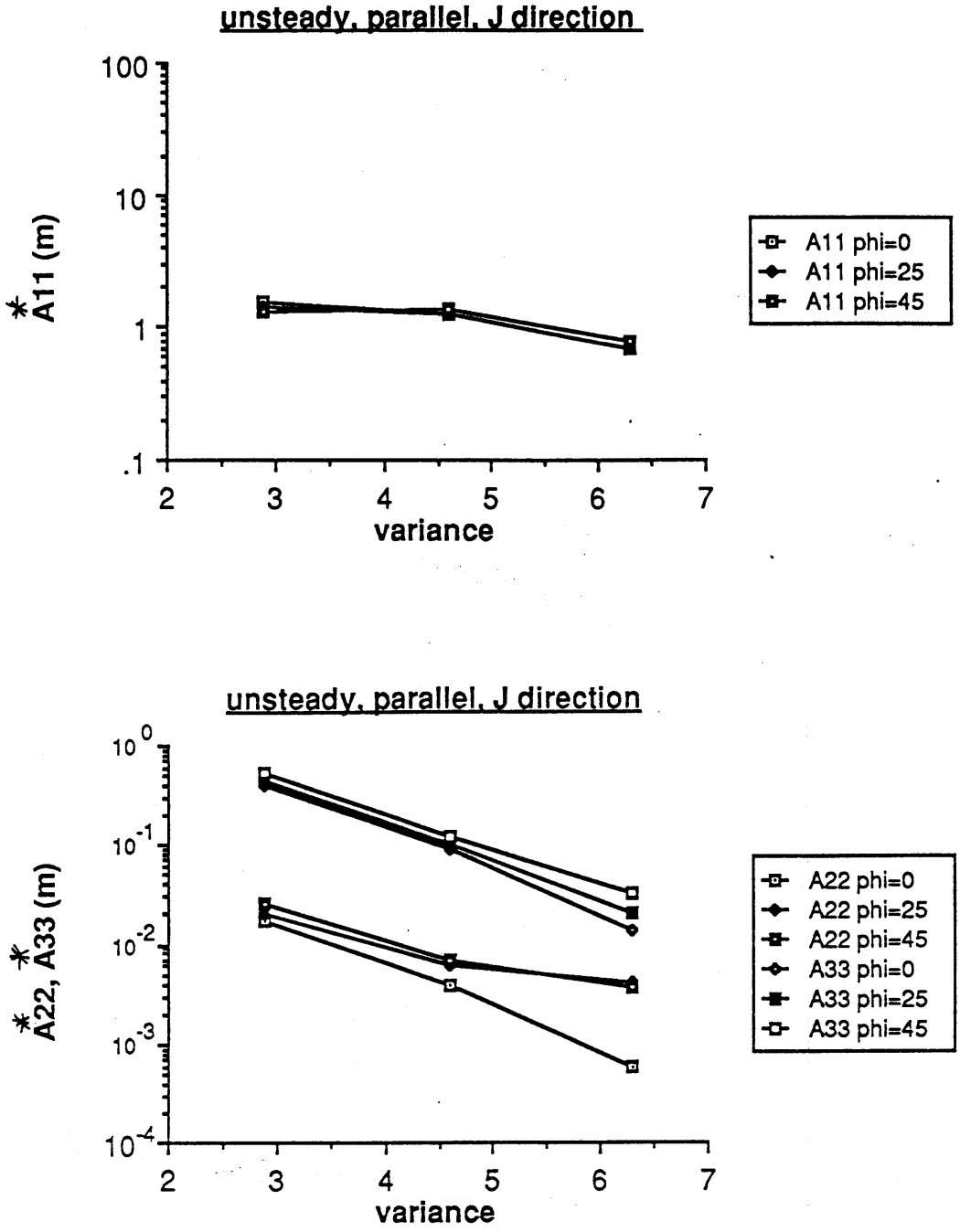

5-8. Principal Components of the Macrodispersivity Tensor for the Case of Unsteady Flow Parallel to Bedding Including Temporal Variability of the Direction of the Hydraulic Gradient.

variability on predicted macrodispersivities becomes greater for less heterogeneous aquifers, for example at the Borden site (Sudicky, 1986). A small variation in the direction of the hydraulic gradient at Borden may be as important as a larger variation at CAFB.

Vertical Anisotropy - Mean Flow Inclined to the Bedding

The second case is flow inclined to bedding in a porous medium that is statistically isotropic in the bedding plane. This case is interesting because in the steady-state case the predicted A_{ij} were very sensitive to the angle θ. The transverse macrodispersivities were also very sensitive to the variance.

Two sets of A_{ij} are calculated, one examining the effect of gradient magnitude variation and the other examining the combined effects of variation in Γ and Ω.

For this example of gradient magnitude variation in the vertical plane, the mean gradient and magnitude are larger than in the horizontal plane. The results are presented in Table 5-6 and Figure 5-9. Comparing the last four columns of Tables 5-3 and 5-6 or comparing Figures 5-5 and 5-9 indicates that variation of the magnitude of the hydraulic gradient has a small effect on macrodispersivity.

The final example, of gradient direction variation with flow oriented at some angle in the vertical plane, is the most interesting case because it combines the largest effects of both spatial and temporal variability. In this case, $\Gamma = 0$ and Ω varies with θ. The results are presented in Table 5-7 and Figure 5-10. A number of interesting aspects of Table 5-7 are worth noting.

The much stronger variability of the gradient direction in the vertical direction results in a much larger increase in A_{33}^* than in A_{22}^*. The transverse principal components of A_{ij} are clearly anisotropic in this case. Had the gradient direction fluctuations been stronger in the horizontal plane, then the A_{22}^* value would have been larger than A_{33}^*.

Another interesting point is that the direction of plume rotation due to the gradient direction variation is in the opposite direction to the rotation due to spatial variability. This opposite rotation is clearly

Table 5-6

CALCULATED MACRODISPERSIVITY COMPONENTS FOR THE CASE OF FLOW INCLINED TO BEDDING INCLUDING THE CONTRIBUTION FROM HYDRAULIC GRADIENT MAGNITUDE VARIABILITY

Group #	σ_f^2	θ deg	Ω deg	λ_1 m	λ_2 m	λ_3 m	γ	K_{11}/K_{33}	$A_{11}^{(u)}$ m	$A_{22}^{(u)}$ m	$A_{13}^{(u)}$ m	$A_{33}^{(u)}$ m	A_{11}^{*} m	A_{22}^{*} m	A_{33}^{*} m	η deg
1	2.9	0.0	0.0	6.9	6.9	0.85	3.35	12.9	0.105	0.0	0.000	0.0000	1.89	0.0	0.000	0.0
	2.9	2.0	15.0	6.9	6.9	0.85	3.31	12.9	0.107	0.0	-0.029	0.0078	1.86	0.0064	0.012	-2.6
	2.9	5.0	33.0	6.9	6.9	0.85	3.16	12.9	0.118	0.0	-0.076	0.0484	1.79	0.038	0.071	-7.2
	2.9	9.0	45.0	6.9	6.9	0.85	2.81	12.9	0.149	0.0	-0.151	0.1530	1.84	0.112	0.196	-15.2
2	4.6	0.0	0.0	12.7	12.7	1.60	6.71	30.8	0.026	0.0	0.000	0.0000	1.31	0.0	0.000	0.0
	4.6	2.0	45.0	12.7	12.7	1.60	6.48	30.8	0.028	0.0	-0.028	0.0280	1.38	0.068	0.088	-8.1
	4.6	5.0	65.0	12.7	12.7	1.60	5.48	30.8	0.039	0.0	-0.082	0.1730	1.87	0.404	0.47	-24.3
	4.6	9.0	69.0	12.7	12.7	1.60	3.89	30.8	0.078	0.0	-0.207	0.5490	3.65	1.18	1.07	-41.7
3	6.3	0.0	0.0	22.5	22.5	2.50	14.40	129.0	0.0057	0.0	0.000	0.0000	0.69	0.0	0.000	0.0
	6.3	2.0	76.0	22.5	22.5	2.50	12.50	129.0	0.0076	0.0	-0.029	0.1130	1.25	0.61	0.49	-44.2
	6.3	5.0	80.0	22.5	22.5	2.50	7.30	129.0	0.0221	0.0	-0.124	0.6990	5.62	3.59	1.45	-66.4
	6.3	9.0	78.0	22.5	22.5	2.50	3.50	129.0	0.0970	0.0	-0.463	2.2100	19.20	10.40	4.28	-65.1

Magnitude Variation: $J = 2.3 \times 10^{-2}$ $\sigma_J^2 = 3.1 \times 10^{-5}$ $\lambda_J = 365$ day

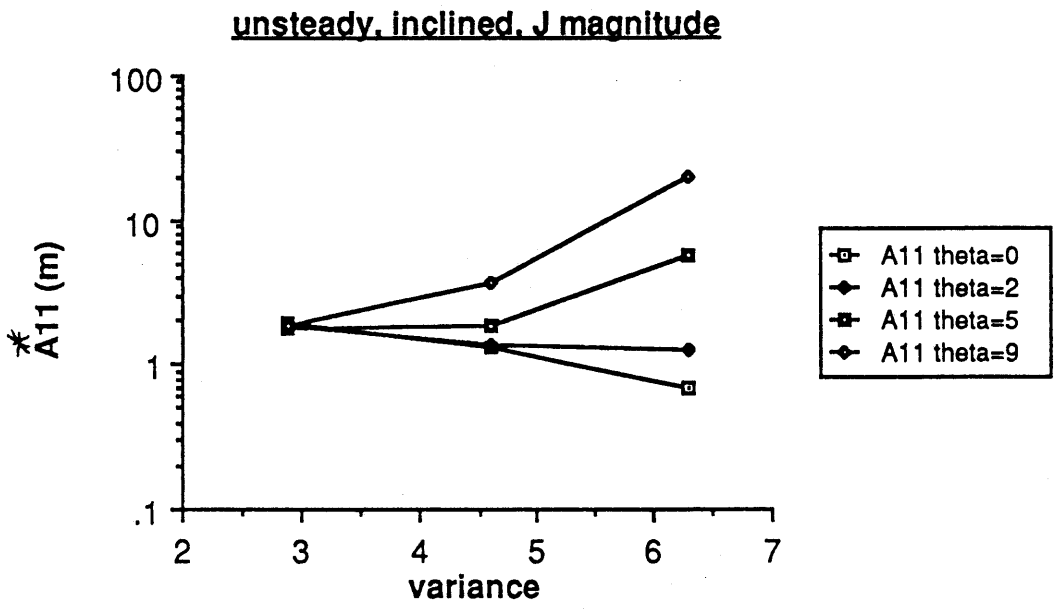

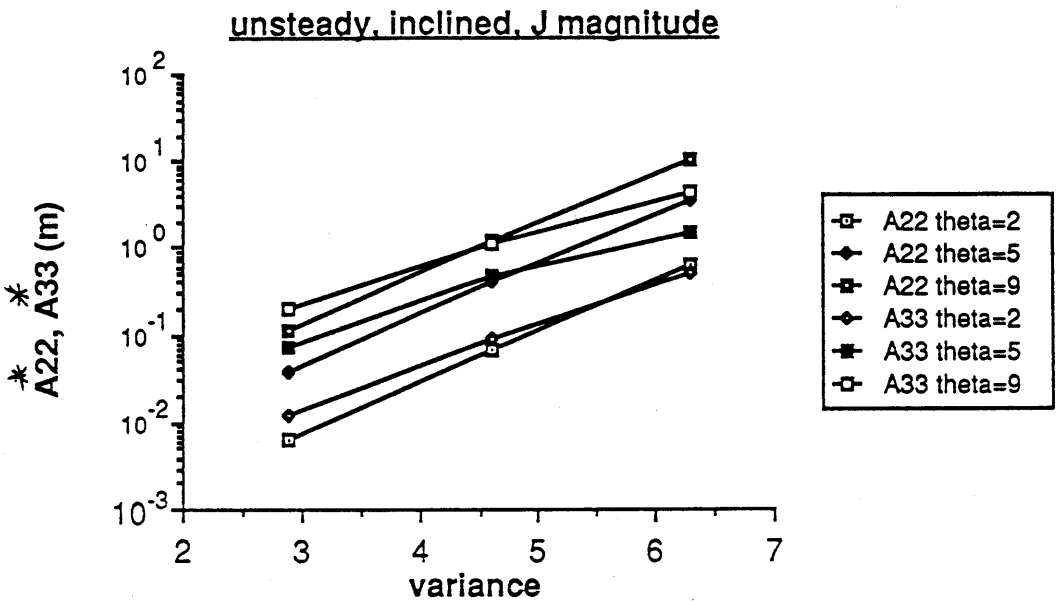

5-9. Principal Components of the Macrodispersivity Tensor for the Case of Unsteady Flow Inclined to Bedding Including Temporal Variability of the Magnitude of the Hydraulic Gradient.

Table 5-7

CALCULATED MACRODISPERSIVITY COMPONENTS FOR THE CASE OF FLOW INCLINED TO BEDDING INCLUDING THE CONTRIBUTION FROM HYDRAULIC GRADIENT DIRECTION VARIABILITY

Group #	σ_f^2	θ deg	Ω deg	λ_1 m	λ_2 m	λ_3 m	γ	K_{11}/K_{33}	$A_{11}^{(u)}$ m	$A_{22}^{(u)}$ m	$A_{13}^{(u)}$ m	$A_{33}^{(u)}$ m	A_{11}^{*} m	A_{22}^{*} m	A_{33}^{*} m	η deg
1	2.9	0.0	0.0	6.9	6.9	0.85	3.35	8.8	0.000	0.0200	0.00	0.480	1.790	0.0200	0.480	0.00
	2.9	2.0	15.0	6.9	6.9	0.85	3.31	8.8	0.036	0.0200	0.13	0.490	1.790	0.0200	0.500	3.51
	2.9	5.0	33.0	6.9	6.9	0.85	3.16	8.8	0.220	0.0220	0.35	0.540	1.900	0.0220	0.560	9.14
	2.9	9.0	45.0	6.9	6.9	0.85	2.81	8.8	0.710	0.0280	0.70	0.690	2.400	0.0280	0.720	15.50
2	4.6	0.0	0.0	12.7	12.7	1.60	6.74	30.8	0.000	0.0049	0.00	0.120	1.290	0.0049	0.120	0.00
	4.6	2.0	45.0	12.7	12.7	1.60	6.51	30.8	0.130	0.0053	0.13	0.130	1.460	0.0053	0.210	-1.20
	4.6	5.0	65.0	12.7	12.7	1.60	5.49	30.8	0.800	0.0074	0.38	0.180	2.400	0.0074	0.710	-2.30
	4.6	9.0	69.0	12.7	12.7	1.60	3.89	30.8	2.530	0.0150	0.95	0.360	4.960	0.0150	2.020	-2.40
3	6.3	0.0	0.0	6.3	6.3	2.50	14.40	129.0	0.000	0.0011	0.00	0.026	0.681	0.0011	0.026	0.00
	6.3	2.0	76.0	6.3	6.3	2.50	12.50	129.0	0.520	0.0015	0.14	0.035	1.460	0.0015	0.710	-17.60
	6.3	5.0	80.0	6.3	6.3	2.50	7.30	129.0	3.220	0.0043	0.57	0.102	5.940	0.0043	4.070	-35.40
	6.3	9.0	78.0	6.3	6.3	2.50	3.50	129.0	10.200	0.0190	2.13	0.450	19.200	0.0190	12.700	-35.40

Gradient Direction Variation: σ_Ω^2 = 870 (degrees)^2 = 0.27 (radians)^2 λ_Ω = 365 days

σ_Γ^2 = 35 (degrees)^2 = 0.011 (radians)^2 λ_Γ = 365 days

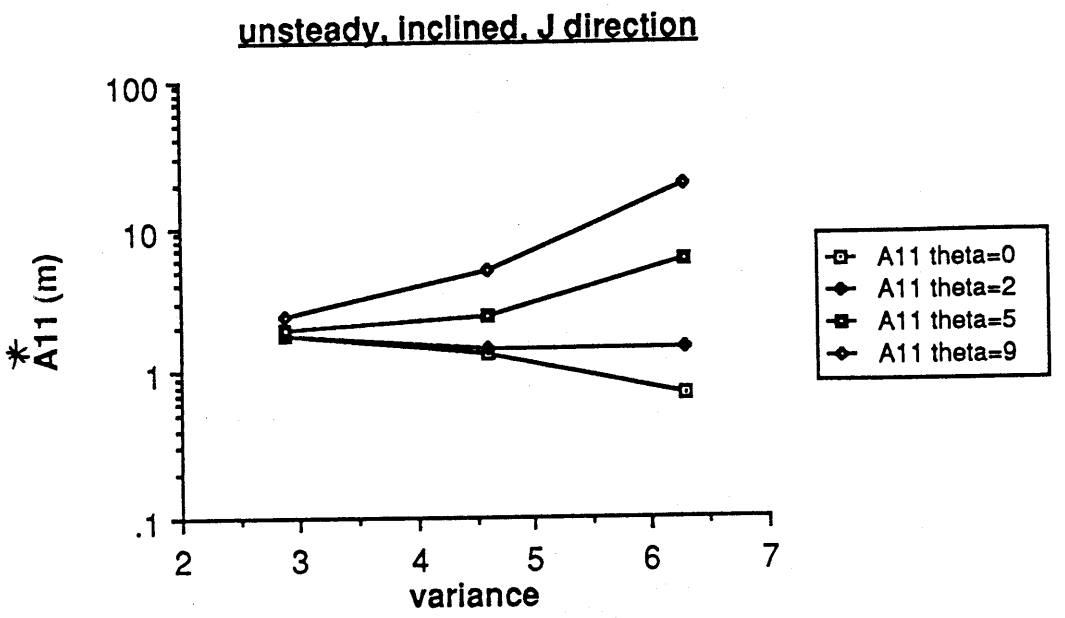

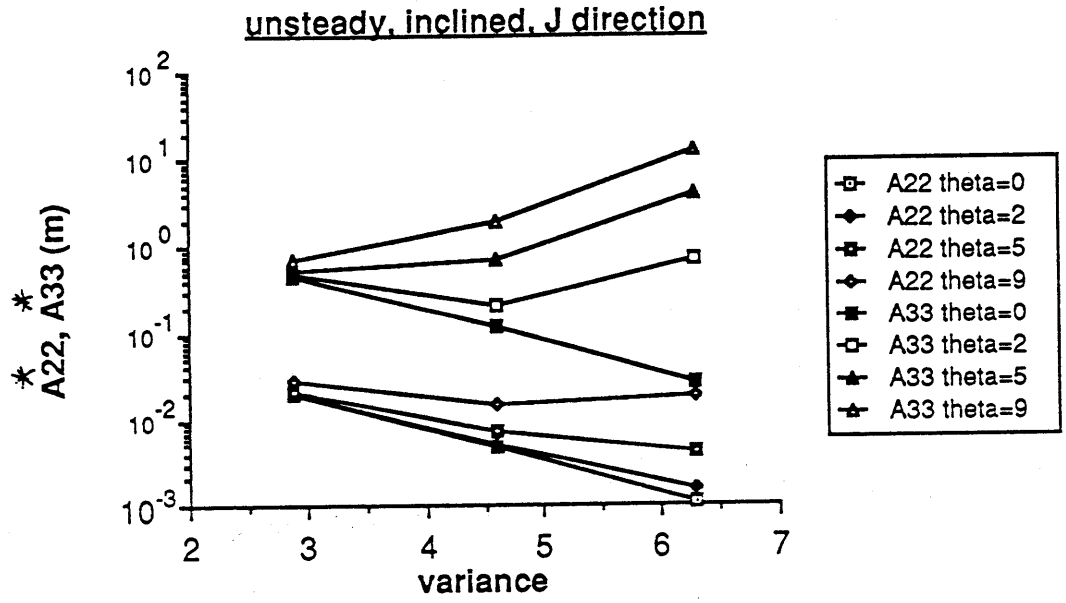

5-10. Principal Components of the Macrodispersivity Tensor for the Case of Unsteady Flow Inclined to Bedding Including Temporal Variability of the Direction of the Hydraulic Gradient.

demonstrated for case of variance of 2.9 where the angle η is positive in Table 5-7 compared to Table 5-3 where for the same case, η was negative. The results for this last case must be viewed with some skepticism because the physical situation is somewhat unrealistic. The hydraulic gradient is oriented downward at angles as large as 70 or 80 from the vertical. The large fluctuations in the direction of the hydraulic gradient (±60 degrees) result in an oscillating flow system.

Discussion - Temporal Variability

Fluctuations in the magnitude of the gradient produce a minor affect on A_{ij} even for the large seasonal parameters that were used for inputs. The temporal variation of the gradient direction does produce significantly increased transverse macrodispersivities in some cases. The largest transverse macrodispersivities were in the vertical direction because the variance of the vertical gradient direction was larger. If the more probable subseasonal parameters are used, then the effect is reduced. Note also that the magnitude of the contribution to A_{ij} due to unsteadiness is larger for less heterogeneous media. The contribution to dispersive flux from unsteady flow obtained in this study agrees with the work of Ackerer and Kinzelbach (1985) who suggested that the longitudinal component would be largely unaffected, but that the transverse components could increase dramatically. However, the forms of the unsteady components developed in this work and in Ackerer and Kinzelbach (1985) are substantially different. In Ackerer and Kinzelbach (1985) the unsteadiness in the velocity components multiply the steady-state macrodispersivities whereas in this work the unsteadiness in the hydraulic gradient is an additive effect.

Although the parameters describing the temporal variability of the hydraulic gradient were only crude estimates, it is clear from the result of the this section that unsteady flow is a potentially important dispersive mechanism that warrants additional study.

Before closing this section, the data from two recently completed tracer tests will be used to show the applicability of the unsteady results to different site conditions. At the Borden experiment, Mackay et al. (1986) noted that the hydraulic gradient was temporally variable. From Mackay et al. (1986) and Sudicky (1986) the following parameters can be obtained

σ_Γ^2 = 10.6 (degrees)^2 = 0.0032 (radians)^2

q/n = 0.091 m/day

σ_f^2 = 0.29

λ_1 = 2.8m

J = 0.0043

λ_3 = 0.12m

Assume q is aligned with J, so $\overline{\Omega} = \overline{\Gamma} = 0$ and that λ_J = 60 days. With the parameters above, the longitudinal and transverse macrodispersivities are 0.62 and 0.013 m, respectively. The transverse term is similar in magnitude to the measured value (see Freyberg, 1986; and Section 1 of this thesis). Recall that the steady theory was unable to reproduce the transverse term. Therefore the unsteadiness at the Borden site may have contributed to the observed dispersivity.

At the site of another large-scale tracer experiment on Cape Cod, Garabedian (1987) measured the variation in hydraulic head with time at a number of wells from which the variation of the gradient direction is determined. Garabedian showed that the center of mass of the plume shifted laterally in response to the hydraulic gradient fluctuations, but that there was a small fluctuation that appeared to be random. The scale of fluctuation of the random component along with several other measured or assumed parameters are:

σ_Γ^2 = 0.75 (degrees)^2

q/n = 0.43 m/day

σ_f^2 = 1.1

λ_1 = 2 m

J = 0.0043

λ_3 = 0.2m

The calculated macrodispersivities are A_{11} = 0.85 m; A_{22} = 0.008 m, which are in general agreement with the measured values determined from the large-scale tracer test of A_{11} = 0.96 m and A_{22} = 0.018 m. Again it appears that unsteadiness does lead to an increased transverse dispersive flux of a magnitude that is comparable with existing tracer-test data.

Section 6

SUMMARY AND RECOMMENDATIONS

At a site located on the Columbus Air Force Base (CAFB), Mississippi, the Tennessee Valley Authority and the Massachusetts Institute of Technology are conducting a Macrodispersion Experiment (MADE) to study the large-scale mixing caused by aquifer heterogeneity. One aim of the MADE project is to develop and evaluate methods of characterizing the spatial variability of hydraulic conductivity at the CAFB site. In particular, the variance and correlation scales of the three-dimensional autocovariance function of the natural logarithm of hydraulic conductivity are required to be able to predict macrodispersivities using recently developed stochastic theories (Gelhar and Axness, 1983; Dagan, 1982, 1984).

Eight possible methods of characterizing variability were implemented: slug tests in piezometers, grain-size distributions, surface geophysics, borehole geophysics, conventional large-scale aquifer tests, mapping of sedimentological facies, laboratory permeameter, and borehole flowmeter. The goal was to find a method that not only characterized the variability accurately, but also could be applied on a routine basis at other sites. Of the possible methods, the borehole flowmeter method appeared to be the most promising and was extensively tested at the CAFB site (Rehfeldt et al., 1988). Less extensive data were collected using methods other than the borehole flowmeter. These secondary data, collected prior to the flowmeter measurements, provided preliminary estimates of the variance and correlation scales that were useful in designing the flowmeter experiments. The methods for collecting the secondary data were applied in much the same way one might use them in a routine site evaluation. Much of the data collected during a routine site evaluation is for reconnaissance purposes to familiarize the investigator with the range of conditions at the site. These measurements are not designed to provide geostatistical information, yet in many cases preliminary geostatistical information can be obtained. The preliminary autocovariance parameters from the analyses of the secondary data were found to be in general agreement with the parameters from the extensive analyses of the flowmeter data.

An extensive set of hydraulic conductivity data (1242 points), collected using a borehole flowmeter technique, was analyzed to obtain the best estimate of the autocovariance parameters. The most likely values for the variance of lnK, the horizontal correlation scale, and the vertical correlation scale are 4.6, 12.7 m and 1.6 m, respectively. Simple approaches were used to quantify the uncertainty in the estimates and produced approximate 95% confidence intervals about the most likely values. The bounding values are 2.9 to 6.3 for the variance, 6.9 m to 22.5 m for the horizontal correlation scale, and 0.7 m to 2.5 m for the vertical correlation scale. Placing a rigorous confidence band on the autocovariance is a difficult problem, and I do not claim to have solved it. Rather, an objective way is presented to evaluate the resulting parameters to determine whether additional, more comprehensive analyses to improve the estimates are justified. The parameter estimates improve slowly with increasing data because the confidence band decreases as the inverse of the square root of the number of samples. Therefore a reduction of the confidence band by a factor of two would require a four-fold increase in the number of data points. It is clear that even with the extensive data set at the CAFB site, the variance and correlation scales could not be determined with certainty and that attempts to do so would require such large amounts of data as to be impossible for practical application. Given that some uncertainty in the covariance parameters is unavoidable, it is encouraging that the preliminary covariance parameters based on secondary measurements (variance of 3.9, horizontal correlation scale of 16 to 30 m, and vertical correlation scale of 1.1 m) fall within the confidence band of the detailed analyses.

The question of whether a random field contains a trend is a difficult problem that will never be answered with certainty in real situations. We approached the question of detrending from the pragmatist's point of view. First of all, from synthetic random fields it is clear that portions of the field of a size up to four or five times the correlation scale can be systematically above or below the ensemble mean. At the CAFB site, where the correlation scale was about 12 m in the horizontal direction, a lense or body of material 50 or 60 m long could legitimately be considered part of the expected behavior of a stationary random field. In addition, what is deemed a trend depends strongly on the scale of the problem being investigated. It is therefore very

important that an investigator understand the scope of the problem before designing a sampling well network and that the design be flexible enough to allow modifications as new information is obtained. With the data collected at the CAFB site it was not possible to show that a trend existed, because the variablity that was observed could all be explained as consistent with a stationary random field. Nonetheless, the measured data were reexamined assuming a trend might be present, for two reasons: 1) to establish a methodology for removing a trend and 2) to see if removing a trend would significantly change the covariance parameter estimates.

After examining the literature, no evidence was found that indicated that the least-squares methods of detrending would yield unsatisfactory results. Polynomial trends of various orders were considered. From the variograms of the residuals it was not possible to decide which order of polynomial was the most appropriate. Only after including information on the path of the tracer plume did it become clear that if a trend was to be removed, it would be of second order. A second-order trend was removed using least-squares appproaches and the variograms of the residuals were corrected for the effects of measurement error, correlated residuals, and estimation bias. The resulting spatial covariance parameters fall well within the confidence range defined for the parameters obtained before detrending. Parameter values that fall within the confidence range cannot be distinguished statistically. Hence, from the viewpoint of the spatial covariance parameter values, the question of whether a second-order trend is superimposed on an otherwise stationary random field is a moot point.

Some uncertainty in the spatial covariance parameters estimated from sample data is inevitable even for very large data sets. By acknowledging this uncertainty, the need for intensive sampling to define "The Autocovariance" largely disappears, and the more pragmatic (and attainable) goal becomes simply a good estimate of the autocovariance. Toward that goal it is encouraging that the preliminary estimates of covariance parameters from the secondary data commonly gathered during routine site investigations are consistent with the more complete analyses of the detailed borehole flowmeter data.

Although the uncertainty in the covariance parameters is itself a concern, it is the effect of that uncertainty on predicted

macrodispersivities that is of most interest. The importance of the parameter uncertainty was assessed by predicting asymptotic macrodispersivities (A_{ij}) using Gelhar and Axness (1983) for the most likely parameter values and the bounding values. The results are summarized in the following table:

	Dispersivity in m	
Dispersivity component	Most likely	Bounding
Longitudinal	0.6-3.2	0.6-17.1
Horizontal transverse	0.0006-1.2	0.0006-10.4
Vertical transverse	0.0006-0.9	0.0006-4.2

This range of A_{ij} is quite large, but recall that the range of the variance and correlation scales are interpreted as 95% confidence intervals. By using a smaller confidence interval, and hence accepting a greater risk that the true values fall outside the interval, a smaller range of A_{ij} would result. In addition to the uncertainty in the variance and correlation scales, the transverse terms are also very sensitive to the angle of inclination for flow inclined to the bedding.

The Columbus site is much more heterogeneous than any other well-studied site to date. The equations in Gelhar and Axness (1983) were obtained assuming small random perturbations. In the case of an isotropic autocovariance ($\lambda_1=\lambda_2=\lambda_3$) Tompson et al. (1988) used a random-walk technique to simulate the transport of solutes through two heterogeneous random porous media using the flow field from Ababou (1988). Their results indicated that for the isotropic case, the predicted value of the longitudinal dispersivity A_{11} using the theory of Gelhar and Axness is quite good for the variance of lnK (σ_f^2) as large as 1.0 and reasonable for σ_f^2 as large as 5.3. In contrast, the theory of Neuman (1987) yields a modest overestimate of A_{11} for $\sigma_f^2=1.0$, but is significantly in error for $\sigma_f^2=5.3$.

The predicted macrodispersivities were obtained under the assumption that the log hydraulic conductivity field is stationary. A tempting solution to the large-variance question is to simply reduce the variance by removing higher-order trends from data. This simple idea ignores one important point: the theoretical results of Gelhar and Axness (1983) assume the mean log conductivity is constant. The theory would need to be extended for the case of a trending mean before any conclusions can

be drawn. If, for example, the hydraulic conductivity decreases monotonically with depth in the aquifer, then a tracer plume in such an aquifer would be sheared as it moved along. That shearing, however, is not dispersion.

An examination of the additional dispersive flux due to unsteady flow was motivated by two factors: 1) the predicted transverse macrodispersivities from the steady-state stochastic theories were sometimes much smaller than observed values, indicating that perhaps a transverse dispersive mechanism had been neglected in the steady analysis, and 2) the flow system at CAFB was temporally variable and there was concern about the effect of unsteadiness on dispersion.

A preliminary analysis of the effect of unsteadiness on dispersion treated the temporally variable hydraulic gradient vector as the primary influence of dispersivity. Although the time series of hydraulic gradient at CAFB were inadequate to perform detailed covariance analyses, preliminary estimates of the variance and correlation scales were obtained and used to demonstrate the magnitude of the unsteady effect.

Variations in the magnitude of the hydraulic gradient had little effect on the predicted macrodispersivities. Variations in the direction of the gradient did significantly increase the dispersive flux in the transverse direction, but upper-bound values of the variability made the actual magnitude of the effect suspect. Nonetheless, unsteady flow was shown to produce enhanced lateral mixing, and the magnitude of the additional dispersion was comparable to measurements at recently completed tracer test sites.

A number of recommendations can be made from this study. Surface geophysics may offer a way to characterize the horizontal variability of hydraulic conductivity. The results from CAFB were encouraging, but inconclusive because the sample spacing was too coarse. Conventional resistivity and SP surveys should be repeated, but with a spacing between measurements of 7m or so. Grain-size samples should be taken at least every 0.76 m (2.5 feet) during the augering of a borehole. That should provide sufficient data to calculate a variogram in the vertical.

We recommend more thorough analysis of the large-scale aquifer test data with particular attention to: (1) the assumptions in Neuman (1972, 1975) that transmissivity, specific yield, and hydraulic (horizontal-vertical) anisotropy remain constant, and (2) an extension of the analysis to the horizontally anisotropic case.

Additional flowmeter measurements should be performed at the CAFB site. The additional wells are not likely to increase the accuracy of the autocovariance parameters, so the well locations should be chosen for reconnaissance of areas currently without data. For instance, a number of wells should be installed well ahead of the plume to aid in gauging future plume speed and direction.

Additional theoretical work is needed. The case of a trending mean hydraulic conductivity field needs to be examined to fully understand the implications of removing a trend from the random field. We finally wish to emphasize that the results of Tompson et al. (1988), which indicated that the theory of Gelhar and Axness (1983) gave a reasonable prediction of longitudinal dispersivity for variances as large as 5.3, apply to the isotropic case only. There is a clear need to expand the simulations to cases of anisotropic porous media. Simulations in an anisotropic case would not be straightforward because of the additional questions of initial conditions, boundary conditions, and the size of the domain. Tompson et al. (1988) suggest that a model with 10^7 nodes or more may be necessary to simulate the anisotropic flow and transport problem properly.

Finally, longer time series of hydraulic head measurements are needed to be able to obtain better estimates of the temporally variable parameters. In particular, nested piezometers are necessary to estimate the vertical hydraulic gradient which is likely to be more variable at the CAFB site. The sampling frequency should be increased from the current monthly interval to bi-weekly and preferably weekly.

REFERENCES

R. Ababou. Three-Dimensional Flow in Porous Media. Doctoral Dissertation, Dept. of Civil Engrg., MIT, Cambridge, MA, Jan. 1988.

P. Ackerer and W. Kinzelbach. Modelization du Transport de Contaminant par la Method de Marche au Hasard: Influence des Variations du Champ D'Ecoulement au Cours de Temps sur la dispersion. The Stochastic Approach to Subsurface Flow, ed. by G. deMarsily, pp. 446-458., 1985.

Albireo, Inc. The Self-Potential Solution to Groundwater, Reservoir, and Geothermal Problems. Company Flyer, Wheat Ridge, CO, 1983, 4 p.

M. Armstrong. Common Problems Seen in Variograms. Mathematical Geology, Vol. 16, No. 3, 1984, pp. 305-313.

G.K. Bhattacharyya and R.A. Johnson. Statistical Concepts and Methods. New York: John Wiley & Sons, 1977, 639 p.

J.R. Benjamin and C.A. Cornell. Probability, Statistics, and Decision for Civil Engineers. New York: McGraw-Hill Book Co., 1970, 684 p.

R.P. Betson, J.M. Boggs, S.C. Young and L.W. Gelhar. Macrodispersion Experiment (MADE): Design of a Field Experiment to Investigate Transport Processes in a Saturated Groundwater Zone. Electric Power Research Institute Interim Report EA-4082, Palo Alto, CA, 1985, 152 p.

Boggs et al. CAFB Site Characterization Report. In Preparation, 1988.

V.A. Bogoslovsky and A.A. Ogilvy. Application of Geophysical Methods for Studying the Technical Status of Earth Dams. Geophysical Prospecting, Vol. 18, 1970, pp. 758-773.

C.F. Chung. Use of the Jackknife Method to Estimate Autocorrelation Functions (or Variograms). G. Verly et al. (eds)., Geostatistics for Natural Resources Characterization, Part 1, 1984, pp. 55-69.

N. Cressie. Fitting Variogram Models by Weighted Least Squares. Mathematical Geology, Vol. 17, No. 5, 1985, pp. 563-586.

N. Cressie. A Nonparametric View of Generalized Covariances for Kriging. Mathematical Geology, Vol. 19, No. 5, 1987, pp. 425-449.

N. Cressie and D.M. Hawkins. Robust Estimation of the Variogram: I. Mathematical Geology, Vol. 12, No. 2, 1980, pp. 115-125.

G. Dagan. Analysis of Flow through Heterogeneous Random Aquifers, 2: Unsteady Flow in Confined Formation. Water Resources Research, Vol. 18, No. 5, 1982, pp. 1571-1585.

G. Dagan. Solute transport in heterogeneous porous formations. Journal of Fluid Mechanics, Vol. 145, 1984, pp. 151-177.

B.M. Davis. Uses and Abuses of Cross-Validation in Geostatistics. Mathematical Geology, Vol. 19, No. 3, 1987, pp. 241-248.

G. deMarsily. Quantitative Hydrogeology; Groundwater Hydrology for Engineers. Orlando: Academic Press, 1986, 440 p.

J.J. Dongarra, J.R. Bunch, C.B. Moler and G.W. Stewart. LINPACK Users' Guide. SIAM, Philadelphia, PA, 1979.

P.A. Dowd. The Variogram and Kriging: Robust and Resistant Estimators. G. Verly et al. (eds)., Geostatistics for Natural Resources Characterization, Part 1, 1984, pp. 91-106.

D.L. Freyberg. A Natural Gradient Experiment on Solute Transport in a Sand Aquifer. 2: Spatial Moments and the Advection and Dispersion of Nonreactive Tracers. Water Resources Research, Vol. 22, No. 13, 1986, pp. 2031-2046.

G. Gambolati and G. Galeati. Comment on "Analysis of Nonintrinsic Spatial Variability by Residual Kriging with Application to Regional Groundwater Levels" by Shlomo P. Neuman and Elizabeth A. Jacobson. Mathematical Geology, Vol. 19, No. 3, 1987, pp. 249-257.

S.P. Garabedian. Large-scale Dispersive Transport in Aquifers: Field Experiments and Reactive Transport Theory. Ph.D. Dissertation, Dept. of Civil Engineering, MIT, Cambridge, MA, 1987.

L.W. Gelhar and C.L. Axness. Stochastic Analysis of Macrodispersion in Three-Dimensionally Heterogeneous Aquifers. Report H-8, Hydorlogy Research Program, New Mexico Institute of Mining and Technology, Socorro, New Mexico, 1981.

L.W. Gelhar and C.L. Axness. Three-Dimensional Stochastic Analysis of Macrodispersion in Aquifers. Water Resources Research, Vol. 19, No. 1, 1983, pp. 161-180.

L.W. Gelhar, A. Mantoglou, C. Welty and K.R. Rehfeldt. A Review of Field-Scale Physical Solute Transport Processes in Saturated and Unsaturated Porous Media. Final Report Prepared for Electric Power Research Institute, Palo Alto, CA, Research Project 2485-5, EPRI EA-4190, 1985.

M.S. Hantush. Analysis of Data from Pumping Tests in Anisotropic Aquifers. Journal of Geophysical Research, Vol. 71, No. 2, 1966, pp. 421-426.

M.S. Hantush and R.G. Thomas. A Method for Analyzing a Drawdown Test in Anisotropic Aquifers. Water Resources Research, Vol. 2, No. 2, 1966, pp. 281-285.

A. Hazen. Experiments upon the Purification of Sewage and Water at the Lawrence Experiment Station. Mass. State Board of Health, 23rd Annual Report, 1892.

P.C. Heigold, R.H. Gilkeson, K. Cartwright and P.C. Reed. Aquifer Transmissivity from Surficial Electrical Methods. Ground Water, Vol. 17, No. 4, 1979, pp. 338-345.

R.J. Hoeksema and P.K. Kitanidis. Analysis of the Spatial Structure of Properties of Selected Aquifers. Water Resources Research, Vol. 21, No. 4, 1985, pp. 563-572.

P. Hufschmied. Die Ermittlung der Durchlässigkeit von Lockergesteins-Grundwasserleitern, eine vergleichende Untersuchung verschiedener Felmethoden. Doctoral Dissertation No. 7397, ETH Zurich, Switzerland, 1983.

P. Hufschmied. Estimation of Three-Dimensional Statistically Anisotropic Hydraulic Conductivity Field by Means of Single Well Pumping Tests Combined with Flowmeter Measurements. Hydrogéologie, No. 2, 1986, pp. 163-174.

D. Huntley and H.M. Mishler. Relationship Between Permeability and Electrical Resistivity in Granular and Fractured-Rock Aquifers. Proceedings, NWWA/EPA Conference on Surface and Borehole Geophysical Methods in Ground Water Investigation. National Water Well Association, Worthington, OH, Feb. 7-9, 1984, pp. 18-36.

M.J. Hvorslev. Time Lag and Soil Permeability in Ground-Water Observations. U.S. Army Corps of Engineers Bulletin, No. 36, 1951.

G.M. Jenkins and D.G. Watts. Spectral Analysis and its Applications. San Francisco: Holden-Day, 1968, 525 p.

A.G. Journel and C.J. Huijbregts. Mining Geostatistics. New York: Academic Press, 1978, 600 p.

W.E. Kelly. Geoelectric Sounding for Estimating Aquifer Hydraulic Conductivity. Ground Water, Vol. 15, No. 6, 1977, pp. 420-425.

P.K. Kitanidis. Statistical Estimation of Polynomial Generalized Covariance Functions and Hydrologic Applications. Water Resources Research, Vol. 19, No. 4, 1983, pp. 901-921.

P.K. Kitanidis. Minimum-Variance Unbiased Quadratic Estimation of Covariances of Regionalized Variables. Mathematical Geology, Vol. 17, No. 2, 1985, pp. 195-208.

P.K. Kitanidis and R.W. Lane. Maximum Likelihood Parameter Estimation of Hydrologic Spatial Processes by the Gauss-Newton Method. Journal of Hydrology, Vol. 79, 1985, pp. 53-71.

W.C. Krumbein and G.D. Monk. Permeability as a Function of the Size Parameters of Unconsolidated Sand. Petr. Technology, 1942, July.

D.R. LeBlanc. Sewage Plume in a Sand and Gravel Aquifer, Cape Cod, Massachusetts. U.S. Geological Survey Water Supply Paper 2018, 1984.

J.L. Lumley and H.A. Panofsky. The Structure of Atmospheric Turbulence. John Wiley , New York, 1964.

D.M. Mackay, D.L. Freyberg, P.V. Roberts, and J.A. Cherry. A Natural Gradient Experiment on Solute Transport in a Sand Aquifer 1. Approach and Overview of Plume Movement. Water Resources Research, Vol. 22, No. 13, 1986,pp. 2017-2029.

A. Mantoglou and J.L. Wilson. The Turning Bands Method for Simulation of Random Fields Using Line Generation by a Spectral Method. Water Resources Research, Vol. 18, No. 5, 1982, pp. 1379-1394.

A. Mantoglou and L.W. Gelhar. Stochastic Modeling of Large-Scale Transient Unsaturated Flow Systems. Water Resources Research, Vol 23, No. 1, 1987a, pp. 37-46.

A. Mantoglou and L.W. Gelhar. Capillary Tension Head Variance, Mean Soil Moisture Content, and Effective Specific Soil Moisture Capacity of Transient Unsaturated Flow in Stratified Soils. Water Resources Research, Vol 23, No. 1, 1987b, pp. 47-56.

A. Mantoglou and L.W. Gelhar. Effective Hydraulic Conductivities of Transient Unsaturaed Flow in Stratified Soils. Water Resources Research, Vol 23, No. 1, 1987c, pp. 57-67.

D.W. Marquardt and S.K. Acuff. Direct Quadratic Spectrum Estimation with irregularly Spaced Data. Time Series Analysis of Irregularly Spaced Data. ed. by E. Parzen, Proceedings of a Symposium held at Texas A & M University, Springer-Verlag, 1983, pp. 211-223.

F. Masch and K. Denny. Grain Size Distribution and Its Effect on the Permeability of Unconsolidated Sands. Water Resources Research, Vol. 2, No. 4, 1966, pp. 665-677.

G. Matheron. The Theory of Regionalized Variables and its Applications. Les Cahiers du Centre de Morphologie Mathématique de Fontainebleau No. 5, 1971, 211 p.

R. L. Naff. A Continuum Approach to the Study and Determination of Field Longitudinal Dispersion Coefficients. Ph.D. Dissertation, New Mexico Institute of Mining and Technology, Socorro, New Mexico, June 1978.

S.P. Neuman. Theory of Flow in Unconfined Aquifers Considering Delayed Response of the Water Table. Water Resources Research, Vol. 8, No. 4, 1972, p. 1031.

S.P. Neuman. Analysis of Pumping Test Data from Anisotropic Unconfined Aquifers Considering Delayed Gravity Response. Water Resources Research, Vol. 11, No. 2, 1975, pp. 329-342.

S.P. Neuman, J. Samper and M. Hernandez. Reply to Comments by G. Gambolati and G. Galeati. Mathematical Geology, Vol. 19, No. 3, 1987, pp. 259-266.

S.P. Neuman and E.A. Jacobson. Analysis of Nonintrinsic Spatial Variability by Residual Kriging with Application to Regional Groundwater Levels. Mathematical Geology, Vol. 16, No. 5, 1984, pp. 499-521.

A.A. Ogilvy, M.A. Ayed and V.A. Bogoslovsky. Geophysical Studies of Water Leakages from Reservoirs. Geophysical Prospecting, Vol. 17, No. 1, 1969, pp. 36-62.

H. Omre. The Variogram and its Estimation. G. Verly et al. (eds)., Geostatistics for Natural Resources Characterization, Part 1, 1984, pp. 107-125.

E.P. Patten, Jr. and G.D. Bennett. Application of Electrical and Radioactive Well Logging to Ground-Water Hydrology. U.S. Geological Survey Water Supply Paper 1544-D, 1963, 60 p.

W.H. Press, B.R. Flannery, S.A. Teukolsky and W.T. Vetterling. Numerical Recipes, The Art of Scientific Computing. Cambridge, England: Cambridge University Press, 1986, 818 p.

M.B. Priestley. Spectral Analysis and Time Series. Vol. 1. Univariate Series. Academic Press, New York. 1981.

K.R. Rehfeldt, P. Hufschmied, L.W. Gelhar and M.E. Schaefer. The Borehole Flowmeter Technique for Measuring Hydraulic Conductivity Variability. Draft of a Topical Report Prepared by MIT for Electric Power Research Institute, Research Project 2485-5, 1988

D. Russo and W.A. Jury. A Theoretical Study of the Estimation of the Correlation Scale in Spatially Variable Fields, 1. Stationary Fields. Water Resources Research, Vol. 23, No. 7, 1987a, pp. 1257-1268.

D. Russo and W.A. Jury. A Theoretical Study of the Estimation of the Correlation Scale in Spatially Variable Fields, 2. Nonstationary Fields. Water Resources Research, Vol. 23, No. 7, 1987b, pp. 1269-1279.

A. Scheidegger. Physics of Flow Through Porous Media. University of Toronto Press, Toronto, Canada, 1960.

F.C. Schweppe. Uncertain Dynamic Systems. Englewood Cliffs, NJ: Prentice-Hall, 1973, 563 p.

L.V.A. Sendlein and H. Yazicigal. Surface Geophysical Techniques in Ground-Water Monitoring Part I. Ground Water Monitoring Review, Fall, 1981, pp. 42-46.

K.P. Seiler. Durchlässigkeit, Porosität und Kornverteilung quartärer Keis-Sand-Ablagerunger des bayerischen Alpenvorlandes. Gas-und Wasserfach, Vol. 114, No. 8, 1973, pp. 353-400.

O. Serra. Fundamentals of Well-Log Interpretation. 1. The Acquisition of Logging Data. New York: Elsevier Science Publ. Co., Developments in Petroleum Science, 15A, 1984, 423 p.

W.E. Sharp. Estimation of Semivariograms by the Maximum Entropy Method. Mathematical Geology, Vol. 14, No. 5, 1982, pp. 457-474.

H.E. Skibitzke and G.M. Robertson. Dispersion in Groundwater Flowing Through Heterogeneous Materials. U.S. Geological Survey Prof. Paper 386B, 1963.

E.A. Sudicky. A Natural Gradient Experiment on Solute Transport in a Sand Aquifer: Spatial Variability of Hydraulic Conductivity and its Role in the Dispersion Process. Water Resources Research, Vol. 22, No. 13, 1986, pp. 2069-2082.

J.F. Sykes, S.B. Pahwa, R.B. Lantz and D.S. Ward. Numerical Simulation of Flow and Contaminant Migration at an Extensively Monitored Landfill. Water Resources Research, Vol. 18, No. 6, 1982, pp. 1687 - 1704.

A.F.B. Tompson, E.G. Vomvoris and L.W. Gelhar. Numerical Simulation of Solute Transport in Randomly Heterogeneous Porous Media: Motivation, Model Development, and Application. Ralph M. Parson Laboratory, Report 316, R88-05, Feb. 1988.

E. Vanmarcke. Random Fields: Analysis and Synthesis. Cambridge: MIT Press, 1983, 382 p.

E.G. Vomvoris. Concentration Variability in Transport in Heterogeneous Aquifers: A Stochastic Analysis. Doctoral Dissertation, Dept. of Civil Engineering, MIT, Cambridge, MA, 1986, 224 p.

J.E. Warren and F.F. Skiba. Macroscopic Dispersion. Transactions, American Institute Min. Metall. Petr. Engineering, Vol. 231, 1964, pp. 215-230.

A.W. Warrick and D.E. Myers. Optimization of Sampling Locations for Variogram Calculations. Water Resources Research, Vol. 23, No. 3, 1987, pp. 496-500.

S.W. Wheatcraft, K.C. Taylor, J.W. Hess and T.M. Morris. Borehole Sensing Methods for Ground-Water Investigations at Hazardous Waste Sites. Desert Research Institute, University of Nevada System, Water Resources Center, Pub. No. 41099, Jan. 1986, 69 p.

S. Wolf. Master of Science Thesis, Dept. of Civil Engineering, MIT, Cambridge, MA, 1988, In Preparation.

M.R.J. Wyllie. The Fundamentals of Well Log Interpretation. Academic Press, 1963, 238 p.

H. Yazicigal and L.V.A. Sendlein. Surface Geophysical Techniques in Ground-Water Monitoring Part II. Ground Water Monitoring Review, Winter, 1982, pp. 56-62.

T.-C. Yeh, L.W. Gelhar and A.L. Gutjahr. Stochastic Analysis of Unsaturated Flow in Heterogeneous Soils, 1, Statistically Isotropic Media. Water Resources Research, Vol. 21, No. 4, 1985a, pp. 447-456.

T.-C. Yeh, L.W. Gelhar and A.L. Gutjahr. Stochastic Analysis of Unsaturated Flow in Heterogeneous Soils, 2, Statistically Anisotropic Media with variable α. Water Resources Research, Vol. 21, No. 4, 1985b, pp. 457-464.

T.-C. Yeh, L.W. Gelhar and A.L. Gutjahr. Stochastic Analysis of Unsaturated Flow in Heterogeneous Soils, 3, Observations and Applications. Water Resources Research, Vol. 21, No. 4, 1985c, pp. 465-471.

A.A.R. Zohdy, G.P. Eaton and D.R. Mabey. Application of Surface Geophysics to Ground-Water Investigations. Book 2, Chapter D1: Techniques of Water-Resources Investigations of the United States Geological Survey, 1974, 115 p.

Appendix A

CONTOUR MAPS OF SOME OF THE SURFACE GEOPHYSICAL MEASUREMENTS AT THE CAFB SITE

The surface geophysical data are presented in this appendix to acquaint the reader with some of the available data. The full set of measurements is available in Boggs et al. (1988). Figure A-1 shows the location of the surface geophysical surveys on the site. Figures A-2, A-3, and A-4 are the contour maps of the direct current resistivity collected by TVA for electrode spacings of 1.52, 3.05, and 6.1 m, respectively. The spacing between measurements is 30.5 m in each direction. The contours for the different electrode spacings (1.52 m, 3.05 m, and 6.10 m) are quite similar, so it is no surprise that the correlation scales estimated in Table 2-5 are also similar. The contours of streaming potential (SP) data (Figure A-5) were collected on a finer grid (15.24 m on a side) than the contours of direct current resistivity. Both the resistivity and SP show significant variability over the site, but whether this variability reflects hydraulic conductivity variability is not clear.

Figure A-6 is an example of the electromagnetic data. It is clear that manmade structures such as electric and telephone cables strongly influence the EM measurements. Away from manmade structures, the EM survey shows little variability and we chose not to use any of the EM data for preliminary covariance analysis.

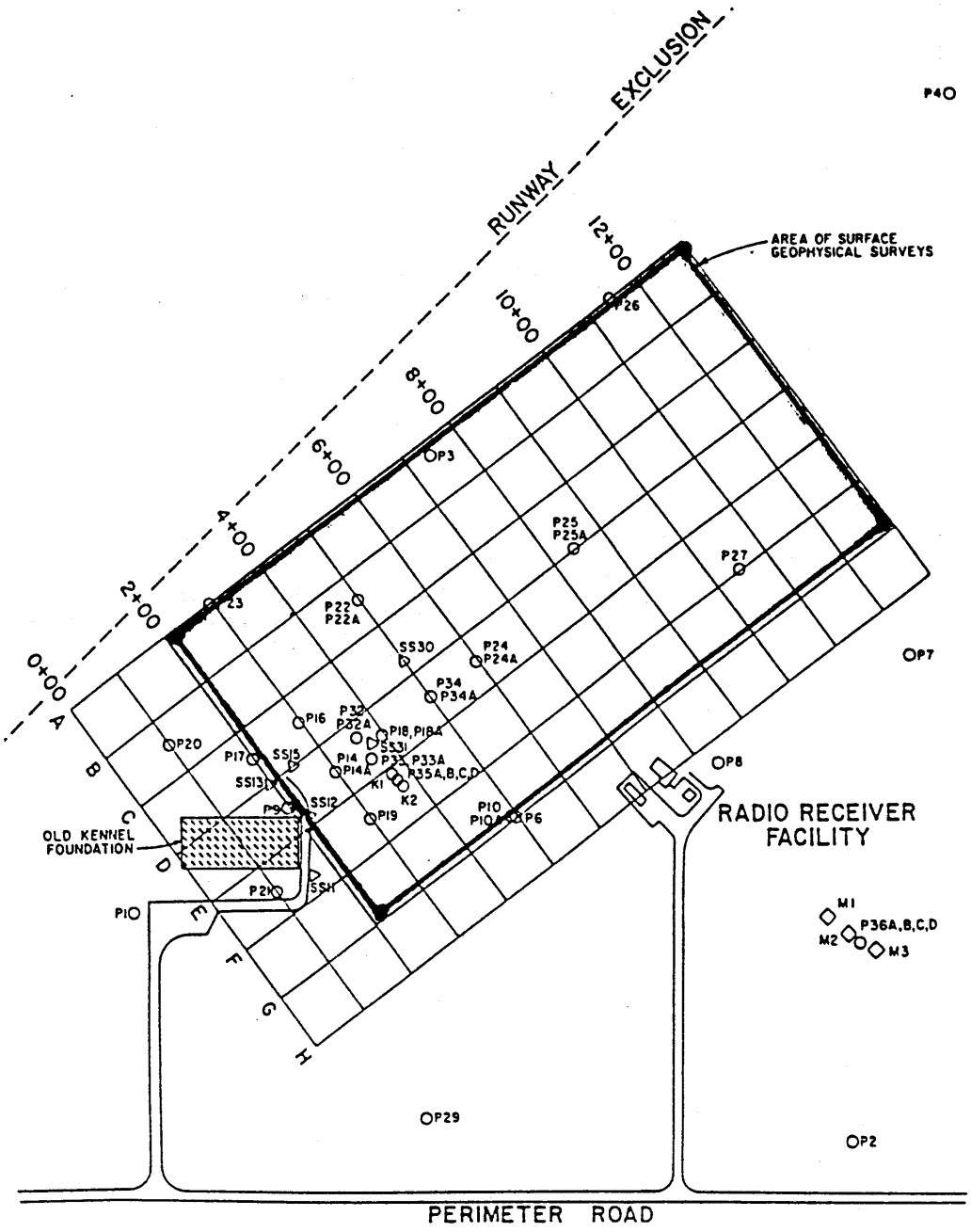

Figure A-1. Area of the Surface Geophysical Survey.

Source: Boggs et al., 1988

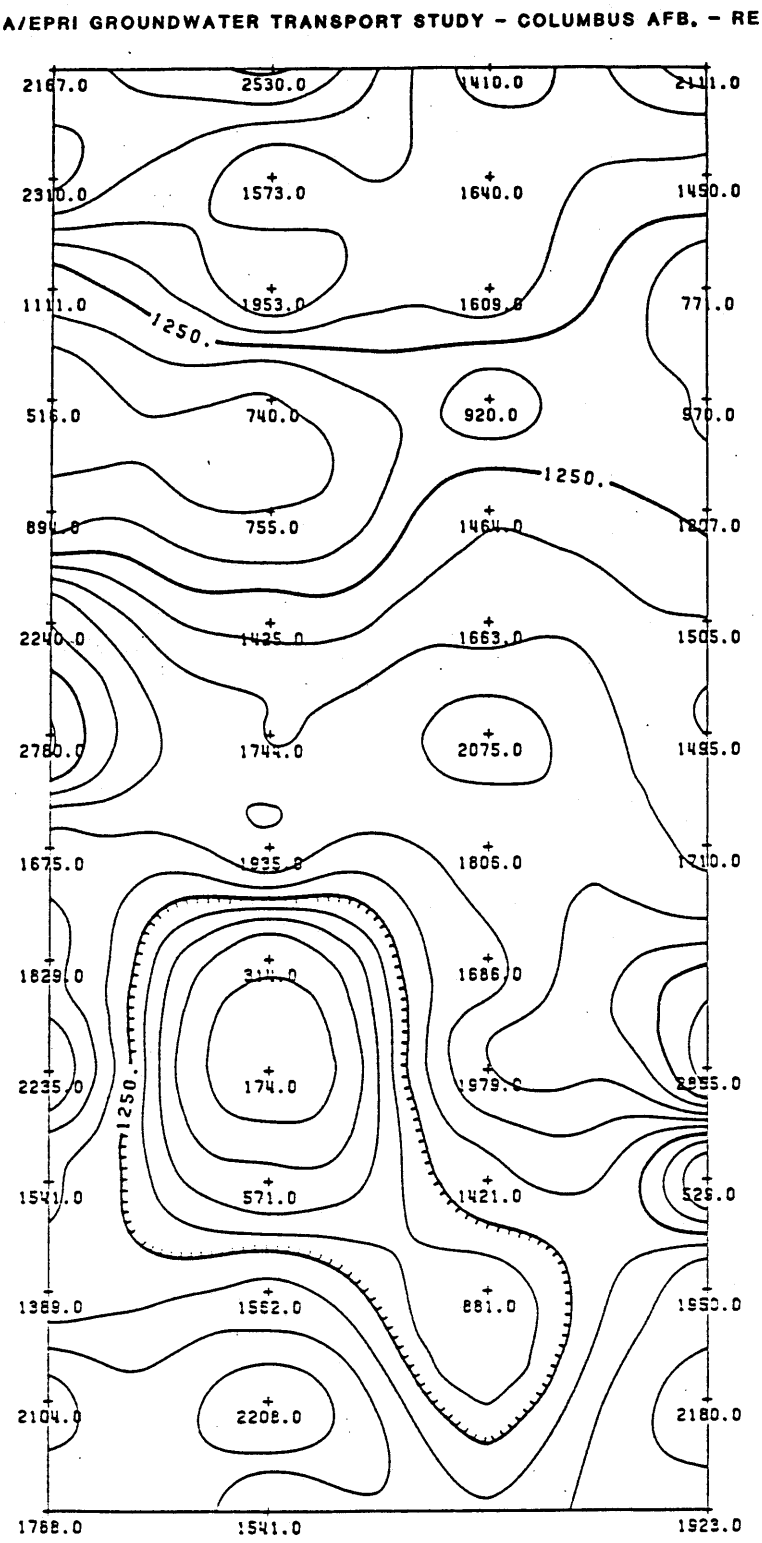

Figure A-2. Conventional Resistivity Survey with the Electrode Spacing of 1.52 m. Contour Interval is 250. Units are Unknown.

Source: Boggs et al., 1988.

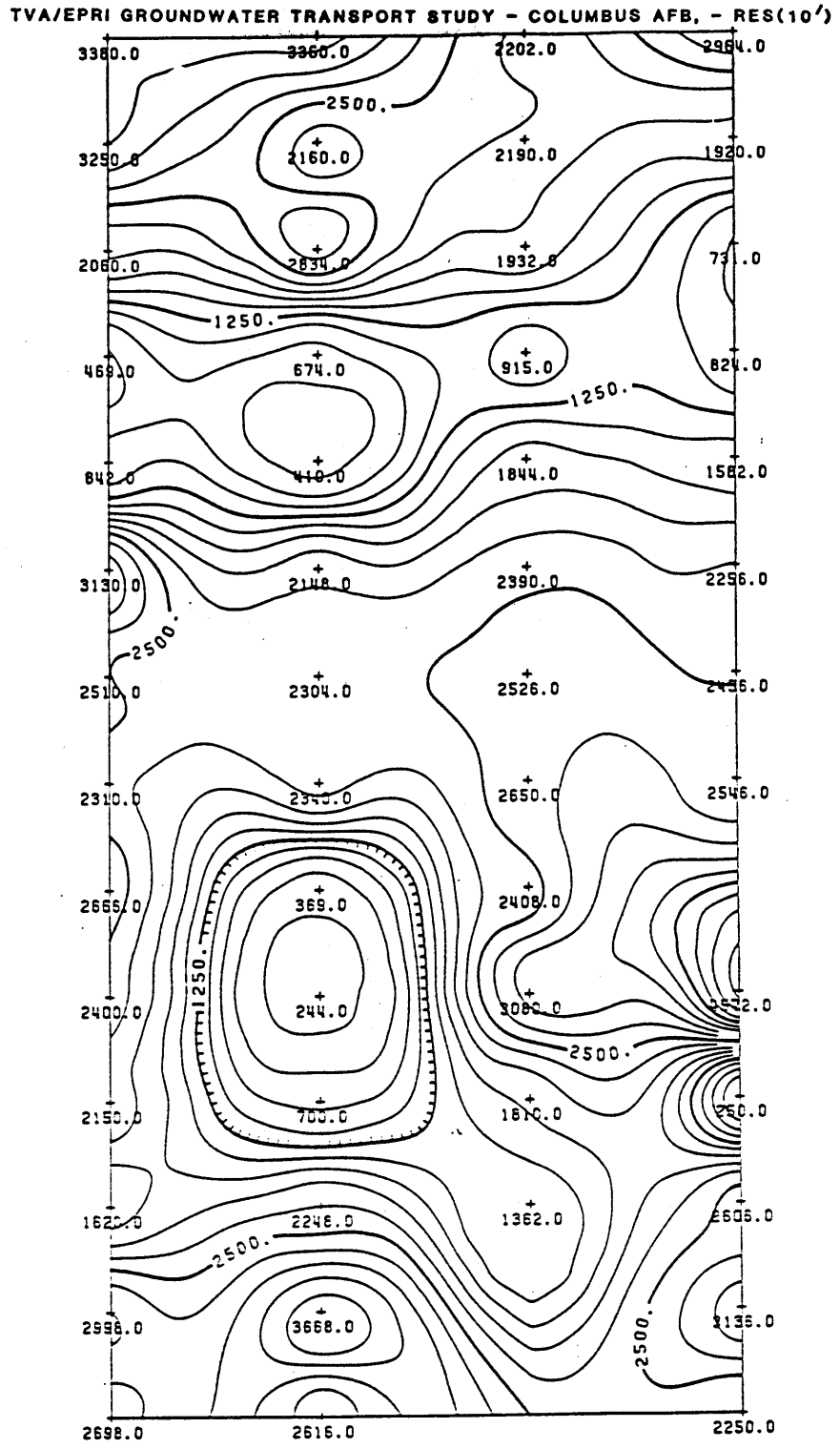

Figure A-3. Conventional Resistivity Survey with the Electrode Spacing of 3.05 m. Contour Interval is 250. Units are Unknown.

Source: Boggs et al., 1988.

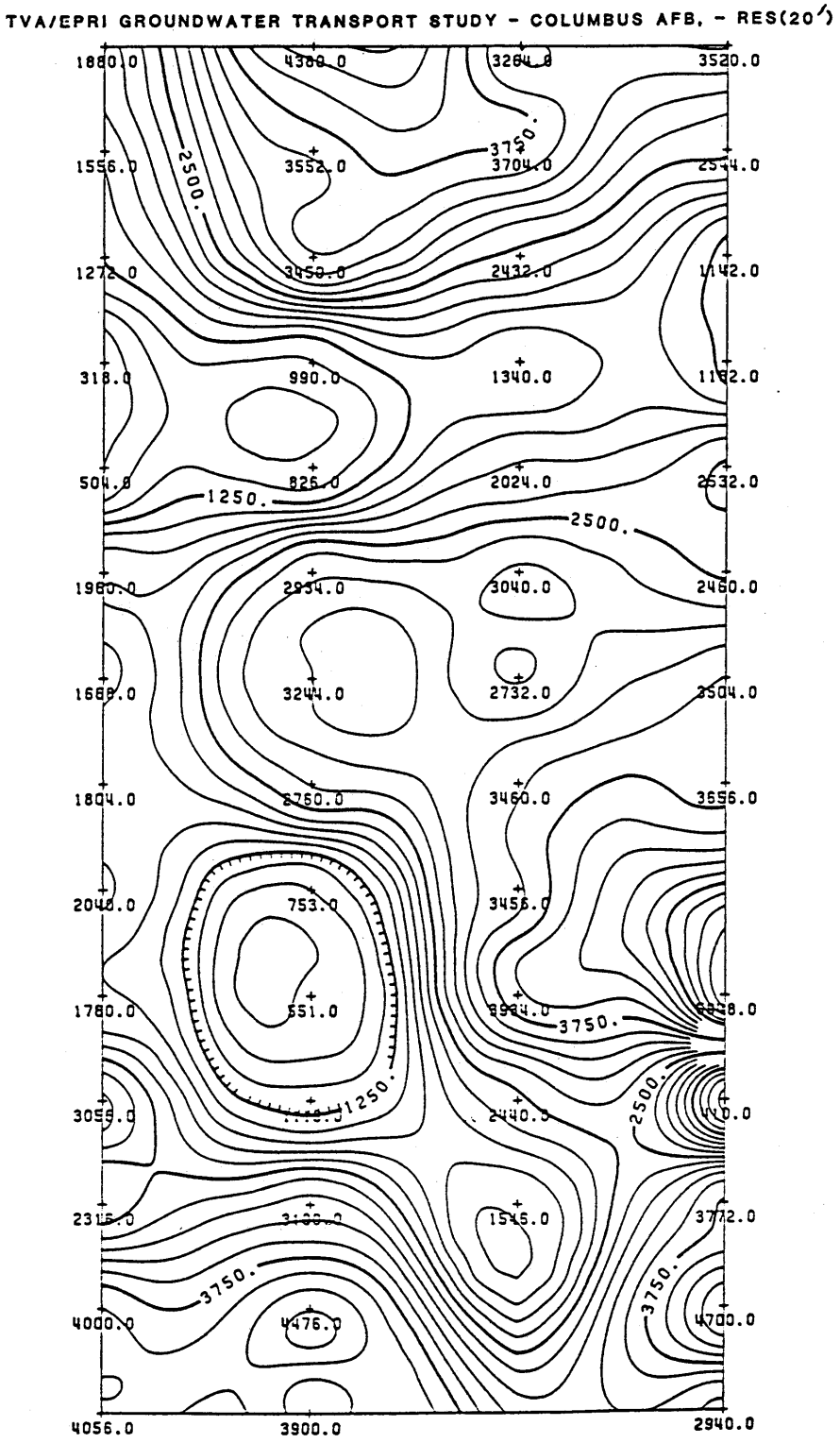

Figure A-4. Conventional Resistivity Survey with the Electrode Spacing of 6.1 m. Contour Interval is 250. Units are Unknown.

Source: Boggs et al., 1988.

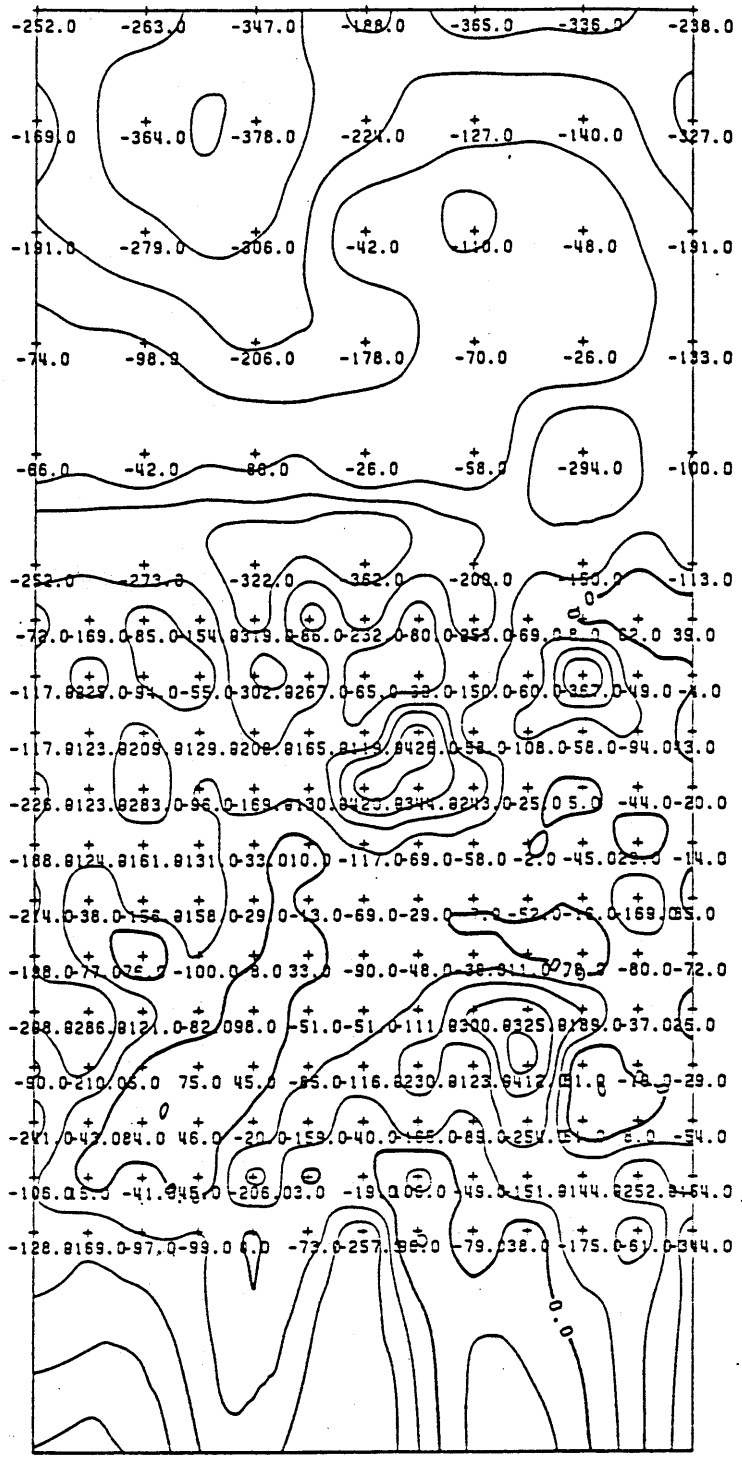

Figure A-5. Streaming Potential. Contour Interval is 100. Units are not Reported.

Source: Boggs et al., 1988.

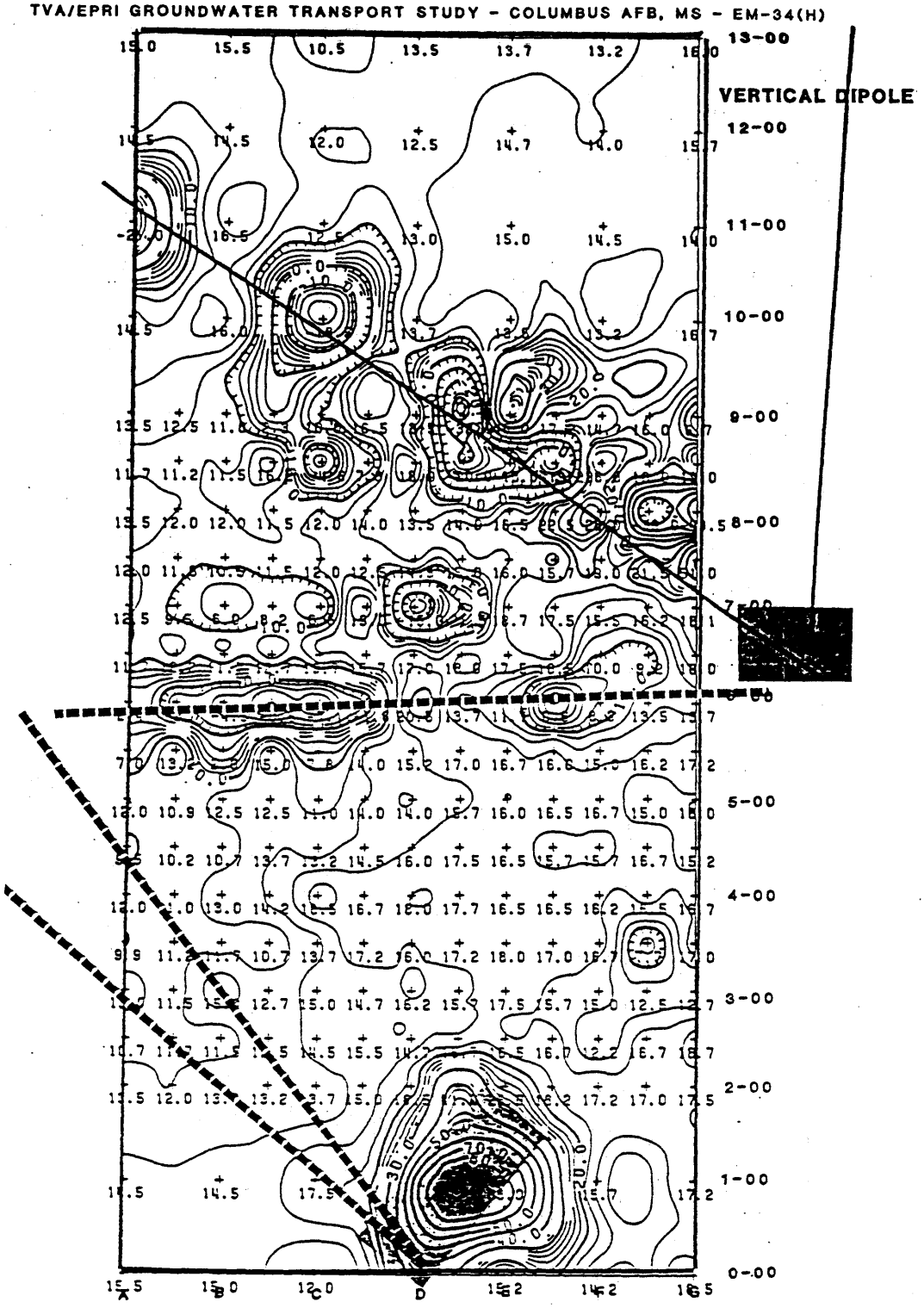

Figure A-6. Electromagnetic Induction (EM-34H) Survey. Buried Cables are Marked.

Source: Boggs et al., 1988.

Appendix B

BOREHOLE GEOPHYSICAL LOGS

Most of the piezometers installed through Fall, 1986, have been geophysically logged and the log profiles are presented in Boggs et al., 1988. The logs of the first six K-wells that are presented in this appendix serve to illustrate common features.

Figure B-1 indicates some variability in the natural gamma production over the depth of the well. Nearly all the variability is associated with the unsaturated zone (above elevation 205 ft) or with the Cretaceous Age marine sediments that form the base of the aquifer (below 180 feet). It is not clear if the small variations between 205 and 180 feet are real or if they represent measurement noise.

The resistance log (Figure B-1) clearly indicates the level of standing water in the well (about 200 ft). Below 200 ft, the only significant kicks in the log occur at 10 foot intervals and indicate the couplings between screened sections.

The density logs (Figure B-2) show significant variation over the depth; however, these logs are sensitive to conditions immediately outside the casing. A comparison of the density log profile from Well K-7 and the discharge profile in Well K-7 flowmeter log illustrates that sensitivity. In Figure B-3, the dips in the discharge profile are the result of incomplete collapse of aquifer material around the casing, permitting flow to leave the well screen and thereby producing a reduction in flow. There are corresponding dips in the density log profile of Well K-7 (Figure B-2). Therefore we suspect that the density logs may be simply an indicator of how much material has collapsed around the outside of the casing.

Some detailed quantitative analysis of the borehole geophysical logs needs to be done to confirm the qualitative impressions discussed above. However we do not expect that the currently available logs will yield information useful for evaluating spatial variability of hydraulic conductivity. We suspect that improvements in the logging methods are possible and could lead to useful surrogate information on hydraulic conductivity. This would require a series of systematic tests of

different well installations and development methods, and different types of logging devices for a small number of wells. If a promising technique is identified through such testing, then a comprehensive logging program should be undertaken.

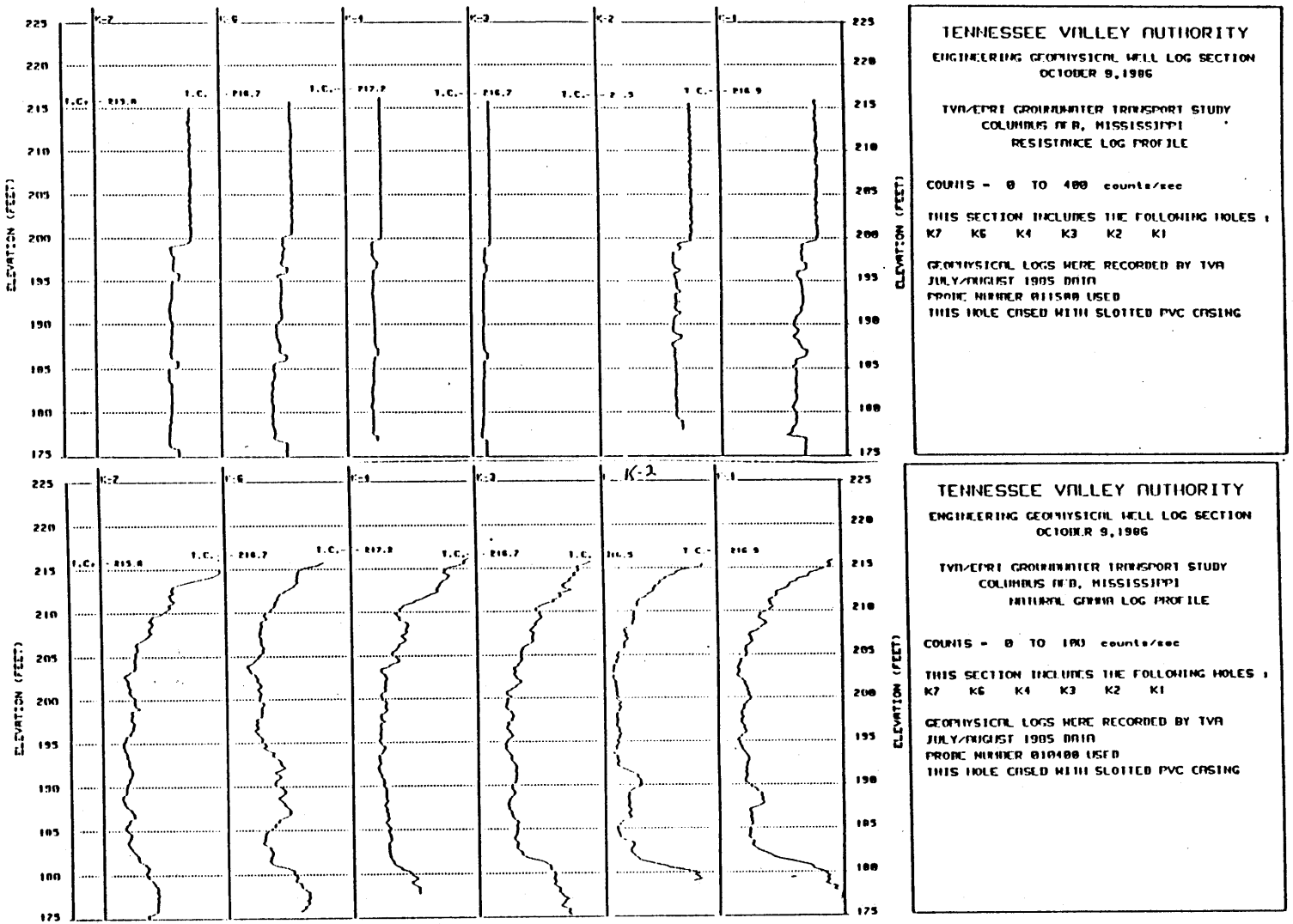

Figure B-1. Electrical Resistance and Natural Gamma Geophysical Log Profiles from Wells K-1 through K-7.

Source: Boggs et al., 1988.

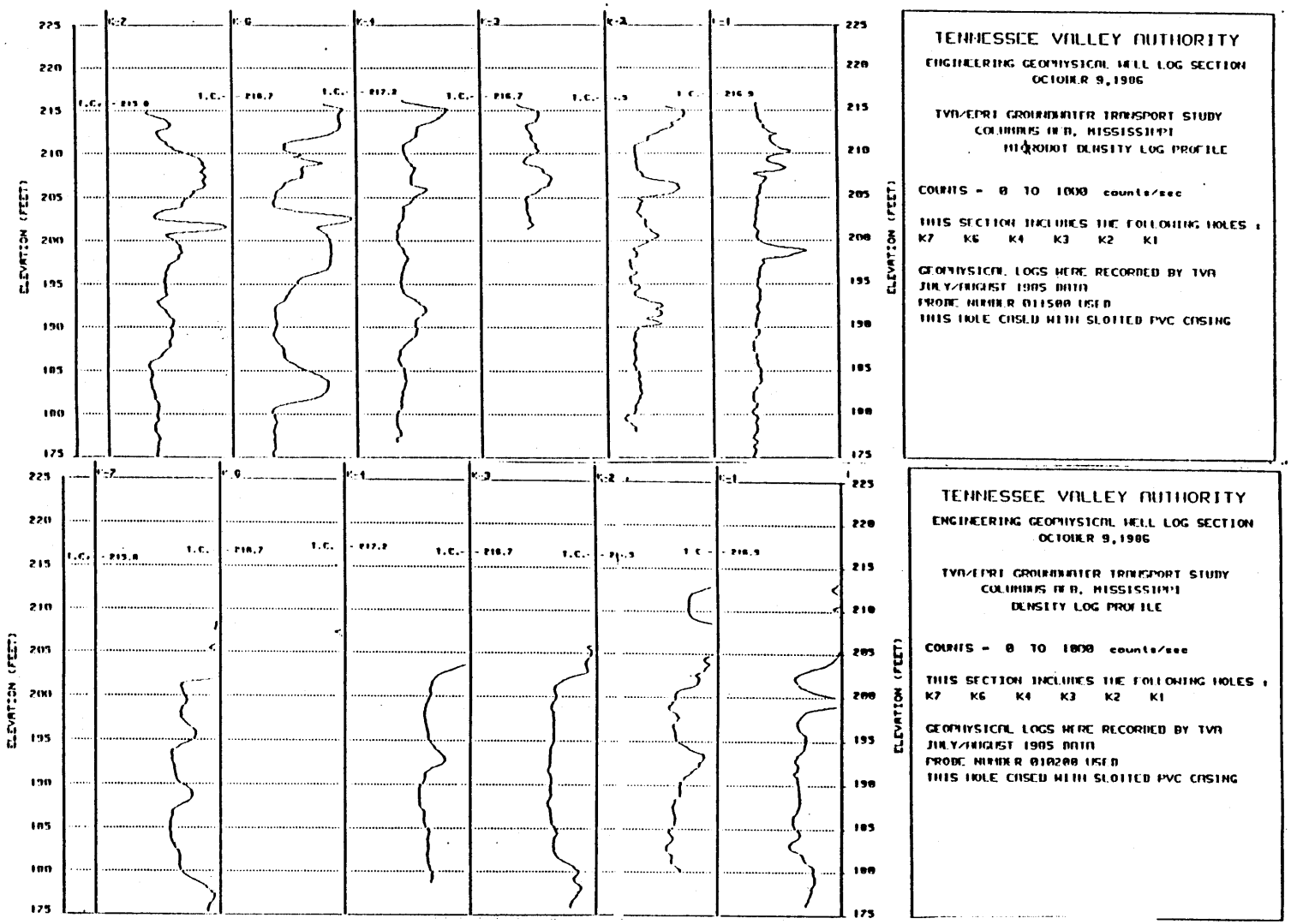

Figure B-2. Density Log Profiles from Wells K-1 through K-7.

Source: Boggs et al., 1988.

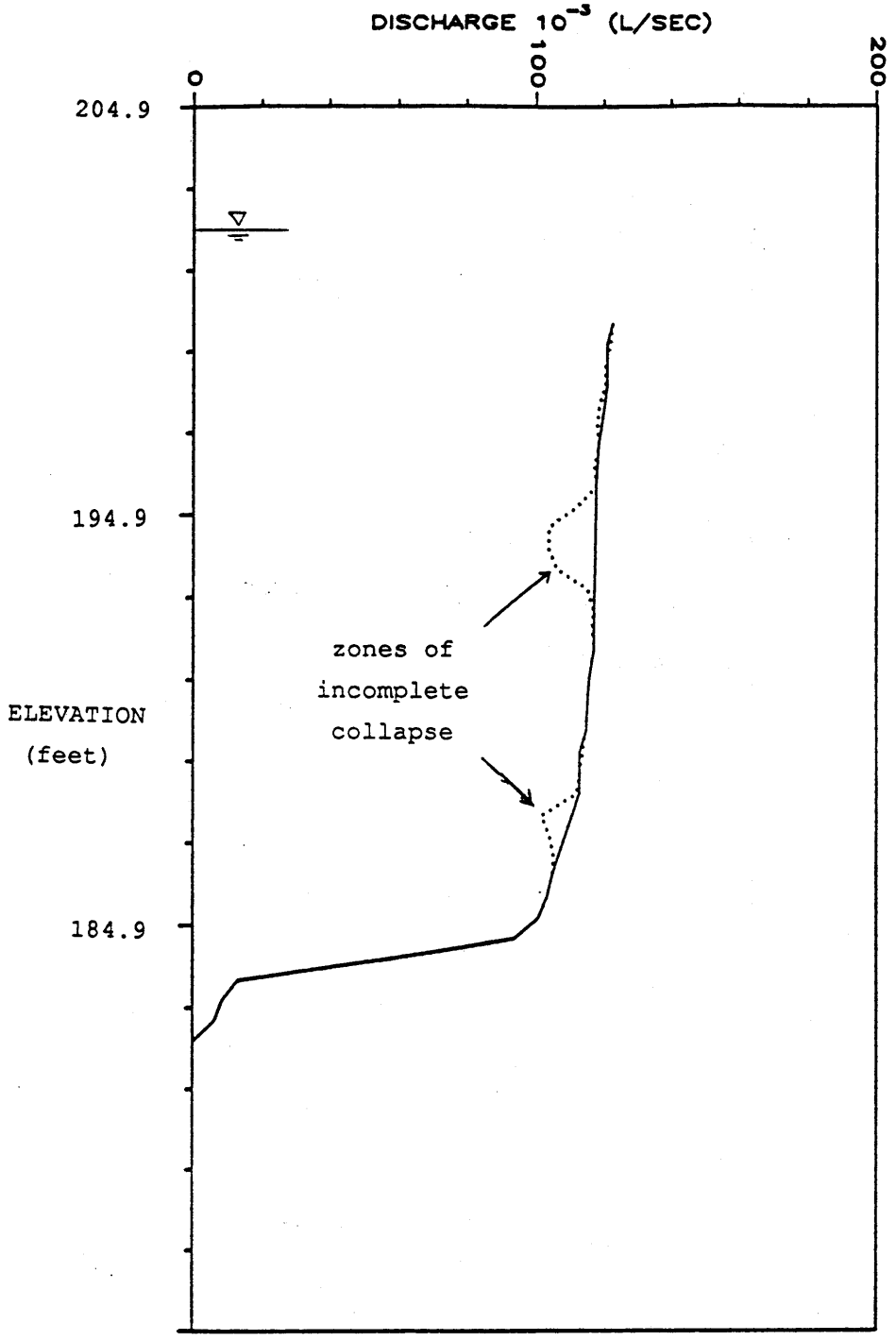

Figure B-3. Discharge Profile in Well K-7 During Pumping.